Title

Superfluid Theory: Vortex Theory of the Phase Transition, Pressure Dependencies in Equilibrated Three-Dimensional Bulk, and Vortex Pair Density in Quenched Two-Dimensional Film

Author

Forrester, Andrew

Publication Date

2012

University of California

Los Angeles

Superfluid Theory:

Vortex Theory of the Phase Transition,

Pressure Dependencies in Equilibrated Three-Dimensional Bulk,

and Vortex Pair Density in Quenched Two-Dimensional Film

A dissertation submitted in partial satisfaction

of the requirements for the degree

Doctor of Philosophy in Physics

by

Andrew Wade Forrester

2012

Abstract of the Dissertation

Superfluid Theory:

Vortex Theory of the Phase Transition,

Pressure Dependencies in Equilibrated Three-Dimensional Bulk,

and Vortex Pair Density in Quenched Two-Dimensional Film

by

Andrew Wade Forrester
Doctor of Philosophy in Physics
University of California, Los Angeles, 2012
Professor Gary A. Williams, Chair

The vortex theory of the helium-4-type superfluid phase transition, in both the 3D-bulk form and 2D-film form, is herein explained and intuitively derived. New evidence is provided supporting the accuracy of the 3D vortex loop theory in equilibrium over all pressures up to the solidification point. We show that the 3D theory consistently describes, within about 200 µK below T_λ, the pressure dependence of the helium superfluid fraction, heat capacity, vortex-loop core diameter, smallest-loop energy, and universal quantity X, which relates to an algebraic combination of the superfluid-fraction and specific-heat critical amplitudes. We suggest that the smallest vortex loops of the theory, with size on the order of angstroms, may be crude approximations for rotons. We also present a new exact analytic solution for the 2D non-equilibrium dynamics of vortex pairs in rapid temperature quenches.

The dissertation of Andrew Wade Forrester is approved.

Robijn F. Bruinsma

Paul H. Roberts

Joseph A. Rudnick

Gary A. Williams, Committee Chair

University of California, Los Angeles
2012

I dedicate this dissertation to everyone – family, friends, teachers, and mentors – who gave encouragement, support, and constructive critical thought along the way towards the completion of this dissertation.

TABLE OF CONTENTS

List of Figures

List of Tables

Acknowledgments

I thank my advisor Gary Williams for providing me the opportunity to work with him in investigating his vortex theory of the superfluid phase transition, for his exceptional pedagogical explanations and presentations, and for his enthusiasm, humor, patience, and good-natured attitude toward the highs, middles, and lows of research. I also thank Subodh Shenoy for his essential contribution to the theory, which has enabled our further research, and for his hospitality, entertaining conversation, and helpful comments. My doctoral committee, including Robijn Bruinsma, Paul Roberts, and Joseph Rudnick, as well as Gary, deserve and receive many thanks for their constructive criticisms and for ensuring that the assumptions and approximations are clearly and prominently stated and that the conclusions are conservative. In particular, I thank Paul Roberts for his detailed criticisms and mathematical suggestions that lead me to a more in-depth explanation of the renormalization flow and fixed points. I thank Han-Ching Chu for her contributions, for her computer programs, which helped as an initial reference for my programs, and for her email correspondence. Thanks also go to John Heidemann, Richard Wales, and everyone else who has contributed to the creation and maintenance of the `uclathes` LaTeX class file (which I only had to slightly edit to conform to the new typographical requirements). With regard to Chapter 4, Gary and I thank Leticia Cugliandolo, Asja Jelić, and William Newman for useful discussions. This work is supported by the U.S. National Science Foundation, Grant DMR 09-06467.

VITA

2003	Los Alamos Summer School (LASS) in Physics.
2004	CERN Summer Student Program.
2005	B.S., Physics and Mathematics, California State University, Long Beach (CSULB).
2007	M.S., Physics, University of California, Los Angeles (UCLA).

CHAPTER 1

Introduction

1.1 Introduction to Superfluidity

A (pure) superfluid is a fluid that flows without viscosity or internal friction. Not just any fluid can reach such a state, and those that do reach it have additional interesting properties that arise from the same mechanisms that allow for superfluidity. Fluids that reach a superfluid phase do so in a manner inconsistent with classical concepts, reaching this phase suddenly below a critical temperature T_{c} specific to each type of sample, and so require a quantum explanation. A fluid capable of superfluidity must be made of particles, quasi-particles[1], or molecules that, when near their collective quantum ground state – usually at what we consider to be very low temperatures – will flow together coherently in unison in a state called (or similar to) a Bose-Einstein condensate (BEC). Bose-Einstein condensation refers to a "condensing" of a detectable or macroscopic number of particles into the same quantum state, and it requires, in part, either low temperatures or high particle densities. A superfluid may come in the form of a "pure" gaseous BEC, where the particles are very weakly interacting[2], or a "non-pure" liquid BEC, where the particles are interacting strongly enough to create cohesion and maintain surface tension. The non-

---

[1] A quasi-particle is an excitation of a many-body system, such as a vibration in a crystal lattice, that has some of the properties of a free particle, such as momentum and position.

[2] For a 3D gas made of non-interacting particles capable of reaching a BEC state, the transition temperature is given by $T_{\mathrm{c}} = (2\pi\hbar^2/k_{\mathrm{B}}m)[N/V/\zeta(2/3)]^{2/3} \approx 3.3125\,(\hbar^2/k_{\mathrm{B}}m)(N/V)^{2/3}$, where N is the number of particles, V is the volume of the gas, m is the mass of each particle, ζ is the Riemann zeta function (with $\zeta(2/3) \approx 2.6124$), k_{B} is the Boltzmann constant, and $\hbar$ is the reduced Planck constant.

pure BEC is said to have a condensate component and a "depletion" component, due to the liquid-cohesion excitations of the interactions. A superfluid is generally composed of some fraction of pure superfluid (the condensate[3], or condensate-plus-depletion) and a remaining fraction of normal, viscous fluid.

The coherence of a superfluid is analogous in some ways to the coherence of laser light and the dissipationless coherence of an electron in an atom, where the behavior is self-reinforced in a kind of "rigid" resonance. As temperature decreases from a normal-fluid phase toward a superfluid phase, the thermal de Broglie wavelength of the particles can become comparable to the average inter-particle distance, meaning that the wave-functions start to overlap and the fluid can transform from a classical fluid to a quantum fluid, where quantum-condensing into a superfluid becomes possible. Although the lack of viscosity is the characteristic "super" fluid-ness property of a superfluid, one can more theoretically or constructively define a superfluid as a fluid in a near-BEC phase with low internal energy, having relatively few quantum excitations beyond its BEC ground state, where the fluid consequently has extremely low entropy and viscosity (or friction or resistance), rapid or "super" heat-conduction, quantized vorticity, and other interesting resultant properties[4]. With enough quantum excitations, the superfluid will change phase, losing its pure superfluid component, and become completely normal-fluid.

One of the simplest examples of a superfluid is superfluid helium, or more specifically, superfluid helium-4. A natural sample of helium contains two stable isotopes, helium-4 (^{4}He) and helium-3 (^{3}He), with about 10,000 more helium-4 atoms than helium-3 atoms in an atmospheric sample.[5] So natural helium can essentially be identified with helium-

---

[3] In a two-dimensional system, such as a thin film of superfluid helium, the pure superfluid is termed a quasicondensate [1], with properties only locally identical to a BEC.

[4] We won't discuss these other interesting properties, which for superfluid helium include Rollin films and self-siphoning, the mechano-caloric effect that creates the fountain effect, the critical velocity, and various sound modes ranging from "zeroth sound" to "sixth sound". What we do discuss, however, provides a foundation that supports understanding of these other phenomena.

[5] The laboratory samples of liquid helium used in Gary Williams' lab have a fraction of helium-3 of approximately 0.3 parts per million.

4. Helium-3 has only been available in experimentally useful quantities since the early 1950s, via the decay of tritium produced in nuclear reactors [2]. It so happens that a pure sample of helium-3 can also become superfluid, but explaining how is more complicated than explaining helium-4 and will be discussed below. In laboratories, liquid superfluidity, or “superliquidity”, has only been observed in samples of helium-4, helium-3, and (more recently, but arguably) hydrogen H_2 [3].[6] Helium is a monatomic substance and the helium-4 atom is a boson, meaning that multiple helium atoms can occupy the same quantum state, due to their integer spin arising from an even number of sub-particles and due to other principles associated with the spin-statistics theorem. (A fermion is a particle with integer-plus-half spin that cannot occupy the same state as other fermions of the same kind, also due to the spin-statistics theorem.) So helium-4, as a boson, has the possibility of directly forming a BEC. Also, helium-4 is such an inert element that at atmospheric pressure it doesn’t liquify until cooled to about 4.2 K and doesn’t freeze into a solid at all. The small mass m of the atoms combined with the weakness of their interaction, yield large quantum mechanical zero-temperature “zero-point” vibrations that prevent freezing to a crystalline solid state; only after applying additional pressure will the helium freeze into a solid. Furthermore, the thermal de Broglie wavelength $\lambda_T = h/\sqrt{2\pi m k_{\mathrm{B}} T}$ of the atoms can be equal to or greater than the average distance between the atoms, qualifying this liquid as a quantum liquid where wavefunctions overlap and the quantum statistics of the BEC are important. Thus helium has the opportunity to simultaneously be in a liquid state and at low enough temperatures to reach a BEC. Helium reaches the superliquid phase under about 2.2 K. See the phase diagrams in Fig.s 1.1 and 1.2 for illustration.

A more complicated example of superfluidity is superconductivity, which is resistance-

---

[6] Although reported as superfluidity in “liquid helium”, the Toennies experiment [3] only used a cluster of 14 to 16 para-hydrogen molecules forming a ring around a linear carbonyl sulfide (OCS) molecule, all encased in a micro-droplet of helium. This system is very different from a macroscopic bulk liquid of hydrogen.

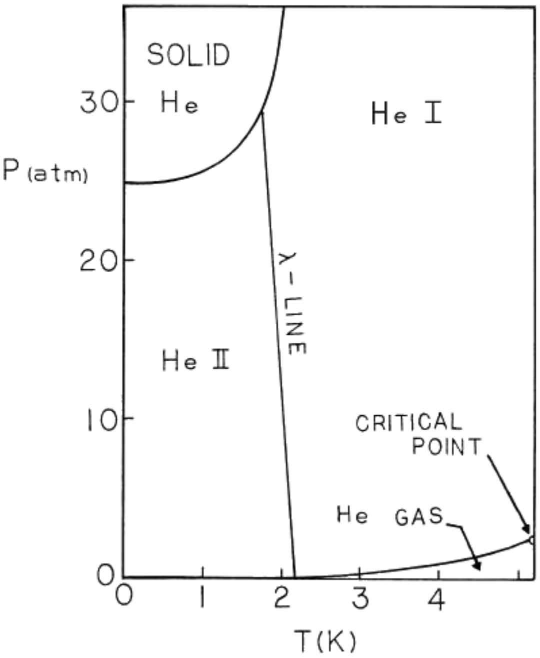

Figure 1.1: Phase diagram 1, 3D bulk helium. He I is normal fluid helium, and He II is superfluid helium. The transition between these two fluid phases occurs on the "lambda"-line, or λ-line. (We'll explain the reason for the use of the λ in this name below in Section 2.1.1.) This phase transition is of particular importance in the superfluid theory discussed here. Note that the range of pressures relevant to this transition is approximately 0 atm to 30 atm (or about 0 bar to 30 bar since 1 atm = 1.01325 bar). Also note that whenever we say "critical", we refer not to the liquid-gas critical point, but to the (normal)fluid-superfluid transition.

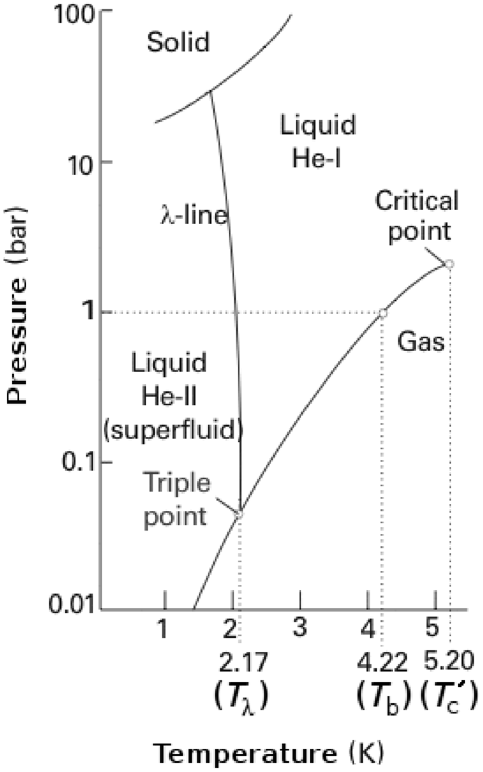

Figure 1.2: Phase diagram 2, also 3D bulk helium. Putting the vertical axis, pressure (in bars now), on a logarithmic scale, it is easier to see the boundary of the gas phase and the triple point, as well as the transition temperatures (T_λ and the boiling temperature T_b) at atmospheric pressure (1 bar). (The triple point temperature is distinct from T_λ, even though they are close and the dashed line for T_λ seems to intersect with the triple point.) Again, we'll refer to the superfluid transition temperature generally as the critical temperature T_c (where for bulk helium $T_\mathrm{c} = T_\lambda$) as distinct from the liquid-gas critical temperature T'_c.

less flow of an electron-fluid through the charged atomic lattice of a metal, alloy, or ceramic material. Again, other interesting quantum effects accompany the frictionless persistent current of the superconducting phase, including magnetic field expulsion of the Meissner effect in type-I superconductors or magnetic vortex-lattice penetration and pinning in type-II superconductors that allows for magnetic levitation and suspension. Since electrons are fermions, with spin-1/2, they cannot directly form a BEC. However, there do exist mechanisms by which fermions can sometimes form pairs, and the resulting composite particle is a boson that can form a BEC. The final condensate is called a fermionic condensate. This phenomenon occurs for electrons in "conventional" superconductors, and the theory that describes how superconductivity arises from these microscopic mechanisms is called BCS theory, named after its creators: Bardeen, Cooper, and Schrieffer. The theory describes how conduction electrons can form so-called "Cooper pairs" by indirectly attracting each other through vibrations in the positively charged crystal lattice of nuclei. There are also many examples of "unconventional" superconductors that are not yet explainable using the BCS theory (or Bogolyubov's formulation) or it's known extensions. Interestingly, the best conductors at room temperature, such as gold, silver, and copper, do not become superconductors at all, while some poorer room-temperature conductors such as beryllium ($T_\mathrm{c} = 26$ mK [4]) and mercury ($T_\mathrm{c} = 4.2$ K [5]) do. Even more interestingly, superconductivity is most easily accessible using ceramic room-temperature insulators such as yttrium-barium-copper-oxide ($YBa_2Cu_3O_7$ or YBCO, with $T_\mathrm{c} \approx 92$ K [7]) that have higher critical temperatures than pure metals.

The case of superfluid helium-3 is even more complicated than superconductivity. The pairing mechanism for the fermionic helium-3 atoms arises from spin fluctuations, with quantum excitations called paramagnons, rather than the BCS interplay between electric forces and lattice vibrations, where the quantum excitations are called phonons. At atmospheric pressure, helium-3 has a superfluid phase transition at about 2.5 mK, and it actually has two additional superliquid phases (superfluids A and A_1) at higher pressure, temperature, and applied magnetic field, than the atmospheric-pressure zero-magnetic-field phase (superfluid B). [8]

There are many other examples of superfluids. Perhaps the simplest example of all is the "pure" BEC, a gaseous superfluid, but this phase was only achieved recently compared to the previously mentioned examples, with the first sample consisting of rubidium atoms cooled below 170 nK. See Tables 1.1 and 1.2 below for a short history of the study of superfluidity. For superconductivity, the present record for the highest critical temperature (at atmospheric pressure) is 138 K, held by a thallium-doped, mercuric-cuprate, $\mathrm{Hg_{0.8}Tl_{0.2}Ba_2Ca_2Cu_3O_{8+\delta}}$. Above this temperature, in fact at room temperature, a quasi-equilibrium quasi-particle BEC of magnons[7] has been created [9]. Another dynamic quasi-equilibrium system strongly couples light and matter into a superfluid in the form of a exciton-polariton[8] BEC [10]. There are also systems of particles, such as the first "pure" fermionic condensate [11], whose interactions are tune-able (using magnetic-field Feshbach resonances) and so can be moved between BCS-type and "pure" BEC superfluidity.[9] One of the most exotic and spectacular examples is a naturally occurring one: a neutron star, a high-density remnant of a massive star gone supernova. These super-dense, super-hot stars can contain both a (fermionic) neutron superliquid, perhaps in two phases, and a (fermionic) proton superconductor! [12, 13] Finally, there is also research on a relatively new and unexplained phenomenon that unifies the concepts of superfluidity and solidity, called supersolidity [14, 15]. It can be found in solid helium-4, for example.

---

[7] Magnons are quanta of magnetic excitations in a magnetically ordered ensemble of magnetic moments.

[8] An exciton is a bound electron-hole particle, and can be found in semiconductor nanostructures, and a polariton is a quasiparticle resulting from strong coupling of an electromagnetic wave or photon with an electric or magnetic dipole-carrying excitation. Examples of polaritons include exciton-polaritons, phonon-polaritons, and plasmon-polaritons, where a plasmon is a quantum of plasma oscillation.

[9] For a reference to an entertaining song involving superfluidity and Feshbach resonances, see Appendix D.

Year	**Event**
1908	Helium first liquified at 4.22 K by H. Kamerlingh Onnes [16].
1911	Discovery of superconductivity (or "supraconductivity") at 4.2 K in solid mercury, cooled with liquid helium, by H. Kamerlingh Onnes [5]. Evidence of a new phase of helium witnessed on the same day, in the same experiment [17], but the discovery and naming of the phase and its properties is slow and gradual over the next 26 years [18].
1924	The concept of Bose-Einstein condensation is introduced by Satyendra Nath Bose and Albert Einstein [19].
1937	Discovery of superfluidity (superliquidity, in the form of frictionless flow through narrow capillaries) at 2.176 K in liquid helium independently by Pyotr Kapitza [20], and John Allen and Don Misener [21]. Papers published in 1938. Kapitza coins the word superfluid. Its relation to the BEC is suggested by Fritz London [22] a few weeks after the publications, but this relationship remains controversial for decades.
1938	A qualitative two-fluid model is proposed by László Tisza [23] (who predicts effects such as temperature waves, dubbed "second sound" by Lev Landau).
1941	A quantitative phenomenological microscopic theory of the two-fluid model is proposed by Lev Landau [24], based on elementary quantum excitations within a quantum liquid, describing thermodynamic and hydrodynamic properties.
1957	BCS theory of superconductivity introduced by John Bardeen, Leon Cooper, and Robert Schrieffer [25], with an independent description in 1958 by Nikolay Bogolyubov, or Bogoliubov [26].
1972	Discovery of what was later proven to be three phases of superfluidity in liquid helium-3 under 2.5 mK by Dave Lee, Bob Richardson, and Doug Osheroff [27].

Table 1.1: A small sample of interesting events in the history of superfluidity.

Year	**Event**
1973	The KT (or BKT) theory of the 2D superfluid phase transition (e.g., for helium films or the 2D XY spin model) introduced by John Kosterlitz and David Thouless (following earlier work by Vadim Berezinskii) [28, 29].
1986	Discovery of first ceramic-compound (copper-oxide, or cuprate) superconductor (La–Ba–Cu–O composition, with $T_c \approx 30$ K) by Alex Müller and Georg Bednorz [30]. In 1987, a similar ceramic superconductor (Y–Ba–Cu–O composition, "YBCO", $T_c \approx 92$ K) with a critical temperature in the experimentally convenient liquid nitrogen region ($T > 77$ K) was discovered by Wu *et alia* [7]. YBCO is the first modernly-defined "high temperature" superconductor.
1994	Discovery of the present record-holding high temperature superconductor ($T_c = 138$ K, using a thallium-doped, mercuric-cuprate with nominal composition $Hg_{0.8}Tl_{0.2}Ba_2Ca_2Cu_3O_{8+\delta}$) by Ron Goldfarb [31] or Dai *et alia* [32].
1995	The first "pure" BEC, a gaseous superfluid, is created by Eric Cornell, Carl Wieman, *et alia* in a dilute vapor of rubidium-87 atoms that was confined by magnetic fields and evaporatively cooled and laser cooled below 170 nK [33].
2000	Discovery of superfluidity in "liquid" clusters of (para)hydrogen H_2 at 0.15 K by Slava Grebenev, Boris Sartakov, Peter Toennies, and Andrei Vilesov [3].
2003	The first "pure" or weakly-interacting fermionic condensate is created by Cindy Regal, Markus Greiner, and Deborah Jin using potassium-40 atoms near a magnetic Feshbach resonance in the BCS-BEC crossover regime [11].
2004	Discovery of supersolidity (predicted in 1969 [34]) in solid helium below 230 mK at up to 66 bar (65 atm) by Eun-Seong Kim and Moses Chan [35].
2006	Creation of room temperature superfluid in a quasi-particle BEC of magnons by Demokritov, Demidov, *et alia* [9].

Table 1.2: Continuation of the timeline in Table 1.1.

1.2 Research Interest and Focus

The study of superfluids and superfluid phase transitions is important and interesting for several reasons. Aside from providing a fuller understanding of fluids in any phase and inspiring novel applications for the superfluid phase, this study continues to provide new insight and discoveries in quantum and collective phenomena, as well as stimulating progress in technology and experimental techniques. An indication of this fundamental importance is that at least 13 out of about 100 Nobel Prizes in physics have been awarded to research on superfluids and superconductors [36]. In particular, the theory that we focus on in this dissertation can also shed light on open questions in related phenomena such as turbulence [37,38]; high-temperature superconductors [39,40]; quark confinement [41]; and quenched systems, the Kibble-Zurek mechanism [42], and cosmological phase transitions [39, 40] during the rapid cooling at the earliest known states of the universe (after the Big Bang or during the "Big Quench", one might say).

The focus of the theoretical research in this dissertation is on two aspects of superfluids. The first aspect is the pressure dependence of various properties (including heat capacity) of a three-dimensional bulk of superfluid helium in equilibrium. The second aspect is the time-evolution of the vortex-pair density in a film or two-dimensional system of a superfluid as it is quenched, that is, as its heat bath temperature is instantaneously dropped further below the critical phase-transition temperature. However, before addressing these two topics in Chapters 3 and 4, we shall cover some preparatory background material on the theories of superfluids in Chapter 2.

Although the theory we discuss has applications to multiple instances of superfluidity, our focus is mainly on liquid helium-4 and related theories that are most relevant to this instance of superfluidity. The topic of Chapter 3 is specifically on the properties of superfluid helium. The topic of Chapter 4, given the rapidity (i.e., instantaneity) of the quench examined, may be most directly applicable to exciton-polariton superfluids [43], supposing that the response of the heat bath is found to be much quicker than the response of the vortices.

CHAPTER 2

Background

In this chapter we shall examine the 3D and 2D versions of the vortex theory of the superfluid phase transition, including equilibrium properties and 2D out-of-equilibrium vortex-pair dynamics of a quench, governed by the Fokker-Planck equation. The 2D theory is in the well-known Kosterlitz-Thouless theory universality class [28,29,44], which includes the 2D XY spin-lattice model phase transition as well as the superfluid film phase transition. The 3D theory is a generalization of both the Kosterlitz-Thouless theory and Landau's theory of excitations underpinning the two-fluid model. Conceptually, however, it may be simplest to start with the 3D vortex theory, and the 2D theory is then seen to be essentially a cross-section of the 3D theory. So, we start with the 3D theory in Section 2.1 and end the chapter with the 2D theory in Section 2.2.

In the theory, we take the pure superfluid condensate for granted, as a kind of background on top of which excitations are added, as is done in Landau's phenomenological excitation theory of the two-fluid model of superfluidity. We therefore simply derive the deviation from the superfluid state. We do not focus on the physics of the condensate, the condensation process itself, or the macroscopic or microscopic wavefunctions of the condensate and its excitations [45–55]. We also do not discuss topics such as the two-fluid hydrodynamic equations [56] or phase order parameters.

To be clear at the outset about the limitations and assumptions of the vortex theory, we shall spell out the aims and approximations of the theory here. These points will be reiterated (and the notation explained) throughout the derivations in the rest of this work. Some of these comments may make more sense in their appropriate context in the derivations and can be skipped at this time. The vortex theory is meant to be a kind of "first order" approximation theory, capturing the basic properties of the phase transition using very little input. Therefore, many simplifications and approximations are made. Specifically, the theory is a renormalization theory, with certain large-scale properties (such as the correlation-length critical exponent) insensitive to small-scale properties (such as the smallest vortex-loop diameter). However, using the theory enables some rough calculations of small-scale parameters (such as a_0 and U) using large-scale parameters (such as T_λ and the critical amplitude A'). The vortex theory, as calculated in this work, does not include phonons (a.k.a. first-sound excitations), maxons, or other excitations such as second-sound excitations, and the vortices are found to explain the main features of the phase transition whereas these other excitation are either known or expected [57] to not significantly affect the behavior at the lambda transition. We assume that the quantum vortices in the theory, being vortex loops in 3D and point-vortex pairs in 2D, each have a single quantum of circulation $\kappa = h/m$ as the most prevalent value of circulation. We assume the vortices are described using equations of classical fluid dynamics; the dipolar flow of fluid caused by the vortices is assumed to be approximately that given by small-core formulas, with momentum p and energy U given by $p = \frac{\pi}{4}\kappa\rho_{\mathrm{s}}^{\mathrm{r}}a^2$ and $U = \frac{1}{4}\kappa^2\rho_{\mathrm{s}}^{\mathrm{r}}a\left\{\ln(a/a_{\mathrm{c}}) + C\right\}$ in 3D and $p = \kappa\sigma_{\mathrm{s}}^{\mathrm{r}}a$ and $U = \frac{\kappa^2\sigma_{\mathrm{s}}^{\mathrm{r}}}{2\pi}\left\{\ln(a/a_0) + C\right\}$ in 2D. These formulas may only be approximately accurate for the smallest vortices, which should properly be modeled using quantum mechanics, and for the larger vortices in 3D (vortex loops), for which the small-core assumption is a simplification since the effective core size a_{c} can be on the order of the (effective) loop diameter size a. The ansatz for the relation between the effective core diameter and the coupling, $a_{\mathrm{c}} = aK^{\theta}\exp(C)$, has been calculated [58] to be applicable for large length scales, but we apply it as an approximation to the smaller length scales as well. We take one of two procedures (that yield numerically equivalent results): when $K \gtrsim 1$ we set $a_{\mathrm{c}} = a$ to keep a_{c} from growing beyond a, or we cut off the renormalization at a threshold $K = 4.15$ before the formula for a_{c} becomes large enough to significantly affect the results. These two methods are numerically equivalent since the cut-off is made well beyond the correlation length, under which the important physics takes place. We take the size of the smallest vortices to be determined by the natural cut-off where, in 3D, the vortex diameter equals the vortex core diameter, or in 2D, where the vortex-pair separation equals the vortex core diameter. Near this natural cut-off length scale, the quantum-mechanical details of the flow pattern become important and may be described by the Gross-Pitaevskii or nonlinear Schrödinger equations, for example. Also, there are certain quantum excitations that may behave similarly to the theoretical vortex loops at this scale, namely, spherical vortices and rotons. It may be reasonable to suspect that there is some agreement in some properties, such as energy or pressure-dependence of energy, between the smallest vortex loops and rotons, for instance, even if they are not strictly identical. In fact we do find a rough agreement between properties of the smallest vortex loops and rotons. In the 2D case, we assume a Villain model approximation to relate the vortex-pair core energy to the smallest-scale coupling, $2U_{\mathrm{core}}/k_{\mathrm{B}}T = \pi^2 K^{\ell 0}$, which is equivalent in our formulation to setting the core parameter C equal to $\pi/2$. And we postulate that the K and e equations remain the same out of equilibrium as they are in equilibrium.

We also should note here that alternate theoretical frameworks exist that are complementary to, but much more mathematically complicated than, the theory we discuss in this dissertation. They are known as field-theoretic perturbative renormalization-group theories, including the epsilon-expansion or $4 - \epsilon$ expansion, so called since it is an expansion in dimension about the fourth dimension. These perturbative theories work well above T_λ and near four dimensions but calculations are extremely difficult below T_λ and in three dimensions. [59–62] They also don't make any reference to quasi-particles, phonons, or rotons, but rather expand the Wilson-Fisher Hamiltonian without ever transforming to collective excitations. Feynman diagrams are a common sight in the literature, representing the integrals and series of the expansions. See, for example, Ref. [63]. We will only implicitly refer to this methodology when comparing some calculations in Chapter 3 using Refs. [64] and [65], which use high-temperature expansions and Monte Carlo simulations within a 3D XY model setting. Note that the vortex theory itself is a (non-perturbative) renormalization-group theory, as we will explain.

2.1 3D Theory: Superfluid Bulk

We will go into great detail in explaining the 3D theory and take a more schematic approach with the 2D theory, since most of the arguments will be the same in both cases.

2.1.1 Data to be Explained

Before jumping into an explanation of the theory, let's quickly examine a couple sets of data that must be explained by the theory. The temperature-dependent plot of specific heat capacity near 2 K, shown in Fig. 2.1, resembles the Greek letter lambda (λ). The specific heat cusps up to a maximum and drops immediately above the transition temperature. This is why the transition has been named the lambda-point or, over the relevant pressures, the lambda-line (as shown in the phase diagrams of Fig.s 1.1 and 1.2). The pressure-dependent transition temperature is called T_λ.

When comparing the theoretical results to these data, it will be more convenient to put the horizontal temperature axis on a logarithmic scale in terms of $\tau = 1 - T/T_\lambda$, what we'll call the "temperature variable". As shown in Fig. 2.2, this spreads out and straightens the data below and near T_λ, making it easier to see what's going on.

Another important set of measurements relates to the "amount of superfluidity" of the superfluid. As will be explained in the next section, the interesting properties of

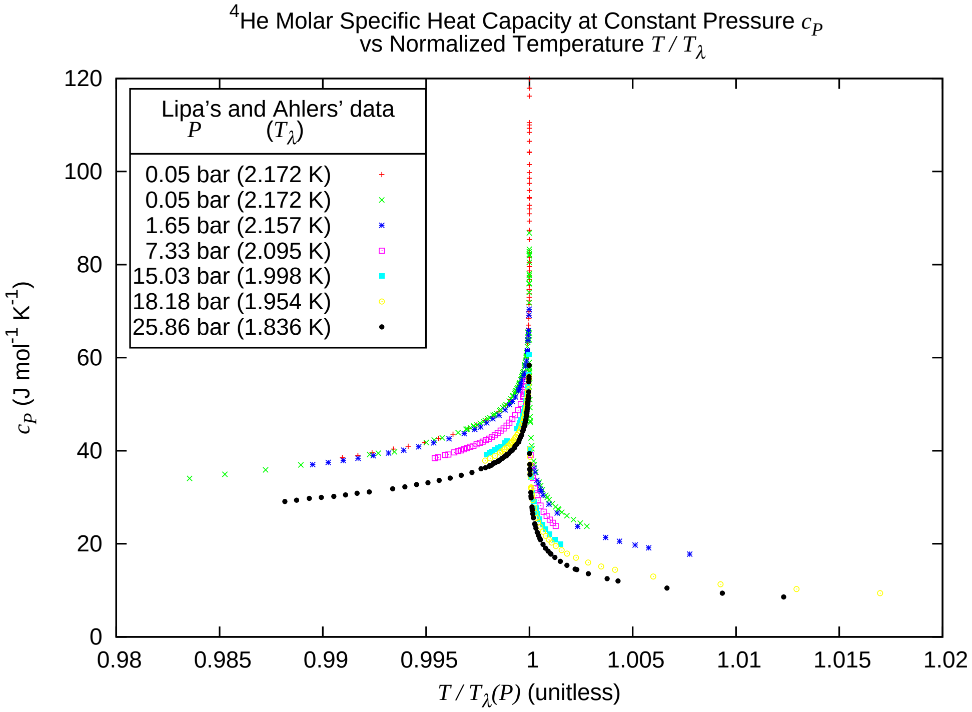

Figure 2.1: The specific heat capacity data, which resembles the Greek letter λ, motivates the "lambda" in the naming schemes associated with 3D bulk superfluid phase transition. This anomaly in the heat capacity was discovered before the zero-viscosity, superfluid property of the helium II phase was discovered. These data are from Lipa *et alia* [66] and Ahlers [67, 68].

a superfluid are maximized at the lowest temperatures and gradually disappear upon heating up to the transition temperature. This is illustrated by the "superfluid fraction" data shown in Fig. 2.3.

We aim to match these superfluid-fraction data, heat-capacity data, and other data, with calculations based on a fairly simple physical model given by the vortex theories.

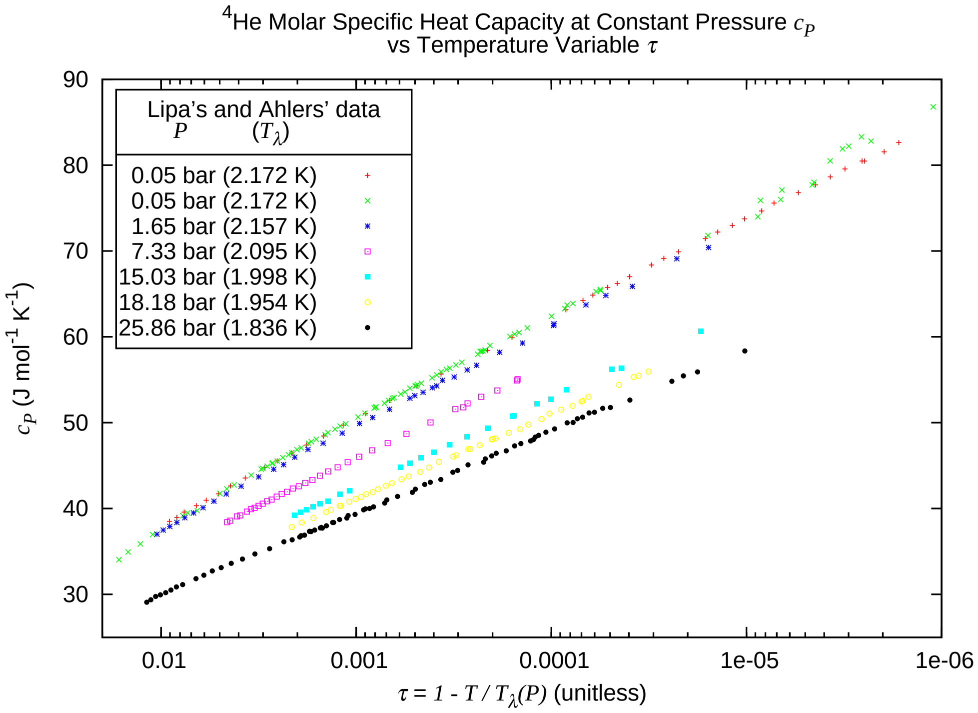

Figure 2.2: With the horizontal axis on a logarithmic scale, it is easier to see the behavior of the heat capacity at temperatures below and near T_λ. Note that in this plot the transition temperature (T_λ, $\tau = 0$) is toward the right, and zero absolute temperature ($T = 0$, $\tau = 1$) is toward the left, so the axis is reversed in terms of τ from the standard direction.

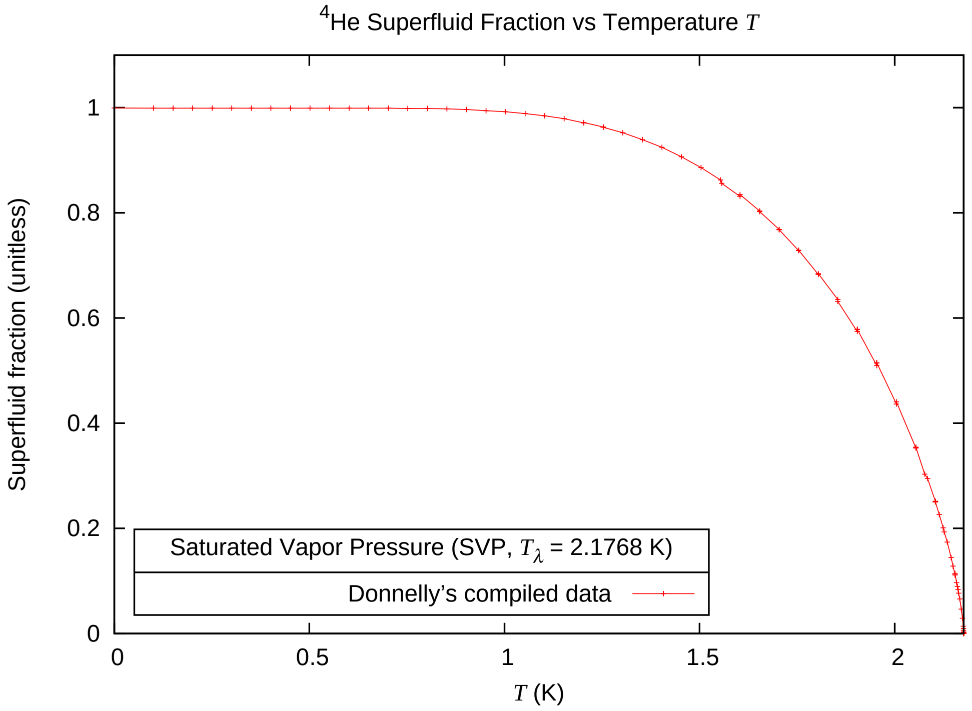

Figure 2.3: Superfluidity is destroyed by heating up to the transition temperature $T_\lambda = 2.1768$ K, while at saturated vapor pressure (which is near zero and reaches about 0.05 bar by T_λ). The superfluid fraction is explained below in Section 2.1.2.1. These data are from Donnelly and Barenghi [69].

2.1.2 Vortex Loop Theory, Concepts

2.1.2.1 excitations and fluid components

The 3D theory – the vortex loop theory of the superfluid phase transition – (with the addition of phonons) builds upon Landau's excitation model [24] that underlies the two-fluid model of superfluidity, first proposed by Tisza [23]. In Landau's model, a real superfluid (which has some friction, viscosity, and entropy at finite temperature) is fundamentally seen to be made of a pure superfluid (which has no friction, viscosity, or entropy) and excitations of that pure superfluid (which are fundamental kinds of quantum-mechanical motions of the superfluid that collectively create viscosity and entropy on larger length-scales).[1] Landau considered a spectrum of quantum excitations described by a energy-momentum "dispersion" relationship, shown in Fig. 2.4, that yields two low-energy excitations: phonons, which are compression-wave or sound modes, and rotons, which were not described in detail physically by Landau but suggested to have some rotational properties and relate to vortices. For these two lowest-energy excitations, the energies for their part of the spectrum are given by

$$\begin{aligned} \varepsilon^{\text{phonon}} &= cp && (2.1)\\ \varepsilon^{\text{roton}} &= \Delta + \frac{(p-p_0)^2}{2\mu_0}, && (2.2) \end{aligned}$$

where c is the speed of sound (speed of phonons) in helium, p is the momentum of the excitation, Δ is the minimum energy of a roton, p_0 is the momentum of the minimal-energy roton, and μ_0 is the effective mass of a roton (when seen as a quasi-particle).

Qualitatively speaking, the portion of the superfluid that is "caught up" in the excitations is seen to be "normal fluid" since it has entropy and viscosity, as the excitations

---

[1] We will ignore the complications arising from "depletion" in the pure superfluid, which separates it into a Bose condensate and a depleted part due to the interactions that keep the helium in a liquid state rather than a gaseous or solid state. See Ref. [70] for more detail.

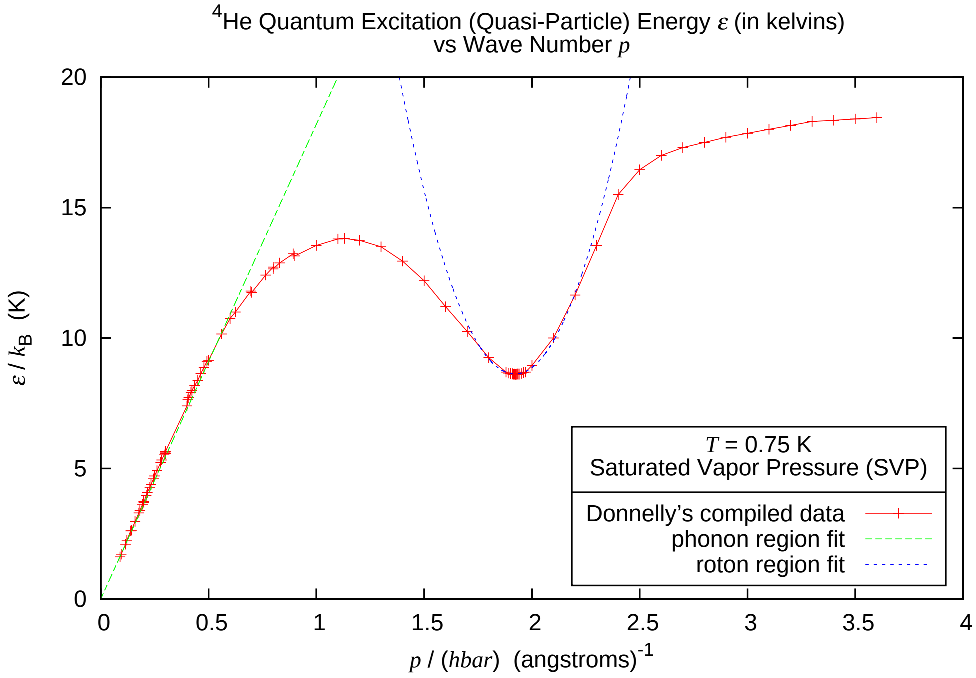

Figure 2.4: The quantum excitation energy-momentum dispersion curve. This curve corresponds to saturated vapor pressure at temperature $T = 0.75$ K. The lowest energy regions of this curve correspond to states dubbed phonons and rotons. (The intermediate range between them with a maximum has states called maxons.) The fits for these data, also provided by Donnelly and Barenghi [69], yield $c = 238.2$ m/s, $\Delta/k_{\mathrm{B}} = 8.62$ K, $p_0/\hbar = 1.921$ Å^{-1}, and $\mu_0 = 0.153m$, where $m = 6.6464759 \times 10^{-27}$ kg is the mass of a helium atom. This curve depends on temperature and pressure such that, for instance, Δ/k_{B} decreases with increasing temperature and pressure, as will be seen in Fig. 3.8.

interact with themselves and the container walls, and it behaves as a regular fluid would behave. So a real superfluid can be seen effectively as a kind of superposition of 1) a pure superfluid component with mass density ρ_{s} and velocity field $\mathbf{v}_{\mathrm{s}}$; and 2) a normal fluid component with mass density ρ_{n} and velocity field $\mathbf{v}_{\mathrm{n}}$. The real superfluid has mass density ρ and momentum density (or mass current-density) $\mathbf{j}$, where

$$\rho = \rho_{\mathrm{n}} + \rho_{\mathrm{s}}, \tag{2.3}$$

$$\mathbf{j} = \rho_{\mathrm{n}}\mathbf{v}_{\mathrm{n}} + \rho_{\mathrm{s}}\mathbf{v}_{\mathrm{s}}. \tag{2.4}$$

The excitations are constantly moving, interacting, and being created and destroyed, but at a particular temperature there is a static distribution of the number of excitations with respect to their energies. As temperature increases, there are more and more elementary excitations, so the fraction of the fluid that is normal increases from zero at zero absolute temperature to one by the critical temperature T_λ. Note that to understand this model at a deeper level would require more detailed explanation of the excitations and how they could create two apparently independent components of fluid. That goal is outside the scope of this dissertation. Still, this decomposition into two fluids is a simple demonstrable experimental truth.

In the Landau model one can calculate how phonons and rotons independently contribute to the normal fluid component:

$$\rho_{\mathrm{n}} = \rho_{\mathrm{n}}^{\mathrm{phonons}} + \rho_{\mathrm{n}}^{\mathrm{rotons}} \tag{2.5}$$

$$\rho_{\mathrm{n}}^{\mathrm{phonons}} = \frac{2\pi^2}{45\hbar^3}\frac{(k_{\mathrm{B}}T)^4}{c^5} \tag{2.6}$$

$$\rho_{\mathrm{n}}^{\mathrm{rotons}} = \frac{2}{3(2\pi)^{3/2}\hbar^3}\, p_0^4 \sqrt{\frac{\mu_0}{k_{\mathrm{B}}T}}\, \exp\!\left(-\frac{\Delta}{k_{\mathrm{B}}T}\right). \tag{2.7}$$

Or more generally, utilizing the full dispersion curve $\varepsilon(p)$,

$$\rho_{\mathrm{n}} = \frac{\hbar^2}{6\pi^2 k_{\mathrm{B}}T}\int_0^{p_{\max}} \frac{\exp\big(\varepsilon(p)/k_{\mathrm{B}}T\big)}{\Big[\exp\big(\varepsilon(p)/k_{\mathrm{B}}T\big)-1\Big]^2}\, p^2\,\mathrm{d}p. \tag{2.8}$$

Using Eq. (2.8), one can calculate the superfluid fraction $\rho_\mathrm{s}/\rho = (\rho - \rho_\mathrm{n})/\rho$, using experimental data for ρ, and find good agreement with the experimental superfluid fraction up to but not including the critical temperature. This comparison is made in Fig. 2.5, along with a plot of the superfluid fraction due to just phonons plus rotons, which compares rather poorly with the data.

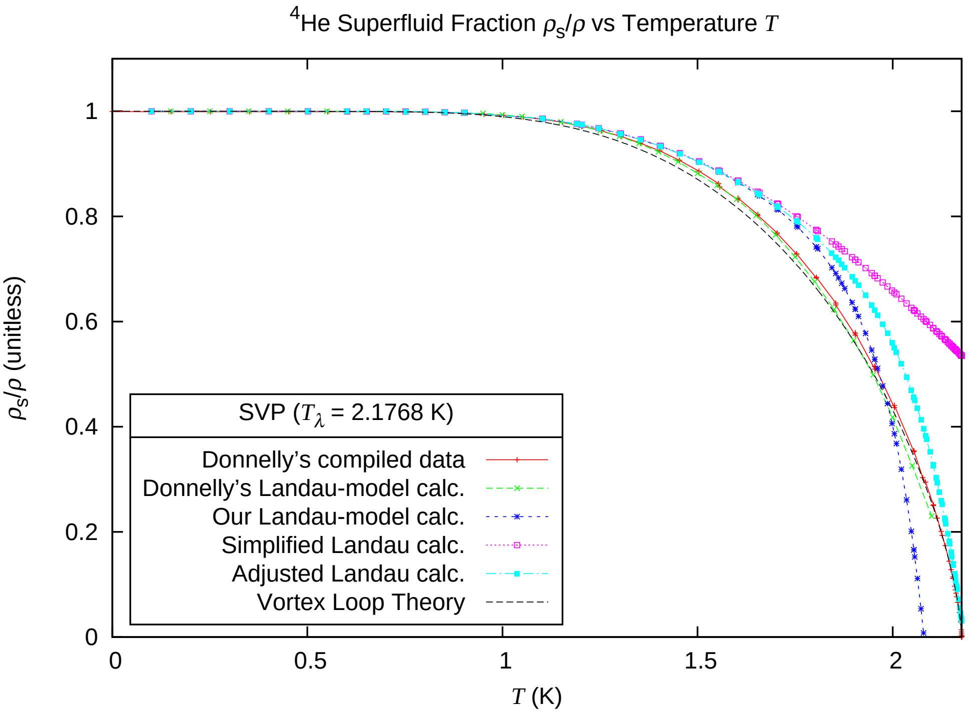

Figure 2.5: Landau's theory, as calculated by Brooks and Donnelly [71] using Eq. (2.8), works well but does not capture the critical behavior of the fluid at the phase transition, as will be shown more clearly in Fig. 2.6. The phonon and roton expressions in Eq.s (2.6) and (2.7), together with temperature- and pressure-dependent Landau parameters Δ, p_0, and μ_0, also given by fits from Brooks and Donnelly [71], yield a similar-looking curve that bows too high and goes to zero below T_λ. Assuming the Landau parameters are constant yields the "Simplified" curve, and adjusting Δ/k_B so that it falls to about 6.7 K instead of 5 K (as seen in [71] Fig. 5) yields the "Adjusted" curve. The vortex-loop-theory calculated curve is included for comparison.

In the vortex loop theory (plus phonons), we extend the Landau model by including vortex-loop excitations of all possible size, from the scale of angstroms (corresponding to the quantum vortex-loop core diameter) to the scale of the system. We suggest that vortex loops with diameters in the range of angstroms can be considered crude approximations to roton excitations. With this in mind we replace Eq. (2.5) with

$$\rho_{\mathrm{n}} \;=\; \rho_{\mathrm{n}}^{\mathrm{phonons}} + \rho_{\mathrm{n}}^{\mathrm{loops}}. \tag{2.9}$$

Actually, we do not include the phonons in our calculations since they only affect the result by about 0.4% near T_λ. Anyway, these vortex loops have dipole flow-fields, and in an applied flow-field they are forced to oppose the flow, analogous to diamagnetic behavior, where dipole magnets oppose an applied magnetic field. Thus the vortex loops act to oppose a flow in a superfluid, destroying what would be a perfect "superflow" in the absence of excitations (at zero absolute temperature). Furthermore, the smallest vortices screen the flow of larger loops, lowering their energy and making them easier to form. At higher temperatures, more and more vortices can form, and the size of the largest vortices (the correlation length, essentially) diverges while their energy approaches zero as the temperature approaches the transition temperature. At the transition temperature, the superflow is completely obstructed. The vortex loop model, in fact, accurately captures the behavior at the phase transition, as can be seen in Fig. 2.5 and more clearly in Fig. 2.6.[2] Whereas the phenomenological Landau theory takes more experimental input and works well at lower temperatures, the vortex loop theory takes less input and works well only very near the transition temperature T_λ. (As we will find out in Section 2.1.5, where we show more theoretical plots, the superfluid-fraction calculations at higher pressures deviate from the experimental data more than at saturated vapor pressure.)

---

[2] The vortex loop theory also explains why a superfluid in a confined space has more pure superfluid, since larger vortex loops are prevented from forming.

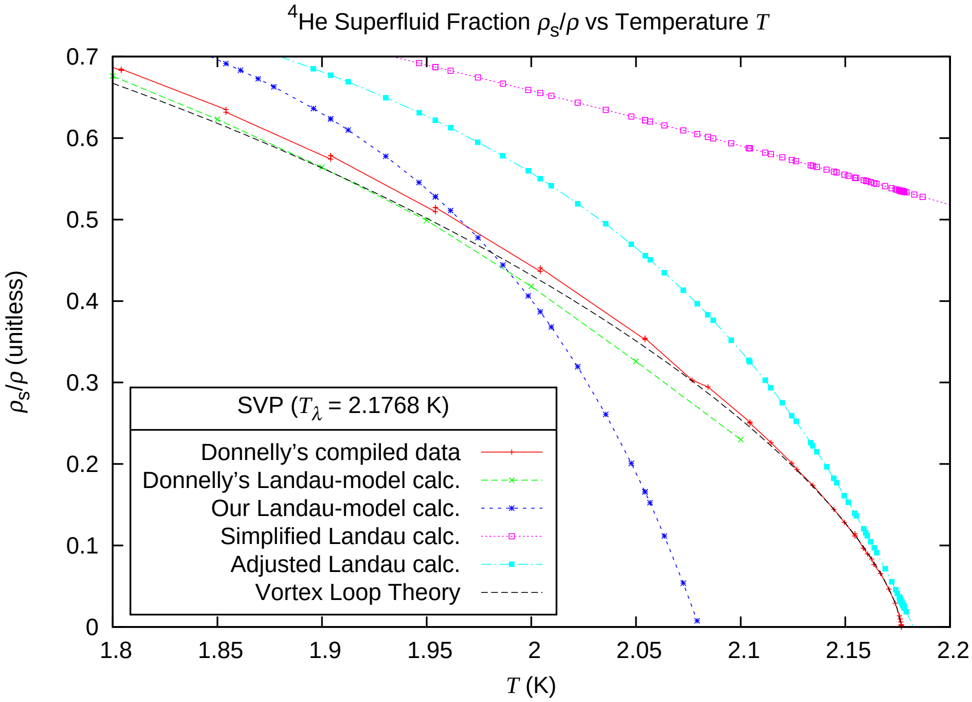

Figure 2.6: Near T_λ the calculations based on Landau's model remain fairly linear when compared with the data the vortex loop theory, which both follow (approximately) a 2/3 power law near T_λ, as will be explained in greater detail later in Chapter 3 and Appendix B. (The critical exponent ν is found to be 0.67168835 rather than 2/3.)

Note again that the vortex loop theory, as calculated in this work, does not include phonons (a.k.a. first-sound excitations), maxons, or other excitations such as second-sound excitations. A hybrid theory could be concocted that includes the phenomenology of the Landau dispersion curve, the effects of vortex loops of all sizes, and the effects of second-sound excitations and perhaps other excitations, but that is beyond the scope of this work.

2.1.2.2 renormalization

Note that at any temperature, at the smallest length-scales, below the length-scales of the excitations, a real superfluid is purely superfluid. The normal fluid is just pure superfluid "caught up" in the activity of the excitations, and so can only be "seen" at length scales larger than the excitations. So the properties of a superfluid, such as the pure superfluid density ρ_{s}, are length-scale dependent. We'll use a superscript "r", standing for "renormalized", to indicate this dependence, with the following justification. The value at a particular length scale depends on the value at the smaller length scales, and so at each stage going up in length scale the value is "renormalized" or recalculated. For instance, at the smallest relevant length-scale on the order of angstroms, $\rho_{\mathrm{s}}^{\mathrm{r}} = \rho$. As one "zooms out" and includes the effects of the smallest loops, $\rho_{\mathrm{s}}^{\mathrm{r}}$ decreases. Including larger and larger loops decreases $\rho_{\mathrm{s}}^{\mathrm{r}}$ further, and as explained above, the smaller vortices influence the effect of the larger vortices, so there is a recalculation at each progressively larger scale that is sensitive to the immediately smaller scale. So to solve for $\rho_{\mathrm{s}}^{\mathrm{r}}$ all the way up to its macroscopic value ρ_{s}, we will need to construct some interconnected equations that allow us to step up in length scale. This is the renormalization procedure of the vortex loop theory, and we shall call its equations scaling or recursion relations. See Table 2.1 for an overview of the notation that summarizes the temperature and length-scale dependence of the fluid component densities.

There is a common nomenclature in theories that use renormalization techniques. The smallest-scale values are called the "bare" values and those at larger scales are called "dressed". At the largest scale one sees the fully dressed quantity, where all the dressing has obstructed the view to the bare quantity. For example, in quantum field theory, particle fluctuations "dress" a bare electron to change its charge and mass at greater distances from the bare particle. In our case, one could say that the activity of the excitations "dress" the superfluid so that at the largest scales one does not see that

Component	Temp. dependence	Length-scale dependence
normal ρ_n	$\rho_\mathrm{n}^{T0} = 0 \quad \rho_\mathrm{n}^{T\lambda} = \rho$	$\rho_\mathrm{n}^{\ell 0} = 0 \quad 0 \le \rho_\mathrm{n}^\mathrm{r} \le \rho_\mathrm{n} \quad \rho_\mathrm{n}^{\ell\infty} = \rho_\mathrm{n}$
pure superfluid ρ_s	$\rho_\mathrm{s}^{T0} = \rho \quad \rho_\mathrm{s}^{T\lambda} = 0$	$\rho_\mathrm{s}^{\ell 0} = \rho \quad \rho \ge \rho_\mathrm{s}^\mathrm{r} \ge \rho_\mathrm{s} \quad \rho_\mathrm{s}^{\ell\infty} = \rho_\mathrm{s}$

Table 2.1: The superfluid component densities. "$T0$" indicates absolute zero temperature, "$T\lambda$" indicates the phase transition temperature, "$\ell 0$" indicates the smallest length scale (on the order of angstroms, corresponding to the quantum vortex-loop core diameter), "$\ell\infty$" indicates the largest length scale (that of the system and the correlation length at T_λ), which we'll take to be ∞, and "r" indicates any length scale ("r" is for "renormalized", explained in the renormalization section). The absence of a length-scale indicator on ρ implies $\ell\infty$.

the bare material is all pure superfluid.

Furthermore, "bare" can refer to an object or quantity at a certain length scale without the usual "dressings" that accompany it. This is a non-physical, out-of-equilibrium, or at least unusual situation. For instance, one may want to examine how certain parts of quantum field theory work with the vacuum fluctuations "turned off", with bare particles and fields interacting. In our case, we will use in one derivation the derivative of the bare energy of a vortex loop, multiplied by a permeability, to integrate up to the dressed energy. So in this sense an individual vortex loop is dressed by the activity of the smaller loops surrounding it.

Note that since we are not including excitations other than vortex loops, we do not have to worry about what length scale to start including their effects. If we included phonons, the pure-superfluid density would first be reduced by the phonons, and the "bare" superfluid density "seen" by the loops would be less than ρ, lowered by as much as 4% by T_λ.

2.1.2.3 model and linear response (permeability)

We shall now construct a conceptual model for the vortex loop theory in this section and continue to use the model in the following sections and derivations. Let's assume there is a very large system of superfluid in a container in thermodynamic equilibrium very near zero absolute temperature, where there is an infinitesimal applied flow $\mathbf{j}^{T0}$. We then heat the system to a higher temperature that is still below T_λ. Before heating, there is essentially no normal fluid and, once the superflow is set up, the flow remains unabating without further intervention due to lack of viscosity. After heating, some normal fluid is created, and the normal fluid comes to rest with respect to the fluid container ($\mathbf{v}_\mathrm{n} = \mathbf{0}$) as it loses energy and momentum to the container wall through interactions between the excitations and the wall. The total flow is reduced and the remaining flow is only in the pure superfluid component: $\mathbf{j} = \rho_\mathrm{s}\mathbf{v}_\mathrm{s}$. We can assume that the initial velocity field $\mathbf{v}^{T0}$ of the initial flow field $\mathbf{j}^{T0} = \rho\mathbf{v}^{T0}$ is retained by the pure superfluid: $\mathbf{v}_\mathrm{s} = \mathbf{v}^{T0}$. We shall call the factor by which the flow reduces μ: $\mathbf{j} = \mu\mathbf{j}^{T0}$. This is analogous to magnetism, $\mathbf{B} = \mu\mathbf{H}$, so we can call μ a permeability. Thus,

$$\begin{aligned}
\mathbf{j} &= \mu\mathbf{j}^{T0} && (2.10)\\
(\rho_\mathrm{s}\mathbf{v}_\mathrm{s}) &= \mu(\rho\mathbf{v}^{T0}) && (2.11)\\
(\rho_\mathrm{s}\mathbf{v}_\mathrm{s}) &= \mu(\rho\mathbf{v}_\mathrm{s}) && (2.12)\\
\mu &= \frac{\rho_\mathrm{s}}{\rho}. && (2.13)
\end{aligned}$$

This μ is the permeability at the largest length scale of the system, the length scale of the container. At smaller length scales, we can define a renormalized permeability based on the renormalized superfluid density:

$$\mu^\mathrm{r} = \frac{\rho_\mathrm{s}^\mathrm{r}}{\rho}. \qquad (2.14)$$

This μ^r is the permeability at any length scale, starting at 1 at the smallest length scale and ending at the superfluid fraction ρ_s/ρ at the largest scale, and it tells how well the superfluid effects (e.g., superflow or superfluid density) “survive” from the smallest scale to the scale in question and permeate the fluid. In the derivations in later sections, we shall refer to this quantity as well as the analogue of magnetic susceptibility, χ, defined by how it relates the flow induced by the vortex loops to the applied flow:

$$\mathbf{j}^{\mathrm{i}} = \chi \mathbf{j}^{T0}, \tag{2.15}$$

so

$$\begin{aligned} \mathbf{j} &= \mathbf{j}^{T0} + \mathbf{j}^{\mathrm{i}} && (2.16) \\ \left(\mu \mathbf{j}^{T0}\right) &= \mathbf{j}^{T0} + \left(\chi \mathbf{j}^{T0}\right) && (2.17) \\ \mu &= 1 + \chi. && (2.18) \end{aligned}$$

2.1.2.4 vortex-loop state variables

We take the quantum vortex loops that are naturally thermally excited in a superfluid to have cores of diameter a_0 on the order of angstroms. What is quantized is the circulation[3] of flow of the vortices, which come in multiples of h/m, where h is Planck’s constant and m is the mass of a helium-4 atom. We assume the single quantum of circulation $\kappa = h/m$ is the most prevalent value. The loops are free to wobble and so are not necessarily circular in shape. They can be quite distorted as they interact with each other and other excitations, and their cores can trace tortuous paths. In fact, we postulate that the perimeter or length L of a loop is what one would expect in a Flory-type minimization of the free energy: $L \propto a^{1/(1-\theta)}$, where a is an approximate diameter of the distorted loop and $\theta = D/[(D+2)(D-2)]$ is similar to the Flory exponent familiar from polymer physics [72, 73], with $\theta = 0.6$ in $D = 3$ dimensions [58, 74].[4] Even with this complicated

---

[3] The circulation of flow of a vortex loop is the line integral of the fluid velocity around a closed loop that encircles the vortex line of the loop. The vortex line for our purposes coincides with the core of the loop.

[4] In Ref. [58], the use of a $1/R$ interaction between vortex segments means that their results (including $\theta = D/(D+2)$) are strictly only valid at $D = 3$. By using the more general interaction $1/R^{(D-2)}$, the

geometry, the resultant flow field of such a wiggly loop can be approximated as that of a circular vortex loop of "best fit" diameter a and effective core size $a_\mathrm{c} < a$, where most of the vortex line remains within this effective core. Note that in our notation a will sometimes represent the diameter of a loop, and it will sometimes represent a length scale, such as in $\rho_\mathrm{s}^\mathrm{r}(a)$, which is the pure superfluid density at length-scale a, including the effect of all vortex loops up to diameter a.

A set of coordinates that describe the state of a circular vortex loop is the diameter a of the loop, the location of the center of the loop $\mathbf{x}$, the direction of motion of the loop $\hat{\mathbf{n}}$, and the momentum (or, more properly, the hydrodynamic impulse) $\mathbf{p}$ of the loop. These are not all independent quantities. We can specify the impulse and direction of propagation in one 3-component vector $\mathbf{p}$, since $\hat{\mathbf{p}} = \hat{\mathbf{n}}$ and the magnitude of the impulse is proportional to the square of the diameter $p = ka^2$, where the proportionality factor k is known ($k \equiv \frac{\pi}{4}\kappa\rho_\mathrm{s}^\mathrm{r}$).[5] Alternatively, we can define a diameter vector $\mathbf{a}$ with magnitude a and direction $\hat{\mathbf{a}} \equiv \hat{\mathbf{n}} = \hat{\mathbf{p}}$. So to describe a vortex loop, we can either use the pair of variables $(\mathbf{x}, \mathbf{p})$ or the pair $(\mathbf{x}, \mathbf{a})$. We will assume that the loops are spatially homogeneously distributed throughout the fluid.

These variables so far discussed determine other properties of vortex loops, such as its self-induced velocity v, flow-moment d, and energy E. First let's write some conventional equations, and then we'll modify them a bit. For the case of a loop with core diameter that is negligible in size compared to the vortex loop diameter, the following expressions for total energy Hamiltonian H (absent an applied flow), self-induced velocity v, and

---

Flory free-energy minimization gives the formula of θ used here. Note that the famous Flory exponent $3/(D+2)$ is different but numerically equal to these other exponents in 3D and was used in earlier incarnations of the vortex theory.

[5] We'll show evidence in the derivation of the K scaling equation that the potential alternate choice of $\frac{\pi}{4}\kappa\rho = \frac{\pi}{4}\kappa\rho_\mathrm{s}^{\ell 0}$ is incorrect.

impulse p are accurate for several core models,

$$
\begin{aligned}
H &= \tfrac{1}{4}\kappa^2\rho a\left[\ln(8a/a_0) - C_1\right] && (2.19)\\
v &= \frac{\kappa}{2\pi a}\left[\ln(8a/a_0) - C_2\right] && (2.20)\\
p &= \tfrac{\pi}{4}\kappa\rho a^2, && (2.21)
\end{aligned}
$$

where Table 2.2 shows values of C_1 and C_2 for various core models [55,75]. We will not find it necessary to pick a specific core model, although we will be able to eventually solve for a pressure-dependent C (defined by Eq. 2.27 below). If the Hamilton equation $v = \partial H/\partial p$ holds, then the vortex loop may be regarded as a quasi-particle excitation [76]. A simple but superficial analysis (as seen in Ref. [75]) follows if one supposes that ρ is constant, so that the derivative yields

Model	C_1	C_2
Solidly rotating core, constant volume	$\frac{7}{4}$	$\frac{1}{4}$
Hollow core, constant volume	2	$\frac{1}{2}$
Hollow core, constant pressure	$\frac{3}{2}$	$\frac{1}{2}$
Hollow core with surface tension	1	0
GP vortex in a Bose condensate	1.62	0.62

Table 2.2: Values of C_1 and C_2 for vortex rings with different core models. The first four are classical models and the last is a quantum model based on the Gross-Pitaevskii (GP) equation, a variant of the Non-Linear Schrödinger (NLS) equation, for a Bose condensate.

$$
\begin{aligned}
\frac{\partial H}{\partial p} &= \frac{1}{2\left(\frac{\pi}{4}\kappa\rho\right)a}\frac{\partial H}{\partial a} && (2.22)\\
&= \frac{\kappa}{2\pi a}\left[\ln(8a/a_0) - C_1 + 1\right], && (2.23)
\end{aligned}
$$

and thus one would expect that if $C_2 = C_1 - 1$, then the loop is a quasi-particle. But this argument is incorrect because any vortex governed by inviscid hydrodynamics (for instance, all of the vortices in Table 2.2, except possibly the third one) obey Hamiltonian dynamics, which lead to $v = \partial H/\partial p$ [77] (whereas only three of the models in Table 2.2 obey $C_2 = C_1 - 1$).

Now we shall modify and expand these relations a bit for the vortex loop theory and for elucidation. Although a_c may be on the same order of magnitude as a for some vortices, we will still use the small-core-size formulas as approximations for all vortices, knowing that this is inaccurate for the large-core vortices.[6] (What matters in the end is not whether this is a good approximation for a particular vortex but whether this is a good relative approximation over the whole renormalization, from small vortices to large ones, and between different temperatures.) Instead of using ρ, we'll use $\rho_\mathrm{s}^\mathrm{r}$, since a vortex loop of a given diameter a will utilize the pure superfluid at its length scale – the smaller vortices having extracted some of the pure superfluid, turning it normal. Thus we have

---

[6] One avenue of adjusting this model toward more accuracy would be to apply the non-small-core hydrodynamic equations found in the works of L. Edward Fraenkel and his student John Norbury, as well as those of Paul Roberts. As a historical aside, we can note that these relatively recent works of the later half of the 20th century and beginning of the 21st century recover, rederive, and expand the vortex theory that had been developed and expounded in the late 19th century by authors such as W.M. Hicks, Frank Dyson, and J.J. Thomson, who were inspired at least in part by the vortex theory of atoms devised by William Thomson ("Lord Kelvin").

the following renormalized quantities:

$$\begin{aligned}
U &= P.E. + K.E. && (2.24)\\
&= U_{\rm core} + K.E. && (2.25)\\
&= \tfrac{1}{4}\kappa^2\rho_{\rm s}^{\rm r}a\left\{\ln(a/a_{\rm c}) + C\right\} && (2.26)\\
C &\equiv \ln 8 - C_1 && (2.27)\\
&= U_{\rm core}/(\tfrac{1}{4}\kappa^2\rho_{\rm s}^{\rm r}a) \pm \text{constants} && (2.28)\\
d &= \tfrac{\pi}{4}\kappa a^2 && (2.29)\\
p &= \rho_{\rm s}^{\rm r}d && (2.30)\\
&= \tfrac{\pi}{4}\kappa\rho_{\rm s}^{\rm r}a^2 && (2.31)\\
E &= U + \mathbf{p}\cdot\mathbf{v}_{\rm s}. && (2.32)
\end{aligned}$$

Although we used a superscript "r" on ρ and μ (and will use it on χ) to indicate renormalization, from now on the "r" will be implicit on every newly introduced quantity that depends on length scale (including those above). The constant C here, which we'll call the core parameter, is related to the vortex core energy per effective diameter length, $U_{\rm core}/a$, as can be seen in Eq. (2.28), where the "constants" depend on which core model is used. We have included the energies U and E of a single loop so far, and will later also discuss the Helmholtz free energy F and the Gibbs free energy G of the liquid due to the loops. (The term $\mathbf{p}\cdot\mathbf{v}_{\rm s}$ in E gives the "Doppler shift" seen by an observer in the stationary normal fluid rest frame.)

The bare vortex loop energy, of which we wrote previously, being the loop energy absent the effect of smaller loops, is given by using the bare, unrenormalized pure superfluid density $\rho_{\rm s}^{\ell 0} = \rho$:

$$\begin{aligned}
U^0 &= \tfrac{1}{4}\kappa^2\rho_{\rm s}^{\ell 0}a\left\{\ln(a/a_{\rm c}) + C\right\} && (2.33)\\
U &= \mu^{\rm r}U^0. && (2.34)
\end{aligned}$$

The effective core diameter a_{c} should be different without the effect of the smaller loops, but we'll assume it is approximately the same as it is with the effect. Note that the bare loop energy at any scale, $U^0(a)$, is not the same quantity as the bare loop energy at the smallest scale $U^{\ell 0}$, but they are the same at the smallest scale: $U^0(a_0) = U^{\ell 0} = U(a_0)$.

2.1.2.5 vortex-loop number densities

At any time t there is a distribution $w(\mathbf{p}, t)$ in the number of vortex loops per volume that have an impulse in a region of volume $\mathrm{d}^3p = \mathrm{d}p_x\,\mathrm{d}p_y\,\mathrm{d}p_z$ in $\mathbf{p}$-state space at $\mathbf{p}$, independent of location $\mathbf{x}$ in a homogeneous system. Let's say the function w has dimensions of cardinality per spatial-volume per impulse-volume. More verbosely, the dimensions are number of loops with their centers in the spatial-volume in question and with impulse in the impulse volume in question, per that spatial-volume and per that impulse-volume. We'll see this confirmed in the equations below. There is also a related distribution $\Gamma(\mathbf{a}, t)$ in the number of vortex loops per volume that have a diameter vector in a region of volume $\mathrm{d}^3a = \mathrm{d}a_x\,\mathrm{d}a_y\,\mathrm{d}a_z$ in $\mathbf{a}$-state space at $\mathbf{a}$, independent of location $\mathbf{x}$ in a homogeneous system. Let Γ have dimensions of cardinality per spatial-volume per diameter-volume, with a similar verbose elaboration as the dimensions of w. Given a system with total fluid volume V and total number of vortices $N(t)$, which can change over time, we have the following relationships:

$$\frac{N(t)}{V} \;=\; \int w(\mathbf{p}, t)\,\mathrm{d}^3p \;=\; \int \Gamma(\mathbf{a}, t)\,\mathrm{d}^3a. \tag{2.35}$$

The relationship $p = ka^2$ dictates that the differentials are related like so, $\mathrm{d}^3p = p^2\mathrm{d}p\,\mathrm{d}\Omega = 2k^3a^5\mathrm{d}a\,\mathrm{d}\Omega = 2k^3a^3\mathrm{d}^3a$ (where Ω is a solid angle), so these number densities are related like so,

$$\Gamma(\mathbf{a}, t) \;=\; 2k^3a^3\,w(\mathbf{a}, t) \tag{2.36}$$

$$\Gamma \;\propto\; a^3 w. \tag{2.37}$$

We will assume that in equilibrium, Γ takes on a Boltzmann distribution[7]:

$$\Gamma_{\mathrm{eq}} \;=\; \frac{A}{a_0^6}\exp(E_{\mathrm{eq}}/k_{\mathrm{B}}T), \tag{2.38}$$

where A is a dimensionless constant that we'll set during our derivations to $4/\pi^2$. Although w will not concern us for now in the 3D theory, we will use the 2D version of w when constructing the 2D Fokker-Planck equation for the non-equilibrium evolution of the vortex distribution. Also, for those who plan on following along and writing the derivations, it may be helpful to read Appendix A right now to get some advice on using or defining Γ.

2.1.2.6 convenient parameters and an ansatz

In this section we will elaborate on a_{c}, the effective core diameter of a vortex loop, so that we can get on to the derivation of the theoretical equations. First, however, we should define some convenient parameters. The equations we derive will involve the dimensionful quantities Γ, U, F, $\rho_{\mathrm{s}}^{\mathrm{r}}$, T, and a. We would rather like to deal with dimensionless parameters that simplify the equations and our upcoming statement about a_{c}. So, let's define the parameters now and their convenience shall be manifest upon their usage.

Let $K_{\mathrm{s}} \equiv a_0(\hbar/m)^2\rho_{\mathrm{s}}^{\mathrm{r}}/k_{\mathrm{B}}T$, where K_{s} will be called the "superfluid parameter". Let $K \equiv (a/a_0)K_{\mathrm{s}} = a(\hbar/m)^2\rho_{\mathrm{s}}^{\mathrm{r}}/k_{\mathrm{B}}T$, where K is called the "coupling". Let $y \equiv (a^6/A)\Gamma$, where y is called the "fugacity"[8]. Let $e \equiv (F/k_{\mathrm{B}}T)(a_0^3/V)$, where e will be called the "Helmholtz parameter", since F is the Helmholtz energy of the liquid due to the loops. Let $r \equiv a/a_0$, where r could be called the "diameter parameter". Let $\ell \equiv \ln(a/a_0)$, where ℓ will be called the "length-scale parameter".

---

[7] There may be some question as to whether it is w, rather than Γ, that takes on the Boltzmann distribution in equilibrium.

[8] The parameter y is commonly called the fugacity, but we have not seen a proof that this is the fugacity as it is usually defined.

We should note some of the notation and properties of these parameters at the smallest relevant length scale of the vortex loop theory, the core diameter a_0. At that scale, where $a = a_0$, we have $r = 1$ and $\ell = 0$. This justifies the notation "$\ell 0$" (short for $\ell = 0$) that's been used to signify this length scale. Also, at this scale K and K_{s} become identical: $K^{\ell 0} = K_{\mathrm{s}}^{\ell 0} = a_0(\hbar/m)^2\rho_{\mathrm{s}}^{\ell 0}/k_{\mathrm{B}}T$. The most frequent use of K_{s} is to find the superfluid fraction (which explains the use of the subscript "s"):

$$\frac{K_{\mathrm{s}}}{K^{\ell 0}} = \frac{K_{\mathrm{s}}}{K_{\mathrm{s}}^{\ell 0}} = \frac{\rho_{\mathrm{s}}^{\mathrm{r}}}{\rho_{\mathrm{s}}^{\ell 0}}. \tag{2.39}$$

The energy of the smallest loop is $U^{\ell 0}/k_{\mathrm{B}}T = \frac{1}{4}(\kappa^2\rho_{\mathrm{s}}^{\ell 0}a_0/k_{\mathrm{B}}T)C = \pi^2 K^{\ell 0}C$. In equilibrium, given that we know Γ_{eq}, we thus know y is $y_{\mathrm{eq}} = (a/a_0)^6\exp(-E_{\mathrm{eq}}/k_{\mathrm{B}}T) \approx (a/a_0)^6\exp(-U_{\mathrm{eq}}/k_{\mathrm{B}}T)$, and so at a_0 this becomes $y_{\mathrm{eq}}^{\ell 0} \approx \exp(-\pi^2 K^{\ell 0}C)$. When examining y_{eq} remember that it can be traced back to the equilibrium vortex-loop distribution and energy:

$$\Gamma = \frac{A}{a_0^6}\left(\frac{a}{a_0}\right)^{-6} y \tag{2.40}$$

$$\frac{U_{\mathrm{eq}}}{k_{\mathrm{B}}T} \approx -\ln\left[\left(\frac{a}{a_0}\right)^{-6} y_{\mathrm{eq}}\right]. \tag{2.41}$$

Finally, let's discuss a_{c}. At the smallest scale, when a loop has an effective diameter a equal to (or near) a_0, there is no room for the loop to make any wiggles, and so the effective core diameter must equal the actual core diameter: $a_{\mathrm{c}}^{\ell 0} = a_0$. At this scale, on the order of angstroms, the true behavior of the loop must actually be described by quantum mechanics, but this simple vortex-loop theory will assume that Eq.s (2.24) to (2.32) are approximately valid down to this scale. (It is the larger loops that are more important to the theory near the phase transition anyway.) We now follow Shenoy [58, 78] and propose an ansatz to describe how a_{c} grows as a loop becomes larger: $a_{\mathrm{c}} \approx aK^{\theta}\exp(C)$. This choice is motivated by the same kind of free-energy-minimizing arguments that were used for determining that $L \propto a^{1/(1-\theta)}$. To see more detail and numerical evidence that supports this ansatz, see Ref. [58]. Note that this expression doesn't match a_0 at the smallest scale, so this is only an approximate relation, especially at smaller scales. A final convenient parameter, for use in the derivations, is $a'_{\mathrm{c}} \equiv a_{\mathrm{c}} / \exp(C) = aK^{\theta}$.

Vortex loop properties	$\kappa = h/m$
	$L = a_0 B (a/a_0)^{1/(1-\theta)}$
	$\theta = D/[(D+2)(D-2)] \quad = \quad 0.6 \qquad \text{(3D)}$
	$p = \frac{\pi}{4}\kappa\rho_{\mathrm{s}}^{\mathrm{r}} a^2$
	$U = \frac{1}{4}\kappa^2 \rho_{\mathrm{s}}^{\mathrm{r}} a \left\{ \ln(a/a_{\mathrm{c}}) + C \right\}$
	$U^0 = \frac{1}{4}\kappa^2 \rho_{\mathrm{s}}^{\ell 0} a \left\{ \ln(a/a_{\mathrm{c}}) + C \right\}$
	$E = U + \mathbf{p}\cdot\mathbf{v}_{\mathrm{s}}$
Convenient parameters	$K_{\mathrm{s}} \equiv a_0 (\hbar/m)^2 \rho_{\mathrm{s}}^{\mathrm{r}}/k_{\mathrm{B}}T$
	$K \equiv (a/a_0) K_{\mathrm{s}} \quad = \quad a(\hbar/m)^2 \rho_{\mathrm{s}}^{\mathrm{r}}/k_{\mathrm{B}}T$
	$y \equiv (a^6/A)\,\Gamma$
	$e \equiv (F/k_{\mathrm{B}}T)(a_0^3/V)$
	$r \equiv a/a_0$
	$\ell \equiv \ln(a/a_0) \qquad (\text{“}\ell 0\text{”} \Rightarrow a = a_0)$
Equilibrium	$\Gamma_{\mathrm{eq}} = (A/a_0^6)\exp(-E_{\mathrm{eq}}/k_{\mathrm{B}}T)$
	$y_{\mathrm{eq}} \approx (a/a_0)^6 \exp(-U_{\mathrm{eq}}/k_{\mathrm{B}}T)$
Smallest scale	$\dfrac{U^{\ell 0}}{k_{\mathrm{B}}T} = \frac{1}{4}\dfrac{\kappa^2 \rho_{\mathrm{s}}^{\ell 0} a_0}{k_{\mathrm{B}}T} C \quad = \quad \pi^2 K^{\ell 0} C$
	$y_{\mathrm{eq}}^{\ell 0} \approx \exp(-\pi^2 K^{\ell 0} C)$
	$a_{\mathrm{c}}^{\ell 0} = a_0$
Ansatz	$a_{\mathrm{c}} \approx a K^{\theta} \exp(C)$
	$a_{\mathrm{c}}' \equiv a_{\mathrm{c}}/\exp(C) \quad \approx \quad a K^{\theta}$

Table 2.3: This summarizes the important vortex loop theory quantities.

2.1.3 Equilibrium Scaling Relations, Derivations

In this section we'll derive the equilibrium recursion relations or scaling relations of the vortex loop theory. These equations will allow us to calculate the properties of helium at any length-scale given known small-scale values. We'll take a less rigorous, more physically qualitative approach than that taken by Shenoy [78], where he uses a duality transformation to switch from a Landau-Ginzburg-Wilson partition function to a vortex-loop plus second-sound/spin-wave partition function.

2.1.3.1 renormalized energy equation (leading to y equation)

We'll use two methods to derive an equation dealing with the vortex loop energy. The first method is simply to take the derivative of the loop energy, but we must treat $\rho_{\mathrm{s}}^{\mathrm{r}}$ and a_{c} as constants. (We've already treated $\rho_{\mathrm{s}}^{\mathrm{r}}$ as a constant when relating the distributions w and Γ and when examining the Hamilton relation.) The second method is inspired by the Kosterlitz-Thouless approach and uses the permeability to integrate up from the smallest-loop energy, using the bare energy U^0 and treating a_{c} as a constant.

Method 1 – Differentiate but ignore the a-dependence of $\rho_{\mathrm{s}}^{\mathrm{r}}$ and a_{c} when differentiating:

$$\begin{aligned}
\frac{\partial}{\partial \ell}\left(\frac{U}{k_{\mathrm{B}}T}\right) &= a\,\frac{\partial}{\partial a}\left(\frac{U}{k_{\mathrm{B}}T}\right) && (2.42)\\
&= a\,\frac{\partial}{\partial a}\left(\frac{1}{k_{\mathrm{B}}T}\tfrac{1}{4}\kappa^2\rho_{\mathrm{s}}^{\mathrm{r}}(a)\,a\left\{\ln(a/a_{\mathrm{c}})+C\right\}\right) && (2.43)\\
&\approx a\frac{1}{k_{\mathrm{B}}T}\tfrac{1}{4}\kappa^2\rho_{\mathrm{s}}^{\mathrm{r}}(a)\,\frac{\partial}{\partial a}\left(a\left\{\ln\left(a/a_{\mathrm{c}}\right)+C\right\}\right) && (2.44)\\
&\approx \frac{a\kappa^2\rho_{\mathrm{s}}^{\mathrm{r}}(a)}{4k_{\mathrm{B}}T}\left(\left\{\ln\left(a/a_{\mathrm{c}}\right)+C\right\}+a\left\{\frac{1}{a}\right\}\right) && (2.45)\\
&= \pi^2\frac{a\kappa^2\rho_{\mathrm{s}}^{\mathrm{r}}(a)}{(2\pi)^2k_{\mathrm{B}}T}\left\{\ln\left(a/a_{\mathrm{c}}'\right)+1\right\} && (2.46)\\
&= \pi^2K\left\{1-\theta\ln K\right\}. && (2.47)
\end{aligned}$$

In integral form, this scaling relation becomes

$$\frac{U(\ell)}{k_{\mathrm{B}}T} = \frac{U(0)}{k_{\mathrm{B}}T} + \pi^2 \int_0^\ell K(\ell') \left\{1 - \theta \ln\left[K(\ell')\right]\right\} \mathrm{d}\ell'. \tag{2.48}$$

Now we transform to the dimensionless parameter y. Given the relation $y_{\mathrm{eq}} \approx (a/a_0)^6 \exp(-U/k_{\mathrm{B}}T) = \exp(6\ell - U/k_{\mathrm{B}}T)$, we have

$$\begin{aligned}
\frac{\partial y_{\mathrm{eq}}}{\partial \ell} &= \frac{\partial}{\partial \ell} \exp(6\ell - U/k_{\mathrm{B}}T) && (2.49)\\
&= y_{\mathrm{eq}} \frac{\partial}{\partial \ell} \left(6\ell - U/k_{\mathrm{B}}T\right) && (2.50)\\
&= y_{\mathrm{eq}} \left\{6 - \frac{\partial}{\partial \ell}\left(\frac{U}{k_{\mathrm{B}}T}\right)\right\} && (2.51)\\
&= y_{\mathrm{eq}} \left\{6 - \pi^2 K \left(1 - \theta \ln K\right)\right\}. && (2.52)
\end{aligned}$$

Thus, we have found one of the scaling relations in terms of y.

Method 2 – Use the permeability to integrate up from the smallest-loop energy, using the bare energy U^0 and ignoring the a-dependence of a_{c} when differentiating:

$$\begin{aligned}
\frac{U(a)}{k_{\mathrm{B}}T} &= \frac{U^0(a_0)}{k_{\mathrm{B}}T} + \int_{a_0}^{a} \mu^{\mathrm{r}}(a')\, \frac{\mathrm{d}}{\mathrm{d}a'}\left(\frac{U^0(a')}{k_{\mathrm{B}}T}\right) \mathrm{d}a' && (2.53)\\
&= \frac{U^0(a_0)}{k_{\mathrm{B}}T} + \int_{a_0}^{a} \mu^{\mathrm{r}}(a')\, \frac{\mathrm{d}}{\mathrm{d}a'}\left(\frac{\kappa^2 \rho_{\mathrm{s}}^{\ell 0}}{4k_{\mathrm{B}}T} a' \left\{\ln(a'/a_{\mathrm{c}}) + C\right\}\right) \mathrm{d}a' && (2.54)\\
&\approx \frac{U(a_0)}{k_{\mathrm{B}}T} + \int_{a_0}^{a} \left(\frac{\rho_{\mathrm{s}}^{\mathrm{r}}(a')}{\rho_{\mathrm{s}}^{\ell 0}}\right) \frac{\kappa^2 \rho_{\mathrm{s}}^{\ell 0}}{4k_{\mathrm{B}}T} \left[\left\{\ln\left(a'/a_{\mathrm{c}}\right) + C\right\} + 1\right] \mathrm{d}a' && (2.55)\\
&= \frac{U(a_0)}{k_{\mathrm{B}}T} + \int_{a_0}^{a} \pi^2 \frac{a' \kappa^2 \rho_{\mathrm{s}}^{\mathrm{r}}(a')}{(2\pi)^2 k_{\mathrm{B}}T} \left\{\ln\left(a'/a'_{\mathrm{c}}\right) + 1\right\} \frac{\mathrm{d}a'}{a'} && (2.56)\\
&= \frac{U(a_0)}{k_{\mathrm{B}}T} + \pi^2 \int_{a_0}^{a} K(a') \left\{1 - \theta \ln\left[K(a')\right]\right\} \frac{\mathrm{d}a'}{a'}. && (2.57)
\end{aligned}$$

In terms of ℓ, this is the same result as Eq. (2.48), and so we obtain the same scaling relation:

$$\frac{\partial y_{\mathrm{eq}}}{\partial \ell} = y_{\mathrm{eq}} \left\{6 - \pi^2 K \left(1 - \theta \ln K\right)\right\}. \tag{2.58}$$

2.1.3.2 renormalized induced-flow equation (leading to K equation)

We'll use two methods to derive an equation dealing with the pure superfluid density (and the induced flow). The first method makes no special additional assumptions. The second method is inspired by the Kosterlitz-Thouless approach and uses a redefined impulse $p = ka^2$ with $k = (\pi/4)\kappa\rho_{\mathrm{s}}^{\ell 0}$, but must thus utilize a poor assumption that $\rho_{\mathrm{s}}^{\mathrm{r}}/\rho_{\mathrm{s}}^{\ell 0} \approx 1$, which is definitely false near T_λ but is approximately true in the 2D case near the critical temperature. This second method is included for comparison and for evidence that the proper expression for the impulse is $p = ka^2$ with $k = (\pi/4)\kappa\rho_{\mathrm{s}}^{\mathrm{r}}$.

In both methods we construct an integral expression for the induced flow $\mathbf{j}^{\mathrm{i}}$ (momentum per volume) due to the vortex loops, and thus find the susceptibility χ and use the relation $\mu = 1 + \chi$. In the absence of an applied flow, the loops' flows cancel out. Since there is an infinitesimal applied flow, a net opposing flow is induced, but the flows still cancel out in all directions perpendicular to the applied flow. So we add up (integrate), over all vortex-loop diameter sizes a, the loops' induced flow in the direction of the applied flow.

Method 1 – Keeping $k = (\pi/4)\kappa\rho_{\mathrm{s}}^{\mathrm{r}}$:

$$\begin{aligned}
\mathbf{j}^{\mathrm{i}} &= \text{(induced momentum per volume due to vortex loops)} && (2.59)\\
&= \int_{a_0}^{\infty} \text{(momentum due to a loop, component in applied-flow direction)} \\
&\qquad\quad \times (\text{\# of loop centers per volume per diameter-volume})\, \mathrm{d}^3 a && (2.60)\\
&= \int_{a_0}^{\infty} \left(p_{\|}(\mathbf{a})\, \hat{\mathbf{j}}^{T0} \right) \Gamma_{\mathrm{eq}}(\mathbf{a})\, \mathrm{d}^3 a && (2.61)\\
&= \int_{a_0}^{\infty} \left(p_{\|}(\mathbf{a})\, \hat{\mathbf{j}}^{T0} \right) \frac{A}{a_0^6} \exp\!\left[-E(\mathbf{a})/k_{\mathrm{B}}T\right] \mathrm{d}^3 a && (2.62)\\
&= \frac{A\hat{\mathbf{j}}^{T0}}{a_0^6} \int_{a_0}^{\infty} p_{\|}(\mathbf{a}) \, \exp\!\Big[-\big\{U(a) + \mathbf{p}(\mathbf{a}) \cdot \mathbf{v}_{\mathrm{s}}\big\}/k_{\mathrm{B}}T\Big]\, \mathrm{d}^3 a && (2.63)\\
&= \frac{A\hat{\mathbf{j}}^{T0}}{a_0^6} \int_{a_0}^{\infty} \int_0^{\pi} \int_0^{2\pi} \left(-p(a)\, \cos\vartheta\right) \exp\!\left[-U(a)/k_{\mathrm{B}}T\right] \\
&\qquad\qquad \times \exp\!\left[p(a)\, v_{\mathrm{s}} \cos\vartheta / k_{\mathrm{B}}T\right] a^2 \sin\vartheta \, \mathrm{d}\phi\, \mathrm{d}\vartheta\, \mathrm{d}a && (2.64)
\end{aligned}$$

$$\begin{aligned}
&\approx \frac{A2\pi\hat{\mathbf{j}}^{T0}}{a_0^6}\int_{a_0}^{\infty}\int_0^{\pi}\left(-p(a)\,\cos\vartheta\right)\exp\left[-U(a)/k_{\mathrm{B}}T\right] \\
&\qquad\qquad \times\left[1+p(a)\,v_{\mathrm{s}}\cos\vartheta/k_{\mathrm{B}}T\right]a^2\sin\vartheta\,\mathrm{d}\vartheta\,\mathrm{d}a && (2.65) \\
&= -\frac{A2\pi\hat{\mathbf{j}}^{T0}v_{\mathrm{s}}}{a_0^6k_{\mathrm{B}}T}\int_0^{\pi}\cos^2\vartheta\,\sin\vartheta\,\mathrm{d}\vartheta\int_{a_0}^{\infty}\left[p(a)\right]^2\exp\left[-U(a)/k_{\mathrm{B}}T\right]a^2\mathrm{d}a && (2.66) \\
&= -\frac{A2\pi\hat{\mathbf{j}}^{T0}(j^{T0}/\rho)}{a_0^6k_{\mathrm{B}}T}\left(\frac{2}{3}\right)\int_{a_0}^{\infty}\left[\frac{\pi}{4}\kappa\rho_{\mathrm{s}}^{\mathrm{r}}a^2\right]^2\exp\left[-U(a)/k_{\mathrm{B}}T\right]a^2\mathrm{d}a && (2.67) \\
&= -\mathbf{j}^{T0}\left(\frac{2}{3}\right)\frac{A2\pi}{a_0^6}\frac{(1/\rho_{\mathrm{s}}^{\ell 0})}{k_{\mathrm{B}}T}\int_{a_0}^{\infty}\left(\frac{\pi}{4}\right)^2\left(\frac{(2\pi)^4(k_{\mathrm{B}}T)^2}{\kappa^2}\right)\left(\frac{a\kappa^2\rho_{\mathrm{s}}^{\mathrm{r}}}{(2\pi)^2k_{\mathrm{B}}T}\right)^2 \\
&\qquad\qquad \times a^5\exp\left[-U(a)/k_{\mathrm{B}}T\right]\frac{\mathrm{d}a}{a} && (2.68) \\
&= -\mathbf{j}^{T0}\left(\frac{2}{3}\right)\frac{A2\pi^3}{4^2}(2\pi)^2\left(\frac{(2\pi)^2k_{\mathrm{B}}T}{a_0\kappa^2\rho_{\mathrm{s}}^{\ell 0}}\right)\int_{a_0}^{\infty}K^2\left(\frac{a}{a_0}\right)^5\exp\left[-\frac{U(a)}{k_{\mathrm{B}}T}\right]\frac{\mathrm{d}a}{a} && (2.69) \\
&\approx -\mathbf{j}^{T0}\frac{A\pi^5}{3}\frac{1}{K^{\ell 0}}\int_{a_0}^{\infty}\left(\frac{a}{a_0}\right)^{-1}K^2y_{\mathrm{eq}}\frac{\mathrm{d}a}{a} && (2.70) \\
&= -\mathbf{j}^{T0}\frac{A\pi^5}{3}\frac{1}{K^{\ell 0}}\int_0^{\infty}\exp(-\ell)\,K^2y_{\mathrm{eq}}\,\mathrm{d}\ell && (2.71) \\
&= \chi_{\mathrm{eq}}\mathbf{j}^{T0}. && (2.72)
\end{aligned}$$

Note that since $\Gamma_{\mathrm{eq}} \approx (A/a_0^6)\exp[-U(a)/k_{\mathrm{B}}T]$, Expressions (2.66) and (2.67) can be considered as integrals of the loop polarizability (proportional to $p^2 \propto a^4$) times the number density, to obtain the susceptibility. Now we use the renormalized version of $\mu = 1 + \chi$:

$$\begin{aligned}
\mu^{\mathrm{r}}(\ell) &= 1+\chi^{\mathrm{r}}(\ell) && (2.73) \\
\frac{\rho_{\mathrm{s}}^{\mathrm{r}}(\ell)}{\rho} &= 1-\frac{1}{K^{\ell 0}}\frac{A\pi^5}{3}\int_0^{\ell}\exp(-\ell')\,K^2y_{\mathrm{eq}}\,\mathrm{d}\ell' && (2.74) \\
\frac{K_{\mathrm{s}}}{K^{\ell 0}} &= 1-\frac{1}{K^{\ell 0}}\frac{A\pi^5}{3}\int_0^{\ell}\exp(-\ell')\,K^2y_{\mathrm{eq}}\,\mathrm{d}\ell' && (2.75) \\
K_{\mathrm{s}} &= K^{\ell 0}-\frac{A\pi^5}{3}\int_0^{\ell}\exp(-\ell')\,K^2y_{\mathrm{eq}}\,\mathrm{d}\ell' && (2.76) \\
\frac{\partial K_{\mathrm{s}}}{\partial\ell} &= -\frac{A\pi^5}{3}\exp(-\ell)\,K^2y_{\mathrm{eq}}. && (2.77)
\end{aligned}$$

Reworking this in terms of K gives us another scaling relation:

$$\begin{aligned}
\frac{\partial K}{\partial \ell} &= \frac{\partial}{\partial \ell}\big(\exp(\ell)\, K_{\mathrm{s}}\big) && (2.78)\\
&= \exp(\ell)\, K_{\mathrm{s}} + \exp(\ell)\, \frac{\partial K_{\mathrm{s}}}{\partial \ell} && (2.79)\\
&= K + \exp(\ell)\left(-\frac{2\pi^5}{3}\exp(-\ell)\, K^2 y_{\mathrm{eq}}\right) && (2.80)\\
&= K - \frac{A\pi^5}{3} K^2 y_{\mathrm{eq}}. && (2.81)
\end{aligned}$$

To match Shenoy's rigorous result [78], we must set $A = 4/\pi^2$ to end up with

$$\frac{\partial K}{\partial \ell} = K - \frac{4\pi^3}{3} K^2 y_{\mathrm{eq}}. \qquad (2.82)$$

Method 2 – Redefining $k = (\pi/4)\kappa\rho_{\mathrm{s}}^{\ell 0}$, and making the bad assumption that $\rho_{\mathrm{s}}^{\mathrm{r}}/\rho_{\mathrm{s}}^{\ell 0} \approx 1$ (and jumping ahead in the derivation to where this method diverges from the previous method):

$$\begin{aligned}
\mathbf{j}^{\mathrm{i}} &\approx -\frac{A 2\pi \hat{\mathbf{j}}^{T0} v_{\mathrm{s}}}{a_0^6 k_{\mathrm{B}} T} \int_0^{\pi} \cos^2\vartheta \, \sin\vartheta \, \mathrm{d}\vartheta \int_{a_0}^{\infty} \big[p(a)\big]^2 \exp\!\big[-U(a)/k_{\mathrm{B}}T\big]\, a^2 \mathrm{d}a && (2.83)\\
&= -\frac{A 2\pi \hat{\mathbf{j}}^{T0} (j^{T0}/\rho)}{a_0^6 k_{\mathrm{B}} T} \left(\frac{2}{3}\right) \int_{a_0}^{\infty} \left[\frac{\pi}{4}\kappa\rho_{\mathrm{s}}^{\ell 0} a^2\right]^2 \exp\!\big[-U(a)/k_{\mathrm{B}}T\big]\, a^2 \mathrm{d}a && (2.84)\\
&= -\mathbf{j}^{T0}\left(\frac{2}{3}\right)\frac{A 2\pi^3}{4^2 a_0^6}\frac{\kappa^2 \rho_{\mathrm{s}}^{\ell 0}}{k_{\mathrm{B}} T} \int_{a_0}^{\infty} a^4 \exp\!\big[-U(a)/k_{\mathrm{B}}T\big]\, a^2 \mathrm{d}a && (2.85)\\
&= -\mathbf{j}^{T0}\left(\frac{2}{3}\right)\frac{A 2\pi^3}{4^2 a_0^6}\frac{(h/m)^2 \rho_{\mathrm{s}}^{\ell 0}}{k_{\mathrm{B}} T} \int_{a_0}^{\infty} a^6 \exp\!\big[-U(a)/k_{\mathrm{B}}T\big]\, \mathrm{d}a && (2.86)\\
&= -\mathbf{j}^{T0}\left(\frac{2}{3}\right)\frac{A 2\pi^3}{4^2}(2\pi)^2\frac{a_0(\hbar/m)^2 \rho_{\mathrm{s}}^{\ell 0}}{k_{\mathrm{B}} T} \int_{a_0}^{\infty} \left(\frac{a}{a_0}\right)^6 \exp\!\big[-U(a)/k_{\mathrm{B}}T\big]\, \frac{\mathrm{d}a}{a_0} && (2.87)\\
&= -\mathbf{j}^{T0}\frac{A\pi^5}{3}K^{\ell 0} \int_{a_0}^{\infty} \left(\frac{a}{a_0}\right)^6 \exp\!\big[-U(a)/k_{\mathrm{B}}T\big]\, \frac{\mathrm{d}a}{a_0} && (2.88)\\
&\approx -\mathbf{j}^{T0}\frac{A\pi^5}{3}K^{\ell 0} \int_{a_0}^{\infty} y_{\mathrm{eq}}\, \frac{\mathrm{d}a}{a_0} && (2.89)\\
&= -\mathbf{j}^{T0}\frac{A\pi^5}{3}K^{\ell 0} \int_{a_0}^{\infty} \left(\frac{a}{a_0}\right) y_{\mathrm{eq}}\, \frac{\mathrm{d}a}{a} && (2.90)\\
&= -\mathbf{j}^{T0}\frac{A\pi^5}{3}K^{\ell 0} \int_{0}^{\infty} \exp(\ell)\, y_{\mathrm{eq}}\, \mathrm{d}\ell && (2.91)
\end{aligned}$$

$$= \quad \chi_{\mathrm{eq}}\,\mathbf{j}^{T0}. \tag{2.92}$$

With the incorrect assumption that $\rho_{\mathrm{s}}^{\mathrm{r}}/\rho_{\mathrm{s}}^{\ell 0} \approx 1$, meaning that χ is very small, we get

$$\begin{aligned}
\mu^{\mathrm{r}}(\ell) &= 1 + \chi^{\mathrm{r}}(\ell) && (2.93)\\
\frac{\rho_{\mathrm{s}}^{\mathrm{r}}(\ell)}{\rho_{\mathrm{s}}^{\ell 0}} &= 1 - \frac{A\pi^5}{3} K^{\ell 0} \int_0^{\ell} \exp(\ell')\, y_{\mathrm{eq}}\, \mathrm{d}\ell' && (2.94)\\
\frac{\rho_{\mathrm{s}}^{\ell 0}}{\rho_{\mathrm{s}}^{\mathrm{r}}(\ell)} &\approx 1 + \frac{A\pi^5}{3} K^{\ell 0} \int_0^{\ell} \exp(\ell')\, y_{\mathrm{eq}}\, \mathrm{d}\ell' && (2.95)\\
\frac{K_{\mathrm{s}}^{\ell 0}}{K_{\mathrm{s}}(\ell)} &\approx 1 + \frac{A\pi^5}{3} K^{\ell 0} \int_0^{\ell} \exp(\ell')\, y_{\mathrm{eq}}\, \mathrm{d}\ell' && (2.96)\\
\frac{1}{K_{\mathrm{s}}(\ell)} &\approx \frac{1}{K^{\ell 0}} + \frac{A\pi^5}{3} \int_0^{\ell} \exp(\ell')\, y_{\mathrm{eq}}\, \mathrm{d}\ell' && (2.97)\\
\frac{\partial\big((K_{\mathrm{s}})^{-1}\big)}{\partial \ell} &\approx \frac{A\pi^5}{3} \exp(\ell)\, y_{\mathrm{eq}}. && (2.98)
\end{aligned}$$

Rewriting in terms of K gives us

$$\begin{aligned}
\frac{\partial(K^{-1})}{\partial \ell} &= \frac{\partial}{\partial \ell}\big(\exp(-\ell)\,(K_{\mathrm{s}})^{-1}\big) \quad = \quad -K^{-1} + \exp(-\ell)\,\frac{\partial\big((K_{\mathrm{s}})^{-1}\big)}{\partial \ell} && (2.99)\\
&\approx -K^{-1} + \exp(-\ell)\frac{A\pi^5}{3}\exp(\ell)\, y && (2.100)\\
&= -K^{-1} + \frac{A\pi^5}{3} y && (2.101)\\
&= -K^{-2}\,\frac{\partial K}{\partial \ell} && (2.102)\\
\frac{\partial K}{\partial \ell} &= K - \frac{A\pi^5}{3} K^2 y, && (2.103)
\end{aligned}$$

which again yields the same result obtained by Shenoy [78] if $A = 4/\pi^2$.

Note that using method 1, one can derive both of the following equations,

$$\begin{aligned}
K_{\mathrm{s}} &= K_{\mathrm{s}}^{\ell 0} - \frac{4\pi^3}{3} \int_0^{\ell} \exp(-\ell')\, K^2 y_{\mathrm{eq}}\, \mathrm{d}\ell' && (2.104)\\
(K_{\mathrm{s}})^{-1} &= (K_{\mathrm{s}}^{\ell 0})^{-1} + \frac{4\pi^3}{3} \int_0^{\ell} \exp(\ell')\, y_{\mathrm{eq}}\, \mathrm{d}\ell', && (2.105)
\end{aligned}$$

but this does not imply that $\rho_{\mathrm{s}}^{\mathrm{r}}/\rho_{\mathrm{s}}^{\ell 0} \approx 1$ since the integrals are different. In contrast, method 2 implies the following equation (that we'll write as an inequality):

$$K_{\rm s} \quad \neq \quad K_{\rm s}^{\ell 0} - \frac{4\pi^3}{3}(K_{\rm s}^{\ell 0})^2 \int_0^{\ell} \exp(\ell')\, y_{\rm eq}\, {\rm d}\ell'. \tag{2.106}$$

2.1.3.3 renormalized free-energy equation (leading to e equation)

This final derivation will be the most qualitative of the derivations. We will use a very crude analogy with the Helmholtz free energy of a gas to discuss the Helmholtz free energy F of the liquid due to the vortex loops, and the assumptions that must be made to match Shenoy's result will perhaps reveal some qualitative information for the reader. Supposing a system at constant temperature and volume, we'll build up the system by integrating up from the smallest scale. We'll use the differential relation

$${\rm d}F \quad = \quad -S\,\cancelto{0}{{\rm d}T} - P\,\cancelto{0}{{\rm d}V} + \mu_{\rm ch}{\rm d}N, \tag{2.107}$$

where S is the entropy of the loops, P is the pressure of the fluid[9], and $\mu_{\rm ch}$ is the chemical potential of the loops. Without including the effects of phonons and other excitations besides the loops, we start with zero free energy at the smallest scales ($F^{\ell 0} = 0$) and find

$$\begin{aligned} F \quad &= \quad F^{\ell 0} + \int \mu_{\rm ch}{\rm d}N & (2.108)\\ &= \quad \mu_{\rm ch}\int {\rm d}N & (2.109)\\ &= \quad \mu_{\rm ch}V\int \Gamma\, {\rm d}^3 a, & (2.110)\end{aligned}$$

---

[9] The thought crossed our minds of considering this to be the pressure of the vortex loops in the gas of excitations, but then our results in Chapter 3 suggest that this should be the fluid pressure.

where we've assumed constant chemical potential. Now let's switch to the convenient parameter $e \equiv (F/k_\mathrm{B}T)(a_0^3/V)$ and examine the equilibrium conditions:

$$\begin{aligned}
e_\mathrm{eq} &= a_0^3 \frac{\mu_\mathrm{ch}}{k_\mathrm{B}T} \int \Gamma_\mathrm{eq}\, \mathrm{d}^3 a && (2.111)\\
&\approx a_0^3 \frac{\mu_\mathrm{ch}}{k_\mathrm{B}T} \int \frac{A}{a_0^6} \exp\bigl[-U(a)/k_\mathrm{B}T\bigr]\; \mathrm{d}^3 a && (2.112)\\
&= \frac{A}{a_0^3} \left(\frac{\mu_\mathrm{ch}}{k_\mathrm{B}T}\right) \int_{a_0}^{\infty} \int \exp\bigl[-U(a)/k_\mathrm{B}T\bigr]\, a^2 \mathrm{d}\Omega\, \mathrm{d}a && (2.113)\\
&= 4\pi A \left(\frac{\mu_\mathrm{ch}}{k_\mathrm{B}T}\right) \int_{a_0}^{\infty} \left(\frac{a}{a_0}\right)^3 \exp\bigl[-U(a)/k_\mathrm{B}T\bigr] \frac{\mathrm{d}a}{a} && (2.114)\\
&= 4\pi A \left(\frac{\mu_\mathrm{ch}}{k_\mathrm{B}T}\right) \int_{a_0}^{\infty} \left(\frac{a}{a_0}\right)^{-3} y_\mathrm{eq} \frac{\mathrm{d}a}{a} && (2.115)\\
&= 4\pi A \left(\frac{\mu_\mathrm{ch}}{k_\mathrm{B}T}\right) \int_{0}^{\infty} \exp(-3\ell)\, y_\mathrm{eq}\, \mathrm{d}\ell. && (2.116)
\end{aligned}$$

Again, to reproduce the results of Shenoy's rigorous derivations [78], we require that $\mu_\mathrm{ch}/k_\mathrm{B}T = -(\pi/4)^2$ as well as $A = 4/\pi^2$:

$$\begin{aligned}
e_\mathrm{eq} &= -4\pi \left(\frac{4}{\pi^2}\right)\left(\frac{\pi}{4}\right)^2 \int_0^\infty \exp(-3\ell)\, y_\mathrm{eq}\, \mathrm{d}\ell && (2.117)\\
&= -\pi \int_0^\infty \exp(-3\ell)\, y_\mathrm{eq}\, \mathrm{d}\ell && (2.118)\\
\frac{\partial e_\mathrm{eq}}{\partial \ell} &= -\pi \exp(-3\ell)\, y_\mathrm{eq}. && (2.119)
\end{aligned}$$

2.1.4 3D Equations Summary

The dimensionless scaling equations derived in the preceding section are summarized below. Here too are the integral form of these equations, using the dimensionful quantities, including a couple equivalent arrangements for two of the equations:

$$\begin{aligned}
\frac{U(a)}{k_{\mathrm{B}}T} &= \frac{U(a_0)}{k_{\mathrm{B}}T} + \int_{a_0}^{a} \frac{1}{4}\frac{\kappa^2 \rho_{\mathrm{s}}^{\mathrm{r}}(a')}{k_{\mathrm{B}}T} \left\{ \ln\left[\frac{a'}{a_{\mathrm{c}}(a')}\right] + C + 1 \right\} \mathrm{d}a' && \text{(2.120a)} \\
&= \frac{U(a_0)}{k_{\mathrm{B}}T} + \pi^2 \int_{a_0}^{a} \frac{a_0 \kappa^2 \rho_{\mathrm{s}}^{\mathrm{r}}(a')}{(2\pi)^2 k_{\mathrm{B}}T} \left\{ 1 - \theta \ln\left[\frac{a' \kappa^2 \rho_{\mathrm{s}}^{\mathrm{r}}(a')}{(2\pi)^2 k_{\mathrm{B}}T}\right] \right\} \frac{\mathrm{d}a'}{a_0} && \text{(2.120b)}
\end{aligned}$$

$$\begin{aligned}
\rho_{\mathrm{s}}^{\mathrm{r}}(a) &= \rho_{\mathrm{s}}^{\mathrm{r}}(a_0) - \frac{4\pi^3}{3} \int_{a_0}^{a} \frac{a_0 (\hbar/m)^2}{k_{\mathrm{B}}T} \left(\frac{\rho_{\mathrm{s}}^{\mathrm{r}}(a')\, a'^2}{a_0^2} \right)^2 \exp\left[-\frac{U(a')}{k_{\mathrm{B}}T}\right] \left(\frac{a'}{a_0}\right)^2 \frac{\mathrm{d}a'}{a_0} && \text{(2.121a)} \\
\frac{1}{\rho_{\mathrm{s}}^{\mathrm{r}}(a)} &= \frac{1}{\rho_{\mathrm{s}}^{\mathrm{r}}(a_0)} + \frac{4\pi^3}{3} \int_{a_0}^{a} \frac{a_0 (\hbar/m)^2}{k_{\mathrm{B}}T} \left(\frac{a'}{a_0}\right)^4 \exp\left[-\frac{U(a')}{k_{\mathrm{B}}T}\right] \left(\frac{a'}{a_0}\right)^2 \frac{\mathrm{d}a'}{a_0} && \text{(2.121b)}
\end{aligned}$$

$$\frac{f(a)}{k_{\mathrm{B}}T} = -\frac{\pi}{a_0^3} \int_{a_0}^{a} \exp\left[-\frac{U(a')}{k_{\mathrm{B}}T}\right] \left(\frac{a'}{a_0}\right)^2 \frac{\mathrm{d}a'}{a_0}, \qquad \text{(2.122)}$$

where $f = F/V$ is the Helmholtz free energy per volume of the fluid due to the vortex loops, $\rho_{\mathrm{s}}^{\mathrm{r}}(a_0) = \rho_{\mathrm{s}}^{\ell 0} = \rho$, and $U(a_0)/k_{\mathrm{B}}T = a_0 \kappa^2 \rho C / 4 k_{\mathrm{B}}T$, since $U(a_0)/k_{\mathrm{B}}T = \pi^2 K^{\ell 0} C$ and $K^{\ell 0} = a_0 (\hbar/m)^2 \rho_{\mathrm{s}}^{\ell 0}/k_{\mathrm{B}}T$. Note that the only parameters that these equations depend on (other than the variables a and T), are ρ, which is an experimentally known function of temperature and pressure, and a_0 and C.

The dimensionless scaling equations, in derivative form, along with the bare boundary values are summarized in Table 2.4. To solve these equations the bare values are needed: $y_{\mathrm{eq}}^{\ell 0} \approx \exp(-\pi^2 K^{\ell 0} C) = \exp(-a_0 \kappa^2 \rho C / 4 k_{\mathrm{B}}T)$, $K_{\mathrm{eq}}^{\ell 0} = a_0 (\hbar/m)^2 \rho_{\mathrm{s}}^{\ell 0}/k_{\mathrm{B}}T = a_0 (\hbar/m)^2 \rho / k_{\mathrm{B}}T$, and $e_{\mathrm{eq}}^{\ell 0} = 0$. Note again these equations depend on the parameters ρ, a_0 and C.

3D Equilibrium Equations in terms of y, K, e	
Interdependent Relations	Bare $\ell = 0$ ("$\ell 0$") Values
$\dfrac{\partial y}{\partial \ell} = y\left\{6 - \pi^2 K\left(1 - \theta \ln K\right)\right\}$	$y(0) = \exp\bigl(-\pi^2 K^{\ell 0} C\bigr) = \exp\left(-\dfrac{\kappa^2}{4}\dfrac{a_0 \rho\, C}{k_{\mathrm{B}} T}\right)$
$\dfrac{\partial K}{\partial \ell} = K - \dfrac{4\pi^3}{3} K^2 y$	$K(0) = \left(\dfrac{\kappa}{2\pi}\right)^2 \dfrac{a_0 \rho}{k_{\mathrm{B}} T}$
$\dfrac{\partial e}{\partial \ell} = -\pi \exp(-3\ell)\, y$	$e(0) = 0$

Table 2.4: This summarizes the 3D equilibrium scaling equations, with small-scale bare boundary values. For aesthetic purposes, the "eq" subscripts are not written. See the main text below for an important caveat.

We should note that for temperatures below T_λ there comes a point in the progression from $\ell = 0$ to larger ℓ when the approximation for a_{c} ($\sim aK^\theta$) exceeds the value of a, namely, when $K \gtrsim 1$. When that point is reached, one can set $a_{\mathrm{c}} = a$ from there onward, and this gets rid of the logarithmic term in the scaling relations, so that one is left with

$$\frac{\partial y}{\partial \ell} = y\left\{6 - \pi^2 K\right\}. \tag{2.123}$$

An alternative method to cope with this situation is to cut off the calculation at a certain threshold value of K before the formula for a_{c} becomes large enough to significantly affect the results. These two methods are numerically equivalent, since the cut-off is made well beyond the correlation length, under which the important under which the important physics takes place. These issues are discussed and illustrated in Appendix B.

2.1.5 Theoretical Plots

We can now present plots produced using the scaling equations in Table 2.4, equations that we noted above depend on the parameters a_0, C, and ρ. We will discuss in Chapter 3 how we can use experimental data to deduce the pressure- (and to some extent the temperature-) dependence of a_0 and C. For now, assume we're dealing with a particular pressure, say $P = 0.05$ bar, and for each temperature there is associated a particular a_0 and C, as well as ρ, which we know as a function of temperature and pressure from Brooks and Donnelly [71]. Thus at this pressure and for every temperature we can calculate all of the bare values of y, K, and e and use the scaling equations to integrate up to any length scale ℓ_{max} we choose. The process of integrating up in length scale can be accomplished by computer program with numerical methods such as Runge-Kutta (we use a fourth-order Runge-Kutta algorithm with step-size $\Delta\ell = 10^{-4}$). The larger ℓ_{max} is, the greater the size of loops that are included in the calculation to drive down the superfluidity, as is shown in Fig. 2.7. By $\ell_{\text{max}} = 10$ the loops have made their full impact; increasing ℓ_{max} beyond about 10 does not change the results much at all. Figures 2.8 and 2.9 show in detail how the vortex loops increase in number and size with increasing temperature. In the following Fig.s 2.10 through 2.16, the theoretical superfluid-fraction and heat-capacity at various pressures over a range of temperatures are shown and compared with the data that we displayed in Section 2.1.1.

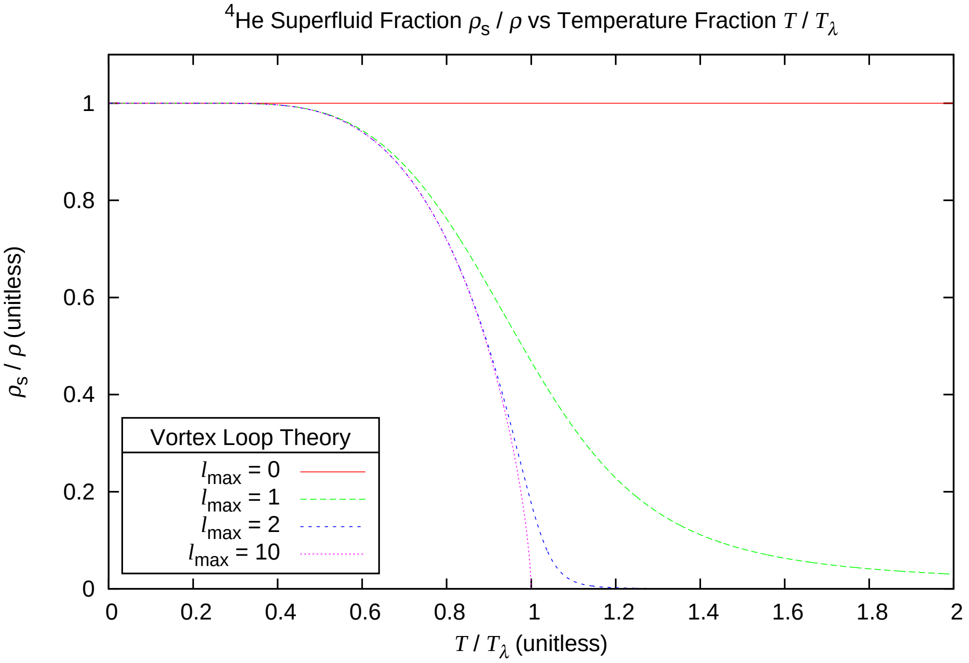

Figure 2.7: The superfluid fraction ρ_s/ρ is driven to zero as temperature increases and vortex loop excitations become more plentiful and larger, on average. At a pressure of $P = 0.05$ bar, and at each temperature, we integrate the scaling equations up in length scale to some $\ell_{\max}$ to calculate the superfluid fraction $\rho_s/\rho = K_s/K^{\ell 0}$. Stringing the points together for a given $\ell_{\max}$, we get the curves above. For $\ell_{\max} = 0$, where no vortex loops are included in the calculation, the superfluid is pure-superfluid at any temperature. For $\ell_{\max} = 1$, which corresponds to including loops of diameter $a = a_0 \exp(1) \approx 6.8$ Å and smaller (since $a_0 \approx 2.5$ Å), a smooth transition from pure-superfluid to normal fluid is seen. At $\ell_{\max} = 2$ ($a_{\max} \approx 1.8$ nm), the transition is much more defined. By $\ell_{\max} = 10$, which corresponds to including loops of diameter $a \approx 5.5$ µm and smaller, the transition is sharp and familiar as the bulk superfluid helium phase transition. Note that this explains why liquid helium near T_λ that is confined in a very small space (on the order of angstroms) will have more pure-superfluid component than a larger sample under the same conditions, and thus leaks through microscopic cracks and holes in a container are to be expected.

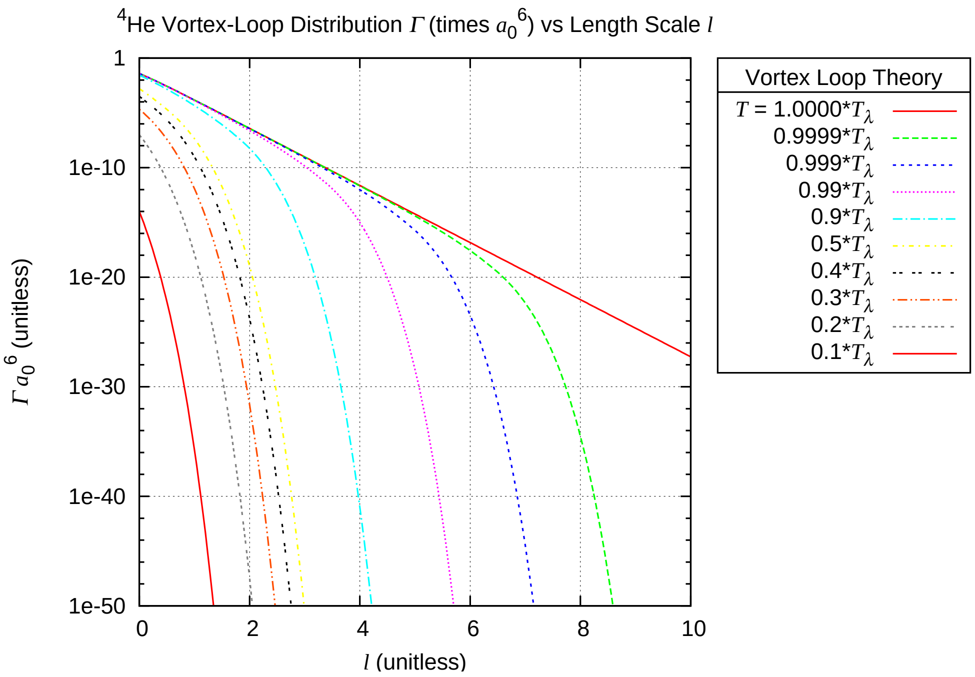

Figure 2.8: As temperature increases, the number of vortex loops at any given length-scale (with corresponding diameter $a = a_0 \exp(\ell)$) increases, with the larger vortex loops multiplying more quickly. As stated in the caption of the previous figure, as temperature increases, the vortex loop excitations become more plentiful and larger, on average. These plots use $\ell_{\text{max}} = 10$.

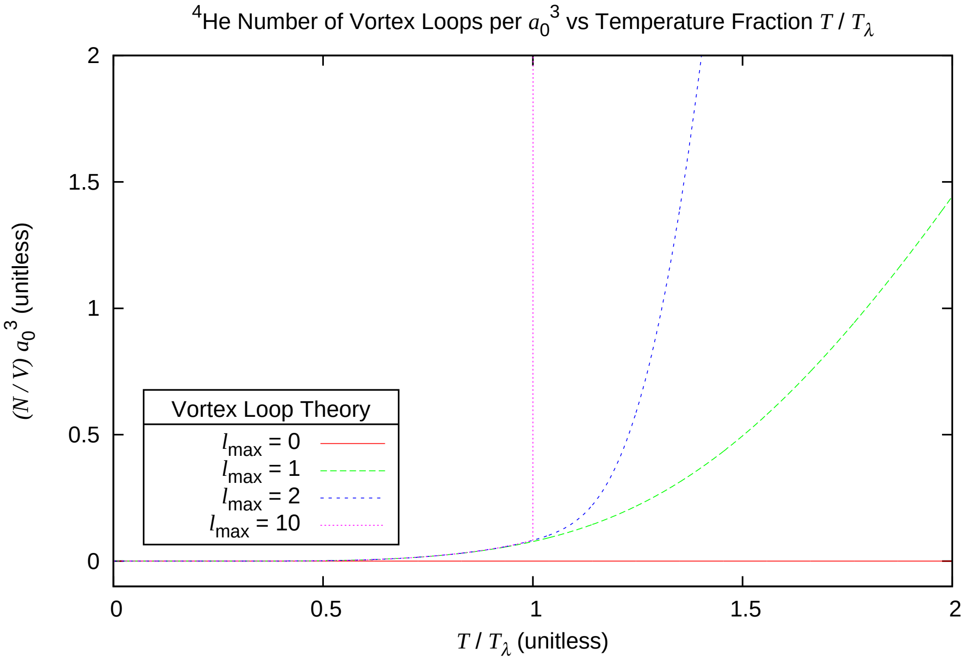

Figure 2.9: To obtain these plots of number density of vortex loops, one can either integrate the loop distribution Γ or multiply the free energy parameter e by a negative factor: $-(4/\pi)^2$. This gives the average number of vortex loops, of any and all diameters, *centered* in a volume a_0^3. In a sharp transition, the number of vortex loops really explodes at the critical temperature T_λ.

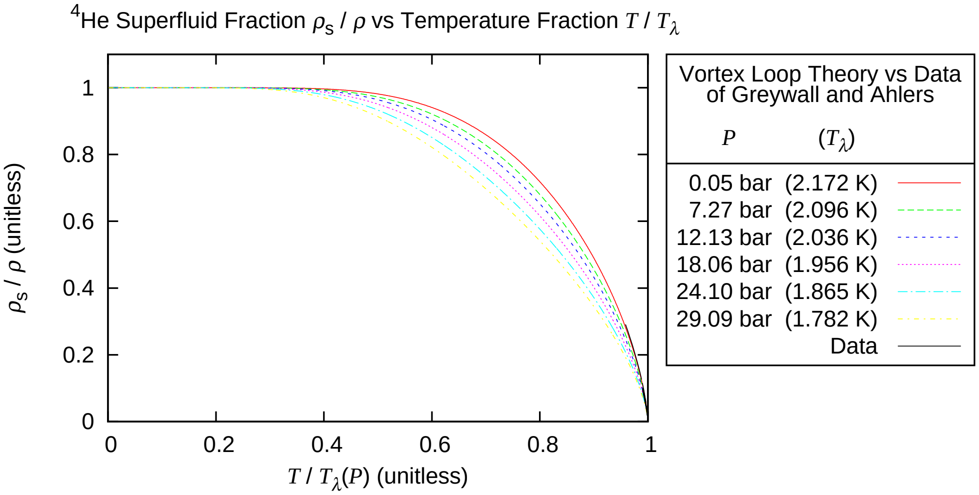

Figure 2.10: This is the first in a series of four figures showing the theoretical superfluid fraction at various pressures (with $\ell_{\max} = 100$). We already showed in Fig.s 2.5 and 2.6 that the superfluid fraction at saturated vapor pressure ($P \lesssim 0.05$ bar) matches the data well over essentially all temperatures but especially near T_λ. Now we will zoom in, over the next three figures, to see how well these six theoretical plots match the data of Greywall and Ahlers [79] near T_λ. In this figure, the data appear as essentially one solid black line in the lower right corner near $T/T_\lambda = 1$.

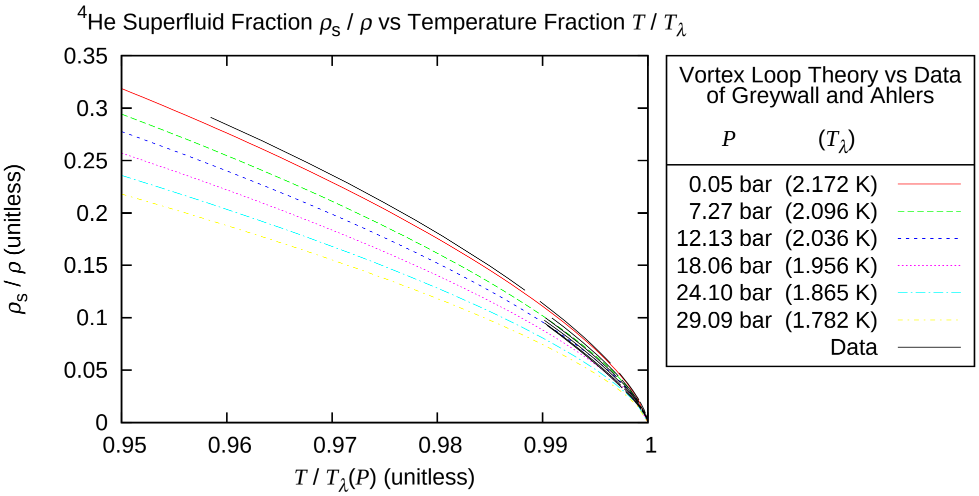

Figure 2.11: This is the second in a series of four figures. Having zoomed in, we can see the data better and can note how the higher pressure curves don't match the data as well as the lower pressure curves. As we zoom in more in the next two figures, we will see that very near T_λ all of the curves match the data quite well.

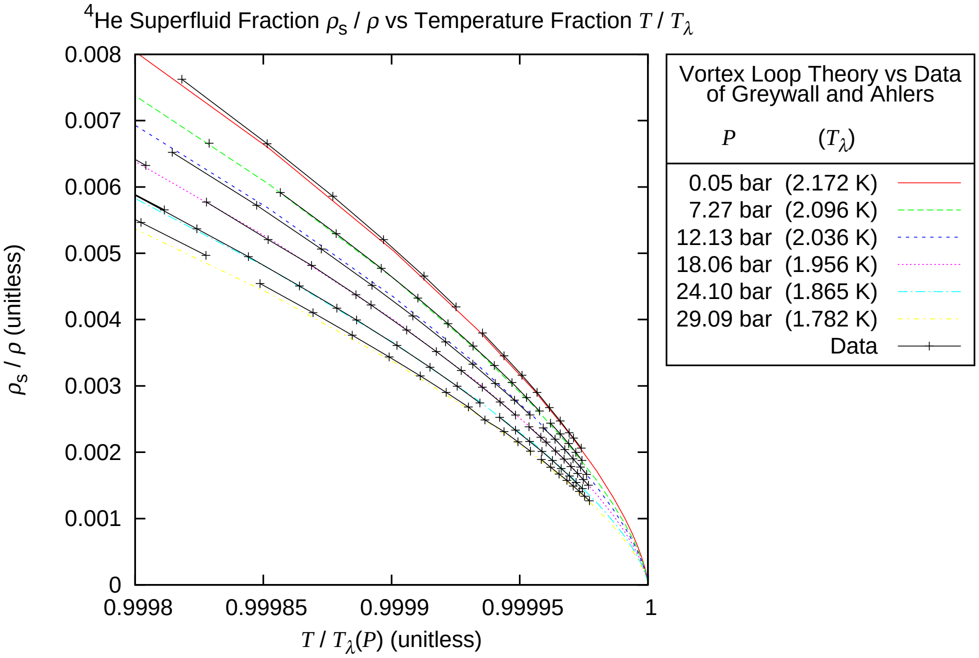

Figure 2.12: This is the third in a series of four figures. Zoomed in to this scale, it becomes feasible to show the individual data points.

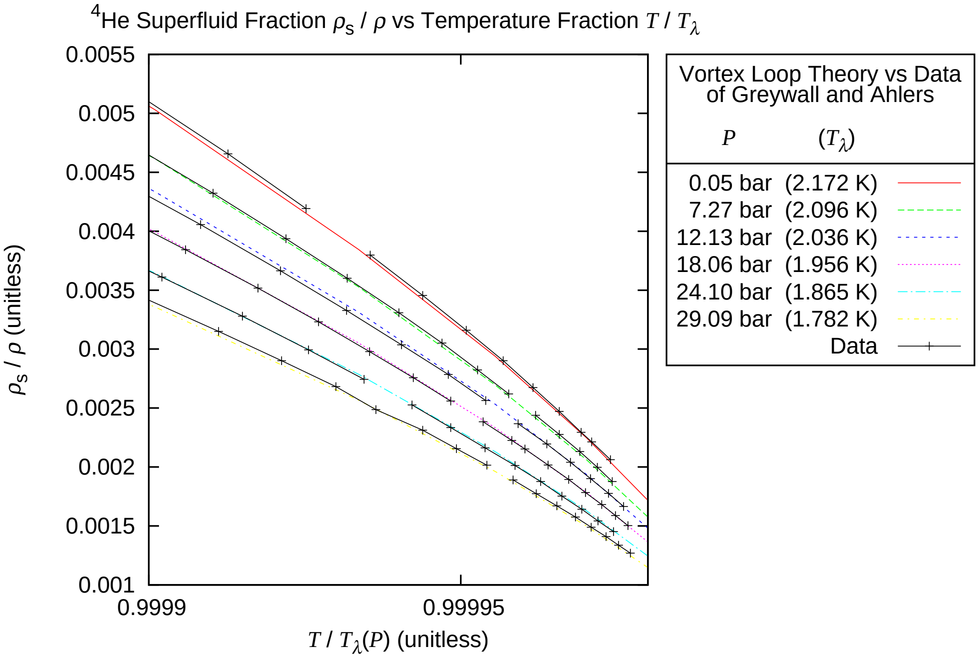

Figure 2.13: This is the fourth in a series of four figures. The theoretical plots match the data well in this range, within about (0.0001)(2 K) = 200 μK of T_λ.

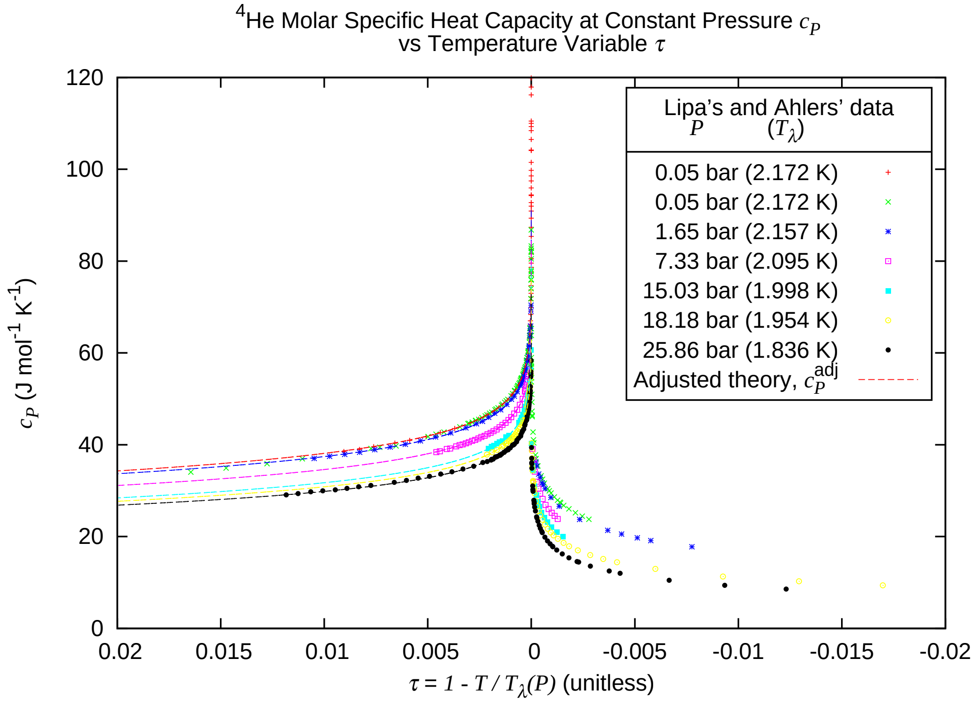

Figure 2.14: This is the first in a series of three figures showing the theoretical constant-pressure molar specific heat capacity at various pressures (with $\ell_{\max} = 100$). Although the overall behavior of the data is clearest in this figure (where we can see the characteristic "lambda" shape shown first in Fig. 2.1), the next two figures will more clearly show how the theoretical plots match the data below and very close to T_λ. (Note here that the horizontal axis, in terms of $\tau = 1 - T/T_\lambda$, is reversed from what one might expect so that lower temperatures are to the left and higher temperatures are to the right. Also note that the theory is "adjusted" and the adjustment is explained in Chapter 3.)

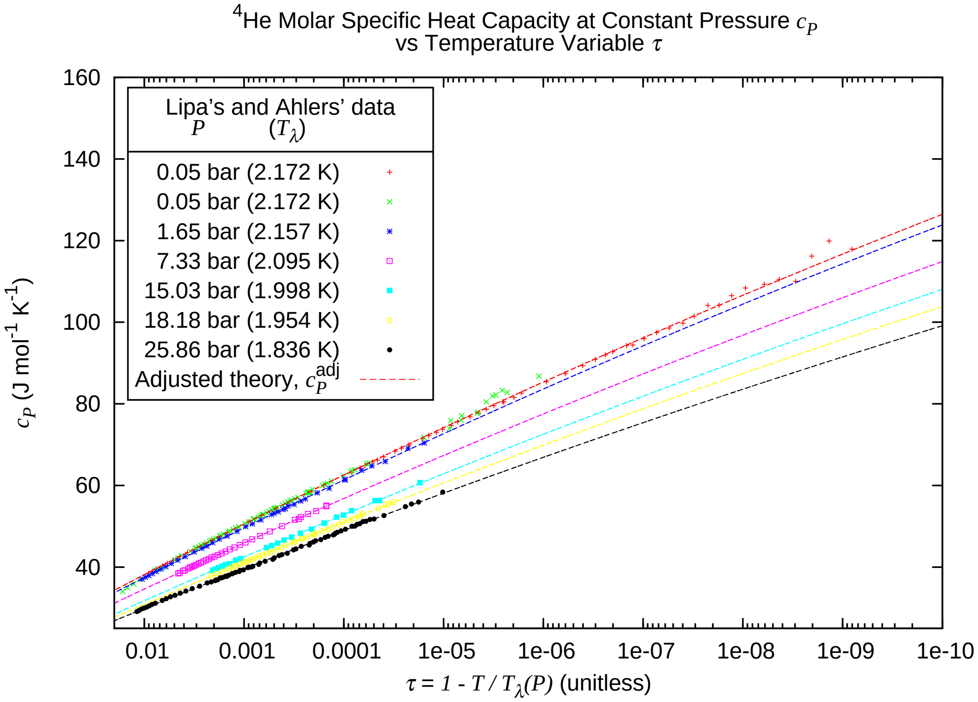

Figure 2.15: This is the second in a series of three figures. It is easier to tell in this image, with the horizontal axis on a logarithmic scale, that the theory accurately reproduces the behavior of the heat capacity for temperatures close to T_λ. (This data was first shown in Fig. 2.2.) Note that the theoretical curves bow slightly downward; in the next figure, we'll see that the curves do indeed reach maximum values at T_λ rather than simply diverging to infinity.

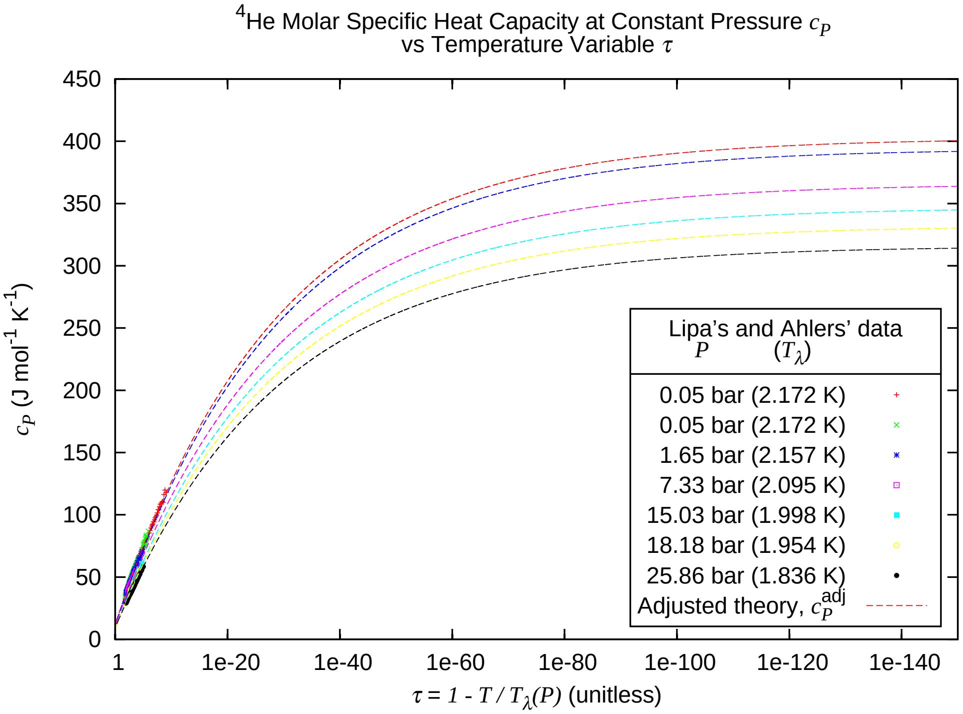

Figure 2.16: This is the third in a series of three figures. Extending the theoretical curves to values extremely close to T_λ (with τ very small), while keeping the horizontal axis on a logarithmic scale, makes it easy to see that the curves reach maximum values (rather than diverging to infinity) at T_λ. The maximum values (which correspond to the experimental critical values, denoted by c_P^{ecr} in Table 3.1) are, from lowest pressure to highest pressure, 400, 394, 366, 347, 332, 310, and 316, with units of J/(K $\cdot$ mol), as indicated on the graph above.

2.2 2D Theory: Superfluid Film

We will now take a very schematic approach in explaining the 2D theory, since we will be using many of the same arguments as were made in the previous section on the 3D theory.

2.2.1 Data to be Explained

Again, let's take a look at some experimental data to know what we'd like the theory to be able to reproduce. We shall focus on the superfluid density (mass per area) σ_s and the superfluid fraction σ_s/σ of a thin film of superfluid (which is composed of a pure superfluid component σ_s and normal fluid component σ_n). In Fig. 2.17 data for five different films of liquid helium-4 are shown, where each film is of a different effective thickness. Further detail is given in the caption, but the main idea is that the vertical axis is proportional to superfluid fraction (where each of the five data sets could be normalized or scaled to have a maximum of $\sigma_\mathrm{s}/\sigma = 1$ at zero absolute temperature), and so we see that the phase transition is similar to the 3D transition (as shown in Fig.s 2.3 and 2.7) except that the transition temperature depends on film thickness (instead of bulk pressure) and the superfluid fraction drops off more quickly at the transition temperature.

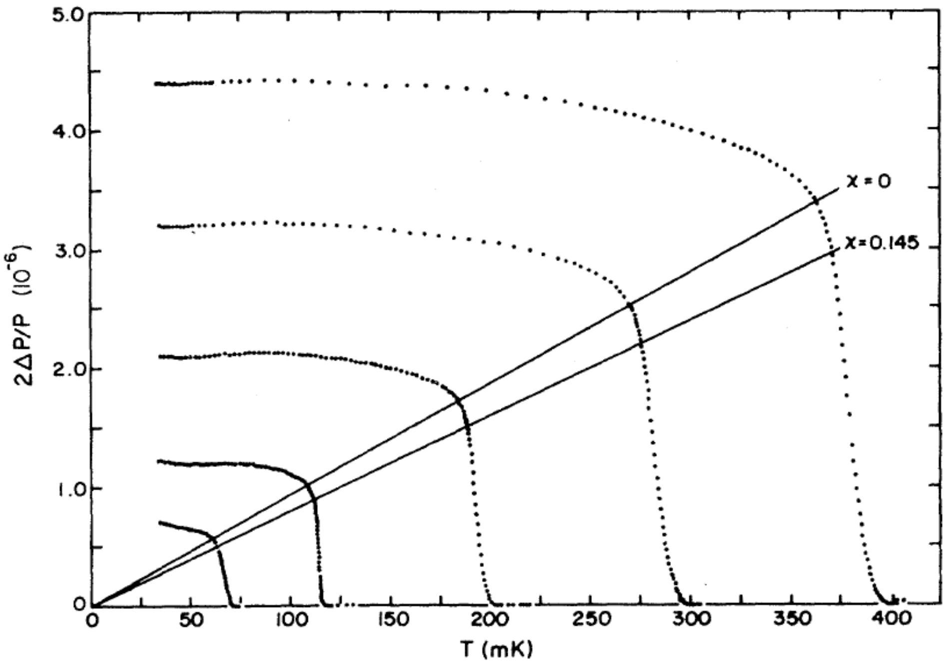

Figure 2.17: These plots relate to the superfluid fraction of 2D systems of superfluid helium, as explained here. The data, from Agnolet, McQueeney, and Reppy [80] Fig. 17, were measured using thin helium films adsorbed on a Mylar substrate attached to a torsional oscillator. The period P of the oscillator decreases with decreasing temperature (below the phase transition) as more fluid becomes pure-superfluid and effectively reduces the mass included in the moment of inertia since it no longer frictionally couples to the oscillator. The plots above show the "reduced period" $2\Delta P/P$ (or $2\left|\Delta P\right|/P$), which happens to be proportional to the superfluid density σ_{s} and fraction $\sigma_{\mathrm{s}}/\sigma$ such that each of the five data sets can be separately normalized or scaled to have a maximum of $\sigma_{\mathrm{s}}/\sigma = 1$ at zero absolute temperature. The fluid coverages range from 29 µmol/m^2 (with $T_{\mathrm{KT}} = 65\,\mathrm{mK}$) to 33 µmol/m^2 (with $T_{\mathrm{KT}} = 371\,\mathrm{mK}$), which may correspond to thicknesses of less than one atomic layer. (The straight lines, relating to geometric hindrance χ, intersect the data at the transition temperatures when χ is set to an appropriate value.) Compare these 2D transitions with the 3D transitions in Fig.s 2.3 and 2.7.

2.2.2 Vortex Pair Theory, Concepts

2.2.2.1 2D cross-section

The 2D theory – the vortex pair theory of the superfluid film phase transition – can be considered essentially a cross-section of the 3D theory. In a very thin film, a would-be vortex loop is realized as pair of point vortices, a vortex pair, where each vortex has a core of diameter a_0 and the rotating flow of one vortex is in the opposite sense of the other vortex. (Vortices with rotation in one direction can be called "antivortices", while the others simply "vortices", so they come in vortex-antivortex pairs.) The pair, each with a quantum of circulation $\kappa = h/m$, induce the same velocity in each other so that they travel together if undisturbed by other excitations, just as a vortex loop travels. Again we'll ignore for the most part the role played by other excitations, since it is the vortex pairs that play the significant role in the phase transition.

Actually, the questions of whether and which point vortices should be identified as paired-up is ambiguous, especially in a chaotic situation with many vortices interacting and passing close to each other, since each vortex interacts with all others with a force that dies off inversely with separation distance (giving a logarithmic interaction energy). We will examine mostly very sparse distributions of vortices where this question is not as ambiguous. But as one example of a practical pair-identifying procedure we quote here a description of the procedure used by Jelić and Cugliandolo [81] in their Monte Carlo simulation (where they use a 2D XY lattice-spin model):

> "The assignment of pairing is, however, a hard problem not free from ambiguity. We used the following simple algorithm. Given a configuration, we first computed and ordered all distances between vortices and antivortices. However, the lattice structure implies that, for sufficiently high density, some vortex (or antivortex) could be at equal distance from two (or more) an-

> tivortices (or vortices). In these cases we chose the pairing at random and we continued the procedure with the remaining defects. With this method we are not sure of finding the optimal pairing but, statistically, we expect all these pairings to be equivalent as far as the distribution of distances is concerned, a feature that we verified numerically."

Another distinction can be made between a point vortex that is bound (paired with another vortex) and a point vortex that is free (not paired with any other vortex). This is similar to the distinction between bound and free astronomical objects. This should be a quantitative, calculable distinction, but we are uncertain how to incorporate the information of all the excitations to make this calculation. We consider all vortices under the critical temperature T_{KT} to be bound and paired. Also, since we are making a theoretical analysis, rather than experimental or simulational measurements, we do not have to do any identifying; all of our vortices will come automatically "pre-paired".

Vortex pairs may be thermally created at a small scale, starting with pair separation of about a_0, and their separation may grow from there. We assume that any pair annihilation takes place only when a pair separation has shrunk back to separation a_0. Annihilation of opposite-sign vortices from different pairs (of any separation) can also occur, but probably not appreciably at the low vortex densities that we examine. Four-vortex annihilation from pair annihilation and other unlikely events are not considered.

A difference that simplifies the 2D case from the 3D case is that, for very thin films, the vortex lines are very short, straight, and perpendicular to the film surface. So, when viewing the film, there only appear to be point vortices, and no wiggling of vortex lines. That means there is no need to consider effective core sizes or any of the Flory-type arguments made in 3D; there is just a simple core size a_0 that doesn't change with pair separation distance. This can change a bit for thicker films and for most films as the transition temperature is approached, where the wiggling becomes more significant and an effective core size could be calculated. However, we will neglect this in our analysis.

Some of the nomenclature of the 2D theory is different too. The critical phase transition temperature is called T_{KT} or T_{BKT} in honor of Kosterlitz, Thouless, and Berezinskii. There is no "T_λ" in 2D because there are no "lambda"-looking plots in 2D. In 3D the heat capacity has a discontinuous cusping (that looks like "lambda" and a divergence) at the critical temperature. The 2D transition has no such cusping or divergence.

Some additional vocabulary will help to distinguish the 2D and 3D cases. There are three broad and fairly useful categories of phase transitions – first-order, second-order, and infinite-order – and this 2D transition is infinite-order. First-order transitions, also known as discontinuous transitions, could be called "sequential" since they involve a latent heat of transformation and so have a mixed-phase regime when one phase is sequentially transformed, bit by bit, into the other phase. Second- and infinite-order transitions, both known as continuous transitions, could be called "immediate" or "instantaneous" since there is no latent heat involved. There is spontaneous symmetry-breaking in second-order transitions, but there is no symmetry-breaking in infinite-order transitions. One might say that second-order phase transitions are characterized by divergences, for instance, in the correlation length. The 3D lambda transition is second-order, it has cusping behavior in the specific heat, and the correlation length (the diameter of largest thermally excited vortex loops) diverges. However, an infinite-order phase transition such as the 2D KT transition also has divergences, for instance, in the correlation length, but no peak in the specific heat (as described in the 1974 paper in Ref. [29]).

2.2.2.2 fluid components and linear response (permeability)

Qualitatively speaking, the portion of the 2D superfluid film that is "caught up" in the flow of the vortex-pair excitations is seen to be "normal fluid" since it has entropy and viscosity, as the excitations interact with themselves and the container boundaries, and it behaves as a regular fluid would behave. So a real 2D superfluid can be seen effectively as a kind of superposition of 1) a pure superfluid component with mass density σ_{s} and velocity field $\mathbf{v}_{\mathrm{s}}$; and 2) a normal fluid component with mass density σ_{n} and velocity field $\mathbf{v}_{\mathrm{n}}$. The real superfluid has mass density σ and momentum density (or mass current-density) $\mathbf{g}$, where

$$\sigma = \sigma_{\mathrm{n}} + \sigma_{\mathrm{s}}, \tag{2.124}$$

$$\mathbf{g} = \sigma_{\mathrm{n}}\mathbf{v}_{\mathrm{n}} + \sigma_{\mathrm{s}}\mathbf{v}_{\mathrm{s}}. \tag{2.125}$$

Densities in 2D are measured “per area” rather than “per volume”. Using the same model and arguments as before, we can relate the superflow-reduction factor (or permeability) to the fluid densities:

$$\mathbf{g} = \mu\mathbf{g}^{T0} \tag{2.126}$$

$$(\sigma_{\mathrm{s}}\mathbf{v}_{\mathrm{s}}) = \mu(\sigma\mathbf{v}^{T0}) \tag{2.127}$$

$$(\sigma_{\mathrm{s}}\mathbf{v}_{\mathrm{s}}) = \mu(\sigma\mathbf{v}_{\mathrm{s}}) \tag{2.128}$$

$$\mu = \frac{\sigma_{\mathrm{s}}}{\sigma}. \tag{2.129}$$

This μ is the permeability at the largest length scale of the system, the length scale of the container. At smaller length scales, we can define a renormalized permeability based on the renormalized superfluid density:

$$\mu^{\mathrm{r}} = \frac{\sigma_{\mathrm{s}}^{\mathrm{r}}}{\sigma}. \tag{2.130}$$

This μ^{r} is the permeability at any length scale, starting at 1 at the smallest length scale and ending at the superfluid fraction $\sigma_{\mathrm{s}}/\sigma$ at the largest scale, and it tells how well the superfluid effects (e.g., superflow or superfluid density) “survive” from the smallest scale to the scale in question and permeate the fluid. The analogue of magnetic susceptibility, χ, is defined by how it relates the flow induced by the vortex pairs to the applied flow:

$$\mathbf{g}^{\mathrm{i}} = \chi\mathbf{g}^{T0}, \tag{2.131}$$

so

$$\begin{aligned} \mathbf{g} &= \mathbf{g}^{T0} + \mathbf{g}^{\mathrm{i}} && (2.132)\\ \left(\mu \mathbf{g}^{T0}\right) &= \mathbf{g}^{T0} + \left(\chi \mathbf{g}^{T0}\right) && (2.133)\\ \mu &= 1 + \chi. && (2.134) \end{aligned}$$

2.2.2.3 vortex-pair state variables

The vortex-pair state variables are mostly the same as those in 3D, but the classical fluid dynamical equations change a bit due to the different geometry. For instance, the impulse of a vortex pair is $p = ka$, where $k \equiv \kappa \sigma_{\mathrm{s}}^{\mathrm{r}}$, whereas for a loop it was $p \propto a^2$. The remaining relations are listed just prior to the beginning of the derivations section.

$$\begin{aligned} v &= \frac{\kappa}{2\pi a} && (2.135)\\ U &= P.E. + K.E. && (2.136)\\ &= 2U_{\mathrm{core}} + \frac{\kappa^2 \sigma_{\mathrm{s}}^{\mathrm{r}}}{2\pi} \ln(a/a_0) && (2.137)\\ &= \frac{\kappa^2 \sigma_{\mathrm{s}}^{\mathrm{r}}}{2\pi} \left\{ \ln(a/a_0) + C \right\} && (2.138)\\ C &\equiv 2U_{\mathrm{core}} / \left(\kappa^2 \sigma_{\mathrm{s}}^{\mathrm{r}} / 2\pi\right) && (2.139)\\ U^0 &= \frac{\kappa^2 \sigma_{\mathrm{s}}^{\ell 0}}{2\pi} \left\{ \ln(a/a_0) + C \right\} && (2.140)\\ U &= \mu^{\mathrm{r}} U^0 && (2.141)\\ d &= \kappa a && (2.142)\\ p &= \sigma_{\mathrm{s}}^{\mathrm{r}} d && (2.143)\\ &= \kappa \sigma_{\mathrm{s}}^{\mathrm{r}} a && (2.144)\\ E &= U + \mathbf{p} \cdot \mathbf{v}_{\mathrm{s}}. && (2.145) \end{aligned}$$

Again, note that we used a superscript “r” on σ and μ (and will use it on χ) to indicate renormalization, but the “r” is implicit on the other quantities that depend on length scale. Here, the core parameter C is related to the vortex core energy as shown in Eq. (2.139).

Supposing that one neglects the a dependence of $\sigma_{\mathrm{s}}^{\mathrm{r}}$, the Hamilton equation $v = \partial U/\partial p$ holds so that a vortex pair may be regarded as a quasi-particle excitation [76].

2.2.2.4 vortex-pair number densities

We have the number density distributions w and Γ, which integrate to give the number density N/A:

$$\frac{N(t)}{A} = \int w(\mathbf{p},t)\,\mathrm{d}^2p = \int \Gamma(\mathbf{a},t)\,\mathrm{d}^2a. \tag{2.146}$$

The relationship $p = ka$ dictates that the differentials are related like so, $\mathrm{d}^2p = p\,\mathrm{d}p\,\mathrm{d}\vartheta = k^2a\,\mathrm{d}a\,\mathrm{d}\vartheta = k^2\mathrm{d}^2a$ (where ϑ is an azimuthal angle), so these number densities are related like so,

$$\Gamma(\mathbf{a},t) = k^2\,w(\mathbf{a},t) \tag{2.147}$$

$$\Gamma \propto w. \tag{2.148}$$

We now make a crude argument as to what w and Γ should be in equilibrium. Take the vortex pairs to be like particles behaving with Maxwell-Boltzmann statistics, given that they are not superimposable in state-space. First let's examine the number of vortex pairs in terms of number (energy-)density $n(\varepsilon)$, which can be broken into a product of the (energy-)density of states $\rho(\varepsilon)$ (number of states per energy) and the occupancy $f(\varepsilon)$ (average number of vortex objects per state with energy ε):

$$N = \int \mathrm{d}N = \int n(\varepsilon)\,\mathrm{d}\varepsilon = \int f(\varepsilon)\,\rho(\varepsilon)\,\mathrm{d}\varepsilon. \tag{2.149}$$

In equilibrium, f is simply the Maxwell-Boltzmann factor $f(\varepsilon) = \exp(-\beta\varepsilon)$ with $\beta \equiv 1/(k_{\mathrm{B}}T)$, and we can find the density of states ρ using Ω_{s}, the number of states, $p = ka$, the vortex-pair impulse/momentum, $h_0 = a_0 p_0 = k a_0^2$, the quantum of action, and V_{phase}, the volume in phase space:

$$\rho \;=\; \frac{\mathrm{d}\Omega_{\text{s}}}{\mathrm{d}\varepsilon} \;=\; \frac{\frac{1}{h_0^2}\mathrm{d}V_{\text{phase}}}{\mathrm{d}\varepsilon} \;=\; \frac{\frac{1}{h_0^2}(\int \mathrm{d}^2x)(\mathrm{d}^2p)}{\mathrm{d}\varepsilon} \;=\; \frac{A}{h_0^2}\,\frac{\mathrm{d}^2p}{\mathrm{d}\varepsilon}. \tag{2.150}$$

Thus, in equilibrium we have

$$N_{\text{eq}} \;=\; \int \exp(-\beta\varepsilon)\,\frac{A}{h_0^2}\,\frac{\mathrm{d}^2p}{\mathrm{d}\varepsilon}\,\mathrm{d}\varepsilon \;=\; \frac{A}{h_0^2}\int \exp(-\beta\varepsilon)\,\mathrm{d}^2p, \tag{2.151}$$

but we also have

$$N_{\text{eq}} \;=\; A\int w_{\text{eq}}(\mathbf{p})\,\mathrm{d}^2p \;=\; A\int \Gamma_{\text{eq}}(\mathbf{a})\,\mathrm{d}^2a, \tag{2.152}$$

so

$$w_{\text{eq}}(\mathbf{p}) \;=\; \frac{\exp\bigl(-\beta\,\varepsilon(\mathbf{p})\bigr)}{h_0^2} \;=\; \frac{\exp\bigl(-\beta\,\varepsilon(\mathbf{p})\bigr)}{k^2 a_0^4}, \tag{2.153}$$

and

$$\Gamma_{\text{eq}}(\mathbf{a}) \;=\; k^2 w_{\text{eq}}(\mathbf{a}) \;=\; \frac{1}{a_0^4}\exp\bigl(-\beta\,\varepsilon(\mathbf{a})\bigr)\,. \tag{2.154}$$

In our usual notation, this is

$$\Gamma_{\text{eq}} \;=\; \frac{1}{a_0^4}\exp\bigl(-U/k_{\text{B}}T\bigr)\,. \tag{2.155}$$

2.2.2.5 convenient parameters and Villain model

Let's define some convenient dimensionless parameters. Let $K \equiv (\hbar/m)^2\sigma_{\text{s}}^{\text{r}}/k_{\text{B}}T$, where K is called the coupling. Let $y \equiv a^4\Gamma$, where y is called the fugacity. Let $e \equiv (F/k_{\text{B}}T)(a_0^2/A)$, where e will be called the "Helmholtz parameter", since F is the Helmholtz energy of the liquid due to the vortex pairs. Let $r \equiv a/a_0$, where r could be called the "diameter parameter". Let $\ell \equiv \ln(a/a_0)$, where ℓ will be called the "length-scale parameter".

To solve for the physically meaningful quantities, once we have done calculations using the dimensionless parameters, we can use the following relations:

$$\begin{aligned} \frac{\sigma_{\mathrm{s}}^{\mathrm{r}}}{\sigma_{\mathrm{s}}^{\ell 0}} &= \frac{K}{K^{\ell 0}} && (2.156) \\ \Gamma &= \frac{1}{a^4}\, y && (2.157) \\ \frac{U_{\mathrm{eq}}}{k_{\mathrm{B}}T} &\approx -\ln\left[\left(\frac{a}{a_0}\right)^{-4} y_{\mathrm{eq}}\right]. && (2.158) \end{aligned}$$

We will use the Villain model [82] for the small-scale core energy, which is conveniently expressed in terms of $K^{\ell 0} = (\hbar/m)^2 \sigma_{\mathrm{s}}^{\ell 0}/k_{\mathrm{B}}T$:

$$2U_{\mathrm{core}}^{\ell 0}/k_{\mathrm{B}}T = \pi^2 K^{\ell 0}. \qquad (2.159)$$

This means, since Eq.s (2.137) and (2.138) imply

$$\begin{aligned} U^{\ell 0}/k_{\mathrm{B}}T &= 2U_{\mathrm{core}}^{\ell 0}/k_{\mathrm{B}}T && (2.160) \\ &= 2\pi K^{\ell 0} C, && (2.161) \end{aligned}$$

that the Villain model is equivalent in this context to setting $C = \pi/2$. This also means that the bare value of y_{eq} is simplified to be $y_{\mathrm{eq}}^{\ell 0} = \exp(-E^{\ell 0}/k_{\mathrm{B}}T) \approx \exp(-U^{\ell 0}/k_{\mathrm{B}}T) = \exp(-\pi^2 K^{\ell 0})$.

Vortex pair properties	$\kappa = h/m$
	$p = \kappa\sigma_{\mathrm{s}}^{\mathrm{r}} a$
	$U = \dfrac{\kappa^2\sigma_{\mathrm{s}}^{\mathrm{r}}}{2\pi}\left\{\ln(a/a_0) + C\right\}$
	$U^0 = \dfrac{\kappa^2\sigma_{\mathrm{s}}^{\ell 0}}{2\pi}\left\{\ln(a/a_0) + C\right\}$
	$E = U + \mathbf{p}\cdot\mathbf{v}_{\mathrm{s}}$
Convenient parameters	$K \equiv (\hbar/m)^2\sigma_{\mathrm{s}}^{\mathrm{r}}/k_{\mathrm{B}}T$
	$y \equiv a^4\Gamma$
	$e \equiv (F/k_{\mathrm{B}}T)(a_0^2/A)$
	$r \equiv a/a_0$
	$\ell \equiv \ln(a/a_0)$
Equilibrium	$\Gamma_{\mathrm{eq}} = (1/a_0^4)\exp(-E/k_{\mathrm{B}}T)$
	$y_{\mathrm{eq}} \approx (a/a_0)^4\exp(-U/k_{\mathrm{B}}T)$
Smallest scale	$\dfrac{U^{\ell 0}}{k_{\mathrm{B}}T} = \dfrac{\kappa^2\sigma_{\mathrm{s}}^{\ell 0}}{2\pi k_{\mathrm{B}}T}C = 2\pi K^{\ell 0}C$
	$= \pi^2 K^{\ell 0}$ (Villain model)
	$y_{\mathrm{eq}}^{\ell 0} \approx \exp(-2\pi K^{\ell 0}C)$
	$\approx \exp(-\pi^2 K^{\ell 0})$ ($\Leftarrow$ Villain)

Table 2.5: This summarizes the important vortex pair theory quantities.

2.2.3 Scaling Relations, Derivations

In this section we'll derive the both the equilibrium and non-equilibrium scaling relations of the vortex pair theory. Again, we'll take a less rigorous, more physically qualitative approach than the type of approach taken by Shenoy [78].

2.2.3.1 renormalized energy equation (leading to y equation)

We use the same two methods as before.

Method 1 – Differentiate but ignore the a-dependence of $\sigma_{\mathrm{s}}^{\mathrm{r}}$ when differentiating:

$$\begin{aligned}
\frac{\partial}{\partial \ell}\left(\frac{U}{k_{\mathrm{B}}T}\right) &= a\,\frac{\partial}{\partial a}\left(\frac{U}{k_{\mathrm{B}}T}\right) && (2.162)\\
&= a\,\frac{\partial}{\partial a}\left(\frac{1}{k_{\mathrm{B}}T}\frac{\kappa^2\sigma_{\mathrm{s}}^{\mathrm{r}}(a)}{2\pi}\left\{\ln(a/a_0)+C\right\}\right) && (2.163)\\
&\approx \frac{1}{k_{\mathrm{B}}T}\frac{\kappa^2\sigma_{\mathrm{s}}^{\mathrm{r}}(a)}{2\pi}a\,\frac{\partial}{\partial a}\big(\ln(a/a_0)+C\big) && (2.164)\\
&= 2\pi\frac{\kappa^2\sigma_{\mathrm{s}}^{\mathrm{r}}(a)}{(2\pi)^2k_{\mathrm{B}}T}a\left(\frac{1}{a}\right) && (2.165)\\
&= 2\pi K. && (2.166)
\end{aligned}$$

In integral form, this scaling relation becomes

$$\frac{U(\ell)}{k_{\mathrm{B}}T} = \frac{U(0)}{k_{\mathrm{B}}T} + 2\pi\int_0^{\ell} K(\ell')\,\mathrm{d}\ell'. \qquad (2.167)$$

Now we transform to the dimensionless parameter y. Given the relation
$y_{\mathrm{eq}} \approx (a/a_0)^4\exp(-U/k_{\mathrm{B}}T) = \exp(4\ell - U/k_{\mathrm{B}}T)$, we have

$$\begin{aligned}
\frac{\partial y_{\mathrm{eq}}}{\partial \ell} &= \frac{\partial}{\partial \ell}\exp(4\ell - U/k_{\mathrm{B}}T) && (2.168)\\
&= y_{\mathrm{eq}}\,\frac{\partial}{\partial \ell}\big(4\ell - U/k_{\mathrm{B}}T\big) && (2.169)\\
&= y_{\mathrm{eq}}\left\{4 - \frac{\partial}{\partial \ell}\left(\frac{U}{k_{\mathrm{B}}T}\right)\right\} && (2.170)\\
&= y_{\mathrm{eq}}\left\{4 - 2\pi K\right\}. && (2.171)
\end{aligned}$$

Method 2 – Use the permeability to integrate up from the energy of the pair of smallest separation, using the bare energy U^0:

$$\frac{U(a)}{k_\mathrm{B}T} = \frac{U^0(a_0)}{k_\mathrm{B}T} + \int_{a_0}^{a} \mu^\mathrm{r}(a')\, \frac{\mathrm{d}}{\mathrm{d}a'}\left(\frac{U^0(a')}{k_\mathrm{B}T}\right) \mathrm{d}a' \tag{2.172}$$

$$= \frac{U^0(a_0)}{k_\mathrm{B}T} + \int_{a_0}^{a} \mu^\mathrm{r}(a')\, \frac{\mathrm{d}}{\mathrm{d}a'}\left(\frac{\kappa^2\sigma_\mathrm{s}^{\ell 0}}{2\pi k_\mathrm{B}T}\left\{\ln(a'/a_0) + C\right\}\right)\mathrm{d}a' \tag{2.173}$$

$$= \frac{U(a_0)}{k_\mathrm{B}T} + \int_{a_0}^{a} \left(\frac{\sigma_\mathrm{s}^\mathrm{r}(a')}{\sigma_\mathrm{s}^{\ell 0}}\right) \frac{\kappa^2\sigma_\mathrm{s}^{\ell 0}}{2\pi k_\mathrm{B}T}\left(\frac{1}{a'}\right) \mathrm{d}a' \tag{2.174}$$

$$= \frac{U(a_0)}{k_\mathrm{B}T} + \int_{a_0}^{a} 2\pi \frac{\kappa^2\sigma_\mathrm{s}^\mathrm{r}(a')}{(2\pi)^2 k_\mathrm{B}T}\frac{\mathrm{d}a'}{a'} \tag{2.175}$$

$$= \frac{U(a_0)}{k_\mathrm{B}T} + 2\pi\int_{a_0}^{a} K(a')\,\frac{\mathrm{d}a'}{a'}. \tag{2.176}$$

In terms of ℓ, this is the same result as Eq. (2.167), and so we obtain the same scaling relation:

$$\frac{\partial y_\mathrm{eq}}{\partial \ell} = y_\mathrm{eq}\left\{4 - 2\pi K\right\}. \tag{2.177}$$

2.2.3.2 renormalized induced-flow equation (leading to K equation)

Again, we'll repeat the two methods from the 3D case. This time the assumption used in method 2 that the superfluid fraction is approximately 1 over all length scales is better than in the 3D case since in 2D $\sigma_\mathrm{s}^\mathrm{r}/\sigma_\mathrm{s}^{\ell 0} \geq 0.851263$ (see Fig. 2.18), at least for temperatures $T \leq T_\mathrm{KT}$.

Method 1 – Keeping $k = \kappa\sigma_\mathrm{s}^\mathrm{r}$:

$$\mathbf{g}^\mathrm{i} = \text{(induced momentum per area due to vortex pairs)} \tag{2.178}$$

$$= \int_{a_0}^{\infty} \text{(momentum due to a pair, component in applied-flow direction)}$$

$$\times\,(\text{\# of pair centers per area per separation-area})\,\mathrm{d}^2a \tag{2.179}$$

$$= \int_{a_0}^{\infty} \left(p_\parallel(\mathbf{a})\,\hat{\mathbf{g}}^{T0}\right)\Gamma_\mathrm{eq}(\mathbf{a})\,\mathrm{d}^2a \tag{2.180}$$

$$= \int_{a_0}^{\infty} \left(p_\parallel(\mathbf{a})\,\hat{\mathbf{g}}^{T0}\right)\frac{1}{a_0^4}\exp\left[-E(\mathbf{a})/k_\mathrm{B}T\right]\mathrm{d}^2a \tag{2.181}$$

$$\begin{aligned}
&= \frac{\hat{\mathbf{g}}^{T0}}{a_0^4}\int_{a_0}^{\infty} p_{\|}(\mathbf{a})\,\exp\Big[-\big\{U(a)+\mathbf{p}(\mathbf{a})\cdot\mathbf{v}_{\mathrm{s}}\big\}/k_{\mathrm{B}}T\Big]\,\mathrm{d}^2a && (2.182)\\
&= \frac{\hat{\mathbf{g}}^{T0}}{a_0^4}\int_{a_0}^{\infty}\int_{-\pi}^{\pi}\big(-p(a)\,\cos\phi\big)\exp\big[-U(a)/k_{\mathrm{B}}T\big] \\
&\qquad\qquad\times\exp\big[p(a)\,v_{\mathrm{s}}\cos\phi/k_{\mathrm{B}}T\big]\,a\,\mathrm{d}\phi\,\mathrm{d}a && (2.183)\\
&\approx \frac{\hat{\mathbf{g}}^{T0}}{a_0^4}\int_{a_0}^{\infty}\int_{-\pi}^{\pi}\big(-p(a)\,\cos\phi\big)\exp\big[-U(a)/k_{\mathrm{B}}T\big] \\
&\qquad\qquad\times\big[1+p(a)\,v_{\mathrm{s}}\cos\phi/k_{\mathrm{B}}T\big]\,a\,\mathrm{d}\phi\,\mathrm{d}a && (2.184)\\
&= -\frac{\hat{\mathbf{g}}^{T0}v_{\mathrm{s}}}{a_0^4k_{\mathrm{B}}T}\int_{-\pi}^{\pi}\cos^2\phi\;\mathrm{d}\phi\int_{a_0}^{\infty}\big[p(a)\big]^2\exp\big[-U(a)/k_{\mathrm{B}}T\big]\,a\,\mathrm{d}a && (2.185)\\
&= -\frac{\hat{\mathbf{g}}^{T0}(g^{T0}/\sigma)}{a_0^4k_{\mathrm{B}}T}\,(\pi)\int_{a_0}^{\infty}[\kappa\sigma_{\mathrm{s}}^{\mathrm{r}}a]^2\exp\big[-U(a)/k_{\mathrm{B}}T\big]\,a\,\mathrm{d}a && (2.186)\\
&= -\mathbf{g}^{T0}\,(\pi)\,\frac{1}{a_0^4}\frac{(1/\sigma_{\mathrm{s}}^{\ell0})}{k_{\mathrm{B}}T}\int_{a_0}^{\infty}\left(\frac{(2\pi)^4(k_{\mathrm{B}}T)^2}{\kappa^2}\right)\left(\frac{\kappa^2\sigma_{\mathrm{s}}^{\mathrm{r}}}{(2\pi)^2k_{\mathrm{B}}T}\right)^2 \\
&\qquad\qquad\times a^4\exp\big[-U(a)/k_{\mathrm{B}}T\big]\,\frac{\mathrm{d}a}{a} && (2.187)\\
&= -\mathbf{g}^{T0}\,(\pi)\,(2\pi)^2\left(\frac{(2\pi)^2k_{\mathrm{B}}T}{\kappa^2\sigma_{\mathrm{s}}^{\ell0}}\right)\int_{a_0}^{\infty}K^2\left(\frac{a}{a_0}\right)^4\exp\left[-\frac{U(a)}{k_{\mathrm{B}}T}\right]\frac{\mathrm{d}a}{a} && (2.188)\\
&\approx -\mathbf{g}^{T0}4\pi^3\frac{1}{K^{\ell0}}\int_{a_0}^{\infty}K^2y_{\mathrm{eq}}\frac{\mathrm{d}a}{a} && (2.189)\\
&= -\mathbf{g}^{T0}\frac{4\pi^3}{K^{\ell0}}\int_{0}^{\infty}K^2y_{\mathrm{eq}}\,\mathrm{d}\ell && (2.190)\\
&= \chi_{\mathrm{eq}}\,\mathbf{g}^{T0}. && (2.191)
\end{aligned}$$

Note that since $\Gamma_{\mathrm{eq}} \approx a_0^{-4}\exp[-U(a)/k_{\mathrm{B}}T]$, Expressions (2.185) and (2.186) can be considered as integrals of the vortex-pair polarizability (proportional to $p^2 \propto a^2$) times the number density, to obtain the susceptibility. Now we use the renormalized version of $\mu = 1+\chi$:

$$\begin{aligned}
\mu^{\mathrm{r}}(\ell) &= 1+\chi^{\mathrm{r}}(\ell) && (2.192)\\
\frac{\sigma_{\mathrm{s}}^{\mathrm{r}}(\ell)}{\sigma} &= 1-\frac{4\pi^3}{K^{\ell0}}\int_0^{\ell}K^2y_{\mathrm{eq}}\,\mathrm{d}\ell' && (2.193)\\
\frac{K}{K^{\ell0}} &= 1-\frac{4\pi^3}{K^{\ell0}}\int_0^{\ell}K^2y_{\mathrm{eq}}\,\mathrm{d}\ell' && (2.194)\\
K &= K^{\ell0}-4\pi^3\int_0^{\ell}K^2y_{\mathrm{eq}}\,\mathrm{d}\ell'. && (2.195)
\end{aligned}$$

This yields the familiar scaling equation,

$$\frac{\partial K}{\partial \ell} = -4\pi^3 K^2 y_{\mathrm{eq}}. \tag{2.196}$$

Method 2 – Redefining $k = \kappa\sigma_{\mathrm{s}}^{\ell 0}$, and making the not-so-bad assumption that $\sigma_{\mathrm{s}}^{\mathrm{r}}/\sigma_{\mathrm{s}}^{\ell 0} \approx 1$ (and jumping ahead in the derivation to where this method diverges from the previous method):

$$\begin{aligned}
\mathbf{g}^{\mathrm{i}} &\approx -\frac{\hat{\mathbf{g}}^{T0} v_{\mathrm{s}}}{a_0^4 k_{\mathrm{B}} T} \int_{-\pi}^{\pi} \cos^2\phi \; \mathrm{d}\phi \int_{a_0}^{\infty} \big[p(a)\big]^2 \exp\big[-U(a)/k_{\mathrm{B}}T\big]\, a\, \mathrm{d}a & (2.197)\\
&= -\frac{\hat{\mathbf{g}}^{T0}(g^{T0}/\sigma)}{a_0^4 k_{\mathrm{B}} T} (\pi) \int_{a_0}^{\infty} \Big[\kappa\sigma_{\mathrm{s}}^{\ell 0} a\Big]^2 \exp\big[-U(a)/k_{\mathrm{B}}T\big]\, a\, \mathrm{d}a & (2.198)\\
&= -\mathbf{g}^{T0} (\pi) (2\pi)^2 \left(\frac{\kappa^2 \sigma_{\mathrm{s}}^{\ell 0}}{(2\pi)^2 k_{\mathrm{B}} T}\right) \int_{a_0}^{\infty} \left(\frac{a}{a_0}\right)^4 \exp\big[-U(a)/k_{\mathrm{B}}T\big] \frac{\mathrm{d}a}{a} & (2.199)\\
&\approx -\mathbf{g}^{T0} 4\pi^3 K^{\ell 0} \int_{a_0}^{\infty} y_{\mathrm{eq}} \frac{\mathrm{d}a}{a} & (2.200)\\
&= -\mathbf{g}^{T0} 4\pi^3 K^{\ell 0} \int_{0}^{\infty} y_{\mathrm{eq}}\, \mathrm{d}\ell & (2.201)\\
&= \chi_{\mathrm{eq}}\, \mathbf{g}^{T0}. & (2.202)
\end{aligned}$$

With the approximately correct assumption that $\sigma_{\mathrm{s}}^{\mathrm{r}}/\sigma_{\mathrm{s}}^{\ell 0} \approx 1$, meaning that χ is very small, we get

$$\begin{aligned}
\mu^{\mathrm{r}}(\ell) &= 1 + \chi^{\mathrm{r}}(\ell) & (2.203)\\
\frac{\sigma_{\mathrm{s}}^{\mathrm{r}}(\ell)}{\sigma} &= 1 - 4\pi^3 K^{\ell 0} \int_0^{\ell} y_{\mathrm{eq}}\, \mathrm{d}\ell' & (2.204)\\
\frac{\sigma_{\mathrm{s}}^{\ell 0}}{\sigma_{\mathrm{s}}^{\mathrm{r}}(\ell)} &\approx 1 + 4\pi^3 K^{\ell 0} \int_0^{\ell} y_{\mathrm{eq}}\, \mathrm{d}\ell' & (2.205)\\
\frac{K^{\ell 0}}{K(\ell)} &\approx 1 + 4\pi^3 K^{\ell 0} \int_0^{\ell} y_{\mathrm{eq}}\, \mathrm{d}\ell' & (2.206)\\
\frac{1}{K(\ell)} &\approx \frac{1}{K^{\ell 0}} + 4\pi^3 \int_0^{\ell} y_{\mathrm{eq}}\, \mathrm{d}\ell' & (2.207)\\
\frac{\partial(K^{-1})}{\partial \ell} &\approx 4\pi^3 y_{\mathrm{eq}}. & (2.208)
\end{aligned}$$

Rearranging, again we get

$$\frac{\partial K}{\partial \ell} = -K^2 \left(-\frac{1}{K^2}\frac{\partial K}{\partial \ell}\right) \tag{2.209}$$

$$
\begin{aligned}
&= -K^2\left(\frac{\partial(K^{-1})}{\partial\ell}\right) && (2.210)\\
&= -4\pi^3K^2y_{\mathrm{eq}}. && (2.211)
\end{aligned}
$$

Note that using method 1, one can derive both of the following equations,

$$
\begin{aligned}
K &= K^{\ell 0} - 4\pi^3\int_0^{\ell} K^2 y_{\mathrm{eq}}\,\mathrm{d}\ell' && (2.212)\\
(K)^{-1} &= (K^{\ell 0})^{-1} + 4\pi^3\int_0^{\ell} y_{\mathrm{eq}}\,\mathrm{d}\ell', && (2.213)
\end{aligned}
$$

but this does not imply that $\sigma_{\mathrm{s}}^{\mathrm{r}}/\sigma_{\mathrm{s}}^{\ell 0} \approx 1$ since the integrals are different. In contrast, method 2 implies the following equation (that we'll write as an approximation):

$$
K \approx K^{\ell 0} - 4\pi^3(K^{\ell 0})^2\int_0^{\ell} y_{\mathrm{eq}}\,\mathrm{d}\ell'. \qquad (2.214)
$$

2.2.3.3 renormalized free-energy equation (leading to e equation)

We use the same crude argument as in the 3D case to write these equations. Taking P to be the force per length in the film, the differential Helmholtz energy of the film is

$$
\mathrm{d}F = -S\,\cancelto{0}{\mathrm{d}T} - P\,\cancelto{0}{\mathrm{d}A} + \mu_{\mathrm{ch}}\mathrm{d}N, \qquad (2.215)
$$

and we take $F^{\ell 0} = 0$. With this we find

$$
\begin{aligned}
F &= F^{\ell 0} + \int \mu_{\mathrm{ch}}\mathrm{d}N && (2.216)\\
&= \mu_{\mathrm{ch}}\int \mathrm{d}N && (2.217)\\
&= \mu_{\mathrm{ch}}A\int \Gamma\,\mathrm{d}^2a, && (2.218)
\end{aligned}
$$

where we've assumed constant chemical potential. Now let's switch to the convenient parameter $e \equiv (F/k_\mathrm{B}T)(a_0^2/A)$ and examine the equilibrium conditions:

$$\begin{aligned}
e_\mathrm{eq} &= a_0^2 \frac{\mu_\mathrm{ch}}{k_\mathrm{B}T} \int \Gamma_\mathrm{eq}\, \mathrm{d}^2 a && (2.219)\\
&\approx a_0^2 \frac{\mu_\mathrm{ch}}{k_\mathrm{B}T} \int \frac{1}{a_0^4} \exp\bigl[-U(a)/k_\mathrm{B}T\bigr]\ \mathrm{d}^2 a && (2.220)\\
&= \frac{1}{a_0^2}\left(\frac{\mu_\mathrm{ch}}{k_\mathrm{B}T}\right) \int_{a_0}^{\infty} \int_{-\pi}^{\pi} \exp\bigl[-U(a)/k_\mathrm{B}T\bigr]\, a\, \mathrm{d}\phi\, \mathrm{d}a && (2.221)\\
&= 2\pi \left(\frac{\mu_\mathrm{ch}}{k_\mathrm{B}T}\right) \int_{a_0}^{\infty} \left(\frac{a}{a_0}\right)^2 \exp\bigl[-U(a)/k_\mathrm{B}T\bigr]\, \frac{\mathrm{d}a}{a} && (2.222)\\
&= 2\pi \left(\frac{\mu_\mathrm{ch}}{k_\mathrm{B}T}\right) \int_{a_0}^{\infty} \left(\frac{a}{a_0}\right)^{-2} y_\mathrm{eq} \frac{\mathrm{d}a}{a} && (2.223)\\
&= 2\pi \left(\frac{\mu_\mathrm{ch}}{k_\mathrm{B}T}\right) \int_{0}^{\infty} \exp(-2\ell)\, y_\mathrm{eq}\, \mathrm{d}\ell. && (2.224)
\end{aligned}$$

We require $\mu_\mathrm{ch}/k_\mathrm{B}T = -1$ to get the usual result:

$$\begin{aligned}
e_\mathrm{eq} &= -2\pi \int_0^\infty \exp(-2\ell)\, y_\mathrm{eq}\, \mathrm{d}\ell && (2.225)\\
\frac{\partial e_\mathrm{eq}}{\partial \ell} &= -2\pi \exp(-2\ell)\, y_\mathrm{eq}. && (2.226)
\end{aligned}$$

2.2.3.4 non-equilibrium superfluid ratio & energy (K, e equations)

We postulate that the K and e equations remain the same out of equilibrium as they were in equilibrium:

$$\begin{aligned}
\frac{\partial K}{\partial \ell} &= -4\pi^3 K^2 y && (2.227)\\
\frac{\partial e}{\partial \ell} &= -2\pi \exp(-2\ell). && (2.228)
\end{aligned}$$

In the derivation above, in Line (2.188), since the applied flow is infinitesimal one can replace the U in the exponent with E and the general y replaces y_eq in the equation. If that explanation is not satisfactory, then one can follow the idea in the comment below Line (2.191) and conclude that the polarizability and screening due to the smaller vortices needs to include the full distribution Γ, and hence, the non-equilibrium y. It's possible that the derivations above need to be reformulated, since they start with Γ_{eq}, to generate the non-equilibrium equations from first principles.

2.2.3.5 non-equilibrium pair distribution (Fokker-Planck Γ equation)

The vortex pairs interact stochastically with other excitations, such as phonons and perhaps second-sound excitations as well as other vortex pairs, so a Fokker-Planck equation should apply with some accuracy to describe the vortex pair distribution Γ out of equilibrium. As shown in the derivation of the general Fokker-Planck equation in Appendix C, the form of the Fokker-Planck equation is

$$\partial_t \mathcal{P}[\mathbf{R}, t] \quad = \quad -\partial_i \left\{ M_1^i(\mathbf{R}, t)\ \mathcal{P}[\mathbf{R}, t] \right\} + \partial_j \partial_k \left\{ M_2^{jk}(\mathbf{R}, t)\ \mathcal{P}[\mathbf{R}, t] \right\}. \tag{2.229}$$

So, given a probability density $\mathcal{P}$ over state-space coordinates $\mathbf{R}$ and time t, to construct the Fokker-Planck equation we have to find the migration holors – the drift terms,

$$M_1^i(\mathbf{R}, t) \quad = \quad \lim_{\Delta t \to 0} \frac{\langle \Delta R_i \rangle_{\Delta t}(\mathbf{R}, t)}{\Delta t}, \tag{2.230}$$

and the diffusion terms,

$$M_2^{jk}(\mathbf{R}, t) \quad = \quad \lim_{\Delta t \to 0} \frac{\left\langle \Delta R_j\, \Delta R_k \right\rangle_{\Delta t}(\mathbf{R}, t)}{2\Delta t}. \tag{2.231}$$

Instead of using a probability density, we shall use number densities (w and Γ), but this should cause no problems; it is really only a question of magnitudes and normalization.

Since the state space includes $\mathbf{p}$ and $\mathbf{x}$ (or $\mathbf{a}$ and $\mathbf{x}$) coordinates, we'll start by looking at $\langle \Delta \mathbf{p} \rangle / \Delta t$, the average force on a vortex pair, and $\left\langle \Delta p_j\, \Delta p_k \right\rangle / 2\Delta t$. First, let's look at the energy and velocity of a pair. The energy of a vortex pair without an applied flow in the fluid is $U \propto (\ln(a/a_0) + C)$, and with an applied (super) flow $\mathbf{v}_{\mathrm{s}}$ the energy is $E = U + \mathbf{p} \cdot \mathbf{v}_{\mathrm{s}}$. The group velocity of a pair relative to the (normal) fluid is $\mathbf{v}'$, with components

$$v_i' \;=\; \frac{\partial E}{\partial p_i} \;=\; \frac{\partial U}{\partial p_i} + v_{\mathrm{s}i} \;=\; v_i + v_{\mathrm{s}i}, \tag{2.232}$$

where $\mathbf{v}$ is the self-induced velocity of the vortex pair. The average force on a pair should be proportional to the velocity of the pair:

$$F_i^{\mathrm{avg}} \;=\; \frac{\langle \Delta p_i \rangle}{\Delta t} \;=\; -\Lambda\, \frac{\partial E}{\partial p_i}\,, \tag{2.233}$$

with proportionality parameter Λ. Since we are considering the applied velocity $\mathbf{v}_{\mathrm{s}}$ to be infinitesimal, this will simplify the remaining analysis. The diffusion, for instance, should be isotropic, so M_2^{jk} should be scalar rather than tensorial. To aid in the analysis, let's define the scalar diffusion term q:

$$M_2^{jk}(\mathbf{R},t) \quad\rightarrow\quad q\,\delta_{jk} \equiv \frac{\big\langle \Delta p_j\, \Delta p_k \big\rangle}{2\Delta t}. \tag{2.234}$$

With an infinitesimal applied flow, the average force also simplifies,

$$M_1^{i}(\mathbf{R},t) \quad\rightarrow\quad \frac{\langle \Delta p_i \rangle}{\Delta t} = -\Lambda\, \frac{\partial U}{\partial p_i}\,, \tag{2.235}$$

and the probability densities should be isotropic in their respective state spaces: $w(\mathbf{p},t) = w(p,t)$ and $\Gamma(\mathbf{a},t) = \Gamma(a,t)$.

Now, considering the vortex-pair interaction with all excitations, the Fokker-Planck equation for w is (with repeating indices summed over and homogeneity of the fluid getting rid of the spatial derivative terms)

$$
\begin{aligned}
\frac{\partial w}{\partial t} &= -\partial_{p_i}\left\{\frac{\langle\Delta p_i\rangle}{\Delta t}w\right\} - w\,\partial_{x_i}\cancelto{0}{\left\{\frac{\langle\Delta x_i\rangle}{\Delta t}\right\}} \\
&\quad +\partial_{p_j}\partial_{p_k}\left\{\frac{\left\langle\Delta p_j\,\Delta p_k\right\rangle}{2\Delta t}w\right\} + w\,\partial_{x_j}\partial_{x_k}\cancelto{0}{\left\{\frac{\left\langle\Delta x_j\,\Delta x_k\right\rangle}{2\Delta t}\right\}} \qquad (2.236) \\
&= -\partial_{p_i}\left\{\frac{\langle\Delta p_i\rangle}{\Delta t}w\right\} + \partial_{p_j}\partial_{p_k}\left\{\frac{\left\langle\Delta p_j\,\Delta p_k\right\rangle}{2\Delta t}w\right\} \qquad (2.237) \\
&= -\partial_{p_i}\left\{-\Lambda k_{\mathrm{B}}T\,\partial_{p_i}\left(\frac{U}{k_{\mathrm{B}}T}\right)w\right\} + \partial_{p_j}\partial_{p_j}\left\{qw\right\} \qquad (2.238) \\
&= \Lambda k_{\mathrm{B}}T\,\partial_{p_i}\left\{\partial_{p_i}\left(\frac{U}{k_{\mathrm{B}}T}\right)w\right\} + q\,\partial_{p_j}\partial_{p_j}\left\{w\right\} \qquad (2.239) \\
&= \boldsymbol{\nabla}_{\mathbf{p}}\cdot\left[\Lambda k_{\mathrm{B}}T\,w\boldsymbol{\nabla}_{\mathbf{p}}\left(\frac{U}{k_{\mathrm{B}}T}\right) + q\boldsymbol{\nabla}_{\mathbf{p}}\left(w\right)\right] \qquad (2.240) \\
\frac{\partial w}{\partial t} &= \frac{1}{p}\frac{\partial}{\partial p}\left[p\left\{\Lambda k_{\mathrm{B}}T\,w\,\frac{\partial}{\partial p}\left(\frac{U}{k_{\mathrm{B}}T}\right) + q\,\frac{\partial w}{\partial p}\right\}\right]. \qquad (2.241)
\end{aligned}
$$

Note that we were able to use the spherical symmetry, or isotropy, of w, U, and q to simplify the derivatives.

We can find the relation between Λ and q by examining the equilibrium situation. In equilibrium, when the distribution w is constant, $\partial w/\partial t = 0$, and $w \propto \exp(U/k_{\mathrm{B}}T)$, we see that Eq. (2.241) requires $q = \Lambda k_{\mathrm{B}}T$. This relation should hold generally as well, and that means generally we have

$$
\begin{aligned}
\frac{\partial w}{\partial t} &= \Lambda k_{\mathrm{B}}T\,\boldsymbol{\nabla}_{\mathbf{p}}\cdot\left[w\boldsymbol{\nabla}_{\mathbf{p}}\left(\frac{U}{k_{\mathrm{B}}T}\right) + \boldsymbol{\nabla}_{\mathbf{p}}\left(w\right)\right] \qquad (2.242) \\
&= \frac{\Lambda k_{\mathrm{B}}T}{p}\frac{\partial}{\partial p}\left[p\left\{w\,\frac{\partial}{\partial p}\left(\frac{U}{k_{\mathrm{B}}T}\right) + \frac{\partial w}{\partial p}\right\}\right]. \qquad (2.243)
\end{aligned}
$$

If we want to rewrite this equation in terms of a and Γ, we can simply make a coordinate transformation using $p = ka$ (where $k \equiv \kappa\sigma_{\mathrm{s}}^{\mathrm{r}}$) and $\frac{\partial}{\partial p} = \frac{\partial a}{\partial p}\frac{\partial}{\partial a} = k^{-1}\frac{\partial}{\partial a}$ and a substitution using $\Gamma \propto w$:

$$\frac{\partial w}{\partial t} = \frac{\Lambda k_{\mathrm{B}} T}{k^2} \frac{1}{a} \frac{\partial}{\partial a}\left[a\left\{w \frac{\partial}{\partial a}\left(\frac{U}{k_{\mathrm{B}}T}\right) + \frac{\partial w}{\partial a}\right\}\right] \tag{2.244}$$

$$\frac{\partial \Gamma}{\partial t} = \frac{\Lambda k_{\mathrm{B}} T}{k^2} \frac{1}{a} \frac{\partial}{\partial a}\left[a\left\{\Gamma \frac{\partial}{\partial a}\left(\frac{U}{k_{\mathrm{B}}T}\right) + \frac{\partial \Gamma}{\partial a}\right\}\right] \tag{2.245}$$

$$= \frac{\Lambda k_{\mathrm{B}} T}{k^2} \boldsymbol{\nabla}_{\mathbf{a}}\cdot \left[\Gamma\, \boldsymbol{\nabla}_{\mathbf{a}}\left(\frac{U}{k_{\mathrm{B}}T}\right) + \boldsymbol{\nabla}_{\mathbf{a}}\,\Gamma\right]. \tag{2.246}$$

We can simplify further using the diffusion time t_0,

$$t_0 = \frac{a_0^2 k^2}{\Lambda k_{\mathrm{B}} T} = \frac{a_0^2 \kappa^2 (\sigma_{\mathrm{s}}^{\mathrm{r}})^2}{\Lambda k_{\mathrm{B}} T} \tag{2.247}$$

$$\frac{\Lambda k_{\mathrm{B}} T}{k^2} = \frac{a_0^2}{t_0}, \tag{2.248}$$

so

$$\frac{\partial \Gamma}{\partial t} = \frac{a_0^2}{t_0} \frac{1}{a} \frac{\partial}{\partial a}\left[a\left\{\Gamma \frac{\partial}{\partial a}\left(\frac{U}{k_{\mathrm{B}}T}\right) + \frac{\partial \Gamma}{\partial a}\right\}\right] \tag{2.249}$$

$$\frac{\partial \Gamma}{\partial \tau} = \frac{1}{r} \frac{\partial}{\partial r}\left[r\left\{\Gamma \frac{\partial}{\partial r}\left(\frac{U}{k_{\mathrm{B}}T}\right) + \frac{\partial \Gamma}{\partial r}\right\}\right], \tag{2.250}$$

where $\tau \equiv t/t_0$ and $r \equiv a/a_0$. And here we insert the scaling relation

$$\frac{\partial}{\partial \ell}\left(\frac{U}{k_{\mathrm{B}}T}\right) = r\frac{\partial}{\partial r}\left(\frac{U}{k_{\mathrm{B}}T}\right) = 2\pi K, \tag{2.251}$$

to get

$$\frac{\partial \Gamma}{\partial \tau} = \frac{1}{r} \frac{\partial}{\partial r}\left[r\frac{\partial \Gamma}{\partial r} + 2\pi K \Gamma\right] \tag{2.252}$$

$$= \boldsymbol{\nabla}_{\mathbf{r}}\cdot \left[\boldsymbol{\nabla}_{\mathbf{r}}\,\Gamma + \frac{2\pi}{r} K\Gamma\right]. \tag{2.253}$$

Noting, as we do in Appendix C, that this Fokker-Planck equation is of the form of a continuity equation,

$$\frac{\partial \rho}{\partial t} = -\boldsymbol{\nabla}\cdot\mathbf{J}, \tag{2.254}$$

where ρ is a density and $\mathbf{J}$ is a current density, we can solve for the number-density current-density,

$$J_a(a) = -\frac{a_0^2}{t_0}\left\{\frac{\partial\Gamma}{\partial a} + \frac{2\pi}{a}K\Gamma\right\} \tag{2.255}$$

$$J_r(r) = -\frac{a_0}{t_0}\left\{\frac{\partial\Gamma}{\partial r} + \frac{2\pi}{r}K\Gamma\right\}, \tag{2.256}$$

so that

$$\frac{\partial\Gamma}{\partial t} = -\boldsymbol{\nabla}_{\mathbf{a}}\cdot\mathbf{J}. \tag{2.257}$$

Due to isotropy, there is only current in the length-scale direction (as opposed to the pair-orientation direction ϕ) in **a**-space.

Finally, let's rewrite these equations in dimensionless terms by defining $\tilde{\Gamma}$ and $\tilde{\mathbf{J}}$ with the following relations,

$$\frac{N}{A/a_0^2} = \int \tilde{\Gamma}\,\mathrm{d}^2r \tag{2.258}$$

$$\tilde{\mathbf{J}} = -\left\{\boldsymbol{\nabla}_{\mathbf{r}}\tilde{\Gamma} + \frac{2\pi}{r}K\tilde{\Gamma}\right\} \tag{2.259}$$

$$\tilde{J}_r = -\left\{\frac{\partial\tilde{\Gamma}}{\partial r} + \frac{2\pi}{r}K\tilde{\Gamma}\right\}, \tag{2.260}$$

so that

$$\frac{\partial\tilde{\Gamma}}{\partial\tau} = -\boldsymbol{\nabla}_{\mathbf{r}}\cdot\tilde{\mathbf{J}} \tag{2.261}$$

$$= \frac{1}{r}\frac{\partial}{\partial r}\left[r\frac{\partial\tilde{\Gamma}}{\partial r} + 2\pi K\tilde{\Gamma}\right]. \tag{2.262}$$

At this point it is worthwhile to read Appendix A, especially if one wishes to follow along and write the derivations for oneself.

2.2.3.6 boundary condition for the Fokker-Planck Γ equation

We should note that in a quench, where energy is being taken out of the system thermally, the smallest vortex-pairs will tend to annihilate as they transfer energy to the heat bath.

Assuming this is the dominant form of energy exchange from the vortex-pairs to the heat bath, we should find that the flow of the number-density of vortex-pairs out of the system (at the smallest length-scale) is equal to the rate of decrease in the total number-density of the vortex-pairs. We can show this using Eq. (2.257), in discrete form:

$$-\int (\boldsymbol{\nabla}_{\mathbf{a}} \cdot \mathbf{J})\, \mathrm{d}^2 a = \int \left(\frac{\Delta\Gamma}{\Delta t}\right) \mathrm{d}^2 a \tag{2.263}$$

$$-\oint \boldsymbol{\nabla}_{\mathbf{a}} \cdot \mathbf{J} \cdot \mathrm{d}\mathbf{a} = \frac{\Delta\left(\int \Gamma\, \mathrm{d}^2 a\right)}{\Delta t} \tag{2.264}$$

$$-J_a(a_{\max})\, 2\pi a_{\max} + J_a(a_0)\, 2\pi a_0 = \frac{\Delta\left(\int \Gamma\, \mathrm{d}^2 a\right)}{\Delta t}, \tag{2.265}$$

and since there is no flow out of the system at the largest length-scale, $J_a(a_{\max}) = 0$, and we have

$$J_a(a_0)\, 2\pi a_0 = \frac{\Delta\left(\int \Gamma\, \mathrm{d}^2 a\right)}{\Delta t} \tag{2.266}$$

$$\tilde{J}_r(1)\, 2\pi = \frac{\Delta\left(\int \tilde{\Gamma}\, \mathrm{d}^2 r\right)}{\Delta \tau}. \tag{2.267}$$

2.2.4 2D Equations Summary

The dimensionless scaling equations derived in the preceding section are summarized below. Here too are the integral form of the equilibrium equations, using the dimensionful quantities, including a couple equivalent arrangements for one of the equations:

$$\frac{U(a)}{k_{\mathrm{B}}T} = \frac{U(a_0)}{k_{\mathrm{B}}T} + 2\pi \int_{a_0}^{a} \frac{\kappa^2 \sigma_{\mathrm{s}}^{\mathrm{r}}(a')}{(2\pi)^2 k_{\mathrm{B}}T} \left(\frac{a'}{a_0}\right)^{-1} \frac{\mathrm{d}a'}{a_0} \tag{2.268a}$$

$$\sigma_{\mathrm{s}}^{\mathrm{r}}(a) = \sigma_{\mathrm{s}}^{\mathrm{r}}(a_0) - 4\pi^3 \int_{a_0}^{a} \frac{(\hbar/m)^2}{k_{\mathrm{B}}T} \left(\frac{\sigma_{\mathrm{s}}^{\mathrm{r}}(a')\, a'}{a_0}\right)^2 \exp\left[-\frac{U(a')}{k_{\mathrm{B}}T}\right] \left(\frac{a'}{a_0}\right) \frac{\mathrm{d}a'}{a_0} \tag{2.269a}$$

$$\frac{1}{\sigma_{\mathrm{s}}^{\mathrm{r}}(a)} = \frac{1}{\sigma_{\mathrm{s}}^{\mathrm{r}}(a_0)} + 4\pi^3 \int_{a_0}^{a} \frac{(\hbar/m)^2}{k_{\mathrm{B}}T} \left(\frac{a'}{a_0}\right)^2 \exp\left[-\frac{U(a')}{k_{\mathrm{B}}T}\right] \left(\frac{a'}{a_0}\right) \frac{\mathrm{d}a'}{a_0} \tag{2.269b}$$

$$\frac{f(a)}{k_{\mathrm{B}}T} = -\frac{2\pi}{a_0^2} \int_{a_0}^{a} \exp\left[-\frac{U(a')}{k_{\mathrm{B}}T}\right] \left(\frac{a'}{a_0}\right) \frac{\mathrm{d}a'}{a_0}, \tag{2.270}$$

where $f = F/A$ is the Helmholtz free energy per area of the film due to the vortex pairs, $\sigma_{\rm s}^{\rm r}(a_0) = \sigma_{\rm s}^{\ell 0} = \sigma$, and $U(a_0)/k_{\rm B}T = \kappa^2\sigma\, C/2\pi k_{\rm B}T$, since $U(a_0)/k_{\rm B}T = 2\pi K^{\ell 0}C$ and $K^{\ell 0} = (\hbar/m)^2\sigma_{\rm s}^{\ell 0}/k_{\rm B}T$. Note that the only parameters that these equations depend on (other than the variables a and T), are σ, which is an experimentally known function of temperature and pressure, and a_0 and C.

The dimensionless equilibrium scaling equations, in derivative form, along with the bare boundary values are summarized in Table 2.6 (using y, K, e) and Table 2.7 (using $\tilde{\Gamma}$, K, e). To solve these equations the bare values are needed: $y_{\rm eq}^{\ell 0} \approx \exp(-2\pi K^{\ell 0}C) = \exp(-\kappa^2\sigma\, C/2\pi k_{\rm B}T)$, $K_{\rm eq}^{\ell 0} = (\hbar/m)^2\sigma_{\rm s}^{\ell 0}/k_{\rm B}T = (\hbar/m)^2\sigma/k_{\rm B}T$, and $e_{\rm eq}^{\ell 0} = 0$. Using the Villain model approximation, which effectively sets $C = \pi/2$, the y bare value becomes $y_{\rm eq}^{\ell 0} \approx \exp(-\pi^2 K^{\ell 0}) = \exp(-\kappa^2\sigma/4k_{\rm B}T)$. Note this time that these equations depend only on the parameter σ and C, but not a_0.

The dimensionless non-equilibrium scaling equations, in derivative form, along with the bare boundary values are summarized in Table 2.8. To solve these equations the bare values are needed as well as an additional condition described in the section above and in the caption of Table 2.8.

2D Equilibrium Equations in terms of y, K, e

Interdependent Relations	Bare $\ell = 0$ ("$\ell 0$") Values
$\dfrac{\partial y}{\partial \ell} = y\,\{4 - 2\pi K\}$	$y(0) = \exp\bigl(-2\pi K^{\ell 0} C\bigr) = \exp\left(-\dfrac{\kappa^2}{4}\dfrac{\sigma}{k_{\mathrm{B}} T}\right)$
$\dfrac{\partial K}{\partial \ell} = -4\pi^3 K^2 y$	$K(0) = \left(\dfrac{\kappa}{2\pi}\right)^2 \dfrac{\sigma}{k_{\mathrm{B}} T}$
$\dfrac{\partial e}{\partial \ell} = -2\pi \exp(-2\ell)\, y$	$e(0) = 0$

Table 2.6: This summarizes the 2D equilibrium scaling equations, in terms of y, K, and e, with small-scale bare boundary values. For aesthetic purposes, the "eq" subscripts are not written. (The Villain approximation used here effectively sets $C = \pi/2$.)

2D Equilibrium Equations in terms of $\tilde{\Gamma}$, K, e

Interdependent Relations	Bare $\ell = 0$ ("$\ell 0$") Values
$\dfrac{\partial \tilde{\Gamma}}{\partial \ell} = -2\pi K \tilde{\Gamma}$	$\tilde{\Gamma}(0) = \exp\left(-\dfrac{\kappa^2}{4}\dfrac{\sigma}{k_{\mathrm{B}} T}\right)$
$\dfrac{\partial K}{\partial \ell} = -4\pi^3 \exp(4\ell)\, K^2 \tilde{\Gamma}$	$K(0) = \left(\dfrac{\kappa}{2\pi}\right)^2 \dfrac{\sigma}{k_{\mathrm{B}} T}$
$\dfrac{\partial e}{\partial \ell} = -2\pi \exp(2\ell)\, \tilde{\Gamma}$	$e(0) = 0$

Table 2.7: This summarizes the 2D equilibrium scaling equations, in terms of $\tilde{\Gamma}$, K, and e (since the non-equilibrium equations are written in terms of $\tilde{\Gamma}$), with small-scale bare boundary values. Note that $\tilde{\Gamma} = (a/a_0)^{-4} y = \exp(-4\ell) y$. For aesthetic purposes, the "eq" subscripts are not written.

2D Non-Equilibrium Equations in terms of $\tilde{\Gamma}$, K, e

Interdependent Relations	Bare $\ell = 0$ ("$\ell 0$") Values
$\dfrac{\partial \tilde{\Gamma}}{\partial \tau} = \dfrac{1}{r}\dfrac{\partial}{\partial r}\left[r\,\dfrac{\partial \tilde{\Gamma}}{\partial r} + 2\pi K \tilde{\Gamma} \right]$	$\tilde{\Gamma}(0,\tau) = \exp\left(-\dfrac{\kappa^2}{4}\dfrac{\sigma}{k_{\mathrm{B}} T} \right)$
$\dfrac{\partial K}{\partial \ell} = -4\pi^3 \exp(4\ell)\, K^2 \tilde{\Gamma}$	$K(0,\tau) = \left(\dfrac{\kappa}{2\pi} \right)^2 \dfrac{\sigma}{k_{\mathrm{B}} T}$
$\dfrac{\partial e}{\partial \ell} = -2\pi \exp(2\ell)\, \tilde{\Gamma}$	$e(0,\tau) = 0$

Table 2.8: This summarizes the 2D non-equilibrium scaling equations, with small -scale bare boundary values. In a numerical simulation of an instantaneous quench, the temperature T starts at some value in the first instant of time $\tau = 0$, and in the next instant $\tau = \Delta\tau$ the temperature is at some lower value. That immediately changes the bare values – or one can take $K(0,\tau)$ to change immediately and enforce continuity on $\tilde{\Gamma}(\ell,\tau)$ at $\ell = 0$, so that $\tilde{\Gamma}$ falls smoothly to it's new lower bare value. We take this latter approach. With the former approach, Eq. (2.267) can be used as the boundary condition. Either way, the results are similar.

2.2.5 Theoretical Plots

We can now present plots produced using the scaling equations in Table 2.6, equations that we noted above depend on the parameter σ. The density σ depends on the thickness of the film, which depends on temperature and vapor pressure. One should be able to use experimental data of σ to calculate $K^{\ell 0}$ and $y^{\ell 0}$ at any film thickness and temperature and integrate the scaling equations up to any desired length scale to know the properties of the superfluid helium film. Alternatively, we use a process described in Appendix B, to calculate each $K^{\ell 0}$ in terms of a critical value $K_{\mathrm{c}}^{\ell 0}$ ($= 0.747852$) that corresponds to the transition temperature: $K^{\ell 0} = (T_{\mathrm{KT}}/T) K_{\mathrm{c}}^{\ell 0}$. Thus, knowing T/T_{KT}, $K^{\ell 0}$ is calculated (and $y^{\ell 0}$ too, since it is a function of $K^{\ell 0}$ anyway). Note that this relationship, in addition to the definition of $K^{\ell 0}$, implies that σ is proportional to T_{KT}, and that since σ increases linearly with increasing film thickness, T_{KT} also increases linearly with film thickness. The proportionality constant is

$$\frac{\sigma}{T_{\mathrm{KT}}} \quad = \quad \frac{k_{\mathrm{B}} K_{\mathrm{c}}^{\ell 0}}{(\hbar/m)^2} \quad = \quad 4.10 \ \mathrm{g/cm^2K}, \tag{2.271}$$

where we've used the critical value $K_{\mathrm{c}}^{\ell 0} = 0.747852$. Furthermore, this argument extends to the superfluid density. In particular, examining the density as the critical temperature is approached, we find that since

$$\lim_{T \to T_{\mathrm{KT}}^-} \frac{\sigma_{\mathrm{s}}}{\sigma} \quad = \quad \lim_{T \to T_{\mathrm{KT}}^-} \frac{\sigma_{\mathrm{s}}^{\ell\infty}}{\sigma^{\ell 0}} \quad = \quad \lim_{T \to T_{\mathrm{KT}}^-} \frac{K^{\ell\infty}}{K^{\ell 0}} \quad = \quad \frac{K^*}{K_{\mathrm{c}}^{\ell 0}}, \tag{2.272}$$

the proportionality constant for the near-critical superfluid density per temperature is

$$\lim_{T \to T_{\mathrm{KT}}^-} \frac{\sigma_{\mathrm{s}}}{T} \quad = \quad \frac{K^*}{K_{\mathrm{c}}^{\ell 0}} \frac{\sigma}{T_{\mathrm{KT}}} \quad = \quad \frac{k_{\mathrm{B}} K^*}{(\hbar/m)^2} \quad = \quad 3.49 \ \mathrm{g/cm^2K}, \tag{2.273}$$

where we've used the critical fixed-point value $K^* = 2/\pi$. This is the famous result of Nelson and Kosterlitz of the universal "jump" line [83], although they cite the value 3.52 g/cm^{2}K. Both of these proportionalities are illustrated in Fig. 2.19.

Again, the process of integrating the scaling equations up in length scale to some ℓ_{max} can be accomplished by computer program with numerical methods such as Runge-Kutta (we use a fourth-order Runge-Kutta algorithm with step-size $\Delta\ell = 10^{-3}$). The larger ℓ_{max} is, the greater the separation of vortex pairs that are included in the calculation to drive down the superfluidity, as is shown in Fig. 2.18. By about $\ell_{\mathrm{max}} = 80$ the pairs have essentially made their full impact; increasing ℓ_{max} beyond 80 does not change the results much at all. Figures 2.20 and 2.21 show in detail how the vortex pairs increase in number and size with increasing temperature. In Fig.s 2.22 and 2.23, two theoretical superfluid-fraction plots are shown (one using the Villain model and one using a modified Villain model), compared with the data that we displayed in Section 2.2.1.

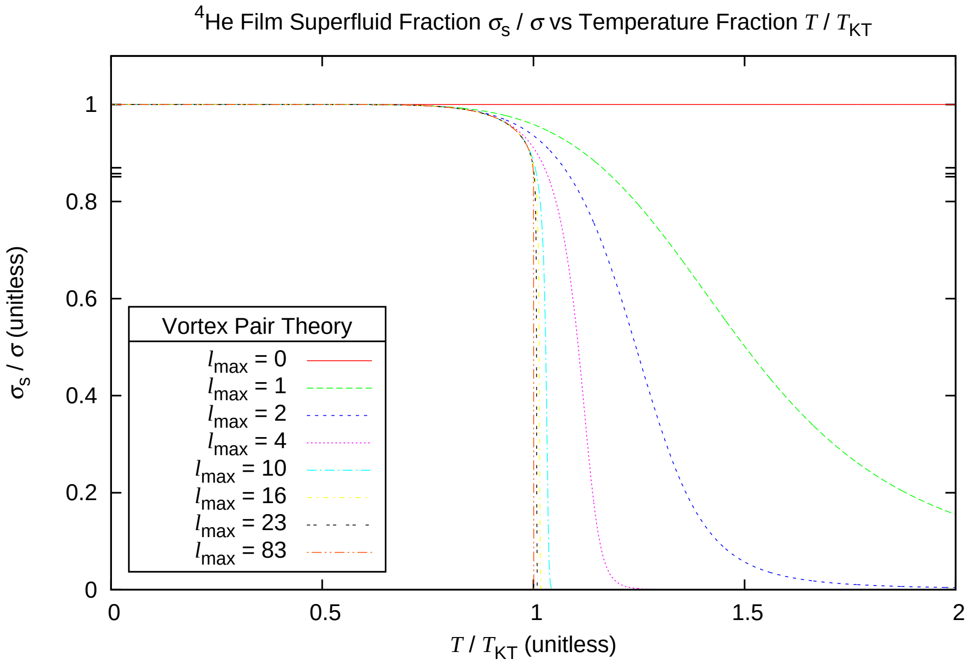

Figure 2.18: The superfluid fraction σ_s/σ is driven to zero as temperature increases and vortex pair excitations become more plentiful and larger, on average. At each temperature, we integrate the scaling equations up in length scale to some ℓ_{max} to calculate the superfluid fraction $\sigma_s/\sigma = K/K^{\ell 0}$. Stringing the points together for a given ℓ_{max}, we get the curves above. For $\ell_{max} = 0$, where no vortex pairs are included in the calculation, the superfluid is pure-superfluid at any temperature. For $\ell_{max} = 1$, which corresponds to including pairs of separation $a = a_0 \exp(1) \approx 6.8$ Å and smaller (since $a_0 \approx 2.5$ Å), a smooth transition from pure-superfluid to normal fluid is seen. By $\ell_{max} = 20$, with pairs of separation $a \approx 10$ cm and smaller, the transition is quite sharp, falling from a value of 0.869702 (marked but unlabeled on vertical axes) to zero over a small temperature interval. The $\ell_{max} = 83$ scale corresponds to $a \approx 10^{26}$ m, the size of observed universe (which is, by the way, not size of universe at present), and at T_{KT} $K/K^{\ell 0} = 0.857343$ (also marked). As $\ell_{max} \to \infty$, at T_{KT} we have $K/K^{\ell 0} \to K^*/K_c^{\ell 0} = (2/\pi)/0.747852 = 0.851263$ (again, marked and unlabeled), where K^* is the critical fixed-point value of K.

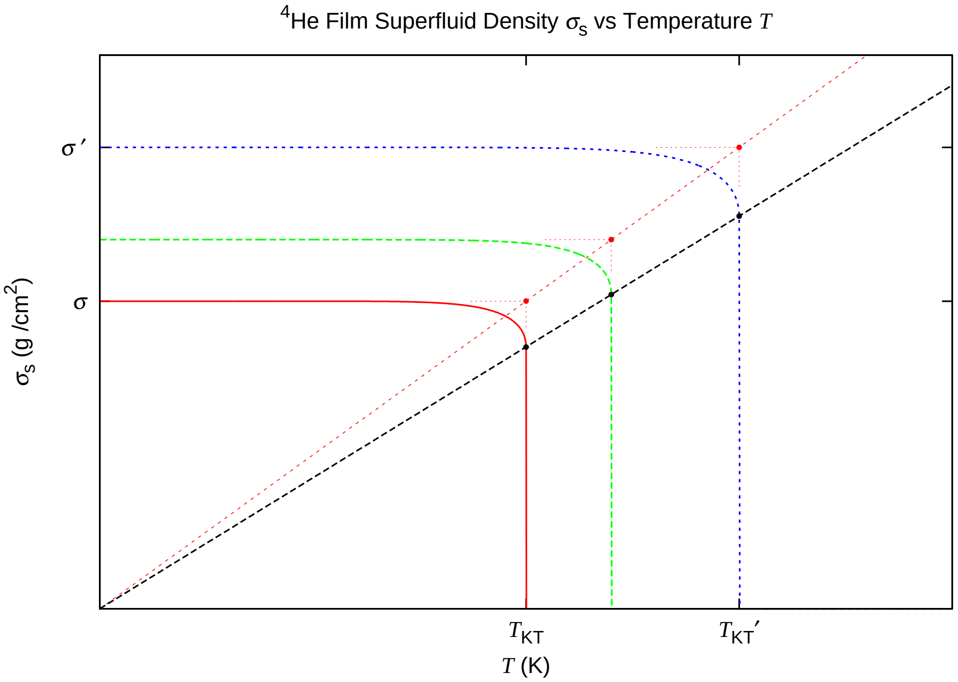

Figure 2.19: The two ratios in Eq. (2.271), $\sigma/T_{\mathrm{KT}} = 4.10\,\mathrm{g/cm^2K}$, and Eq. (2.273), $\lim_{T\to T_{\mathrm{KT}}^-}(\sigma_{\mathrm{s}}/T) = 3.49\ \mathrm{g/cm^2K}$, are illustrated with the two straight lines in this graph. The line with greater slope shows that the critical temperature T_{KT} scales linearly with the film thickness or density σ. The line with smaller slope is the famous result of Nelson and Kosterlitz of the universal "jump" line, where the macroscopic superfluid density jumps to zero at T_{KT}. The critical jump value of σ_{s} increases linearly with critical temperature T_{KT} and the film thickness or density σ.

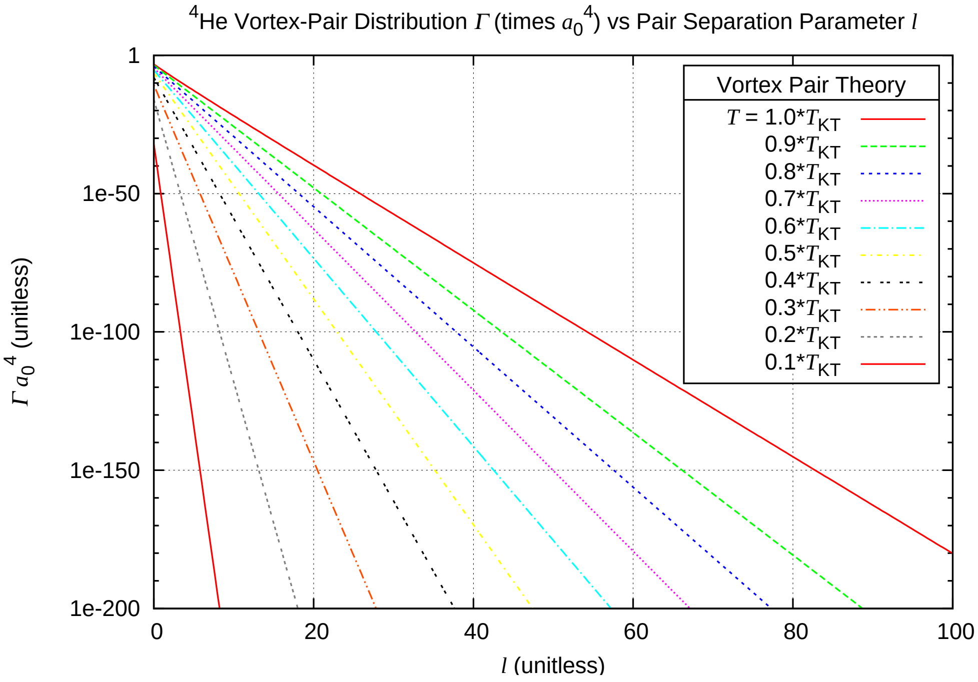

Figure 2.20: As temperature increases, the number of vortex pairs at any given length-scale (with corresponding separation $a = a_0 \exp(\ell)$) increases, with the larger vortex pairs multiplying more quickly. As stated in the caption of the previous figure, as temperature increases, the vortex pair excitations become more plentiful and larger, on average. These plots use $\ell_{\max} = 100$.

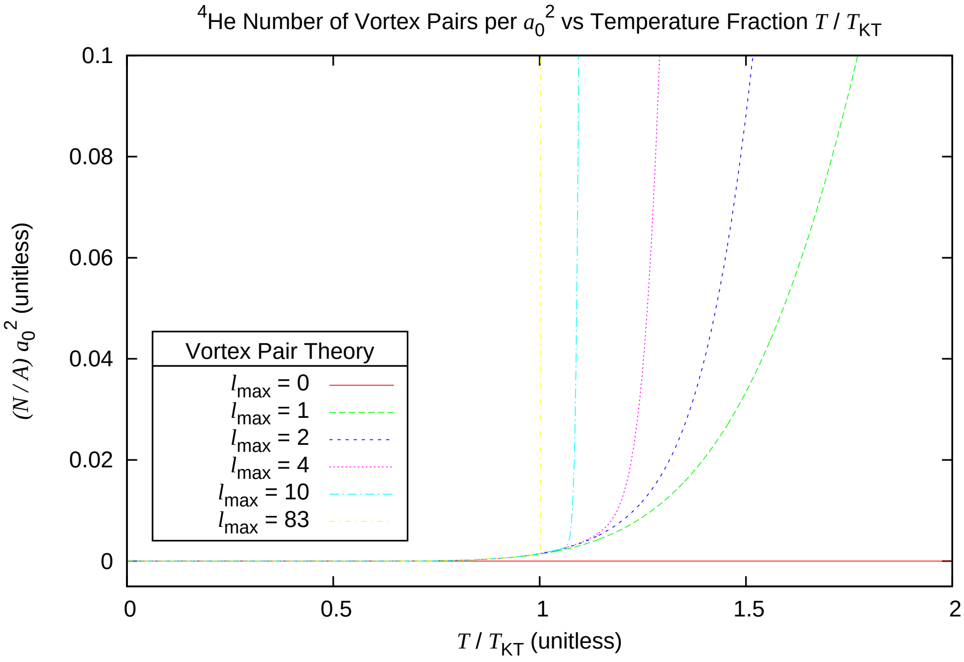

Figure 2.21: To obtain these plots of number density of vortex pairs, one can either integrate the pair distribution Γ or multiply the free energy parameter e by a negative factor: -1. This gives the average number of vortex pairs, of any and all pair-separations, *centered* in an area a_0^2. In a sharp transition, the number of vortex loops really explodes at the critical temperature T_{KT}.

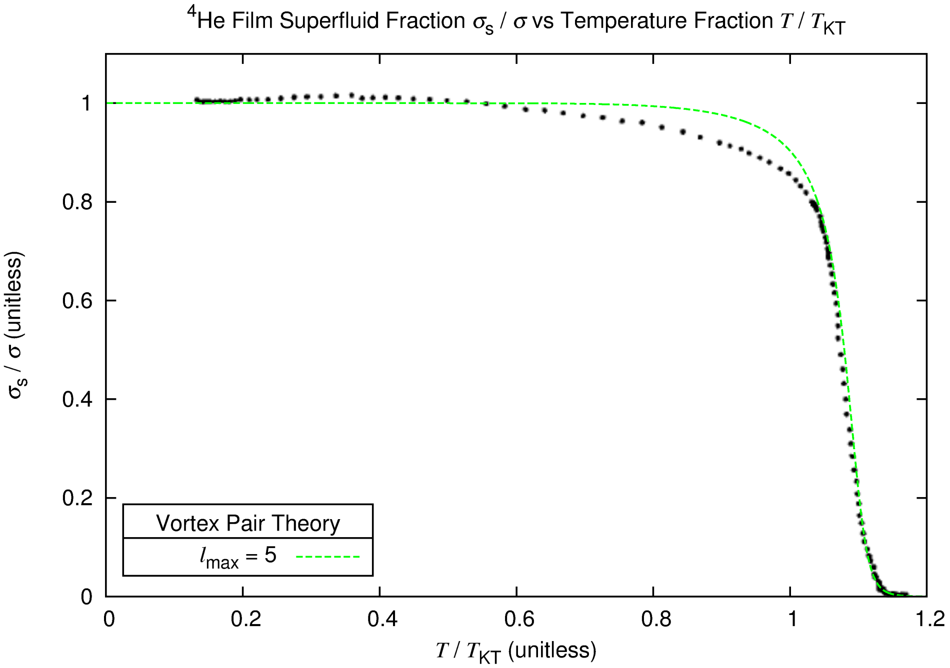

Figure 2.22: This is the first of two figures showing how the vortex pair theory compares to and generally agrees with one of the data sets of Agnolet *et alia* [80] shown in Fig. 2.17. The deviation between the two plots is adjusted in the next figure. An $\ell_{\max}$ of about 5 is required to match the tail of the transition. Just considering the size and shape of the apparatus (enabling a maximum separation probably on the order of centimeters), one would expect $\ell_{\max} \approx 19$. But since these data were gathered from a dynamic system (using a torsion oscillator with frequency on the order of kilohertz) rather than a static system, there are finite-frequency effects: the larger vortex pairs cannot move and respond as quickly as the smaller pairs in canceling out the superflow, so the larger vortex pairs are left out of the superfluid fraction calculation, emulating the finite-size effect of reducing $\ell_{\max}$ [74]. According to Hieda, Matsuda, *et alia* [84], a frequency of about $f = 1$ kHz should correspond to a size (or diffusion length) of about $\sqrt{14D/\omega} = (14 \text{ nm})\sqrt{(180 \text{ MHz})/f} = 6$ µm, or $\ell_{\max} \approx 10$, on a gold substrate, where the diffusion constant D strongly depends on the kind of substrate. It is possible that the nature of Mylar and the construction of the system reduce this figure further to 5.

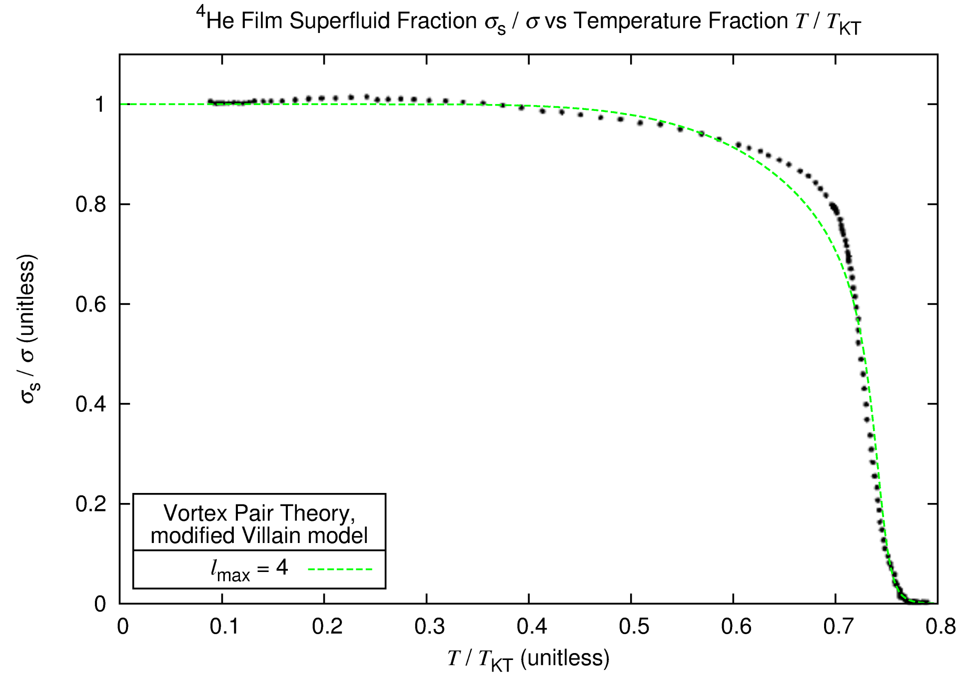

Figure 2.23: This is the second of two figures showing how the vortex pair theory compares to and generally agrees with one of the data sets of Agnolet *et alia* [80] shown in Fig. 2.17. The main difference between this and the previous figure is that the Villain model approximation, which is $2U_{\mathrm{core}}/k_{\mathrm{B}}T = \pi^2 K^{\ell 0}$, has been altered here to be $2U_{\mathrm{core}}/k_{\mathrm{B}}T = \frac{1}{2}\pi^2 K^{\ell 0}$. Perhaps a reduction of the core energy by 3/4 rather than 1/2 would produce an even more satisfying match, but more investigation would have to be done to confirm that the new Villain approximation is appropriate for the experimental system that produced these data. In another experiment, Cho and Williams [85] measured a core energy of about half the Villain value, and found data that resemble this theoretical plot a bit more. Note that $\ell_{\mathrm{max}} = 4$ was used in this theoretical plot to match the tail of the transition, which is not significantly different from the match achieved with $\ell_{\mathrm{max}} = 5$ in the previous figure.

CHAPTER 3

3D Equilibrium under Pressure

3.1 Vortex-Loop Thermodynamics of Superfluid Helium-4 under Pressure

It has been shown previously by Williams [86, 87] and Shenoy [58, 78] that the vortex loop theory of the superfluid phase transition accurately describes, at saturated vapor pressure, the critical behavior of the superfluid fraction and the heat capacity of helium-4 at T_λ. We presently show that the theory in its current state consistently describes the pressure dependence of the superfluid fraction and the heat capacity, in agreement with the expectations of universality, as well as the pressure dependence of the vortex-loop core diameter and the smallest-loop energy. We suggest that the smallest vortex loops of the theory may be crude approximations for rotons. Additionally, we present calculations of a quantity X introduced by Ferer [88] that relates to an algebraic combination of the superfluid-fraction and specific-heat critical amplitudes, and we find that it is indeed universal.

The vortex theory has two non-universal parameters, a_0 and C, which must be obtained from experimental data[1] and will be explained below. From these parameters all of the equilibrium thermodynamics of the fluid can be derived – including the distribution and energies of the vortex loops, the superfluid fraction, and the heat capacity –

---

[1] We use an equivalent but less obviously non-universal pair $K^{\ell 0}$ and C, and in our quantitative arguments below, we use experimental superfluid critical amplitudes to obtain their pressure dependence.

within about 200 µK below T_λ and, as we'll see, over all relevant pressures.

Let us summarize the derivation of the results before presenting them, starting with Eq. (3.8) and Fig. 3.7. The quantized circulation of the vortex loops is $\kappa = h/m$, where h is Planck's constant and m is the mass of the helium-4 atom. The core of a loop has a diameter a_0 on the order of angstroms. The loops are generally thermally excited and distorted out of a circular shape into a loop with many wiggles. Still, the fluid velocity flow field of a given distorted loop can be approximated by a "best fit" circular loop with diameter a and core diameter a_c such that most of the wiggles occur within its core. On average, the dipole flow field of the loops orient to oppose an applied flow in the fluid, similar to a diamagnetic effect of electric current loops. As the effect of the loops is included, from the smallest loops to the largest, in a renormalized calculation upon a pure superfluid background, the superfluid fraction is decreased, from 1 at the smallest scale (a_0) to ρ_s/ρ at the largest scales, where ρ is the fluid density and ρ_s is the bulk, large-scale pure superfluid density. Thus the superfluid density is a renormalized, length-scale dependent quantity, which we'll denote with a superscript "r", $\rho_\mathrm{s}^\mathrm{r}(a)$, and a thus also refers to length scale. (To reduce clutter we will not use an "r" superscript on most other length-scale dependent quantities, and for those quantities we'll use a superscript "$\ell\infty$" to indicate the macroscopic value.) We take the bare superfluid density $\rho_\mathrm{s}^\mathrm{r}(a_0)$ to be the fluid density: $\rho_\mathrm{s}^\mathrm{r}(a_0) \equiv \rho_\mathrm{s}^{\ell 0} = \rho$. (As with $\rho_\mathrm{s}^{\ell 0}$ we will generally use a superscript "$\ell 0$" to denote the bare, smallest length-scale value.) The renormalized energy of a vortex loop is $U = \frac{1}{4}\kappa^2 \rho_\mathrm{s}^\mathrm{r} a\{\ln(a/a_\mathrm{c}) + C\}$, where the "core parameter" C relates to the energy per effective-diameter-length of the vortex core. Although we use classical fluid dynamical expressions, such as that for the energy U, we find that the energy magnitude and pressure-dependence of the smallest vortex "loop" of diameter a_0 approximately matches that of the roton quantum excitation. Let V, T, and P be the volume, absolute temperature, and absolute pressure of the system of fluid, respectively, and let k_B be the Boltzmann constant. Let F be the Helmholtz free energy of the fluid due to the vortex loops and $f = F/V$ be same free energy per fluid volume. The following dimensionless parameters are also useful: the "superfluid parameter" $K_{\rm s} \equiv a_0(\hbar/m)^2\rho_{\rm s}^{\rm r}/k_{\rm B}T$, the "coupling" $K \equiv (a/a_0)K_{\rm s} = a(\hbar/m)^2\rho_{\rm s}^{\rm r}/k_{\rm B}T$, the "fugacity"[2] $y = (a/a_0)^6\exp(-U/k_{\rm B}T)$, the "Helmholtz parameter" $e \equiv (F/k_{\rm B}T)(a_0^3/V)$, and the "length scale parameter" $\ell = \ln(a/a_0)$. So "$\ell 0$", or $\ell = 0$, corresponds to a_0, and for "$\ell\infty$", $\ell = 10$ is generally large enough for our calculations. An ansatz of the theory, with some evidence from the numerical simulations of Chattopadhyay, Mahato, and Shenoy [58], is that the effective core diameter relates to the effective diameter, coupling, and core parameter by $a_{\rm c} = aK^\theta\exp(C)$, where $\theta = D/[(D+2)(D-2)] = 0.6$ (for $D = 3$ dimensions) is similar to the Flory exponent familiar from polymer physics. This relation for $a_{\rm c}$ was calculated to be applicable for large length scales, but we apply it to all length scales. It can only be approximately true at the smallest scales, since $a_{\rm c}$ must approach a_0 for the smallest loops.

With this background we can now present the scaling relations of the theory, first in dimensionful integral form:

$$\frac{U(a)}{k_{\rm B}T} = \frac{U(a_0)}{k_{\rm B}T} + \pi^2\int_{a_0}^{a}\frac{a_0\kappa^2\rho_{\rm s}^{\rm r}(a')}{(2\pi)^2k_{\rm B}T}\left\{1-\theta\ln\left[\frac{a'\kappa^2\rho_{\rm s}^{\rm r}(a')}{(2\pi)^2k_{\rm B}T}\right]\right\}\frac{{\rm d}a'}{a_0} \tag{3.1}$$

$$\frac{1}{\rho_{\rm s}^{\rm r}(a)} = \frac{1}{\rho_{\rm s}^{\rm r}(a_0)} + \frac{4\pi^3}{3}\int_{a_0}^{a}\frac{a_0(\hbar/m)^2}{k_{\rm B}T}\left(\frac{a'}{a_0}\right)^4\exp\left[-\frac{U(a')}{k_{\rm B}T}\right]\left(\frac{a'}{a_0}\right)^2\frac{{\rm d}a'}{a_0} \tag{3.2}$$

$$\frac{f(a)}{k_{\rm B}T} = -\frac{\pi}{a_0^3}\int_{a_0}^{a}\exp\left[-\frac{U(a')}{k_{\rm B}T}\right]\left(\frac{a'}{a_0}\right)^2\frac{{\rm d}a'}{a_0}, \tag{3.3}$$

where, again, $\rho_{\rm s}^{\rm r}(a_0) = \rho$, and $U(a_0)/k_{\rm B}T = a_0\kappa^2\rho C/4k_{\rm B}T$, since $U(a_0)/k_{\rm B}T = \pi^2K^{\ell 0}C$ and $K^{\ell 0} = a_0(\hbar/m)^2\rho_{\rm s}^{\ell 0}/k_{\rm B}T$. Note that the only parameters that these equations depend on (other than the variables a and T), are ρ, which is an experimentally known function of temperature and pressure, and a_0 and C. (We use a fourth order polynomial fit of helium density data from Brooks and Donnelly [71] to approximate ρ.) If we rewrite

---

[2] The parameter y is commonly called the fugacity, but we have not seen a proof that this is the fugacity as it is usually defined.

these equations in dimensionless derivative form,

$$\frac{\partial y}{\partial \ell} = y\left\{6 - \pi^2 K\left(1 - \theta \ln K\right)\right\} \tag{3.4}$$

$$\frac{\partial K}{\partial \ell} = K - \frac{4\pi^3}{3}K^2 y \tag{3.5}$$

$$\frac{\partial e}{\partial \ell} = -\pi \exp(-3\ell)\, y, \tag{3.6}$$

where $y(0) = \exp(-\pi^2 K^{\ell 0} C)$, $K(0) = K^{\ell 0}$, and $e(0) = 0$, and if we do not expand $K^{\ell 0}$ in terms of its definition as shown above, then there are only two parameters that determine the solution: $K^{\ell 0}$ and C. If one wishes to describe the thermodynamics in terms of superfluid fraction instead of fluid densities, then there is no need to use ρ since these two parameters are sufficient. In that sense, the vortex loop theory depends on two, rather than three, non-universal parameters. Note that a_0, C, and $K^{\ell 0}$ all depend on temperature and pressure.

Eq.s (3.4) and (3.5) have a fixed point, that is, a point (K^*, y^*) in the K-y plane, such that $\partial y/\partial \ell\,(K^*, y^*) = 0$ and $\partial K/\partial \ell\,(K^*, y^*) = 0$. Actually, there are two fixed points, but one of them is not physically relevant while the other is relevant. It is easy to solve for the fixed points, the relevant point being $(K^*, y^*) = (0.38750818971, 0.062421005458)$. (See Appendix B for this calculation and explanation of the physical relevance.) If C and $K^{\ell 0}$ are chosen such as to cause K and y to approach this fixed point as ℓ increases, then[3] K_{s} and $\rho_{\mathrm{s}}^{\mathrm{r}}$ behave asymptotically as a^{-1} (since K becomes constant) and approach zero as ℓ approaches infinity. Of all behaviors that $\rho_{\mathrm{s}}^{\mathrm{r}}$ may take, this is the slowest approach to zero possible and represents the point of critical phase transition. The faster approaches to zero represent temperatures above T_λ, and the other possibility is $\rho_{\mathrm{s}}^{\mathrm{r}}$ approaches a non-zero constant, meaning there is superfluidity on the macroscopic scale and the temperature is below T_λ.

Such a pair $(C, K^{\ell 0})$ that lead to this fixed point are a critical pair $(C_{\mathrm{c}}, K_{\mathrm{c}}^{\ell 0}) =$

---

[3] Keep the definitions $K_{\mathrm{s}} \equiv a_0(\hbar/m)^2\rho_{\mathrm{s}}^{\mathrm{r}}/k_{\mathrm{B}}T$ and $K \equiv (a/a_0)K_{\mathrm{s}}$ in mind for the next few statements.

$(C(T_\lambda), K^{\ell 0}(T_\lambda))$, and they only depend on pressure. To find a critical pair, one can select a value for C_c, then vary $K^{\ell 0}$ and use the equations and some numerical technique to step K and y out with ℓ, and the closer $K^{\ell 0}$ is to its critical value $K_\mathrm{c}^{\ell 0}$, the more the plots of K and y will approach constant values over larger length-scales before veering off. Example plots illustrating this process are included in Fig.s 3.1, 3.2, and 3.3. This is how we solve for $K_\mathrm{c}^{\ell 0} = a_0(\hbar/m)^2 \rho_\mathrm{s}^{\ell 0}/k_\mathrm{B} T_\lambda$, starting with some C_c and using a fourth-order Runge-Kutta method, without yet knowing a_0, ρ, or T_λ, all of which depend on pressure and two of which depend on temperature (where those temperature dependencies must cancel out). At this point we can find sets of critical pairs, but we do not know what pressures they correspond to. Note that we must solve for $K_\mathrm{c}^{\ell 0}$ to double (floating point) precision, with many significant digits, because this allows us to examine temperatures very close to T_λ, as we'll explain parenthetically below.

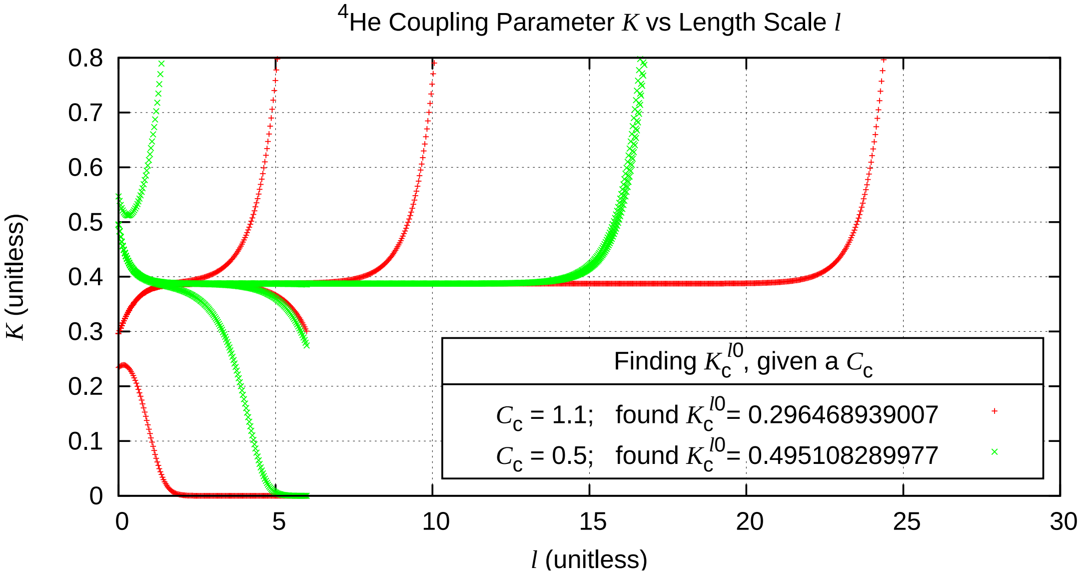

Figure 3.1: Given a critical core parameter, say $C_{\rm c} = 1.1$, an initial $K^{\ell 0}$ is chosen and an initial variation $\Delta K^{\ell 0}$. (We chose $K_{\rm i}^{\ell 0} = 5$ and $\Delta K_{\rm i}^{\ell 0}$=5 since we assume $K_{\rm c}^{\ell 0}$ should be somewhere between 0 and 10.) We use fourth order Runge-Kutta to step out K (and y) in terms of ℓ, and if K blows up (exceeds 0.8, say) then $K^{\ell 0}$ is too large and we decrease it by $\Delta K^{\ell 0}/2$ on the next go around, or if K implodes (decreases after $\ell = 6$) then $K^{\ell 0}$ is too small and we increase it by $\Delta K^{\ell 0}/2$ on the next go around. In this manner, after each go (i.e., each application of Runge-Kutta to step out K), we find a more precise approximation of the $K_{\rm c}^{\ell 0}$ associated with the given $C_{\rm c}$, and the plots of K stay constant at the fixed-point value $K^* = 0.38750818971$ for longer stretches over ℓ.

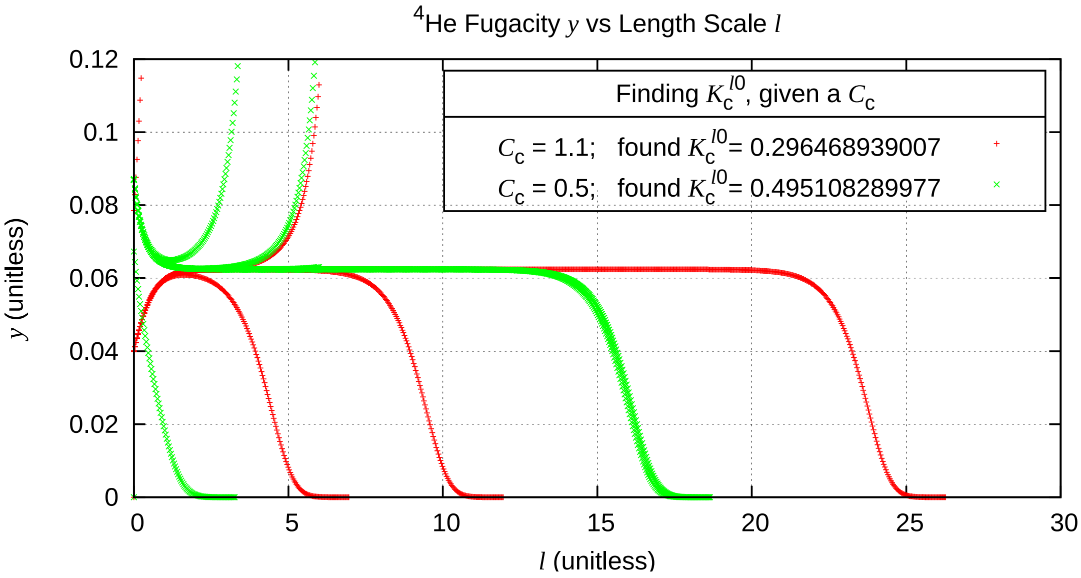

Figure 3.2: The process described in Fig. 3.1 could equivalently utilize y instead of K. As a more precise approximation of $K_c^{\ell 0}$ is found, the plots of y stay constant at the fixed-point value $y^* = 0.062421005458$ for longer stretches over ℓ.

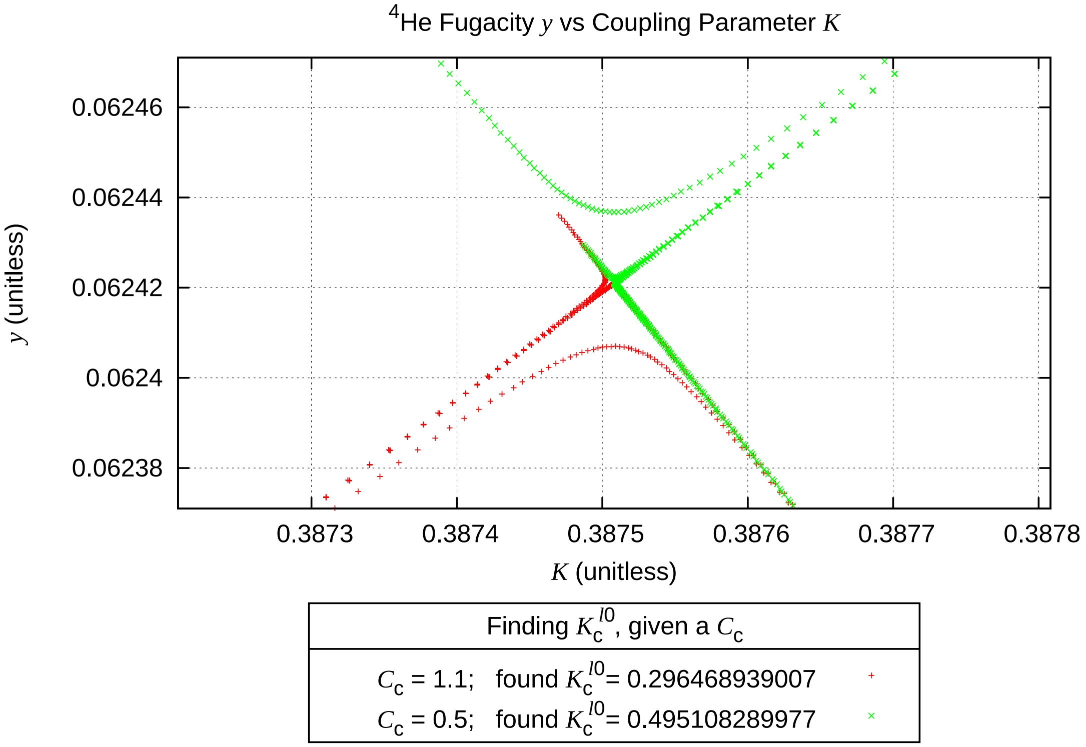

Figure 3.3: The process described in Fig.s 3.1 and 3.2 can be shown in the K-y plane, where the approach to the fixed point $(K^*, y^*) = (0.38750818971, 0.062421005458)$ as ℓ increases becomes apparent. If the $K^{\ell 0}$ chosen in sufficiently close to the critical value $K_c^{\ell 0}$ (associated with the given C_c) then the "flow" of the (K, y) points with increasing ℓ comes very close to the fixed point. The flow swoops away at some point, unless $K^{\ell 0}$ is chosen exactly to be $K_c^{\ell 0}$. This is the renormalization-group (RG) flow near the fixed point.

Given a critical pair with an as yet unknown pressure, we can solve for $K^{\ell 0}$ at all other normalized temperatures T/T_λ using the relation $K^{\ell 0}/K^{\ell 0}_{\mathrm{c}} = T_\lambda/T$ inherent in the definitions. (From this relation we can see that if we want to resolve temperatures T very close to $T_\lambda \approx 2$ K, then we must solve for $K^{\ell 0}_{\mathrm{c}}$ to great precision.) Unfortunately, since we do not know the temperature dependence of C, we cannot extrapolate more values of C from C_{c}, but we assume near the critical temperature T_λ that $C \approx C_{\mathrm{c}}$. (This is why the theory is only accurate near T_λ, but it could be made more accurate by inserting experimental knowledge of the temperature dependence of C.) Again using the Runge-Kutta method, we use various pairs of C and $K^{\ell 0}$ near T_λ to create a plot of superfluid fraction versus relative temperature. Replicating this process for multiple critical pairs, we can compare the multiple resulting plots with experimental plots find the pressure dependence of C_{c}, $K^{\ell 0}_{\mathrm{c}}$, and $K^{\ell 0}$, as well as C near T_λ. The key in making the comparison is that, at any pressure, the superfluid fraction near T_λ follows a power law,

$$\frac{K^{\ell\infty}_{\mathrm{s}}}{K^{\ell 0}} = \frac{\rho_{\mathrm{s}}}{\rho} = A'\tau^{\nu}, \tag{3.7}$$

where $\tau = (1-T/T_\lambda)$, with a critical exponent ν and a critical amplitude A' that depends on pressure. Extending the fixed-point analysis above, one can solve analytically for ν in terms of K^*, where $\nu = 2/(-1+\sqrt{1+4x})$ with $x = \pi^2 K^*[1-\theta(1+\ln K^*)]$, and we get $\nu = 0.67168835$, in agreement with the best simulation calculations to date [64, 65]. (See Appendix B for the procedure to calculate ν and an alternate method of calculating $K^{\ell 0}_{\mathrm{c}}$.) By fitting data of Greywall and Ahlers [79] to this power law using our value for ν (see Fig. 3.4), we find the pressure dependence of A' (see Fig. 3.5) and invert the relationship to find a pressure for a given amplitude. In this way we link each critical pair (C_{c},$K^{\ell 0}_{\mathrm{c}}$), via its resulting critical amplitude, to a pressure and obtain a fit for $C_{\mathrm{c}}(P)$ and $K^{\ell 0}_{\mathrm{c}}(P)$ shown in Fig. 3.6.

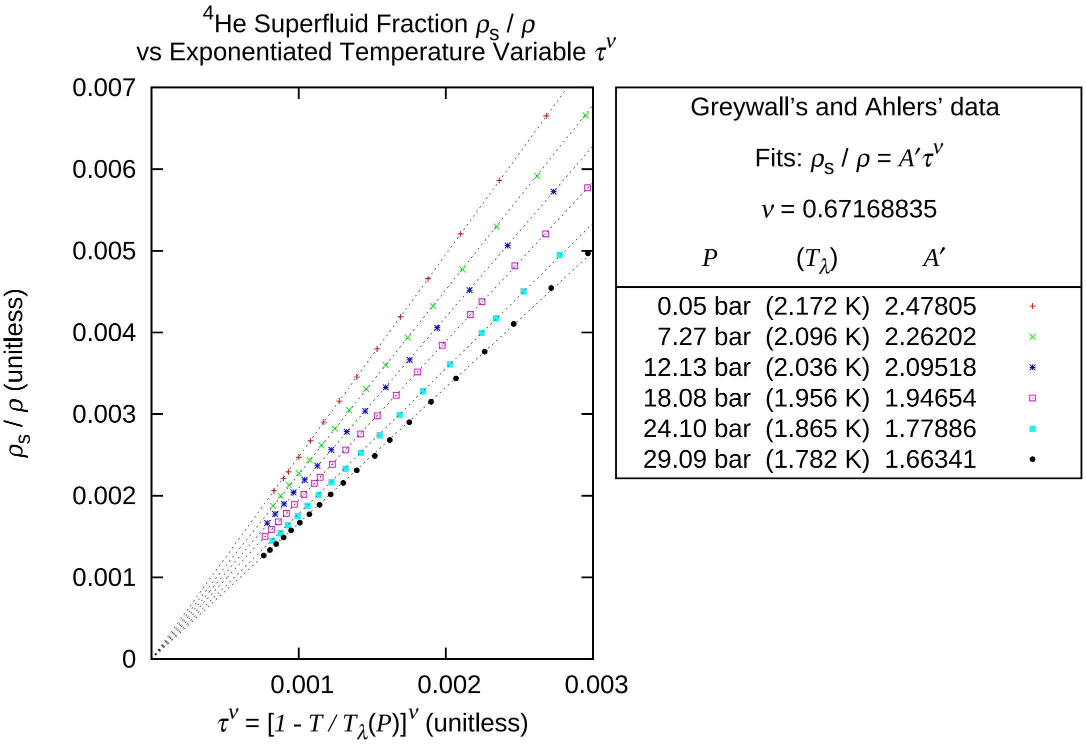

Figure 3.4: These fits of Greywall's and Ahlers' data [79] allow for the pressure characterization of A' and thus the rest of the parameters, including C_{c} and $K_{0\mathrm{c}}$. The fits were performed from T_λ, where $\tau = 0$, down to $\tau = 1.75 \times 10^{-4}$, or $\tau^\nu \approx 3 \times 10^{-3}$. For greater τ, the superfluid fraction starts to deviate from this power law, eventually approaching a constant 1 towards zero absolute temperature, where $\tau = 1$.

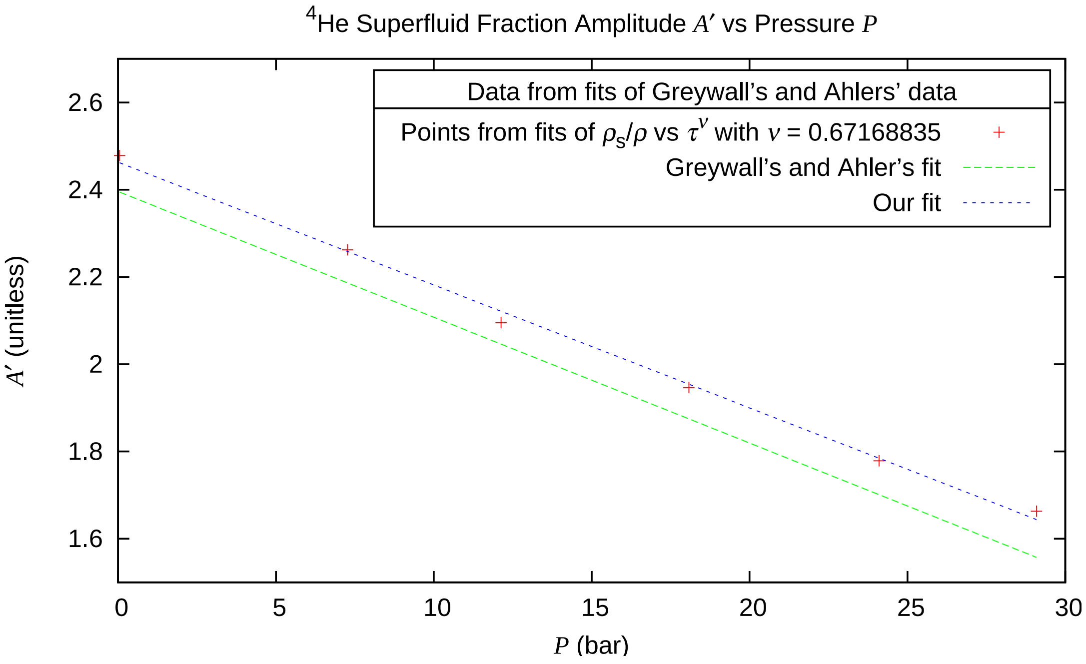

Figure 3.5: Plotting the amplitudes found in Fig. 3.4, we find a fit for the pressure dependence of A'. Our fit, $2.463-(0.02815 \text{ bar}^{-1})P$, assumes a constant critical exponent $\nu = 0.67168835$, whereas Greywall's and Ahlers' fit, $2.396 - (0.02883 \text{ bar}^{-1})P$, takes the critical exponent to be another fitting parameter that is found to oscillate between 0.66 and 0.68 around our value of ν.

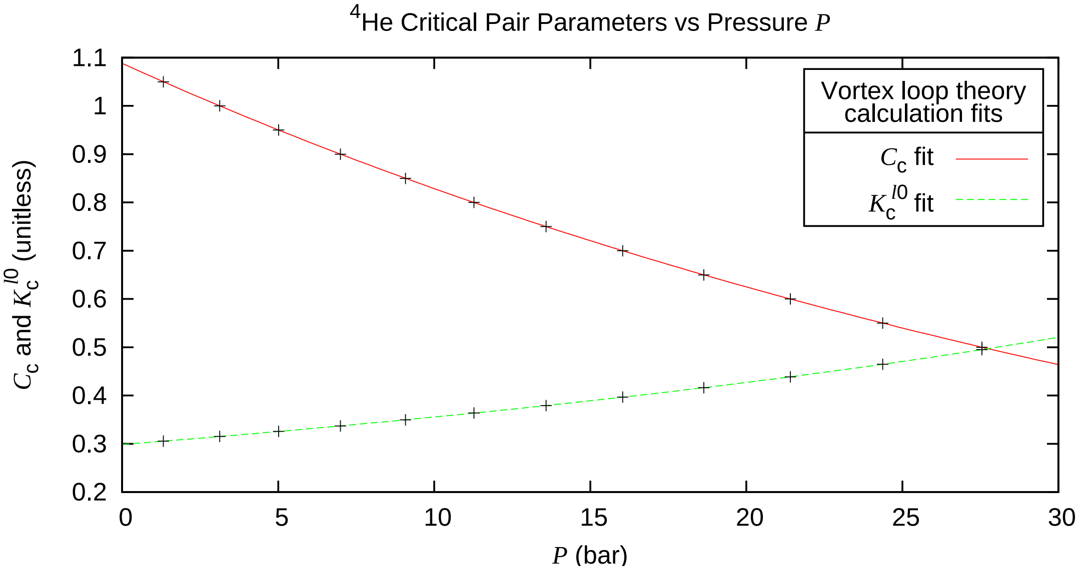

Figure 3.6: Each critical pair $(C_c, K_c^{\ell 0})$ yields a plot of superfluid fraction ρ_s/ρ with a certain critical amplitude A'. Using the relationship between A' and pressure P shown in Fig. 3.5 we can link each critical pair to a pressure, shown here. Note that the core parameter C relates to the core energy of the vortex loops, and since this is lower at higher pressures, one would expect that it is easier for vortex loops to form at higher pressures and that the superfluid fraction would thus more easily be reduced. This logic is confirmed in Fig. 3.4.

With this pressure dependence found, we can use $K_{\mathrm{c}}^{\ell 0}(P)$ along with experimental data of $T_\lambda(P)$ and $\rho(T,P)$ to find the temperature and pressure dependence of the core diameter a_0 using the definition of $K^{\ell 0}$ and its relation to $K_{\mathrm{c}}^{\ell 0}$:

$$a_0(T,P) \;=\; \left(\frac{m}{\hbar}\right)^2 \frac{k_{\mathrm{B}} T_\lambda(P)}{\rho(T,P)} K_{\mathrm{c}}^{\ell 0}(P). \tag{3.8}$$

This relation holds over all temperatures. Comparing plots of $a_0(P)/a_0(0)$ at T_λ and 0.3 K with a similar plot of data from Glaberson [89] at 0.3 K, shown in Fig. 3.7, we find a similar trend.

We can also now examine the energy of the smallest vortex loops, again using $K_{\mathrm{c}}^{\ell 0}$:

$$U^{\ell 0}(T_\lambda, P) = \pi^2 K_{\mathrm{c}}^{\ell 0}(P)\, C_{\mathrm{c}}(P)\, k_{\mathrm{B}} T_\lambda(P). \tag{3.9}$$

This relation only holds near T_λ, as indicated, since we only know C near that temperature. In Fig. 3.8, a plot of this energy (in kelvins) versus pressure is shown along with neutron scattering data collected by Brooks and Donnelly [71] of the (minimum) roton energy at T_λ. Roughly the same pressure dependence is apparent. We suggest that these smallest vortex loops may be crude approximations for rotons.

The physical structure of rotons and their relation to other excitations is a controversial topic with a rich body of research, but our results do lend a small amount of support to the idea of a rough relationship between rotons and the smallest vortex loops. Here, we quote some of the literature that seems to leave this relationship an open possibility and one paper that strongly supports it. From Roberts and Berloff [54] we find these statements:

> “One of the goals of these calculations was to clarify Onsager’s concept of the roton as ‘the ghost of a vanished vortex ring.’ One can hope that the transition from the vortex ring to the sound pulse and the concomitant loss of vorticity would occur close to the roton minimum in energy-momentum

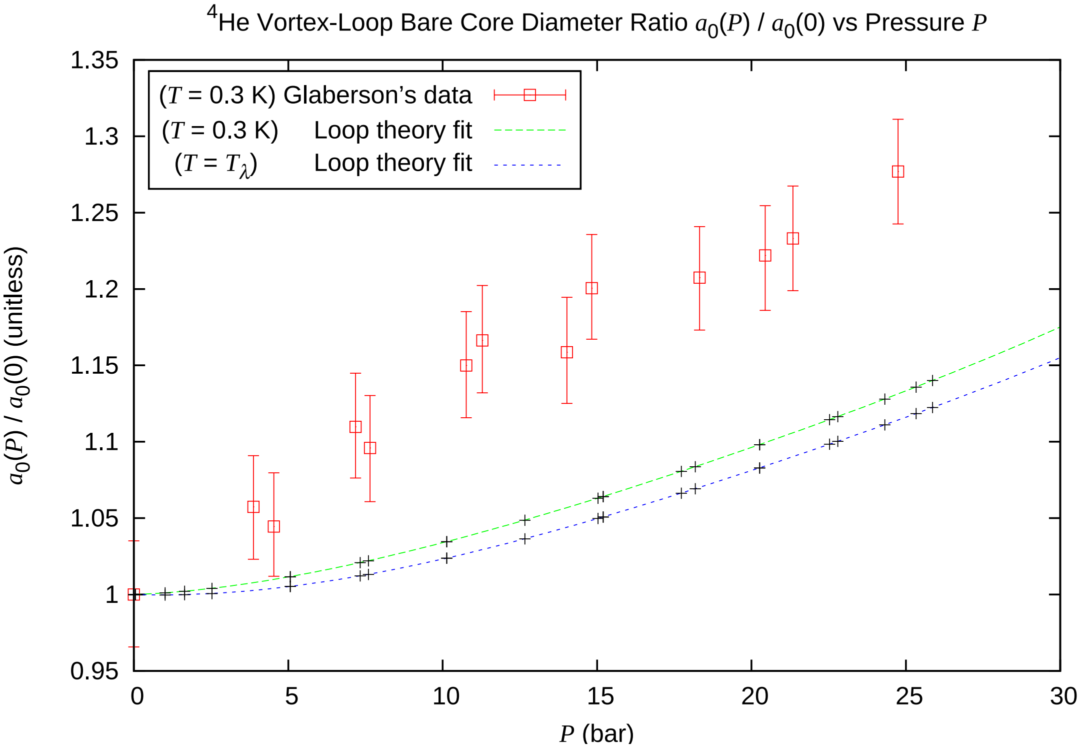

Figure 3.7: Here we compare measurements of Glaberson [89] with our backward-engineered values of a_0, using Eq. (3.8). The trends are similar. The difference reaches about 10% at 25 bar. We should note that the experimental measurements are based on an assumption of circular vortex loops [90] while the loops should actually be distorted [91]. The difference between these plots also may suggest that one or more of our simplifying assumptions is slightly inaccurate. (For example, the assumption that small-effective-core equations can be used for larger loops is perhaps an oversimplification.)

> space, or (more probable) close to the point where the group velocity and the phase velocity are equal (the Landau critical velocity u_L). Their calculations show that indeed there is a point on the $p\mathcal{E}-$ plane where the ring ceases to exist and where $u_L = \partial E/\partial p$, but this point lies far from the roton minimum. It remains to be seen whether the idea of the roton as a ghostly vortex ring will ever be vindicated. As one has a great variety of potentials that lead to the Landau dispersion curve one can tune the parameters so that the line $\mathcal{E} = u_L p$, meets the $p\mathcal{E}-$ curve for the family of the vortex rings, to allow this sequence of vortex rings to be terminated at a lower energy and momentum level. Whether this process will lead to coalescence with the roton minimum is not yet clear."

We also find statements by various others [92] that the rotons may be "ghosts of a Bragg peak". This and other perspectives such as the roton-as-"ghost of a vanished vortex ring" may not be contradictory but roughly correct given different limits. Here is strong support for the roton-vortex connection from a paper by Galli, Cecchetti, and Reatto [48]:

> "Our computation vindicates many arguments of Feynman and gives them a quantitative basis. Exactly at $q = q_R$ a simple dipolar flow due to backflow is present like in a small vortex ring."

But this is tempered by later statements from Reatto and Galli [49]:

> "...we find that the [roton] excitations [of several models] have in a varying degree characters of single particle, of non quantized smoke ring and of collective excitation. ...This study has shown that none of the models introduced so far capture the full complexity of rotons."

Finally, we can move toward finding the pressure dependence of the loop-theory heat capacity. By construction, the theory is based on parameters that, when set, correspond

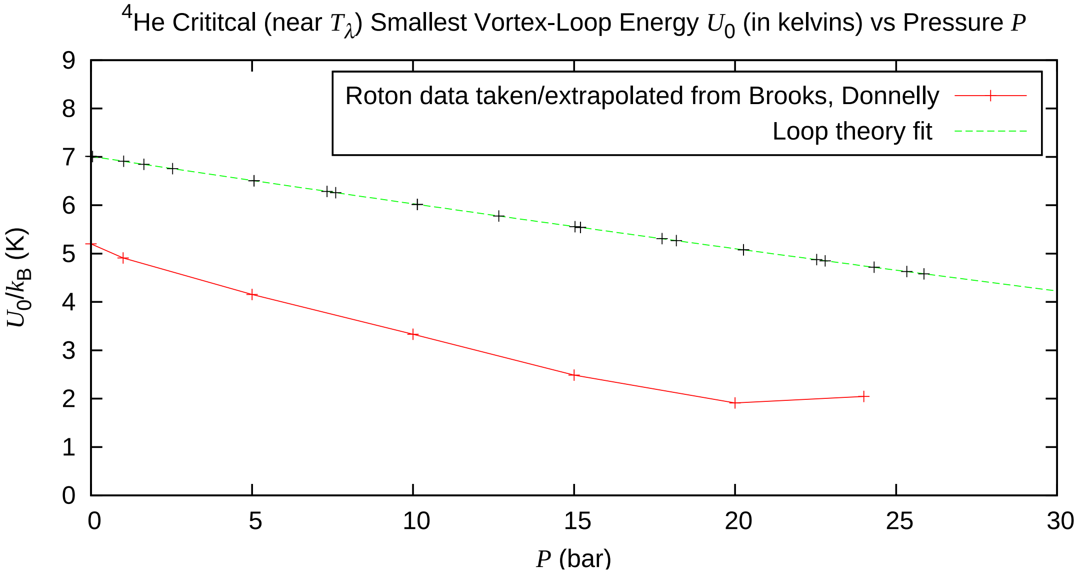

Figure 3.8: Here we plot the roton energy (minimum or gap) at T_λ, taken from extrapolations done by Brooks and Donnelly [71], along with the energy of the smallest vortex loops. Given that the extrapolations are made using sparse data, there should be large error bars on these data. We find rough agreement in magnitude and pressure dependence. More accuracy, and perhaps better agreement with these imprecise data, could be found using a proper quantum description of the smallest loops, rather than the crude, classical-fluids description that we've applied to this atomic-scale phenomenon. Note that as temperature decreases, these roton energies increase, so that by 0.75 K (at saturated vapor pressure) the roton energy $\Delta/k_B = 8.62$ K, as was seen in Fig. 2.4.

to a constant pressure. So it is easiest to calculate heat capacities at constant pressure, rather than constant volume. Thus we'll compare theoretical values to available experimental values of the molar specific heat capacity at constant pressure c_P^{exp}. So let's first see how to calculate the loop-theory specific heat c_P^{loop} using the variables of the theory.

At constant pressure, the total heat capacity is

$$C_P \;=\; -T\left(\frac{\partial^2 G}{\partial T^2}\right)_P \;=\; -T\left(\frac{\partial^2 F}{\partial T^2}\right)_P - TP\left(\frac{\partial^2 V}{\partial T^2}\right)_P , \tag{3.10}$$

where $G = F + PV$ is the Gibbs free energy of the fluid. We use $F = ek_{\mathrm{B}}TV/a_0^3$, thus the derivative of F above expands into derivatives of e, V, and a_0. The derivatives of V and a_0 can be rewritten in terms of derivatives of ρ: given $\rho = M/V$ with a constant total system mass M, we have $(\partial V/\partial T)_P = -(V/\rho)\,(\partial\rho/\partial T)_P$, and given Eq. (3.8) we have $(\partial a_0/\partial T)_P = -(a_0/\rho)\,(\partial\rho/\partial T)_P$. It is also more convenient for us to differentiate e with respect to $K^{\ell 0}$ rather than with respect to T, so we use

$$T\left(\frac{\partial}{\partial T}\right)_P \;=\; T\,\frac{\partial K^{\ell 0}}{\partial T}\,\frac{\partial}{\partial K^{\ell 0}} \;=\; -K_0\left(\frac{\partial}{\partial K_0}\right)_P . \tag{3.11}$$

In the end we convert to specific heat using the relation $c_P = (V_{\mathrm{m}}/V)C_P$, where $V_{\mathrm{m}} = N_{\mathrm{A}}m/\rho$ is the molar volume of helium, N_{A} being the Avogadro constant. All of this yields the following result, where we've used the gas constant $R = k_{\mathrm{B}}N_{\mathrm{A}}$ and put the terms in order of largest-in-magnitude to smallest:

$$\begin{aligned}
c_P^{\mathrm{loop}} \;=\;\; & Rm\frac{1}{\rho a_0^3}\left[-K_0^2\left(\frac{\partial^2 e}{\partial {K_0}^2}\right)_P\right] - N_{\mathrm{A}}m\frac{TP}{\rho}\left(-\frac{1}{\rho}\left(\frac{\partial^2\rho}{\partial T^2}\right)_P\right) \\
& + Rm\frac{1}{\rho a_0^3}\left[+\left\{4\frac{T}{\rho}\left(\frac{\partial\rho}{\partial T}\right)_P\right\}K_0\left(\frac{\partial e}{\partial K_0}\right)_P + \left\{-2\frac{T^2}{\rho}\left(\frac{\partial^2\rho}{\partial T^2}\right)_P - 8\frac{T}{\rho}\left(\frac{\partial\rho}{\partial T}\right)_P\right\}e\right] \\
& - N_{\mathrm{A}}m\frac{TP}{\rho}\left(2\frac{1}{\rho^2}\left(\frac{\partial\rho}{\partial T}\right)_P^2\right) + Rm\frac{1}{\rho a_0^3}\left[\left\{-2\frac{T^2}{\rho^2}\left(\frac{\partial\rho}{\partial T}\right)_P^2\right\}e\right] .
\end{aligned} \tag{3.12}$$

The last term is negligible since it never contributes more than 0.04% to the total.

Via Eq. (3.12) and the scaling relations, each critical pair $(K_{\mathrm{c}}^{\ell 0}(P), C_{\mathrm{c}}(P))$ yields a plot of specific heat versus relative temperature, and near T_λ the loop theory plots follow a power law plus an offset,

$$c_P^{\mathrm{loop}} = B'_{\mathrm{loop}} \tau^{-\alpha} + c_P^{\mathrm{lcr}}, \tag{3.13}$$

with an overall positive critical exponent $-\alpha = 3\nu - 2 = 0.015065057$ given by a Josephson relation [93] (so that the vortex loop theory exactly satisfies Josephson scaling), and a critical amplitude B'_{loop} and offset component c_P^{lcr} that both depend on pressure. The offset c_P^{lcr} is the loop-theory critical value of c_P, for $\tau = 0$ at T_λ. Since c_P reaches a maximum at T_λ, the critical amplitude is a negative number. The experimental heat capacity also takes this form near T_λ:

$$c_P^{\mathrm{exp}} = B'_{\mathrm{exp}} \tau^{-\alpha} + c_P^{\mathrm{ecr}}. \tag{3.14}$$

Since we find exactly the $\tau^{-\alpha}$ behavior seen in experiment, our results give support to the idea that it is the vortex loops of the loop theory, in particular the larger loops, that produce the cusping (or "singular") critical behavior of the heat capacity.

In addition to the loop contribution to the specific heat, there is a background part due primarily to the atomic interactions that cause the helium to be liquid rather than gas, and to a much lesser extent due to phonons, and to an unknown but probably small extent due to second-sound excitations [57]. Since we have not included these other phenomena in the Helmholtz parameter e, we expect c_P^{lcr} to be different from c_P^{ecr}.

Since the amplitude B'_{loop} is another non-universal quantity that depends on the other non-universal, bare parameters at the scale a_0, which we have seen are somewhat approximate, we do not expect B'_{loop} to match B'_{exp} precisely. What we do expect, however, is that the pressure dependencies of both amplitudes to match due to arguments of universality given by Rudnick and Jasnow [63] and Ferer [88], so their ratio should be approximately constant. In comparing theoretical plots of c_P^{loop} to data of Lipa *et alia* [66] and Ahlers [67, 68], we find that the ratio $B'_{\mathrm{exp}}/B'_{\mathrm{loop}}$ is essentially a constant 0.26 over all pressures, mostly within about 5% of that value, in agreement with the expectations of universality. See Table 3.1 for all the values. To illustrate that the vortex loop theory accurately captures the critical behavior of the specific heat capacity, we have computed an adjusted theoretical specific heat,

$$c_P^{\mathrm{adj}} \;=\; \left(\frac{B'_{\mathrm{exp}}}{B'_{\mathrm{loop}}}\right) c_P^{\mathrm{loop}} + c_P^{\mathrm{nl}}, \tag{3.15}$$

where $c_P^{\mathrm{nl}} = c_P^{\mathrm{ecr}} - (B'_{\mathrm{exp}}/B'_{\mathrm{loop}})c_P^{\mathrm{lcr}}$ is the "non-loop" background, and plotted c_P^{adj} along with the experimental data in Fig. 3.9.

The amplitude ratio indicates the theory produces a specific heat amplitude about four times larger than experiment. As we said, the vortex loop theory is not expected to give a precise description of the heat capacity amplitude, but perhaps with a more accurate parameterization of a_0, the theory could do better. For instance, if second-sound excitations are considered, they should contribute in reducing the superfluidity, decreasing $\rho_{\mathrm{s}}^{\ell 0}$ from the value ρ that we used, thereby increasing a_0, since $a_0 \propto 1/\rho_{\mathrm{s}}^{\ell 0}$. This would then reduce the specific heat since $c_P^{\mathrm{loop}} \propto 1/a_0^3$. We know that including phonons will not change the result much since they only reduce $\rho_{\mathrm{s}}^{\ell 0}$ by about 0.4%.

A final calculation we present is that of the universal quantity X, introduced by Ferer [88], which in our notation is equivalent to

$$X_{\mathrm{He}} \;=\; \frac{|B'|/R}{V_{\mathrm{m}\lambda}} \left(\frac{T_\lambda V_{\mathrm{m}\lambda}}{A'}\right)^3, \tag{3.16}$$

where B' is the specific heat capacity critical amplitude (either experimental or "loop" theoretical), $V_{\mathrm{m}\lambda}$ is the helium molar volume at T_λ, A' is the superfluid fraction critical amplitude, and R is the gas constant. In Table 3.2, we compare values of $X_{\mathrm{He}}^{\mathrm{loop}}$, the theoretical (unadjusted) X_{He}, at different pressures to other experimental calculations of X_{He}. We find, interestingly, that the theoretical values are more stable than the

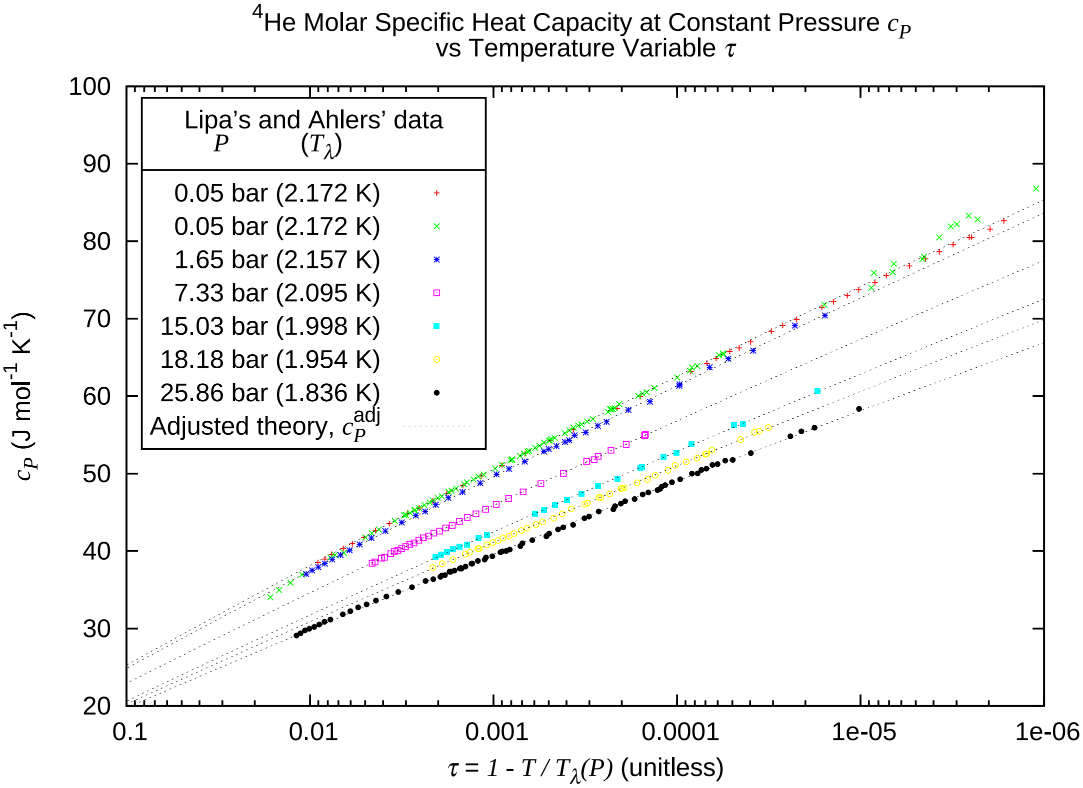

Figure 3.9: Here are data of Lipa *et alia* [66] and Ahlers [67, 68] with the adjusted theoretical plots of the specific heat capacity. The vortex loop theory of the superfluid phase transition captures the criticality of the specific heat and does so universally, over all relevant pressures. The experimental fit for saturated vapor pressure (0.05 bar) was performed using Lipa's data from $\tau = 4 \times 10^{-3}$ to 1×10^{-7}. The fits for higher pressures were performed using Ahler's data over their full domain. (Note the axis reversal putting 0 K leftward and T_λ rightward.)

P (bar)	B'_{exp} (unit*)	c_P^{ecr} (unit*)	B'_{loop} (unit*)	c_P^{lcr} (unit*)	c_P^{nl} (unit*)	$B'_{\text{exp}}/B'_{\text{loop}}$ (unitless)	% diff from avg (0.259)
0.05	−388.0	400.1	−1397	1372	19.14	0.2777	7.1
1.65	−382.1	394.0	−1406	1381	18.68	0.2717	4.8
7.33	−355.0	365.8	−1401	1377	16.76	0.2534	−2.2
15.03	−337.5	346.6	−1328	1308	13.99	0.2542	−1.9
18.18	−322.7	331.9	−1286	1269	13.48	0.2510	−3.2
22.53	−299.6	309.5	−1223	1210	13.16	0.2449	−5.5
25.87	−306.5	315.8	−1173	1164	11.76	0.2613	0.8

Table 3.1: The unidentified unit above is unit* = J/(K · mol). Columns 2–5 show the fit parameters for the experimental data and vortex-loop-theory calculations using Eq.s (3.13) and (3.14). Columns 6 and 7 show the parameters that adjust the theoretical calculations to match the data, as in Eq. (3.15). The important result is that the critical amplitude ratios in column 7 are quite constant, in agreement with the expectations of universality [63, 88]. The average critical amplitude ratio (0.259) and the percentage differences from this average are given in column 8.

experimental values, but too high by a factor of approximately 4 since B'_{loop} is likewise too high by that same factor, as discussed above.

To summarize, we have shown (in this chapter and in Fig. 2.13) that the vortex loop theory of the superfluid phase transition consistently describes, within about 200 μK below T_λ, the pressure dependence of the helium superfluid fraction, heat capacity, vortex-loop core diameter, smallest-loop energy, and universal quantity X. We have suggested that the smallest vortex loops, with size on the order of angstroms, may be crude approximations for rotons. In fact, we've shown in Fig. 3.9 that the heat capacity is characterized

P (bar)	$10^{-4} * {}^1X_{\mathrm{He}}$ (unit**)	$10^{-3} * {}^2X_{\mathrm{He}}$ (unit**)	$10^{-4} * X_{\mathrm{He}}^{\mathrm{exp}}$ (unit**)	$10^{-4} * X_{\mathrm{He}}^{\mathrm{loop}}$ (unit**)
0.05	2.06	3.11	2.41	8.84
1.65	2.02	3.07	2.36	8.84
7.33	1.99	3.01	2.20	8.84
15.03	2.02	3.10	2.21	8.83
18.18	1.99	3.10	2.18	8.83
22.53	1.96	3.12	2.12	8.82
25.87	2.19	3.47	2.26	8.82

Table 3.2: The unidentified unit above is unit** $= R(\mathrm{mol/cm^3})(\mathrm{K \cdot cm^3/mol})^3$. The universality of X is demonstrated by its near-constancy over all relevant pressures. Columns 2 and 3 are calculated by Ferer [88], where ${}^1X_{\mathrm{He}}$ assumes critical exponents $\alpha = -0.02$ and $\nu = 0.669$, whereas ${}^2X_{\mathrm{He}}$ assumes $\alpha = 0$ and $\nu = 2/3$, and B' in this case is based on a logarithmic expansion rather than a power law expansion since $\alpha = 0$. Our calculations in columns 4 and 5 are based on $\alpha = -0.015065057$ and $\nu = 0.67168835$. Note that $X_{\mathrm{He}}^{\mathrm{exp}}$ has approximately equal or lesser variation than Ferer's values and is within about 5% of its average, 2.25. Interestingly, $X_{\mathrm{He}}^{\mathrm{loop}}$ has much less variation, although it's off by a factor of approximately 4, since $B'_{\mathrm{loop}}/B'_{\mathrm{exp}} \approx 4$.

well, with some adjustments to the theory described above, within about 0.2 K below T_λ.

CHAPTER 4

2D Non-Equilibrium Quench

4.1 Exact Solution for Critical Quenches of 2D Superfluids

In this chapter an exact analytic solution for the dynamics of vortex pairs is obtained for rapid temperature quenches of a 2D superfluid, or superfluid film. This gives new insights into the behavior of the vortex decay, which is completely determined by the initial distribution of thermal vortices. It is proposed that there is no breakdown of dynamic scaling even for quenches starting at and above the critical temperature, as previously suggested; logarithmic corrections to the dynamics are only the result of logarithmic corrections to the initial vortex distributions. The solution also verifies that there is no "creation" of vortices depending on the quench rate as predicted by the Kibble-Zurek theory, but only decay of the initial vortices.

Although the phase-ordering kinetics of temperature-quenched thermodynamic systems have been studied for many decades [94], there are few exact results for the dynamics of the recovery to equilibrium, most of which have only been found for model systems with no physical relevance [95], though recently an exact solution for the decay of "hull" areas in the two-dimensional Ising model has been found [96]. Nevertheless, progress in the field has been made by asserting that dynamic scaling should apply to a quenched system, that for a system with non-conserved order parameter the dynamics will be characterized by a growing length scale $\xi(t) = \xi_0 \, t^{1/z}$, where $z \approx 2$ is the dynamical exponent of model A in the classification of Halperin and Hohenberg [97] and t is the time from the quench-to-low-temperature. Scaling holds if solutions involving a length scale r only depend on the ratio r/ξ. The growing length scale characterizes the domain growth of the topological defects of the order parameter as the system becomes completely ordered at long times. A phenomenological dimensional argument [98] is commonly used to predict the time dependence of the decaying defect density:

$$\rho(t) \quad \propto \quad \xi^{-n} \quad \propto \quad t^{-n/z}, \tag{4.1}$$

where n is the number of components of the order parameter. Superfluids are in the $n = 2$ universality class, where the defects are quantized vortices, so if $z = 2$ then dynamic scaling predicts a $1/t$ decay of the vortex density. Computer simulations of spin systems that vary n gave general agreement with Eq. (4.1), though only at long time and length scales, and the simulations were only carried out starting from the disordered state above T_c [99].

However, a problematic case for dynamic scaling has been two-dimensional superfluids, where the defects are the vortex pairs of the Kosterlitz-Thouless theory [29] characterizing the equilibrium phase transition occurring at the critical temperature T_KT. The above arguments would give a vortex density decaying as t^{-1} for quenches from well above T_KT to very low temperatures. Simulations of the XY model however gave a decay exponent initially closer to -0.75, and which only at very long times approached the value of -1 [81, 100, 101]. This behavior could be modeled as a $\ln(t)/t$ variation, but this would seem to require a dynamic length scale varying as $(t/\ln t)^{1/z}$, which has been cited [102] as a breakdown of dynamic scaling. To further complicate the issue, numerical solutions of the Fokker-Planck equation for vortex pairs carried out by two of us [103] for quenches starting from T_KT showed a rather different form for the decay, as $1/(t \ln t)$, and quenches from initial temperatures below T_KT showed a temperature-dependent decay that became considerably more rapid than an exponent of -1 as the starting temperature was reduced.

Here we show that an exact solution to the Fokker-Planck equation for instantaneous quenches easily explains the apparently anomalous behavior listed above. The solution satisfies dynamic scaling, and yields a key insight that the quench dynamics depends crucially on the vortex-pair distribution function at the initial temperature $T_{\rm i}$. The logarithmic corrections to the vortex decay are postulated to arise from logarithmic corrections to the power-law behavior of the initial distributions, and not from any breakdown of dynamic scaling.

The starting point is the Fokker-Planck equation for the vortex pair distribution function [104] as used in Ref. [103],

$$\frac{\partial \Gamma}{\partial t} \;=\; \frac{1}{r}\frac{\partial}{\partial r}\left(r\,\frac{\partial \Gamma}{\partial r} + 2\pi K\,\Gamma\right), \tag{4.2}$$

where $\Gamma(r,t)$ is the distribution function for pairs of separation r at time t from the instantaneous quench, with r measured in units of the vortex core radius a_0, t in units of the diffusion time $a_0^2/2D$ with D the vortex diffusion constant, and Γ in units of a_0^4. In the limit of the low vortex densities that we consider, any terms higher order in Γ can be neglected in Eq. (4.2). The variable $K = \hbar^2\sigma_{\rm s}/m^2k_{\rm B}T$ is the dimensionless ratio of areal superfluid density to temperature, and the starting value of Γ at $r = 1$ and $t = 0$ is $\Gamma_0 = \exp(-\pi^2 K_{0\rm i}/2)$, using the Villain approximation for the vortex core energy. At longer length scales, K is renormalized from its small-scale value K_0 (initially $K_{0\rm i}$) by the Kosterlitz scaling relation [29]

$$\frac{\partial K}{\partial r} \;=\; -4\pi^3 r^3 K^2 \Gamma. \tag{4.3}$$

At $t = 0$, the initial condition is that the system is equilibrated to a thermal bath at the temperature $T_{\rm i}$, corresponding to the initial $K_{\rm i}$ as determined from Eq. (4.3). For quenches starting from below $T_{\rm KT}$ we can make the approximation that $K_{\rm i}$ is effectively a constant, since the spatial renormalization from Eq. (4.3) is rapid, changing from the small-scale $K_{0\rm i}$ to the renormalized $K_{\rm i}$ over a length scale that can be less than a core radius. The equilibrium distribution then varies as ${\Gamma_0}' \, r^{-2\pi K_{\rm i}}$, where ${\Gamma_0}'$ is slightly smaller than Γ_0 due to the renormalization. Since the KT transition is a line of critical points, all quenches starting at $T_{\rm i} \leq T_{\rm KT}$ are critical quenches [105].

Immediately after the quench, the temperature of the heat bath $T_{\rm f}$ is lower than its initial temperature $T_{\rm i}$ but the pure superfluid density $\sigma_{\rm s}$ has not yet changed, so K in Eq.s (4.2) and (4.3) takes on the new much larger value $K_{\rm f}$. Again, for quenches starting from below $T_{\rm KT}$, the time dependence of $K_{\rm f}$ is minimal (as well as the space dependence), recovering after the quench to a superfluid fraction of one in less than a diffusion time [103]. The thermal bath now acts as a delta-function sink to absorb the out-of-equilibrium smallest pairs at $r = 1$ as they annihilate there, and this net annihilation goes on until the pair density falls to the equilibrium value at $T_{\rm f}$ (which for a quench to, e.g., $T_{\rm f} = 0.1\, T_{\rm KT}$ can be 20 orders of magnitude smaller than the starting value).

In the limit of constant $K_{\rm i}$ and $K_{\rm f}$, we can solve Eq. (4.2) for $t > 0$ by separation of variables, writing

$$\Gamma(r,t) \quad = \quad F(w)\, f(t), \tag{4.4}$$

where $w = r/t^{1/z}$ is the dynamic scaling variable (and F and f are not related to the free energies defined in previous chapters). Using the chain rule, Eq. (4.2) then can be written

$$\frac{1}{f}\frac{\partial f}{\partial t} t^{2/z} \quad = \quad \frac{1}{F}\left[\frac{\partial^2 F}{\partial w^2} + \frac{1}{w}\frac{\partial F}{\partial w}\left(1 + 2\pi K_{\rm f}\right) + \frac{w\, t^{2/z}}{z\, t}\frac{\partial F}{\partial w}\right]. \tag{4.5}$$

This equation separates if and only if $z = 2$, and taking the separation constant as $-\alpha/z$ yields the two equations

$$\frac{1}{f}\frac{\partial f}{\partial t} + \frac{\alpha}{z\, t} \quad = \quad 0 \tag{4.6}$$

$$\frac{\partial^2 F}{\partial w^2} + \frac{1}{w}\frac{\partial F}{\partial w}(1 + 2\pi K_{\rm f}) + \frac{w}{z}\frac{\partial F}{\partial w} + \frac{\alpha}{z} F \quad = \quad 0. \tag{4.7}$$

These are straightforward to solve, and the solution for (4.7) finite at $w = 0$ (i.e., $t \to \infty$) is

$$F(w) \;=\; \beta\ {}_1F_1\!\left[\frac{\alpha}{2},\, 1+\pi K_\mathrm{f},\, -\frac{w^2}{2z}\right], \tag{4.8}$$

where the function ${}_1F_1$ is the confluent hypergeometric function of the first kind, and β is a constant. To satisfy the boundary condition $\Gamma(r,0) = {\Gamma_0}'\, r^{-2\pi K_\mathrm{i}}$ at $t = 0$, the large-w expansion of the hypergeometric function requires $\alpha = 2\pi K_\mathrm{i}$, and

$$\beta \;=\; {\Gamma_0}' \left(\frac{G(1+\pi K_\mathrm{f} - \pi K_\mathrm{i})}{(2z)^{\pi K_\mathrm{i}}\, G(1+\pi K_\mathrm{f})}\right), \tag{4.9}$$

where G is the Euler gamma function (usually written as Γ). The full solution for the distribution function then becomes

$$\Gamma(r,t) \;=\; \beta\ {}_1F_1\!\left[\pi K_\mathrm{i},\, 1+\pi K_\mathrm{f},\, -\frac{r^2}{2z\, t^{2/z}}\right]\ t^{-2\pi K_\mathrm{i}/z}. \tag{4.10}$$

This is evaluated in Fig. 4.1a for a quench from $T_\mathrm{i} = 0.9\ T_\mathrm{KT}$ to $T_\mathrm{f} = 0.1\ T_\mathrm{KT}$, corresponding to parameter values ${\Gamma_0}' = 2.576 \times 10^{-4}$, $K_\mathrm{i} = 0.814$, and $K_\mathrm{f} = 7.479$. With no adjustable parameters, this is seen to give a precise description of the numerical results.

The time dependence of the vortex pair density (in units of a_0^2) is found by integrating the distribution function,

$$\begin{aligned} \rho(t) \;&=\; \int_1^\infty \Gamma(r,t)\, 2\pi r\, \mathrm{d}r && (4.11)\\ &=\; 2\pi\,\beta \left(\frac{z\,(2\pi K_\mathrm{f})}{(2\pi K_\mathrm{i} - 2)}\right)\ {}_1F_1\!\left[\pi K_\mathrm{i} - 1,\, \pi K_\mathrm{f},\, -\frac{t^{-2/z}}{2z}\right]\ t^{-(2\pi K_\mathrm{i} - 2)/z}. && (4.12) \end{aligned}$$

The hypergeometric function in this case rises rapidly from zero until the time $t \approx 1$ where it becomes constant and equal to one. Beyond that point the time dependence is then accurately $t^{-z_\mathrm{scale}/z}$, where

$$z_\mathrm{scale} \;=\; 2\pi K_\mathrm{i} - 2 \;=\; 4\,\frac{\sigma_\mathrm{s}(T_\mathrm{i})}{\sigma_\mathrm{s}(T_\mathrm{KT})}\,\frac{T_\mathrm{KT}}{T_\mathrm{i}} - 2 \tag{4.13}$$

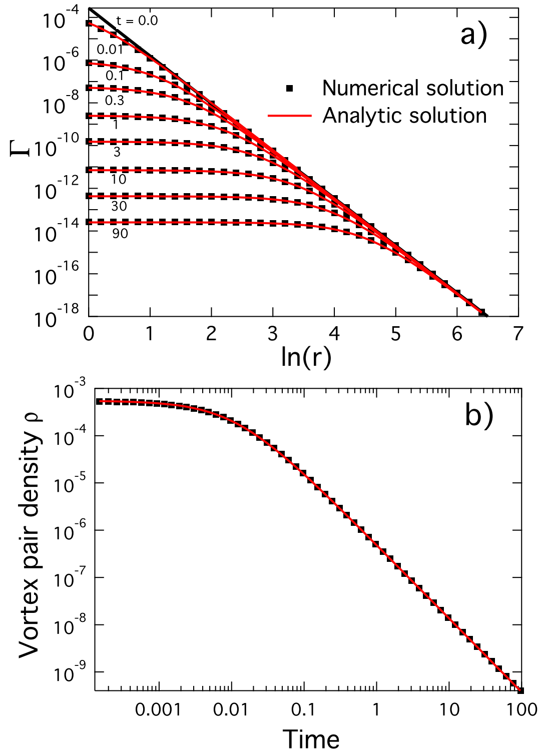

Figure 4.1: Comparison of the numerical and analytic solutions for the vortex distribution function and vortex pair density as functions of time, for an instantaneous quench from 0.9 T_{KT} to 0.1 T_{KT}.

is the dynamic exponent first considered by Minnhagen and co-workers [106].[1] This is just the variation observed earlier [103], but at that time it was not clear that in fact two dynamic exponents are involved in the solution, $-2/z$ and $-(2\pi K_{\mathrm{i}} - 2)/z$. Figure 4.1b shows the time decay of the vortex density for the same parameters as in Fig. 4.1a, where at long times the decay is $t^{-1.557}$.

The exact solutions show that Eq. (4.1) is simply not correct for quenches starting below T_{KT}. Right at T_{KT} (and probably at higher temperatures), z_{scale} takes the value of

---

[1] The second equality in Eq. (4.13) holds due to the definition of K and because, at T_{KT}, $K = K_{\mathrm{c}}$ equals the fixed-point value $K^* = 2/\pi$.

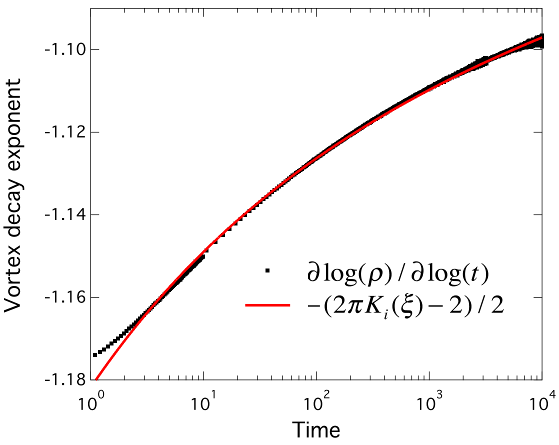

Figure 4.2: Comparison of the numerically computed slope of the vortex decay curve at $T_{\rm KT}$ in Ref. [103] with the exponent $-z_{\rm scale}/z$ using $K_{\rm i}(r)$ at the location $r = \xi = \xi_0\, t^{1/2}$.

2 at long length scales, and it is certainly possible that this could be related to $n = 2$ of the superfluid universality class. However, we are unaware of any direct relation between these quantities.

At initial temperatures higher than about 0.95 $T_{\rm KT}$ the above analysis begins to fail because the initial vortex distribution is no longer accurately a power law. Right at $T_{\rm KT}$ there is a strong logarithmic correction to $K_{\rm i}$ such that $2\pi K_{\rm i}$ approaches the KT value of 4 ($K_{\rm i} = 2/\pi$) only at extremely large pair separations (it is 4.373 at $r = 10$ and 4.197 at $r = 1000$). It is still possible to proceed if one notes that in Eq. (4.2) the derivatives are only important near $r = \xi$, since at smaller length scales the distribution is nearly flat, while at larger scales it falls off rapidly. The solutions of Eq.s (4.10) and (4.12) should remain approximately valid, but now $2\pi K_{\rm i}$ has to be regarded as the local value at $r = \xi$, i.e., it becomes time-dependent. This in turn means that the vortex density decay exponent $-z_{\rm scale}/z$ will be time-dependent, approaching -1 only at very long times.

We can check this scenario for a quench from $T_{\rm KT}$ by numerically evaluating $K_{\rm i}$ from

Eq. (4.3) as a function of length scale and computing the decay exponent $-(2\pi K_{\rm i}-2)/2$ at the corresponding times found from $r = \xi$. This can then be directly compared to Eq. (4.12) by numerically finding the slope of the vortex density decay curve for the quench from $T_{\rm KT}$ in Fig. 2 of Ref. [103] as a function of time, shown as the data points in Fig. 4.2 of this paper (roundoff error becomes appreciable at long times in the data since ρ becomes very small). Since ξ_0 is not uniquely determined by the above analysis, we have matched the computed exponent (solid curve in Fig. 4.2) to the data at one point, arbitrarily taken to be $t = 100$, which yields $\xi_0 = 11.5$. The agreement over more than three orders of magnitude in t between the data and the computation shows without any doubt that the $1/(t \ln t)$ behavior seen in [103] was entirely due to the log corrections to $K_{\rm i}$ in the initial distribution. The value of $\xi_0 = 11.5$ is also quite reasonable, since it causes a scaling plot of $t^{2\pi K_i}\Gamma$ versus r/ξ to match well with the similar scaling plot in Fig. 7b of Ref. [81].

The same idea can be applied to quenches from well above $T_{\rm KT}$, though less is known about the vortex distribution. The distribution has been calculated in Ref. [81] for a quench from $2\,T_{\rm KT}$, but only out to $r \approx 50$, where it falls off as $r^{-3.5}$. This would suggest an initial density decay exponent of $-(3.5-2)/2 = -0.75$, which is just the initial value seen in the simulations [81,100,101]. It will be interesting if simulations on larger lattices show a large-distance distribution exponent increasing towards the value of -4, which would explain the observed $\ln(t)/t$ behavior [107].

A further consequence of the exact solution for the quench is that it validates the conclusion in Ref. [103] that there is no “creation” of vortices in a quench, but only monotonic decay of the existing thermal vortices. This is contrary to the prediction of Kibble and Zurek [42] that excess vortices will be created in a superfluid quench, with higher densities appearing the faster the quench rate. The numerical studies found just the opposite result, that actually more vortices were left over at $T_{\rm f}$ following a slower quench, since in that case the system spends more time at higher temperatures where the thermal vortex density is higher. The present results verify that no excess vortices are created even for an instantaneous quench. Although our results only apply to quenches at and below T_{KT}, the same result has now been seen in XY model simulations [81] for quenches starting from $2\,T_{\mathrm{KT}}$, where the variation with quench rate was entirely similar to the numerical results [103].

Quenches from low to high temperature can also be studied, at least numerically, shown in Fig. 4.3. The vortex density increases as $t^{1/2}$, indicating proportionality to ξ. The distribution shows the smallest pairs being rapidly populated, as expected from the thermal injection at $r = 1$, with the larger pairs only appearing at late times.

In summary, we propose an exact solution for the vortex density following a critical quench in two-dimensional superfluids. The solution highlights the key role of the initial vortex distribution, and this allows a consistent explanation of the logarithmic deviations seen in earlier work as being due to logarithmic corrections in the initial distributions. It will be important to check the validity of the solution by carrying out XY model simulations for quenches starting below T_{KT}, looking for the increasingly rapid decay of the vortex density predicted by Eq. (4.12).

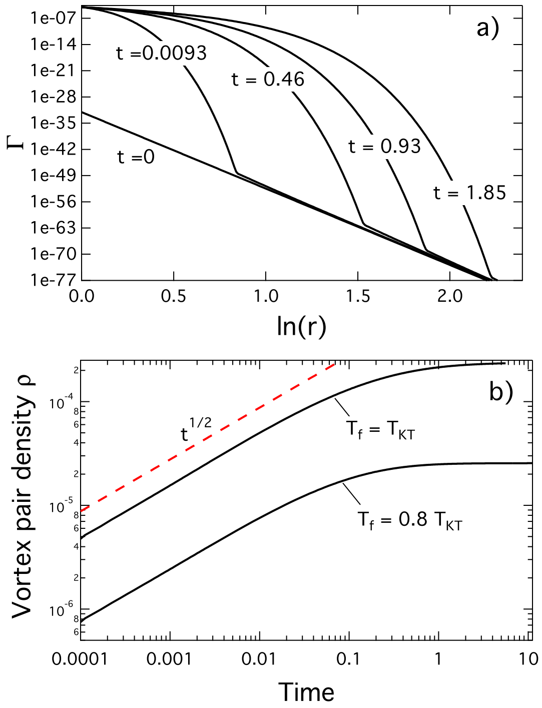

Figure 4.3: a) Pair distribution function for an instantaneous upwards quench from 0.1 to 0.8 T_{KT}. b) Vortex density versus time for upward quenches from 0.1 to 0.8 and 1.0 T_{KT}. The dashed curve shows the $t^{1/2}$ variation.

APPENDIX A

Note on Vortex Distribution Definitions

There are a number of ways that the vortex distribution, or number-of-vortices per state-space-volume, can be defined. In the main text of this dissertation we chose a couple definitions that were suitable for the initial derivations but may not have been the most convenient in the later stages of analysis. In this appendix we suggest a couple other useful definitions for those who wish to re-derive our results or continue this research. (We'll just examine the 3D definitions here, but the 2D definitions follow analogously.)

The initial definitions, given previously, are the following:

$$\frac{N}{V} = \int \Gamma \, \mathrm{d}^3 a, \tag{A.1}$$

where N is the number of vortex loops in a system of volume V and $\Gamma(\mathbf{a})$ (or Γ) is the number of vortex loops with diameter and directionality (of motion) given by $\mathbf{a}$ (as explained in Section 2.1.2.4) per state volume $\mathrm{d}^3 a$, centered at $\mathbf{a}$; and

$$\frac{N}{V} = \frac{1}{a_0^3} \int \tilde{\Gamma} \, \frac{\mathrm{d}^3 a}{a_0^3}, \tag{A.2}$$

where $\tilde{\Gamma}$ is simply the dimensionless form of the distribution, $\tilde{\Gamma} = a_0^6 \Gamma$. (Only the 2D version of $\tilde{\Gamma}$ was defined in the main text, in Section 2.2.3.5.)

The as-yet unstated definitions are the following:

$$\frac{N}{V} = \frac{1}{a_0^3} \int G \, \mathrm{d}\ell, \tag{A.3}$$

where $G(\ell)$ (or G) is the number of vortex loops of diameter $a = a_0 \exp(\ell)$ per length-scale parameter increment $\mathrm{d}\ell$, centered at ℓ; and

$$\frac{N}{V} = \int D \, \mathrm{d}L, \tag{A.4}$$

where $D(L)$ (or D) is the number of vortex loops of vortex-line length (or perimeter) L per length increment $\mathrm{d}L$, centered at L.

Ironically, using the dimensionless distribution G probably makes it easier to keep track of the units than using the dimensionful Γ. Also, G is more appropriate than Γ for use in writing the computer programs, since ℓ is used to parametrize the variables rather than a. Note that the angular dependence of Γ is integrated out when transforming to G. Although the variables K, y, and e are often used in the programs, the equations can be easily be re-written in terms of K, G, and e (instead of the mildly jarring K, Γ, and e), and the results can be expressed in terms of the superfluid fraction, vortex distributions, and total number-density of vortices.

The distribution D may be the best choice when comparing to results of simulations and experiments carried out by other groups (for example, Nguyen and Sudbø [108]) since D is what they tend to measure. So it would probably be best to use G in the program equations and calculations and then convert to D in the end for comparison. (It may be fruitful to derive the equations in terms of D too, in case there are some simplifications in some of the equations.)

APPENDIX B

Flows, Fixed Points, Bare Values, and the Critical Exponent ν

In this appendix we will show how to use the so-called renormalization flows and fixed points of the 2D and 3D scaling relations to calculate the critical ($T = T_c$) bare ($\ell = 0$) values of K and y as well as the critical exponent ν of the 3D case.

First, let's generally describe the renormalization flows and fixed points. Both the 2D and the 3D scaling equations are of the form

$$\frac{\partial K}{\partial \ell} = \mathcal{F}(K, y) \tag{B.1}$$

$$\frac{\partial y}{\partial \ell} = \mathcal{G}(K, y), \tag{B.2}$$

where the derivative functions $\mathcal{F}(K, y)$ and $\mathcal{G}(K, y)$ are given in the following table. Note that the length scale variable ℓ, which is the renormalization parameter, does not appear explicitly in the derivative functions. These equations are therefore called *autonomous*

2D	3D
$\mathcal{F}_2(K, y) = -A_2 K^2 y$ $A_2 = 4\pi^3$ $\mathcal{G}_2(K, y) = y\,(4 - 2\pi K)$	$\mathcal{F}_3(K, y) = K - A_3 K^2 y$ $A_3 = 4\pi^3/3$ $\mathcal{G}_3(K, y) = y\left[6 - \pi^2 K\,(1 - \theta \ln K)\right]$ $\theta = 0.6$

Table B.1: The 2D and 3D scaling equation derivative functions.

since the slope of a solution curve in the K-y plane is "self-governed" by the values of K and y, without reference to the value of ℓ. In particular, supposing one of $\mathcal{F}$ and $\mathcal{G}$ is nonzero, one can divide the two differential equations to find the slope in the K-y plane:

$$\frac{\partial K}{\partial y} = \frac{\mathcal{F}}{\mathcal{G}}(K, y) \qquad \text{or} \qquad \frac{\partial y}{\partial K} = \frac{\mathcal{G}}{\mathcal{F}}(K, y). \tag{B.3}$$

So the scaling equations quantify how the values (K, y) change or "renormalize" in the K-y plane as the length parameter ℓ is changed, independent of the actual value of ℓ. Each curve in the K-y plane that obeys these equations (and hence is directed and parametrizable by ℓ) can be called a *renormalization trajectory* and taken together these trajectories are called a *renormalization flow*, or a "renormalization group flow", or an "RG flow". Pick a particular starting point or region and the scaling equations determine how the variables "flow" along trajectories that run through that region. However, at some points both differential equations may be zero, and such a point is called a stationary or fixed point, with the flow stopped at that point. Some trajectories may begin infinitesimally close to a fixed point, or they may end at a fixed point, or they may begin or end at the "edges" of the domain of the equations, or they may even loop around in a closed circuit. Some trajectories may come nowhere near a fixed point and others may may pass by, arbitrarily close to a fixed point.

With this orientation, we can now move on to calculations in the 2D and 3D cases.

B.1 2D Renormalization Flow Calculations

Let's find the fixed points of the 2D scaling relations. Any fixed point (K^*, y^*) will cause the scaling relations to be zero:

$$\frac{\partial K}{\partial \ell}(K^*, y^*) = -A_2 K^{*2} y^* = 0 \tag{B.4}$$

$$\frac{\partial y}{\partial \ell}(K^*, y^*) = y^*(4 - 2\pi K^*) = 0, \tag{B.5}$$

where $A_2 = 4\pi^3$. By inspection, we can see that $y^* = 0$ is necessary and sufficient for both of the equations to be zero, with K^* being arbitrary. This is a line of fixed points on the K-axis, at the edge of the physically relevant domain, $K \in (0, \infty)$ and $y \in (0, \infty)$. But there are two interesting points within this line of fixed points: the point coinciding with $K = 0$, which drives $\partial K/\partial \ell$ to zero independent of y, and the point coinciding with $K = 2/\pi$, which drives $\partial y/\partial \ell$ to zero independent of y. We'll see that $(K^*, y^*) = (2/\pi, 0)$ is a particularly physically relevant fixed point that corresponds to the critical temperature T_{KT}. We'll see that the fixed point at the origin, $(K^*, y^*) = (0, 0)$, is not physically relevant, but it is interesting in that it is associated with singular trajectories emanating from (infinitesimally close to) the origin.

Besides the stationary, point solutions, which remain the same regardless of the value of ℓ, we can find non-trivial flows off of the K-axis. Off of the fixed-points, the 2D solution curves are still quite simple though, because the slopes are independent of the variable y. This is because y cancels out when dividing $\mathcal{F}$ and $\mathcal{G}$:

$$\frac{\partial y}{\partial K} = \frac{\mathcal{G}}{\mathcal{F}}(K, y) = \frac{y\,(4 - 2\pi K)}{A_2 K^2 y} \tag{B.6}$$

$$= \frac{4 - 2\pi K}{A_2 K^2}, \tag{B.7}$$

for $y \neq 0$ and $K \neq 0$. So we can simply integrate to solve for $y(K)$, starting at some arbitrary point $(K_{\mathrm{i}}, y_{\mathrm{i}})$ and proceeding over an interval along the K-axis $[K_{\mathrm{i}}, K]$ or $[K, K_{\mathrm{i}}]$, so long as none of these variables equal zero at any point during the integration:

$$y(K) = y_{\mathrm{i}} + \int_{K_{\mathrm{i}}}^{K} \frac{\partial y}{\partial K}(K')\, \mathrm{d}K' = y_{\mathrm{i}} + \int_{K_{\mathrm{i}}}^{K} \frac{4 - 2\pi K'}{A_2 K'^2}\, \mathrm{d}K' \tag{B.8}$$

$$= y_{\mathrm{i}} + \frac{4}{A_2}\left[\frac{1}{K} - \frac{1}{K_{\mathrm{i}}}\right] + \frac{2\pi}{A_2} \ln\!\left(\frac{K}{K_{\mathrm{i}}}\right). \tag{B.9}$$

The solution curves described by formula (B.9) are all the same shape, "echoing" each other up and down the y-axis, as illustrated in Fig. B.1 below. Note that for $y > 0$, $\partial K/\partial \ell < 0$ so K decreases with increasing ℓ, and for $y < 0$, $\partial K/\partial \ell > 0$ so K increases with increasing ℓ. With the axis-orientation in Fig. B.1, that translates to mean that the solution trajectories flow leftward above the K-axis ($y > 0$) and rightward below the K-axis ($y < 0$), except at $K = 0$.

The slope of formula (B.9) approaches infinity as K approaches zero, but we can start over with the scaling equations and take the $K = 0$ case by itself to see what we get. We find that $\partial K/\partial\ell = 0$ but $\partial y/\partial\ell = 4y$, so that $y(\ell) = y_{\mathrm{i}} \exp(4\ell)$, where y_{i} is any real number. So along the line $K = 0$, there are two trajectories (one with $y_{\mathrm{i}} < 0$ and one with $y_{\mathrm{i}} > 0$) that exponentially flee from the origin, and one stationary "trajectory" (with $y_{\mathrm{i}} = 0$), which is the fixed point at the origin.

Taking a solution curve that appears to intersect the K-axis, if we follow a point that moves along such a curve according to a parametrization using ℓ, we find that very close to the K-axis, where y is very small, both $\partial K/\partial\ell$ and $\partial y/\partial\ell$ are very small, so that the progress made in traversing the flow is slow as ℓ changes. Such a trajectory gets infinitesimally close to the K-axis but never intersects this line of fixed points. Note that all the fixed points with $K^* < 2/\pi$ are repulsive, with two trajectories flowing away from each of them, and all the fixed points with $K^* > 2/\pi$ are attractive, with two trajectories flowing toward each of them. This is apparent by examining Fig. B.1. The attractive fixed points are called stable fixed points since any point-flow starting near such a point will remain close, whereas the repulsive fixed points are called unstable for the opposite reason. The fixed point at $K^* = 2/\pi$ could be called semi-stable since a quarter of all the nearby point-flows (with $y > 0$ and $K < K^*$) are repelled and exhibit unstable behavior, but the rest remain near and show stable behavior as ℓ increases.

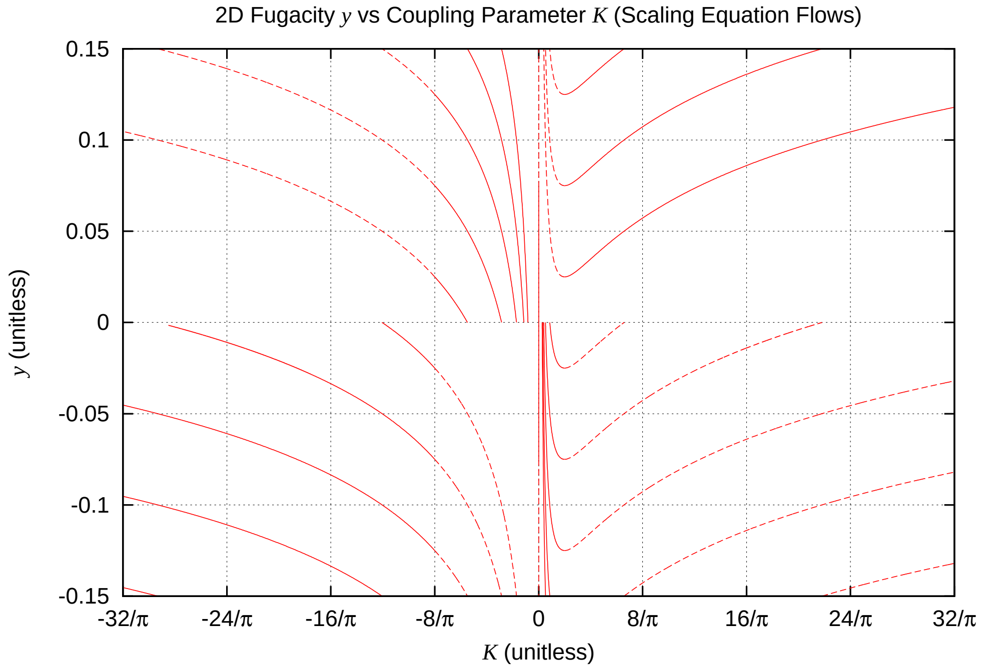

Figure B.1: Here are some representative flow trajectories, or solution curves, for the 2D scaling relations referred to in Eq.s (B.4) and (B.5). There is a line of fixed-points along the K-axis ($y = 0$). When parametrized by the length-scale variable ℓ, these solution trajectories flow leftward above the K-axis ($y > 0$) and rightward below the K-axis ($y < 0$), except at $K = 0$, where the trajectories exponentially flow away from the origin. (The solid and dashed portions of the curves indicate that the curves flow from the solid region to the dashed region.) A given line that appears to intersect the K-axis can be extended across the axis, but separate parametrizations must be used to describe the extended line since flows do not cross the line of fixed points. Although trajectories across whole K-y plane are shown here, only the upper right quadrant is physically relevant.

So far we have not discussed what values ℓ should take at any point on these solution curves. To answer that question, we use the Villain model to determine the relationship between the bare ($\ell = 0$) values of K and y. As discussed in Section 2.2.2.5, our use of the Villain model implies

$$y^{\ell 0} \;=\; \exp(-\pi^2 K^{\ell 0}). \tag{B.10}$$

We can rephrase this as $\ell = 0$ along the curve

$$y \;=\; \exp(-\pi^2 K) \tag{B.11}$$

in the K-y plane. This curve is shown in Fig. B.2, along with representative trajectories that originate from this line. Note that there are two kinds of trajectories from this curve: one type of trajectory ends at a fixed point and another gets directed towards a diverging y value with K heading to zero. There is a critical, boundary trajectory that gets directed to the fixed point $(K^*, y^*) = (2/\pi, 0)$. Physically, the trajectories with K converging to zero represent temperatures above T_{KT}, where $\sigma_{\mathrm{s}}^{\mathrm{r}}/\sigma = K/K^{\ell 0}$ converges to zero as ℓ goes to infinity. The trajectories with K converging to a non-zero finite value represent temperatures below T_{KT}, where $\sigma_{\mathrm{s}}^{\mathrm{r}}/\sigma = K/K^{\ell 0}$ converges to a non-zero finite value. So we see that the fixed point $(2/\pi, 0)$ represents the critical ($T = T_{\mathrm{KT}}$) macroscopic ($\ell \to \infty$) point in K-y space, and tracing its associated trajectory back to the bare-values Villain curve allows one to find the critical bare values of K and y. Actually, since the trajectories are known analytically by Eq. (B.9), and the Villain curve is known analytically, we can solve analytically for these bare values. We get $K_{\mathrm{c}}^{\ell 0} = 0.74785242$ and $y_{\mathrm{c}}^{\ell 0} = 6.2297289 \times 10^{-4}$.

With this knowledge of the bare critical values of K and y, we can determine the temperature of a given physical trajectory that originates from the Villain model curve. Since by definition $K^{\ell 0}/K_{\mathrm{c}}^{\ell 0} = T_{\mathrm{KT}}/T$, the bare value $K^{\ell 0}$ corresponds directly to temperature by $K^{\ell 0} = K_{\mathrm{c}}^{\ell 0}(T_{\mathrm{KT}}/T)$.

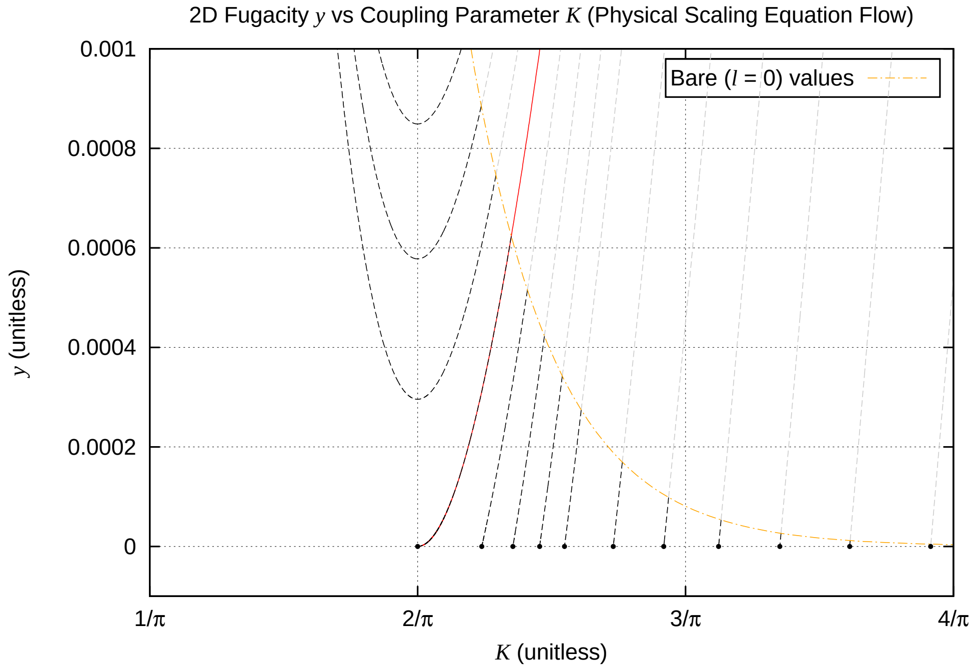

Figure B.2: Here, in black dashed curves, are some representative physically relevant renormalization trajectories, or solution curves for the 2D scaling relations referred to in Eq.s (B.4) and (B.5). This is a zoomed-in view of the upper right quadrant of Fig. B.1, near the fixed point at $K = 2/\pi$. All of the black dashed trajectories start from the Villain model exponential curve given by $y^{\ell 0} = \exp(-\pi^2 K^{\ell 0})$. (The gray dashed trajectories show the continuation of the trajectories to unphysical negative-ℓ-valued locations.) The trajectories that end at fixed points are at temperatures equal to or less than T_{KT}, with the critical trajectory at T_{KT} reaching $(K^*, y*) = (2/\pi, 0)$ as ℓ goes to infinity. The remaining trajectories represent temperatures above T_{KT}. Using the relationship $K^{\ell 0} = K_{\mathrm{c}}^{\ell 0}(T_{\mathrm{KT}}/T)$, these trajectories correspond to the temperature fractions T/T_{KT} between 1.075 and 0.6. The critical trajectory is highlighted with a solid red curve.

B.2 3D Renormalization Flow Calculations

B.2.1 Fixed Point Analysis

Let's find the fixed points of the 3D scaling relations. Any fixed point (K^*, y^*) will cause the scaling relations to be zero:

$$\begin{aligned}\frac{\partial K}{\partial \ell}(K^*, y^*) &= K^* - A_3 {K^*}^2 y^* &= 0 \qquad &\text{(B.12)}\\ \frac{\partial y}{\partial \ell}(K^*, y^*) &= y^*\left[6 - \pi^2 K^*\left(1 - \theta \ln K^*\right)\right] &= 0, \qquad &\text{(B.13)}\end{aligned}$$

where $A_3 = 4\pi^3/3$ and $\theta = 0.6$. At first glance, the origin $(K, y) = (0, 0)$ may seem to be a fixed-point solution, but since $\partial y/\partial \ell$ is not defined at $K = 0$ (due to the logarithm), the origin cannot be a fixed point. However, we will find that it is an unstable, repulsive point. Having determined that $K^* \neq 0$, we can immediately solve Eq. (B.12) for y^* in terms of K^* and get rid of y^* in Eq. (B.13):

$$\begin{aligned}y^* &= \frac{1}{A_3 K^*} \qquad &\text{(B.14)}\\ 0 &= 6 - \pi^2 K^*\left(1 - \theta \ln K^*\right). \qquad &\text{(B.15)}\end{aligned}$$

Equation (B.15) is transcendental and can be solved for K^* using some numerical technique or a calculator, where the technique is automatic. Solving yields two possible values for K^*, and plugging each of these values into Eq. (B.14) gives us the y^* values for these two fixed points. The fixed points are

$$\begin{aligned}(K_1^*, y_1^*) &= (4.1467664169,\ \ 0.005833135603) \qquad &\text{(B.16)}\\ (K_2^*, y_2^*) &= (0.38750818971, 0.062421005458). \qquad &\text{(B.17)}\end{aligned}$$

The 3D scaling relations do not generally simplify in the same way that the 2D scaling relations simplify, so to find the flow pattern we numerically solve by stepping out by increments $\Delta\ell$ starting from $\ell = 0$. (One special but unphysical case we can solve quickly is that of $y = 0$, where we find that $\partial y/\partial \ell = 0$ and $\partial K/\partial \ell = K$, so that $K(\ell) = K_{\mathrm{i}} \exp(\ell)$, where K_{i} is any positive real number.) Before solving numerically, first we can do some further calculations, using what's called linear stability analysis, to characterize the flow very near the two fixed points that we found and eventually use this information to calculate the critical exponent ν. To do this analysis, we linearize the scaling relations, expanding about a fixed point (K^*, y^*) by making the substitutions $K = K^* + \delta K$ and $y = y^* + \delta y$ and getting rid of higher-order terms in δK and δy, where $\delta K/K^* \ll 1$ and $\delta y/y^* \ll 1$. For the K equation, we get this:

$$\begin{align}
\delta \frac{\partial K}{\partial \ell} &= \frac{\partial K}{\partial \ell}\,(K^* + \delta K, y^* + \delta y) - \cancelto{0}{\frac{\partial K}{\partial \ell}\,(K^*, y^*)} \tag{B.18}\\
&= (K^* + \delta K) - A_3 (K^* + \delta K)^2 (y^* + \delta y) \tag{B.19}\\
&= (K^* + \delta K) - A_3 \left(K^{*2} + 2K^*\delta K + \cancel{\delta K^2}\right)(y^* + \delta y) \tag{B.20}\\
&= (K^* + \delta K) - A_3 \left(K^{*2} + 2K^*\delta K\right) y^* - A_3 \left(K^{*2} + \cancel{2K^*\delta K}\right)\delta y \tag{B.21}\\
&= \cancelto{0}{\left[K^* - A_3 y^* K^{*2}\right]} + \delta K - 2A_3 K^* y^* \delta K - A_3 K^{*2} \delta y \tag{B.22}\\
&= \left[1 - 2A_3 K^* y^*\right] \delta K - \left[A_3 K^{*2}\right] \delta y \tag{B.23}\\
&= \left[1 - 2A_3 K^* \left(\frac{1}{A_3 K^*}\right)\right] \delta K - \left[A_3 K^{*2}\right] \delta y \tag{B.24}\\
&= -\delta K - \left[A_3 K^{*2}\right] \delta y. \tag{B.25}
\end{align}$$

We do the same for the y equation, and use the approximation

$$\begin{align}
\ln(K^* + \delta K) &= \ln\big(K^*(1 + \delta K/K^*)\big) \tag{B.26}\\
&= \ln K^* + \ln(1 + \delta K/K^*) \tag{B.27}\\
&\approx \ln K^* + \delta K/K^*, \tag{B.28}
\end{align}$$

since $\ln(1 + x) = x - x^2/2 + x^3/3 - x^4/4 + \cdots$, for $|x| < 1$. For the y equation we get this:

$$\begin{align}
\delta\,\frac{\partial y}{\partial \ell} &= \frac{\partial y}{\partial \ell}\,(K^* + \delta K, y^* + \delta y) - \cancelto{0}{\frac{\partial y}{\partial \ell}\,(K^*, y^*)} \tag{B.29}\\
&= (y^* + \delta y)\left[6 - \pi^2(K^* + \delta K)\left(1 - \theta \ln(K^* + \delta K)\right)\right] \tag{B.30}\\
&= y^*\left[6 - \pi^2(K^* + \delta K)\left(1 - \theta \ln(K^* + \delta K)\right)\right] \nonumber\\
&\quad + \left[6 - \pi^2(K^* + \cancel{\delta K})\left(1 - \theta \ln(K^* + \cancel{\delta K})\right)\right]\delta y \tag{B.31}\\
&= y^*\left[\cancelto{0}{6 - \pi^2 K^*\left(1 - \theta \ln K^*\right)}\right] \nonumber\\
&\quad + y^*\left[-\pi^2 K^*\left(-\theta\delta K/K^*\right) - \pi^2\delta K\left(1 - \theta \ln(K^* + \cancel{\delta K})\right)\right] \tag{B.32}\\
&\quad + \left[\cancelto{0}{6 - \pi^2 K^*\left(1 - \theta \ln K^*\right)}\right]\delta y \tag{B.33}\\
&= \pi^2 y^*\left[\theta - \left(1 - \theta \ln K^*\right)\right]\delta K \tag{B.34}\\
&= \pi^2 y^*\left[\theta\left(1 + \ln K^*\right) - 1\right]\delta K \tag{B.35}\\
&= -\pi^2 y^*\left[1 - \theta\left(1 + \ln K^*\right)\right]\delta K. \tag{B.36}
\end{align}$$

These linear approximations can be rewritten as a matrix equation, with a matrix called the fixed-point stability matrix:

$$\delta\begin{pmatrix} \partial K/\partial \ell \\ \partial y/\partial \ell \end{pmatrix} = \begin{bmatrix} -1 & -b \\ -c & 0 \end{bmatrix}\begin{pmatrix} \delta K \\ \delta y \end{pmatrix}, \tag{B.37}$$

where the constants

$$\begin{align}
b &= A_3 K^{*2} \tag{B.38}\\
c &= \pi^2 y^*\left[1 - \theta\left(1 + \ln K^*\right)\right] \tag{B.39}
\end{align}$$

take on different values depending on which fixed point is used. We will find that the product of b and c, which we'll call x, is an important quantity:

$$
\begin{aligned}
x \equiv bc &= A_3 K^{*2} \pi^2 y^* \left[1 - \theta\left(1 + \ln K^*\right)\right] && \text{(B.40)} \\
&= \pi^2 A_3 K^{*2} \left(\frac{1}{A_3 K^*}\right) \left[1 - \theta\left(1 + \ln K^*\right)\right] && \text{(B.41)} \\
&= \pi^2 K^* \left[1 - \theta\left(1 + \ln K^*\right)\right] . && \text{(B.42)}
\end{aligned}
$$

Note that the differential vector on the left-hand-side of Eq. (B.37), $\delta\big(\partial K/\partial\ell\,, \partial y/\partial\ell\big)$, not only represents the change in the flow-rate vector from a fixed point to a nearby point, but (since the fixed point has a zero-vector flow rate) also represents the flow-rate vector at the nearby point. Given this fact, the equation

$$
\delta \begin{pmatrix} \partial K/\partial\ell \\ \partial y/\partial\ell \end{pmatrix} = \lambda \begin{pmatrix} \delta K \\ \delta y \end{pmatrix} \tag{B.43}
$$

represents the situation where the flow-rate vector at a point near the fixed point equals some constant multiple λ of the displacement from the fixed point. For real-valued constants, this means that the flow is either directly away from (for positive values) or directly toward (for negative values) the fixed point. Using the linearized matrix form of the flow direction, this becomes an eigenvalue equation with the stability matrix:

$$
\begin{bmatrix} -1 & -b \\ -c & 0 \end{bmatrix} \begin{pmatrix} \delta K \\ \delta y \end{pmatrix} = \lambda \begin{pmatrix} \delta K \\ \delta y \end{pmatrix} , \tag{B.44}
$$

Solving for the eigenvalues λ, we get

$$
\begin{aligned}
0 &= \begin{vmatrix} -1-\lambda & -b \\ -c & -\lambda \end{vmatrix} = \lambda(1+\lambda) - bc = \lambda^2 + \lambda - x && \text{(B.45)} \\
\lambda &= \tfrac{1}{2}\left(-1 \pm \sqrt{1+4x}\right) && \text{(B.46)} \\
&= \tfrac{1}{2}\left(-1 \pm \sqrt{1 + 4\pi^2 K^* \left[1 - \theta\left(1 + \ln K^*\right)\right]}\right) , && \text{(B.47)}
\end{aligned}
$$

which gives us two eigenvalues per fixed point:

$$\lambda_{1\mathrm{a}} = -0.5 + i\,4.279 \tag{B.48}$$

$$\lambda_{1\mathrm{b}} = -0.5 - i\,4.279 \tag{B.49}$$

$$\lambda_{2\mathrm{a}} = 1.488 \tag{B.50}$$

$$\lambda_{2\mathrm{b}} = -2.488. \tag{B.51}$$

We've already noted that the positive and negative eigenvalues correspond to outward and inward paths from and to a fixed point, but what do the complex eigenvalues mean? To answer that question, we can examine the general solution of the flow near the fixed point in terms of the eigenvectors and their eigenvalues.

We can and will solve for the (unit) eigenvectors $\mathbf{u}_{\mathrm{a}}$ and $\mathbf{u}_{\mathrm{b}}$ associated with each eigenvalue, but first we treat them abstractly. It may help to use a different notation for the flow-rate vector in this analysis. Defining the displacement vector $\boldsymbol{\epsilon}$ by

$$\boldsymbol{\epsilon} \equiv \begin{pmatrix} \delta K \\ \delta y \end{pmatrix}, \tag{B.52}$$

the flow-rate vector (along an eigenvector direction) can be rewritten by switching the differentials as

$$\delta \begin{pmatrix} \partial K/\partial \ell \\ \partial y/\partial \ell \end{pmatrix} = \frac{\partial}{\partial \ell} \begin{pmatrix} \delta K \\ \delta y \end{pmatrix} \tag{B.53}$$

$$= \frac{\partial \boldsymbol{\epsilon}}{\partial \ell}\,. \tag{B.54}$$

The eigenvalue equation then becomes

$$\frac{\partial \boldsymbol{\epsilon}}{\partial \ell} = \lambda\, \boldsymbol{\epsilon}, \tag{B.55}$$

with the apparent general solution being

$$\boldsymbol{\epsilon} = \chi_{\mathrm{a}} \exp(\lambda_{\mathrm{a}}\, \Delta\ell)\; \mathbf{u}_{\mathrm{a}} + \chi_{\mathrm{b}} \exp(\lambda_{\mathrm{b}}\, \Delta\ell)\; \mathbf{u}_{\mathrm{b}}, \tag{B.56}$$

with χ_a and χ_b being very small with respect to K^* and y^*.

The general solution for the eigenvectors, where a unit eigenvector is written in K- and y-components as $\mathbf{u} = (u_K, u_y)$, is found in the following manner. Solving

$$\begin{bmatrix} -1 & -b \\ -c & 0 \end{bmatrix} \begin{pmatrix} u_K \\ u_y \end{pmatrix} = \begin{pmatrix} -u_K - bu_y \\ -cu_K \end{pmatrix} = \lambda \begin{pmatrix} u_K \\ u_y \end{pmatrix}, \tag{B.57}$$

we find the components of the eigenvector relate to each other by the relation

$$u_y = -\frac{c}{\lambda} u_K. \tag{B.58}$$

In general, since λ can be complex, the eigenvector components can also be complex. Taking u_K to be real, the solution is

$$\mathbf{u} = \begin{pmatrix} \dfrac{1}{\sqrt{1 + c^2/\left|\lambda\right|^2}} \\ \dfrac{-c/\lambda}{\sqrt{1 + c^2/\left|\lambda\right|^2}} \end{pmatrix}, \tag{B.59}$$

so that $\mathbf{u} \cdot \mathbf{u}^* = 1$, where $\mathbf{u}^*$ is the complex conjugate of $\mathbf{u}$. (Be sure not to confuse the two meanings of the asterisk – one indicating a fixed point, the other indicating complex conjugate.)

With this information, we can see what the complex eigenvalues imply. Using Euler's (complex analysis) formula, $\exp(ix) = \cos(x) + i \sin(x)$, a complex number in an exponential function can be translated into an exponential factor (associated with the real part) and a sinusoidal factor (associated with the imaginary part). To see exactly what happens with the solution in Eq. (B.56) for the first fixed point, one needs to incorporate the fact that the eigenvalues of are conjugates of each other ($\lambda_{2\mathrm{b}} = \lambda_{2\mathrm{a}}^*$), and the eigenvectors are complex, and together this should annihilate all the imaginary components of the flow. Without getting into too much detail, it is reasonable to expect that the complex eigenvalues imply a spiraling motion (due to the imaginary part) and an inward motion (due to the negative real part). This suspicion is confirmed by the numerical solution of the flow and by the fixed-point classification in Ref. [109], where the first fixed point is seen to be a stable spiral ("O type") point and the second fixed point is seen to be a hyperbolic or saddle ("X type") point. (See Ref. [110] for further classification vocabulary.)

B.2.2 Flow Investigation

Now we will examine how these flow trajectories look when they are numerically computed. We will make a final analytic calculation of the critical exponent ν after examining the flows and interpreting where the critical behavior arises. We could solve for approximate, asymptotic solutions for the trajectories in various regimes, but we will proceed with a numerical, visual exploration for now. Due to the somewhat complicated nature of the flow, we will have to show the flow in several figures with different coordinate scales.

First we examine the flow near the second fixed point in Fig. B.3. The technique used to produce the inward and outward trajectories was to first step out from the fixed point $(K_2^*, y_2^*) = (0.387508, 0.0624210)$ using the eigenvector components determined by Eq. (B.59), and then take further steps using the scaling relations. The stepping increment $\Delta\ell$ is set to a positive number for the outward trajectories to trace them in the forward direction with ℓ increasing, and $\Delta\ell$ is set to a negative number for the inward trajectories to trace them in the backward direction with ℓ decreasing. The other eight curves were generated by choosing nearby starting points and stepping out (forward and backward) with the scaling relations. The arrows indicate the forward flow direction for each trajectory.

The next plot in Fig. B.4 shows a wider view that includes both fixed points, and it shows the inward spiraling flow near the second fixed point. The even wider view

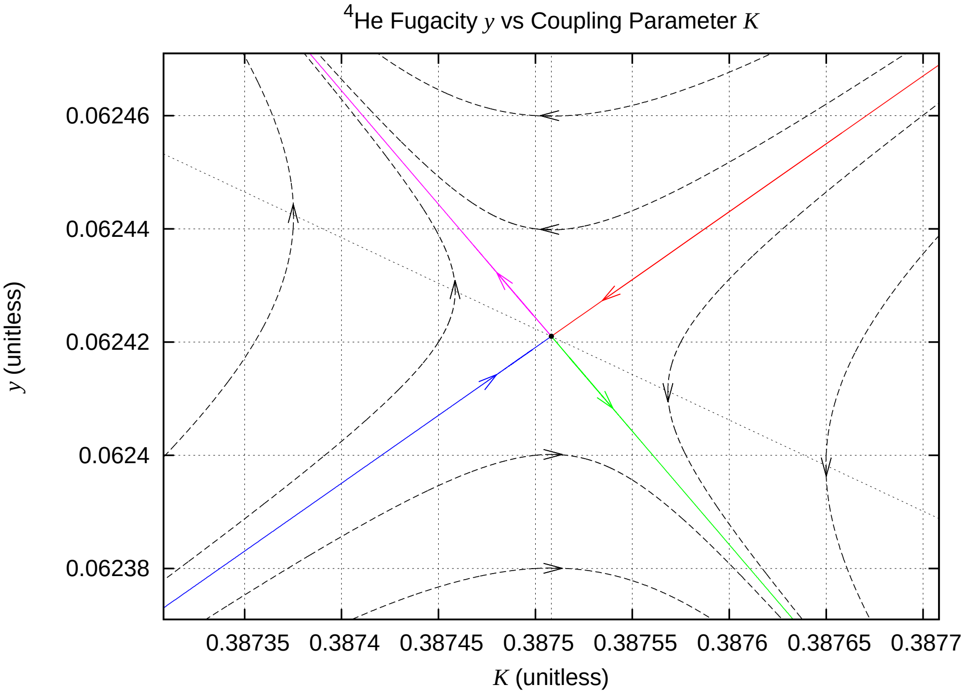

Figure B.3: Here are some representative renormalization trajectories near the second fixed point $(K_2^*, y_2^*) = (0.387508, 0.0624210)$, with arrows to indicate the forward flow directions. Note that the y-derivative is zero for all trajectories along the line $y = y_2^*$, which is highlighted with a dotted line, and the K-derivative for all is zero for all trajectories along the curve $y = 1/(A_3 K)$, also highlighted with a dotted line. This can be confirmed by examining the scaling relations.

in Fig. B.5 shows a larger, triangular pattern in the flow, and it is apparent from both Fig.s B.4 and B.5 that the red and blue trajectories that end on the hyperbolic fixed point both begin at (or infinitesimally close to) the origin. However, we know that the red curve cannot touch or intersect the K-axis (with $y = 0$) since we already know from our earlier parenthetical comment that the trajectory along that axis remains there (since $\partial y/\partial \ell = 0$) with K given by $K(\ell) = K_\mathrm{i} \exp(\ell)$ (since $\partial K/\partial \ell = K$). So the red trajectory and any other trajectory seen above the K-axis must always have a positive y-value, even if it becomes very close to zero. We find that the green trajectory that is repelled directly

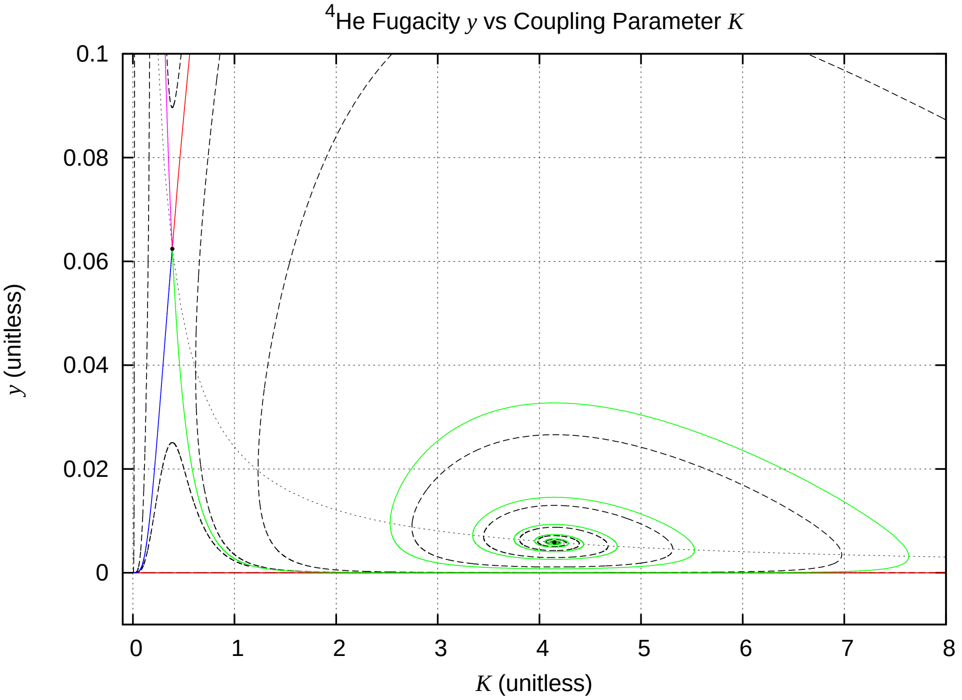

Figure B.4: In this view of the renormalization flow, the spiral fixed point $(K_1^*, y_1^*) = (4.146766, 0.00583314)$ is seen as well as the hyperbolic fixed point (K_2^*, y_2^*) $= (0.387508, 0.0624210)$. Note that the "turn-around" points on the spirals coincide with the dotted-line curve $y = 1/(A_3K)$.

away from the hyperbolic fixed point is "captured" by and ends at the spiral fixed point. The other outward-bound trajectory in magenta diverges in y, with K going to zero. So we find that two trajectories (the magenta and green) originate from the hyperbolic fixed point, and all other trajectories come from the origin. All trajectories inside the region delineated by the blue and red curves end at the spiral fixed point. All trajectories outside of this region mimic the blue-and-magenta or red-and-magenta paths and end with y diverging and K converging to zero. These facts may be easier to discern with the help of Fig.s B.6 and B.7, which use logarithmic scales on one or more axes.

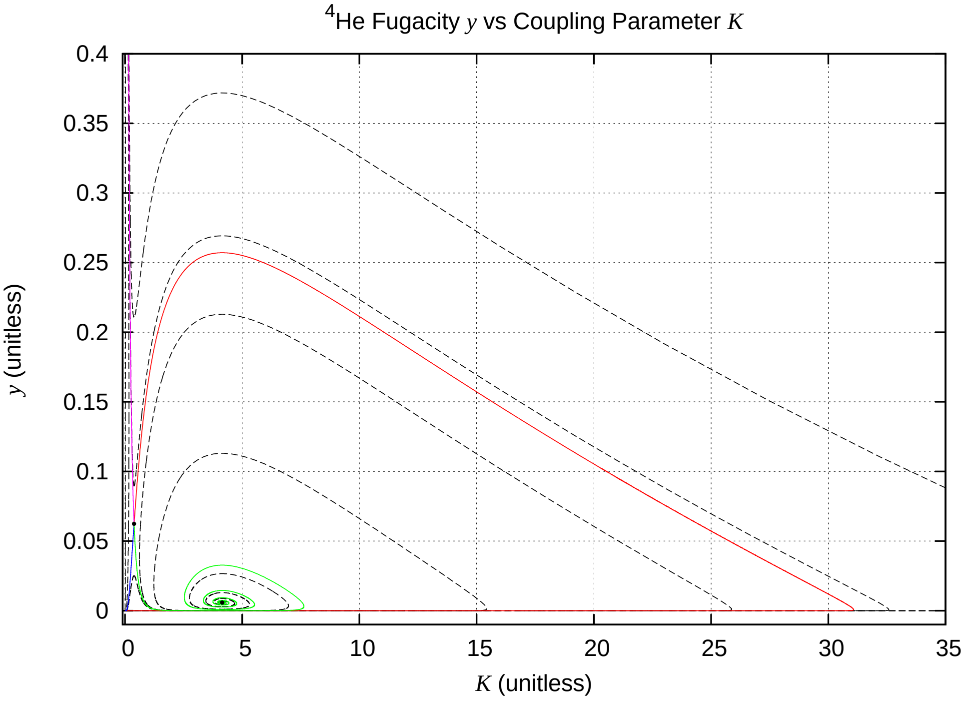

Figure B.5: In this view of the renormalization flow, the larger-scale triangular flow pattern is visible.

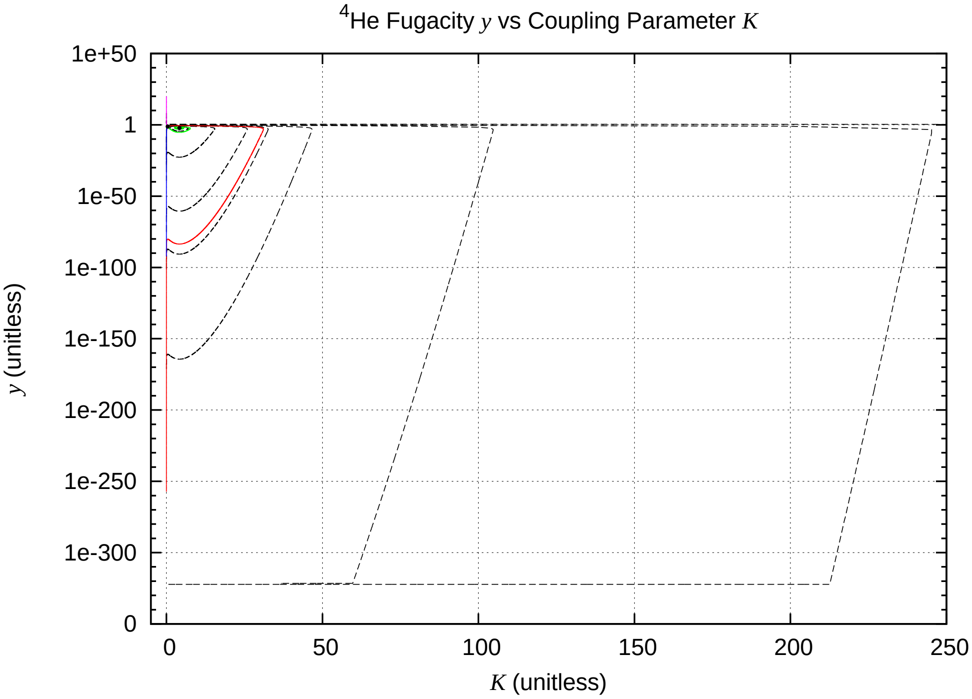

Figure B.6: With the y-axis in logarithmic scale, it is easier to see how the outer trajectories come from underneath the red trajectory to then swoop up and around, as seen in Fig. B.5, to form a triangular flow pattern and then bend upward and head toward $(0, \infty)$. The flat portions of the trajectories at the bottom of the graph are artifacts of the numerical limits of the double floating-point digits in the computation.

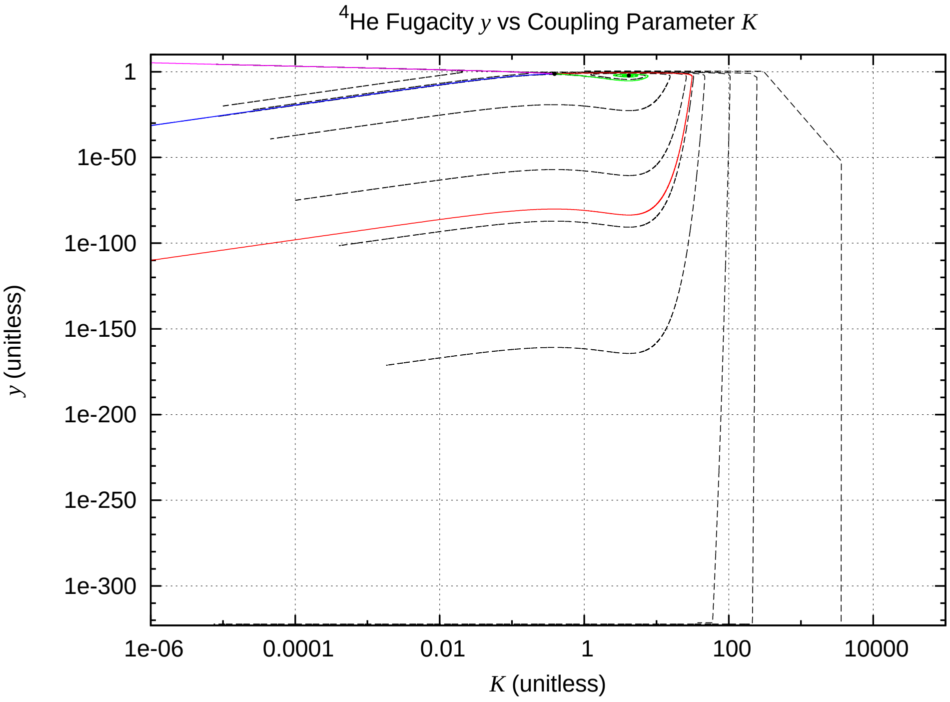

Figure B.7: With the y- and K-axes both in logarithmic scale, the behavior near the origin and near $K = 0$ becomes more apparent. Trajectories between the red and blue lines begin "at" the origin and end at the spiral fixed point. Trajectories outside of this region also begin at the origin but mimic the blue-and-magenta or red-and-magenta paths and end with y diverging and K converging to zero. The strange bend in the rightmost trajectory is an artifact from the program algorithm, which was not designed for such large values of K.

With the nature of the flow pattern above the K-axis understood, one can begin to understand the flow pattern over the whole domain, including the unphysical flow below the K-axis. In Fig. B.8 it is apparent that the triangular pattern above the K-axis is part of a larger "elbow" pattern that repeats and "echoes" up and down the y-axis, much like the 2D flow pattern repeated. It is just at the K-axis and at the fixed points that this pattern is disturbed.

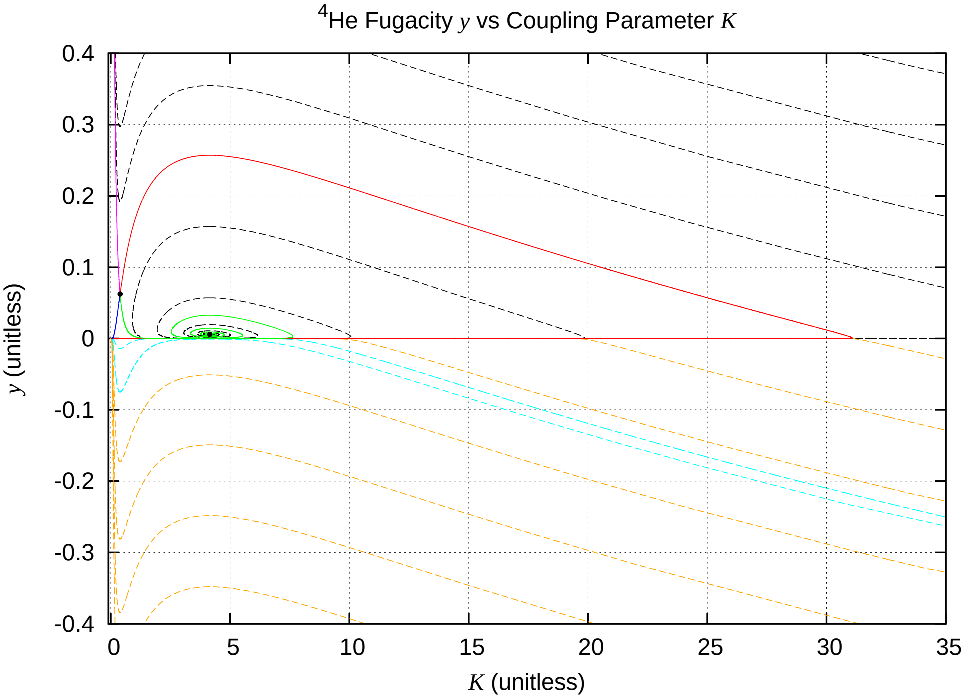

Figure B.8: The renormalization flow across the whole domain shows a repeating "elbow" pattern that repeats and is only disturbed near the K-axis and the fixed points. The orange and cyan curves all start from the origin, some of them skim along near the K-axis, and all of them end in a downward sloping orientation.

As is discussed in Section 2.1.4, the 3D Equations Summary, when calculating these flows one must either manually limit the size of a_c by changing the y scaling relations for

$K \gtrsim 1$ from

$$\frac{\partial y}{\partial \ell} = y\left\{6 - \pi^2 K\left(1 - \theta \ln K\right)\right\} \tag{B.60}$$

to

$$\frac{\partial y}{\partial \ell} = y\left\{6 - \pi^2 K\right\} \tag{B.61}$$

or cut short the renormalization at a certain threshold value of K before the formula for a_{c} becomes large enough to significantly affect the results. These alternatives make intuitive sense when viewing the renormalization flow of the new scaling relation in Eq. (B.61). Taken together with the same K scaling relation as before,

$$\frac{\partial K}{\partial \ell} = K - A_3 K^2 y, \tag{B.62}$$

we can perform the same fixed-point and linear stability analysis as before to help investigate and calculate the flow. We find a hyperbolic fixed point (K_3^*, y_3^*) with

$$K_3^* = \frac{6}{\pi^2} = 0.607927 \tag{B.63}$$

$$y_3^* = \frac{1}{A_3 K^*} = \frac{1}{8\pi} = 0.0397887, \tag{B.64}$$

since $A_3 = 4\pi^3/3$. There is also a repulsive fixed point at the origin. Numerically solving for the flow across the whole upper quadrant of the K-y plane, using the same techniques already described, yields the trajectories in Fig. B.9. This flow is only valid for the region $K \gtrsim 1$; for the region $K < 1$ we use the flow re-illustrated in Fig. B.10 for direct comparison. (See the caption of Fig. B.10 for further comments.) Putting the two together results in Fig. B.11, which finally shows the physical flow of the 3D scaling relations.

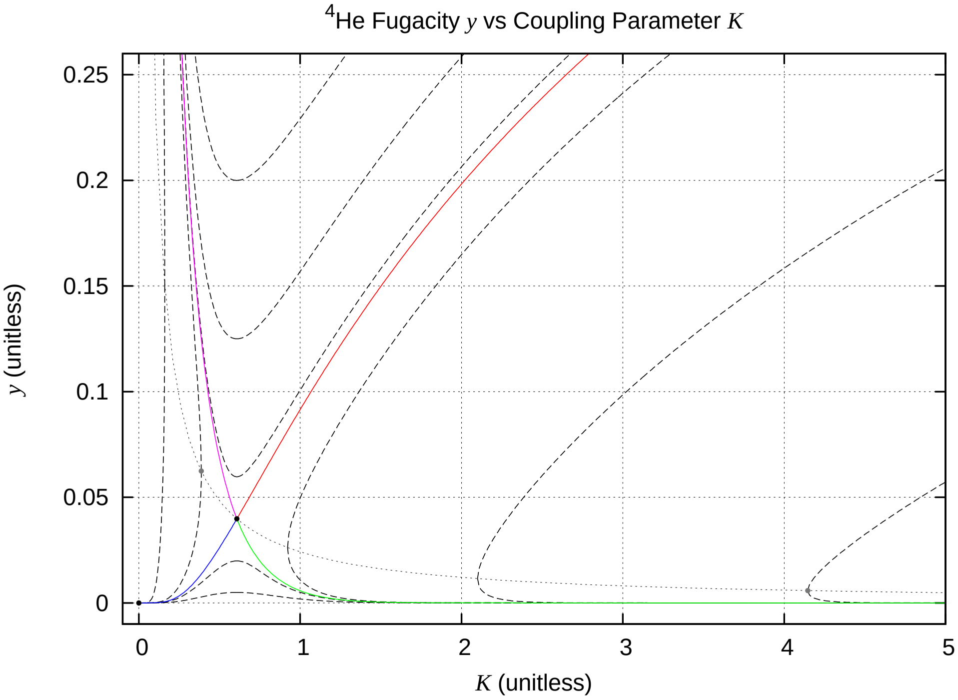

Figure B.9: With the altered y scaling relation in Eq. (B.61), which is only valid for $K \gtrsim 1$, the flow changes and loses the spiral fixed point. There is a repulsive fixed point at the origin and a hyperbolic fixed point at $(K_3^*, y_3^*) = (0.607927, 0.0397887)$.

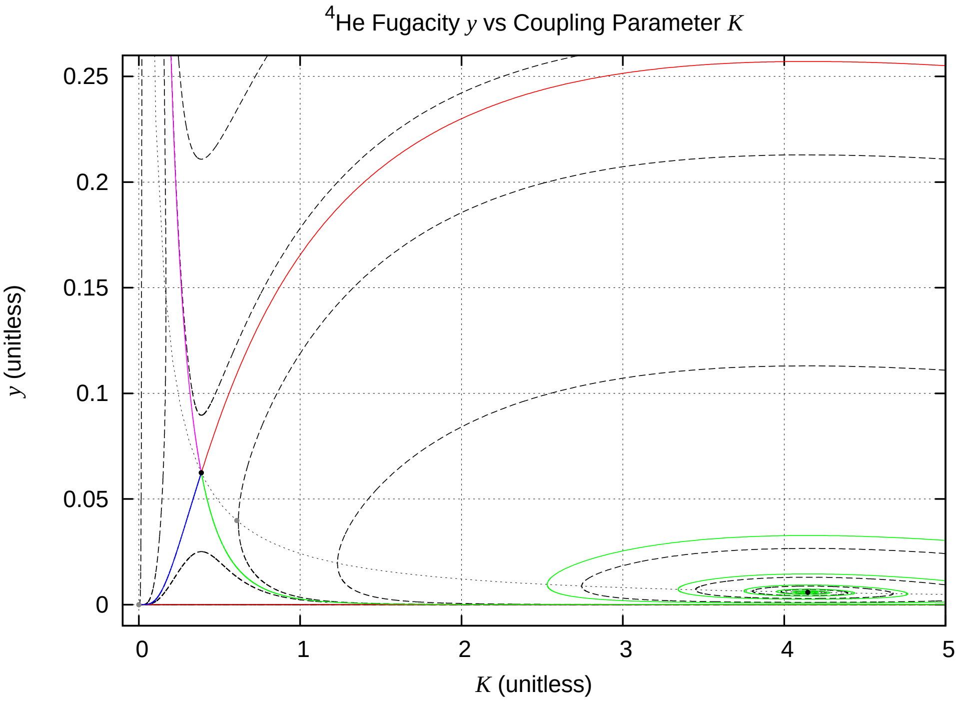

Figure B.10: This is the renormalization flow with the y scaling relation in Eq. (B.60), re-illustrated for direct comparison and synthesis with the flow in Fig. B.9. Note that for flow trajectories near the K-axis (but above the red curve) – trajectories that will turn out to be physically relevant – the flow stops moving downward and starts to curve upwards at $K = K_1^* = 4.15$ (where $\partial y/\partial \ell = 0$) to embark on a spiral towards the lower-right fixed point. At this value of K the miscalculation of a_c is significant enough to fundamentally change the behavior of the flow. One can either cut off the renormalization trajectories at a threshold value of about $K = K_1^*$, to prevent this pathological influence, or transfer to the flow in Fig. B.9 at $K = 1$ (or at least before $K = K_1^*$). In Fig. B.11 we show the flow given the latter choice.

The trajectories in Fig. B.11 must start from bare ($\ell = 0$) values that obey the relation

$$y^{\ell 0} \;=\; \exp(-\pi^2 K^{\ell 0} C). \tag{B.65}$$

As is discussed in Chapter 3, we take the value of C to be approximately constant over temperature (at least near T_λ) and equal to its critical $T = T_\lambda$ value, C_c. A particular value of C corresponds to a particular pressure. The two bare-value exponential curves shown in Fig. B.11 represent the extremal curves of the lowest and highest pressures possible in superfluid helium: $C = 1.1$ goes with $P \approx 0$ bar and $C = 0.4$ goes with $P \approx 30$ bar. This pressure correspondence is explained in detail in Chapter 3 and shown in Fig. 3.6. Some representative trajectories from these bare-value curves are shown, and we can finally see that for the physical flow there are two flow regions separated by a critical boundary trajectory. As is explained in more detail in Chapter 3, the upward-leftward flow corresponds to temperatures above T_λ, where $\rho_\mathrm{s}^\mathrm{r}/\rho = K_\mathrm{s}/K^{\ell 0} = \exp(-\ell)\, K/K^{\ell 0}$ goes to zero as ℓ increases, and the downward-rightward flow corresponds to temperatures below T_λ, where $\rho_\mathrm{s}^\mathrm{r}/\rho = \exp(-\ell)\, K/K^{\ell 0}$ can converge to a non-zero finite value as ℓ increases.

The attractive paths toward the hyperbolic fixed point are the critical trajectories, and tracing the paths backwards from the fixed point allows one to calculate the critical bare value of K, $K_\mathrm{c}^{\ell 0}$, for a given value of C and a certain pressure. This is one way to calculate $K_\mathrm{c}^{\ell 0}$, different from the trial-and-error forward-trajectory method described in Chapter 3. The value one calculates for $K_\mathrm{c}^{\ell 0}$ will depend on the step size (in terms of $\Delta\ell$ or perhaps a K-y-space distance increment in terms of ΔK and Δy) and the desired precision given the particular method used. The latter trial-and-error method is preferable when one is looking for a value of $K_\mathrm{c}^{\ell 0}$ appropriate for use in forward-trajectory calculations of various quantities. We use this trial-and-error method for our calculations.

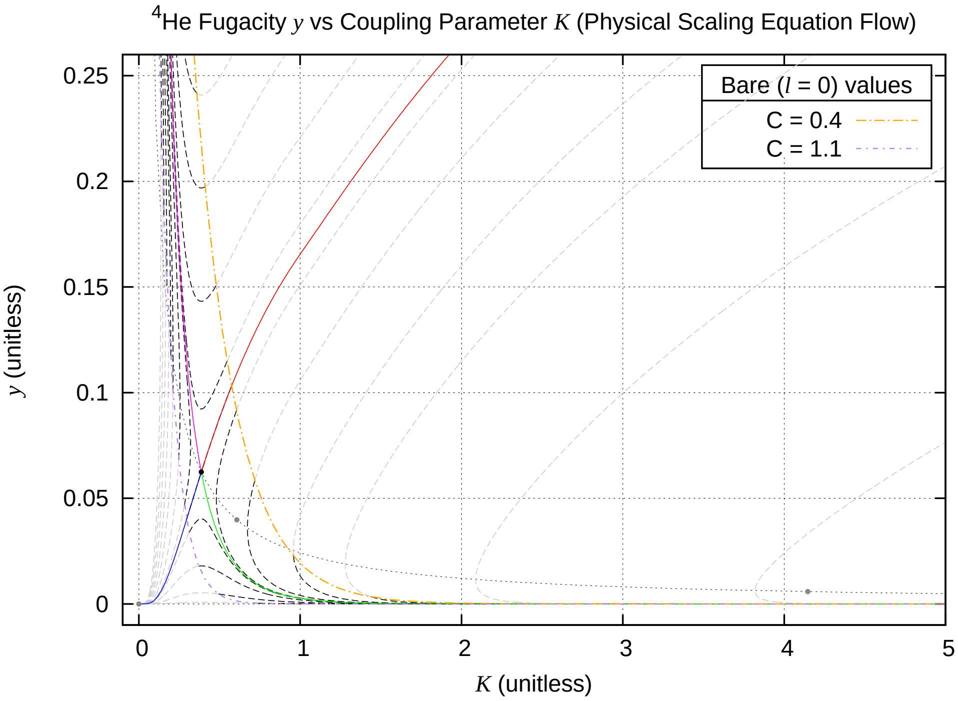

Figure B.11: Here, in black dashed curves, are some representative physically relevant renormalization trajectories, or solution curves for the 3D scaling relations referred to in Eq.s (B.60–B.62). All of the black dashed trajectories start from a bare-value exponential curve given by $y^{\ell 0} = \exp(-\pi^2 K^{\ell 0} C)$, which depends on C. (The gray dashed trajectories show the continuation of the trajectories to unphysical negative-ℓ-valued locations.) The trajectories flowing upward-leftward correspond to temperatures above T_λ, and those flowing downward-rightward correspond to temperatures below T_λ. The critical trajectories at T_λ reach the hyperbolic fixed point $(K_2^*, y*_2) = (0.387508, 0.0624210)$ as ℓ goes to infinity. Using the relationship $K^{\ell 0} = K_{\mathrm{c}}^{\ell 0}(T_{\mathrm{KT}}/T)$, these trajectories correspond to the temperature fractions T/T_λ of 1, $\{1.05, 1.2, 1.4, 1.6, \ldots\}$, and $\{0.95, 0.8, 0.6, 0.4, \ldots\}$. The critical trajectories are highlighted with solid red and blue curves. As is explained in detail in Chapter 3, $C = 1.1$ and $C = 0.4$ correspond to pressures $P \approx 0$ bar and $P \approx 30$ bar, respectively.

B.2.3 Critical Exponent Calculation

We can extract a bit more information from the linear stability analysis within our flow analysis (or "RG analysis"). The eigenvalue $\lambda_{2\mathrm{b}} = -2.488$ is associated with the critical trajectories toward the hyperbolic fixed point. The eigenvalue $\lambda_{2\mathrm{a}} = 1.488$ on the other hand characterizes the flow away from the fixed point at temperatures away from T_λ. Using a standard RG calculation found in the literature [78, 111, 112] and explained in text books [113], we can quantify this relationship to temperature with a critical exponent ν in the power law

$$\frac{\rho_{\mathrm{s}}}{\rho} \propto (\Delta T)^{\nu}, \tag{B.66}$$

where $\Delta T \equiv T - T_\lambda$ and

$$\nu = \frac{1}{\lambda_{2\mathrm{a}}}. \tag{B.67}$$

Recall that the connection between ρ_{s}/ρ and K and y comes from the relation $\rho_{\mathrm{s}}/\rho = \lim_{\ell\to\infty} \exp(-\ell) K/K^{\ell 0}$. For many of our calculations, particularly in Chapter 3, we have preferred to use the quantity $\tau \equiv (1 - T/T_\lambda)$ rather than ΔT, so we can rewrite this power law as

$$\frac{\rho_{\mathrm{s}}}{\rho} = A' \tau^{\nu}, \tag{B.68}$$

with the numerical value of ν being

$$\begin{aligned} \nu &= \frac{1}{\lambda_{2\mathrm{a}}} = \frac{2}{-1 + \sqrt{1 + 4x_2}} && \text{(B.69)} \\ &= \frac{2}{-1 + \sqrt{1 + 4\pi^2 K_2^* \left[1 - \theta\left(1 + \ln K_2^*\right)\right]}} && \text{(B.70)} \\ &= 0.67168835, && \text{(B.71)} \end{aligned}$$

since $K_2^* = 0.38750818971$.

APPENDIX C

Derivation of a Fokker-Planck Equation

The subtitle of this appendix is “Drift and Diffusion of a Probability Density in State Space”. Sections C.5 and C.6 function as sub-appendices. Although this derivation is more general than needed for the usage of the Fokker-Planck equation in this dissertation, it should be useful for anyone interested in extending this research to higher dimensions ($D \geq 3$). For an example in arbitrary dimensions, see Ref. [114].

C.1 Probabilistic Properties

To derive a Fokker-Planck equation, which deals with probabilities, we should start by stating the probabilistic notation and properties we will use. The probability that event A occurs is $P[A]$. Summing over all possible mutually exclusive events must yield a total of one: $\sum_A P[A] = 1$. If one includes non-exclusive events, the probability sum can exceed one, so any sums will be performed over mutually exclusive events.[1] When summations are not involved, the events named can be partially or fully simultaneous, allowing illustration using Venn diagrams with overlapping regions. The probability that both A and B occur is a joint probability $P[A, B]$. The probability that A occurs given that B occurs is a conditional probability $P[A|B]$. A joint-conditional probability

---

[1] For example, let’s say a coin is flipped with colored sides where one side is red and the other is half-red half-blue. Take the set of events to be $A = A1 =$ “the upper side has red on it” and $A = A2 =$ “the upper side has blue on it”. Although this may seem like a reasonable all-inclusive set of events, both may simultaneously occur and $\sum_A P[A] = 1.5 \neq 1$.

property follows:

$$P[A,B] \;=\; P[A|B]\; P[B]. \tag{C.1}$$

This property can be illustrated nicely with a Venn diagram. This property generalizes in many ways, for instance, $P[A,B,C] = P[A|B,C]\; P[B,C]$. However, we will not need any of these generalizations.

Let's say the state of an object exhibiting Brownian motion is described by a stochastic variable $A(t)$. Let the notation $P[A(t), A'(t'), A''(t'')]$ denote the probability that the object occupies the state A'' at time t'', A' at time t', and A at time t.[2] Since the object must occupy a particular state at time t', we have the following relation,

$$\sum_{A'} P[A(t), A'(t'), A''(t'')] \;=\; P[A(t), A''(t'')], \tag{C.2}$$

given that there are a countable number of states available. Given a continuum of states, we have

$$\int \mathrm{d}X'\; p[X(t), X'(t'), X''(t'')] \;=\; p[X(t), X''(t'')], \tag{C.3}$$

where p is a probability distribution or probability density instead of a probability P. This general property is displayed in the Chapman-Kolmogorov equation:

$$\int \mathrm{d}X_i\; p[X_1, \ldots, X_{i-1}, X_i, X_{i+1}, \ldots, X_n] \;=\; p[X_1, \ldots, X_{i-1}, X_{i+1}, \ldots, X_n]. \tag{C.4}$$

Here are some more properties that help elucidate the meaning of the probabilities and probability distributions:

$$\begin{array}{rclrcl}
\sum_A P[A] & = & 1 & \int \mathrm{d}X\; p[X] & = & 1 \\
\sum_A P[A|B] & = & 1 & \int \mathrm{d}X\; p[X|Y] & = & 1 \\
\sum_{A,B} P[A,B] & = & 1 & \int \mathrm{d}X\,\mathrm{d}Y\; p[X,Y] & = & 1 \\
\sum_A P[A,B] & = & P[B] & \int \mathrm{d}X\; p[X,Y] & = & p[Y] \\
\sum_B P[A,B] & = & P[A] & \int \mathrm{d}Y\; p[X,Y] & = & p[X]
\end{array}$$

---

[2] This is slightly sloppy notation since the function P must know about both A and t. We'll eventually use more proper notation, such as $P[A;t]$, in the next section.

Note that P is always dimensionless (or has dimensions of "probability") but a probability density $p[X]$ has dimensions of $[X]^{-1}$, where $[X]$ is the dimension, such as length or energy, of the stochastic variable X. A probability density $p[X, Y, Z|U, V]$ has dimensions of $[X]^{-1}[Y]^{-1}[Z]^{-1}$.

C.2 A Fokker-Planck Equation

We will now derive a very general (forward) Fokker-Planck equation (FPE), which describes the time-evolution of a probability density in state space, considering drift and diffusion but not higher-order migration. [3] In this derivation we start with an integral equation expressing two probabilistic properties we introduced in the last section, we use Taylor expansions, pull the integral out of the derivatives, and absorb the integral into definitions of some quantities to change to a differential equation, and we finally reduce the number of terms by assuming higher-order-derivative terms are negligible.

We use a d-dimensional stochastic variable $\mathbf{R}$ to represent the state of a Brownian object. It may simply represent position or it may include quantum numbers as well as position, velocity, momentum, or other state variables. We assume that the quantum numbers, if there are any, are large enough that differences in them can be considered small, so $\mathbf{R}$ can be considered continuous: $\mathbf{R} \in \mathbb{R}^d$. [4] We also assume that probability distributions such as $p[\mathbf{R}]$ are continuous and differentiable so we can take derivatives.

Using (1) the last equation from the previous section, $p[X] = \int \mathrm{d}Y\ p[X, Y]$, and (2)

---

[3] I consider this derivation an improvement over and abstraction of the derivations by Chandrasekhar [115] and Wilde and Singh [116], where the conceptual steps are made clear and the abstractions are explained in the appendices.

[4] $\mathbf{R}$ is a univalent holor of plethos d. (A holor is a mathematical entity that is made up of one or more independent quantities. A holor may be multiply-indexed, like a tensor, but its transformation properties, under rotation, say, are not necessarily specified.) $\mathbf{R}$ doesn't necessarily transform as a Euclidean vector, so it shouldn't be called a vector to prevent confusion amongst physicists.

the joint-conditional probability property $p[X,Y]=p[X|Y]\ p[Y]$, we have

$$\begin{aligned} p[\mathbf{R}(t+\Delta t)] &= \int \mathrm{d}^d R'\ p[\mathbf{R}(t+\Delta t),\mathbf{R}'(t)] && \text{(C.5)} \\ &= \int \mathrm{d}^d R'\ p[\mathbf{R}(t+\Delta t)|\mathbf{R}'(t)]\ p[\mathbf{R}'(t)]. && \text{(C.6)} \end{aligned}$$

We should switch to a more rigorous notation to aid in the impending mathematical manipulations:

$$p[\mathbf{R},t+\Delta t] = \int \mathrm{d}^d R'\ p[\mathbf{R}|\mathbf{R}';\Delta t,t]\ p[\mathbf{R}',t]. \tag{C.7}$$

We shall approximate this exact relationship by Taylor-expanding each side, but again we should change notation. The notation above makes the joint-conditional property more apparently true, but a different notation will be more suitable for the Taylor expansions. Let's define a change-in-state holor $\boldsymbol{\xi}\equiv\Delta\mathbf{R}=\mathbf{R}-\mathbf{R}'$, denoting the change from $\mathbf{R}'$ to $\mathbf{R}$. We'll use $\boldsymbol{\xi}$ in the equations below rather than $\Delta\mathbf{R}$ because the differential $\mathrm{d}^d\xi$ looks better than $\mathrm{d}^d(\Delta R)$. We can rewrite the above equation like so:

$$p[\mathbf{R},t+\Delta t] = \int \mathrm{d}^d \xi\ p[\mathbf{R}-\boldsymbol{\xi},\boldsymbol{\xi};\Delta t,t]\ p[\mathbf{R}-\boldsymbol{\xi},t]. \tag{C.8}$$

Note that $\mathrm{d}^d R'=(-1)^d \mathrm{d}^d\xi$, but if we change the direction or sense of the integrations, then we can replace $\int \mathrm{d}^d R'$ with $\int \mathrm{d}^d\xi$. [5] Now we can apply on the left side a one-dimensional Taylor expansion (see Sub-Appendix C.5) about time t in terms of Δt and apply on the right side a multi-dimensional product Taylor expansion (also see Sub-Appendix C.5) about state $\mathbf{R}$ in terms of $-\boldsymbol{\xi}$, and we'll define a new quantity in the last

---

[5] Please inform the author if something is wrong with that last step; it seems suspect.

step:

$$\begin{aligned}
&\sum_{n=0}^{\infty}\frac{(\Delta t)^n}{n!}\partial_t{}^n p[\mathbf{R},t] && \text{(C.9)}\\
&\quad= \int \mathrm{d}^d\xi \sum_{|\alpha|\geq 0}\frac{(-\xi)^\alpha}{\alpha!}\partial_R^\alpha\left\{p[\mathbf{R},\boldsymbol{\xi};\Delta t,t]\ p[\mathbf{R},t]\right\} && \text{(C.10)}\\
&\quad= \sum_{|\alpha|\geq 0}(-1)^\alpha\partial_R^\alpha\left\{\frac{1}{\alpha!}\left(\int \mathrm{d}^d\xi\ \xi^\alpha\ p[\mathbf{R},\boldsymbol{\xi};\Delta t,t]\right)p[\mathbf{R},t]\right\} && \text{(C.11)}\\
&\quad= \sum_{|\alpha|\geq 0}(-1)^\alpha\partial_R^\alpha\left\{\frac{\langle\xi^\alpha\rangle_{\Delta t}(\mathbf{R},t)}{\alpha!}\ p[\mathbf{R},t]\right\}, && \text{(C.12)}
\end{aligned}$$

where we've defined $\langle\xi^\alpha\rangle_{\Delta t}(\mathbf{R},t)$ by

$$\langle\xi^\alpha\rangle_{\Delta t}(\mathbf{R},t) \equiv \int \mathrm{d}^d\xi\ \xi^\alpha\ p[\mathbf{R},\boldsymbol{\xi};\Delta t,t], \tag{C.13}$$

which gives the elements of a mean-transition-increment holor to a state $\mathbf{R}$ at time t during a time Δt. Actually, this defines one holor for every set of multi-indices α with the same magnitude. While we're at it, let's define a set of "migration holors", which are also sometimes called kinetic terms (pg 55 of [117]) or generalized diffusion tensors [118],

$$M_{|\alpha|}^{\{\alpha\}}(\mathbf{R},t) \equiv \lim_{\Delta t\to 0}\frac{\langle\xi^\alpha\rangle_{\Delta t}(\mathbf{R},t)}{\alpha!\Delta t}, \tag{C.14}$$

which are mean-transition-rate holors, giving mean rates of various transitions in state space. For more elaboration on the meaning of this notation, see Sub-Appendix C.6. After we divide both sides of the equation by Δt, we can write the resulting equation in terms of these migration holors. In applications, the limit in the definition above may actually have Δt go to some small non-zero value, since there may be wild fluctuations on small time-scales but a smoother behavior when averaged over a small non-zero duration.

Now, after cancelling the first term[6] in each series, dividing by Δt, and letting Δt be

---

[6] Since $\left\langle\xi^{\langle 0,0,\ldots,0\rangle}\right\rangle_{\Delta t}(\mathbf{R},t) = \int \mathrm{d}^d\xi\ \xi^{\langle 0,0,\ldots,0\rangle}\ p[\mathbf{R},\boldsymbol{\xi};\Delta t,t] = \int \mathrm{d}^d\xi\ p[\mathbf{R},\boldsymbol{\xi};\Delta t,t] = 1$, the first term in the series on the right is $p[\mathbf{R},t]$, as is the first term in the series on the left.

small enough[7], we get

$$\sum_{n=1}^{\infty} \frac{(\Delta t)^{n-1}}{n!} {\partial_t}^n p[\mathbf{R}, t] \;=\; \sum_{|\alpha|\geq 1} (-1)^{\alpha} \partial_R^{\alpha} \left\{ \frac{\langle \xi^{\alpha} \rangle_{\Delta t}(\mathbf{R}, t)}{\alpha! \Delta t} \; p[\mathbf{R}, t] \right\} \tag{C.15}$$

$$= \sum_{|\alpha|\geq 1} (-1)^{\alpha} \partial_R^{\alpha} \left\{ M_{|\alpha|}^{\{\alpha\}}(\mathbf{R}, t) \; p[\mathbf{R}, t] \right\}. \tag{C.16}$$

If we expand these series out, we can switch the right side into Einstein summation notation:

$$\partial_t \, p[\mathbf{R}, t] + \frac{\Delta t}{2} {\partial_t}^2 p[\mathbf{R}, t] + \frac{(\Delta t)^2}{6} {\partial_t}^3 p[\mathbf{R}, t] + \cdots \tag{C.17}$$

$$= \; -\partial_i \left\{ M_1^i(\mathbf{R}, t) \; p[\mathbf{R}, t] \right\} + \partial_j \partial_k \left\{ M_2^{jk}(\mathbf{R}, t) \; p[\mathbf{R}, t] \right\} \tag{C.18}$$

$$- \, \partial_\ell \partial_m \partial_n \left\{ M_3^{\ell m n}(\mathbf{R}, t) \; p[\mathbf{R}, t] \right\} + \cdots \tag{C.19}$$

Now, to get the Fokker-Planck equation we seek, we just assume all terms except the first term on the left side and the first two terms on the right side are negligible:

$$\boxed{\partial_t \, p[\mathbf{R}, t] \;=\; -\partial_i \left\{ M_1^i(\mathbf{R}, t) \; p[\mathbf{R}, t] \right\} + \partial_j \partial_k \left\{ M_2^{jk}(\mathbf{R}, t) \; p[\mathbf{R}, t] \right\}} \tag{C.20}$$

As implied in the general definition above, these two migration holors are defined by

$$M_1^i(\mathbf{R}, t) \;\equiv\; \lim_{\Delta t \to 0} \frac{\langle \Delta R_i \rangle_{\Delta t}(\mathbf{R}, t)}{\Delta t}, \tag{C.21}$$

$$M_2^{ij}(\mathbf{R}, t) \;\equiv\; \lim_{\Delta t \to 0} \frac{\left\langle \Delta R_i \, \Delta R_j \right\rangle_{\Delta t}(\mathbf{R}, t)}{2 \Delta t}. \tag{C.22}$$

M_1^i can be called the drift holor since it describes the mean drift through state space. M_1^{ij} can be called the diffusion holor since it describes the mean diffusion through state space, like a diffusion tensor describes real-space diffusion.

C.3 A Note

It is important to note that the Fokker-Planck equation is a continuity equation: it is a local conservation of probability equation. An example of a continuity equation is the

---

[7] If Δt must go to zero, then only one term will remain on the left side.

charge continuity equation in electrodynamics,

$$\partial_t \rho \;=\; -\boldsymbol{\nabla}\cdot\mathbf{J} = -\partial_i J^i, \tag{C.23}$$

where ρ is the charge density and $\mathbf{J}$ is the charge current density (in real space). Likewise, the Fokker-Planck equation can be written in this form and we can solve for the probability current density (in state space):

$$\begin{aligned} \partial_t\, p[\mathbf{R},t] &= -\partial_i \left\{ M_1^i(\mathbf{R},t)\; p[\mathbf{R},t] - \partial_j \Big[M_2^{ij}(\mathbf{R},t)\; p[\mathbf{R},t] \Big] \right\}, &\text{(C.24)}\\ J^i &= M_1^i(\mathbf{R},t)\; p[\mathbf{R},t] - \partial_j \Big[M_2^{ij}(\mathbf{R},t)\; p[\mathbf{R},t] \Big]\,. &\text{(C.25)} \end{aligned}$$

The total probability (usually assumed to be one) could be lost or gained at the boundaries of the state space if there is a loss or gain in the number of Brownian objects, or the Fokker-Planck equation could be reformulated in terms of number-density rather than probability density (of Brownian objects). Furthermore, one could add a source-sink term if there is injection/creation or loss/annihilation of Brownian objects within the boundaries of the state space.

C.4 A Warning

It seems that many times when the Fokker-Planck equation is used, it comes in a simplified form where the diffusion holor has been pulled out of one derivative:

$$\partial_t\, p[\mathbf{R},t] \;=\; \partial_i \left\{ -M_1^i(\mathbf{R},t)\; p[\mathbf{R},t] + M_2^{ij}(\mathbf{R},t)\; \partial_j\, p[\mathbf{R},t] \right\}. \tag{C.26}$$

In the cases where M_2 is constant or nearly constant, this is perfectly justifiable. But this (often unexplained) sleight of pen is performed in cases where M_2 is dependent on $\mathbf{R}$, and the reason for this move may be a kind of “pragmatism”: the equation may just be too hard to solve in its original form, so M_2 is pulled out of one derivative to make it solvable.

C.5 Taylor Series

One-dimensional Taylor Series

A one-dimensional function $f : \mathbb{R} \to \mathbb{R}$ that is analytic equals its Taylor series in some interval. We can write the Taylor series in what could be called the "derivative series form" like so,

$$f(x+h) \;=\; \sum_n \frac{h^n}{n!}\, \mathrm{d}_x^n f(x), \tag{C.27}$$

where d_x^n is shorthand for $(\mathrm{d}/\mathrm{d}x)^n = \mathrm{d}^n/\mathrm{d}x^n$.

Multi-dimensional Taylor Series in Multi-index Notation

A multi-dimensional Taylor series of an analytic function $f : \mathbb{R}^n \to \mathbb{R}$ can be nicely written in what is called multi-index notation. We have $\mathbf{x} \in \mathbb{R}^n$ and $f(\mathbf{x}) \in \mathbb{R}$, and the multi-index α is an n-tuple of non-negative-integer-valued indices in $\mathbb{N}^n$. Here are the notational properties and definitions:

- $\alpha \in \mathbb{N}^n$
- $\alpha = \langle \alpha_1, \ldots, \alpha_n \rangle$
- Magnitude of α: $|\alpha| \equiv \alpha_1 + \cdots + \alpha_n$
- Factorial of α: $\alpha! \equiv \alpha_1! \cdots \alpha_n!$
- $x^\alpha \equiv x_1^{\alpha_1} \cdots x_n^{\alpha_n}$
- $\partial_x^\alpha = \partial_1^{\alpha_1} \cdots \partial_n^{\alpha_n} = (\partial/\partial x_1)^{\alpha_1} \cdots (\partial/\partial x_n)^{\alpha_n} = \dfrac{\partial^{|\alpha|}}{\partial x_1^{\alpha_1} \cdots \partial x_n^{\alpha_n}}$

Given these definitions the Taylor series of f about $\mathbf{x}$ in terms of elements of $\mathbf{h}$ is

$$f(\mathbf{x}+\mathbf{h}) \;=\; \sum_{|\alpha|\geq 0} \frac{h^\alpha}{\alpha!}\, \partial_x^\alpha f(\mathbf{x}). \tag{C.28}$$

Expanding this out, one gets what one expects:

$$\begin{aligned}
f(\mathbf{x}+\mathbf{h}) &= \frac{h^{\langle 0,0,\ldots,0\rangle}}{\langle 0,0,\ldots,0\rangle!}\,\partial_x^{\langle 0,0,\ldots,0\rangle} f(\mathbf{x}) \\
&\quad + \Bigg(\frac{h^{\langle 1,0,\ldots,0\rangle}}{\langle 1,0,\ldots,0\rangle!}\,\partial_x^{\langle 1,0,\ldots,0\rangle} f(\mathbf{x}) + \frac{h^{\langle 0,1,\ldots,0\rangle}}{\langle 0,1,\ldots,0\rangle!}\,\partial_x^{\langle 0,1,\ldots,0\rangle} f(\mathbf{x}) \\
&\qquad + \cdots + \frac{h^{\langle 0,0,\ldots,1\rangle}}{\langle 0,0,\ldots,1\rangle!}\,\partial_x^{\langle 0,0,\ldots,1\rangle} f(\mathbf{x}) \Bigg) \\
&\quad + \Bigg(\frac{h^{\langle 2,0,\ldots,0\rangle}}{\langle 2,0,\ldots,0\rangle!}\,\partial_x^{\langle 2,0,\ldots,0\rangle} f(\mathbf{x}) + \frac{h^{\langle 1,1,\ldots,0\rangle}}{\langle 1,1,\ldots,0\rangle!}\,\partial_x^{\langle 1,1,\ldots,0\rangle} f(\mathbf{x}) \\
&\qquad + \cdots + \frac{h^{\langle 1,0,\ldots,1\rangle}}{\langle 1,0,\ldots,1\rangle!}\,\partial_x^{\langle 1,0,\ldots,1\rangle} f(\mathbf{x}) \\
&\qquad + \frac{h^{\langle 0,2,\ldots,0\rangle}}{\langle 0,2,\ldots,0\rangle!}\,\partial_x^{\langle 0,2,\ldots,0\rangle} f(\mathbf{x}) + \cdots + \frac{h^{\langle 0,1,\ldots,1\rangle}}{\langle 0,1,\ldots,1\rangle!}\,\partial_x^{\langle 0,1,\ldots,1\rangle} f(\mathbf{x}) \\
&\qquad + \cdots + \frac{h^{\langle 0,0,\ldots,2\rangle}}{\langle 0,0,\ldots,2\rangle!}\,\partial_x^{\langle 0,0,\ldots,2\rangle} f(\mathbf{x}) \Bigg) \\
&\quad + \cdots \qquad \text{(C.29)} \\
&= f(\mathbf{x}) + h_i\,\partial_x^i f(\mathbf{x}) + \frac{1}{2} h_j h_k\,\partial_x^j \partial_x^k f(\mathbf{x}) + \cdots \qquad \text{(C.30)}
\end{aligned}$$

1D Taylor Series of a Product of Functions

The product of two Taylor series is the Taylor series of the product:

$$f(x+h)\,g(x+h) = (fg)(x+h) \qquad \text{(C.31)}$$

and

$$\begin{aligned}
\left[\sum_{n=0}^{\infty} \frac{h^n}{n!}\,\partial_x^n f(x)\right]\left[\sum_{m=0}^{\infty} \frac{h^m}{m!}\,\partial_x^m g(x)\right] &= \sum_{\ell=0}^{\infty} \frac{h^\ell}{\ell!}\,\partial_x^\ell (fg)(x) \qquad \text{(C.32)} \\
&\equiv \sum_{\ell=0}^{\infty} \frac{h^\ell}{\ell!}\,\partial_x^\ell \{ f(x)\,g(x) \}\,. \qquad \text{(C.33)}
\end{aligned}$$

Here's a proof using combinatorics:

$$\begin{aligned}
f(x+h)\,g(x+h) &= \left[\sum_{n=0}^{\infty}\frac{h^n}{n!}\,\partial_x^n f(x)\right]\left[\sum_{m=0}^{\infty}\frac{h^m}{m!}\,\partial_x^m g(x)\right] && \text{(C.34)}\\
&= \sum_{\ell=0}^{\infty}\sum_{m=0}^{\ell}\frac{h^\ell}{(\ell-m)!m!}\,\partial_x^{\ell-m} f(x)\,\partial_x^m g(x) && \text{(C.35)}\\
&\quad \ell \equiv n+m,\ \text{so } n=\ell-m && \text{(C.36)}\\
&= \sum_{\ell=0}^{\infty}\frac{h^\ell}{\ell!}\left(\sum_{m=0}^{\ell}\frac{\ell!}{m!(\ell-m)!}\partial_x^{\ell-m} f(x)\,\partial_x^m g(x)\right) && \text{(C.37)}\\
&= \sum_{\ell=0}^{\infty}\frac{h^\ell}{\ell!}\left(\sum_{m=0}^{\ell}\binom{\ell}{m}\partial_x^{\ell-m} f(x)\,\partial_x^m g(x)\right) && \text{(C.38)}\\
&= \sum_{\ell=0}^{\infty}\frac{h^\ell}{\ell!}\,\partial_x^\ell\{f(x)\,g(x)\} && \text{(C.39)}\\
&= \sum_{\ell=0}^{\infty}\frac{h^\ell}{\ell!}\,\partial_x^\ell (fg)(x) && \text{(C.40)}\\
&= (fg)(x+h) && \text{(C.41)}
\end{aligned}$$

Multi-index Taylor Series of a Product of Functions

The product of two Taylor series is the Taylor series of the product:

$$f(\mathbf{x}+\mathbf{h})\,g(\mathbf{x}+\mathbf{h}) = (fg)(\mathbf{x}+\mathbf{h}) \qquad \text{(C.42)}$$

and

$$\begin{aligned}
\left[\sum_{|\alpha|=0}^{\infty}\frac{h^\alpha}{\alpha!}\,\partial_x^\alpha f(\mathbf{x})\right]\left[\sum_{|\beta|=0}^{\infty}\frac{h^\beta}{\beta!}\,\partial_x^\beta g(\mathbf{x})\right] &= \sum_{|\gamma|=0}^{\infty}\frac{h^\gamma}{\gamma!}\,\partial_x^\gamma (fg)(\mathbf{x}) && \text{(C.43)}\\
&\equiv \sum_{|\gamma|=0}^{\infty}\frac{h^\gamma}{\gamma!}\,\partial_x^\gamma\{f(\mathbf{x})\,g(\mathbf{x})\}\,. && \text{(C.44)}
\end{aligned}$$

Here's a proof using combinatorics:

$$
\begin{aligned}
f(\mathbf{x}+\mathbf{h})\, g(\mathbf{x}+\mathbf{h}) &= \left[\sum_{|\alpha|=0}^{\infty} \frac{h^\alpha}{\alpha!}\, \partial_x^\alpha f(\mathbf{x})\right] \left[\sum_{|\beta|=0}^{\infty} \frac{h^\beta}{\beta!}\, \partial_x^\beta g(\mathbf{x})\right] && \text{(C.45)}\\
&= \sum_{|\gamma|=0}^{\infty} \sum_{|\beta|=0}^{|\gamma|} \frac{h^\gamma}{(\gamma-\beta)!\beta!}\, \partial_x^{\gamma-\beta} f(\mathbf{x})\, \partial_x^\beta g(\mathbf{x}) && \text{(C.46)}\\
& \qquad \gamma \equiv \alpha+\beta, \text{ so } \alpha = \gamma-\beta && \text{(C.47)}\\
&= \sum_{|\gamma|=0}^{\infty} \frac{h^\gamma}{\gamma!} \left(\sum_{|\beta|=0}^{|\gamma|} \frac{\gamma!}{\beta!(\gamma-\beta)!} \partial_x^{\gamma-\beta} f(\mathbf{x})\, \partial_x^\beta g(\mathbf{x}) \right) && \text{(C.48)}\\
&= \sum_{|\gamma|=0}^{\infty} \frac{h^\gamma}{\gamma!} \left(\sum_{|\beta|=0}^{|\gamma|} \binom{\gamma}{\beta} \partial_x^{\gamma-\beta} f(\mathbf{x})\, \partial_x^\beta g(\mathbf{x}) \right) && \text{(C.49)}\\
&= \sum_{|\gamma|=0}^{\infty} \frac{h^\gamma}{\gamma!}\, \partial_x^\gamma \{f(\mathbf{x})\, g(\mathbf{x})\} && \text{(C.50)}\\
&= \sum_{|\gamma|=0}^{\infty} \frac{h^\gamma}{\gamma!}\, \partial_x^\gamma (fg)(\mathbf{x}) && \text{(C.51)}\\
&= (fg)(\mathbf{x}+\mathbf{h}). && \text{(C.52)}
\end{aligned}
$$

$$
\binom{\gamma}{\beta} = \binom{\gamma_1}{\beta_1}\binom{\gamma_2}{\beta_2}\cdots\binom{\gamma_n}{\beta_n}. \qquad \text{(C.53)}
$$

C.6 Migration Holors M

Given that $\mathbf{R} \in \mathbb{R}^d$ is a stochastic variable that describes the state of a Brownian object, that $\boldsymbol{\xi} = \Delta\mathbf{R}$ is a stochastic change in the state variable $\mathbf{R}$, that $p[\mathbf{R}, \boldsymbol{\xi}; \Delta t, t]$ is the probability that the Brownian object transitions to a state $\mathbf{R}$ at time t by a change $\boldsymbol{\xi}$ with duration Δt, and that $\alpha \in \mathbb{N}^d$ is a multi-index as defined in Section C.2, we define $\langle \xi^\alpha \rangle_{\Delta t}(\mathbf{R}, t)$, which are elements of a mean-transition-increment holor[8] to a state $\mathbf{R}$ at

---

[8] A holor is a mathematical entity that is made up of one or more independent quantities. A holor may be multiply-indexed, like a tensor, but its transformation properties, under rotation, say, are not necessarily specified.

time t over a time Δt, by

$$\langle \xi^\alpha \rangle_{\Delta t}(\mathbf{R}, t) \;\equiv\; \int \mathrm{d}^d\xi \;\xi^\alpha \; p[\mathbf{R}, \boldsymbol{\xi}; \Delta t, t]. \tag{C.54}$$

For example, with a 4D ($d = 4$) state-space, if $\alpha = \langle 0, 3, 1, 2\rangle$, then $\xi^\alpha = \xi_1^{\alpha_1}\xi_2^{\alpha_2}\cdots\xi_d^{\alpha_d} = {\xi_2}^3\xi_3{\xi_4}^2$ and

$$\begin{aligned}\langle \xi^\alpha \rangle_{\Delta t}(\mathbf{R}, t) \;&=\; \left\langle {\xi_2}^3\xi_3{\xi_4}^2 \right\rangle_{\Delta t}(\mathbf{R}, t) &\text{(C.55)}\\ &=\; \int \mathrm{d}\xi_1\,\mathrm{d}\xi_2\,\mathrm{d}\xi_3\,\mathrm{d}\xi_4 \;{\xi_2}^3\xi_3{\xi_4}^2 \; p[\mathbf{R}, \boldsymbol{\xi}; \Delta t, t]. &\text{(C.56)}\end{aligned}$$

Now we define a migration holor $M_{|\alpha|}^{\{\alpha\}}(\mathbf{R}, t)$ by

$$M_{|\alpha|}^{\{\alpha\}}(\mathbf{R}, t) \;\equiv\; \lim_{\Delta t\to 0} \frac{\langle \xi^\alpha \rangle_{\Delta t}(\mathbf{R}, t)}{\alpha!\Delta t}, \tag{C.57}$$

where

$$\{\alpha\} \;\equiv\; \left\{ \bigcup_j \{j\}_{\alpha_j} \right\} \;=\; \{i_1, i_2, \ldots, i_{|\alpha|}\}, \tag{C.58}$$

and $\{j\}_{\alpha_j}$ means a multiset consisting of α_j instances of the number j. For example, again taking a 4D state-space with $\alpha = \langle 0, 3, 1, 2\rangle$, we have $|\alpha| = 6$ and

$$\begin{aligned}\{\alpha\} \;&=\; \left\{ \bigcup_j \{j\}_{\alpha_j} \right\} \;=\; \big\{ \{1\}_0 \cup \{2\}_3 \cup \{3\}_1 \cup \{4\}_2 \big\} &\text{(C.59)}\\ &=\; \big\{ \{\} \cup \{2, 2, 2\} \cup \{3\} \cup \{4, 4\} \big\} &\text{(C.60)}\\ &=\; \{2, 2, 2, 3, 4, 4\} &\text{(C.61)}\\ &=\; \{i_1, i_2, i_3, i_4, i_5, i_6\}, &\text{(C.62)}\end{aligned}$$

thus

$$\begin{aligned}M_{|\alpha|}^{\{\alpha\}}(\mathbf{R}) \;&=\; \lim_{\tau\to 0} \frac{\langle \xi^\alpha \rangle_\tau(\mathbf{R})}{\alpha!\tau} \;=\; \lim_{\tau\to 0} \frac{\left\langle {\xi_2}^3\xi_3\,{\xi_4}^2 \right\rangle_\tau(\mathbf{R})}{3!1!2!\tau} &\text{(C.63)}\\ &=\; M_6^{\{2,2,2,3,4,4\}}(\mathbf{R}) &\text{(C.64)}\\ &=\; M_6^{222344}(\mathbf{R}) \;=\; M_6^{422234}(\mathbf{R}) \;=\; M_6^{423224}(\mathbf{R}) &\text{(C.65)}\\ &=\; \cdots &\text{(C.66)}\end{aligned}$$

APPENDIX D

Online Videos: Visualization and Entertainment

- Superfluid helium demonstrations.

  `<http://www.youtube.com/watch?v=2Z6UJbwxBZI>`

- Simple bubble rings that grow and slow down as they approach a boundary.

  `<http://www.bubblerings.com/bubblerings/>`

- Dolphins creating and playing with bubble vortex rings!

  `<http://www.youtube.com/watch?v=TMCf7SNUb-Q>`

- Vortex-loop reconnection, which relates to friction, turbulence, and phonon generation in a superfluid

  `<http://physics.aps.org/articles/v1/26>`

- A superfluid song

  YouTube video title: Song A Day #264: Quantum Decoupling Transition in a One-Dimensional Feshbach-Resonant (Superfluid)

  `<http://www.youtube.com/watch?v=FIXRXMMlZBM>`

  This is simply the title and abstract of a paper by Sheehy and Radzihovsky [119], performed as a song set to music.

REFERENCES

[1] Yu. Kagan, V.A. Kashurnikov, A.V. Krasavin, N.V. Prokofev, and B.V. Svistunov, Phys. Rev. A **61**, 043608 (2000) “Quasicondensation in a Two-Dimensional Interacting Bose Gas”; ScienceDaily (March 25, 2009) “Flatland Physics Probes Mysteries Of Superfluidity” `<http://www.sciencedaily.com/releases/2009/03/090325132340.htm>` (accessed 2012 April 27); P. Cladé, C. Ryu, A. Ramanathan, K. Helmerson, and W.D. Phillips, Phys. Rev. Lett. **102**, 170401 (2009) “Observation of a 2D Bose Gas: From Thermal to Quasicondensate to Superfluid”; Yu. Kagan, B.V. Svistunov, and G.V. Shlyapnikov, Sov. Phys. JETP **66**, 314 (1987) [Zh. Eksp. Teor. Fiz. **93**, 552 (1987)]

[2] A.J. Leggett, Rev. Mod. Phys. **71**, S318 (1999) “Superfluidity”; **76**, 999 (2004) “Nobel Lecture: Superfluid ^{3}He: The Early Days as Seen by a Theorist”

[3] S. Grebenev, B. Sartakov, J.P. Toennies, and A.F. Vilesov, Science **289**, 1532 (2000) “Evidence for Superfluidity in Para-Hydrogen Clusters Inside Helium-4 Droplets at 0.15 Kelvin”

[4] R.L. Falge Jr., Phys. Lett. A **24**, 579 (1967) “Superconductivity of Hexagonal Beryllium”

[5] H.K. Onnes, Commun. Phys. Lab. Univ. Leiden **124c**, 1 (1911) H.K. Onnes, Commun. Phys. Lab. Univ. Leiden **124c** and/or **124g**, 1 (1911); “On the sudden change in the rate at which the resistance of mercury disappears”; Akad. van Wetenschappen **14**, 818 (1911) “On the sudden rate at which the resistance of mercury disappears”; these articles are supposedly available at the website `<www.dwc.knaw.nl/english/academy/digital-library/>`, according to Ref. [6]

[6] M.N. Wilson, IEEE Transactions on Applied Superconductivity **PP**, 1 (2011) “100 Years of Superconductivity and 50 Years of Superconducting Magnets”

[7] M.K. Wu, J.R. Ashburn, C.J. Torng, P.H. Hor, R.L. Meng, L. Gao, Z.J. Huang, Y.Q. Wang, and C.W. Chu, Phys. Rev. Lett. **58**, 908 (1987) “Superconductivity at 93 K in a New Mixed-Phase Y-Ba-Cu-O Compound System at Ambient Pressure”

[8] J. Karimäki, Report Series in Physical Sciences, Report No. 74, University of Oulu, Finland (2012) “Structure and Dynamics of Vortices in Superfluid Helium-3”; See Figure 2.4 on page 20 for a phase diagram.

[9] S.O. Demokritov, V.E. Demidov, O. Dzyapko, G.A. Melkov, A.A. Serga, B. Hillebrands, and A.N. Slavin, Nature **443**, (7110) 430 (2006) “Bose-Einstein Condensation of Quasi-Equilibrium Magnons at Room Temperature under Pumping”

[10] D. Sanvitto, F.M. Marchetti, M.H. Szymańska, G. Tosi, M. Baudisch, F.P. Laussy, D.N. Krizhanovskii, M.S. Skolnick, L. Marrucci, A. Lemaître, J. Bloch, C. Tejedor, and L. Viña, Nature Phys. **6**, 527 (2010) "Persistent Currents and Quantized Vortices in a Polariton Superfluid"; J. Kasprzak, M. Richard, S. Kundermann, A. Baas, P. Jeambrun, J.M.J. Keeling, F.M. Marchetti, M.H. Szymaska, R. André, J.L. Staehli, V. Savona, P.B. Littlewood, B. Deveaud, and Le Si Dang, Nature **443**, 409 (2006) "Bose-Einstein Condensation of Exciton Polaritons"

[11] C.A. Regal, M. Greiner, and D.S. Jin, Phys. Rev. Lett. **92**, 040403 (2004) "Observation of Resonance Condensation of Fermionic Atom Pairs"

[12] D. Pines and M.A. Alpar, Nature **316**, 27 (1985) "Superfluidity in neutron stars"

[13] D. Page, M. Prakash, J.M. Lattimer, and A.W. Steiner, Phys. Rev. Lett. **106**, 081101 (2011) "Rapid Cooling of the Neutron Star in Cassiopeia A Triggered by Neutron Superfluidity in Dense Matter"

[14] D.E. Galli and L. Reatto, J. Phys. Soc. Jpn. **77**, 111010 (2008) "Solid ^{4}He and the Supersolid Phase: from Theoretical Speculation to the Discovery of a New State of Matter? A Review of the Past and Present Status of Research"

[15] S. Balibar, Nature **464**, 176 (2010) "The enigma of supersolidity"

[16] H.K. Onnes, Commun. Phys. Lab. Univ. Leiden **108** (1908); Commun. K. Onnes Lab., Leiden No. 108 Sec. 6 (1908); Proc. Roy. Acad. Amsterdam **11**, 168 (1908); KNAW, Proceedings, 11, 1908-1909, Amsterdam, 168 (1909) "The Liquefaction of Helium"; the article is supposedly available at the website `<www.dwc.knaw.nl/english/academy/digital-library/>`, according to Ref. [6]

[17] D. van Delft and P. Kes, Physics Today, September (2010) "The Discovery of Superconductivity"

[18] D.F. Brewer (ed.) and V.L. Ginzburg, Prog. Low Temp. Phys. **10**, 1 (1986) "High-Temperature Superconductivity: Some Remarks"; See the footnote on page 13 for a one-paragraph overview of the timeline of discovery of the superfluid helium phase.

[19] A. Einstein, Sitzungsber. Kgl. Preuss. Akad. Wiss. **1924**, 261 (1924); S.N. Bose, Z. Phys. **26**, 178 (1924)

[20] P. Kapitza, Nature **141**, 74 (1938) "Viscosity of Liquid Helium below the λ-Point"

[21] J.F. Allen and A.D. Misener, Nature **141**, 75 (1938) "Flow of Liquid Helium II"

[22] F. London, Nature **141**, 643 (1938) "The λ-Phenomenon of Liquid Helium and the Bose-Einstein Degeneracy"

[23] L. Tisza, Nature **141**, 913 (1938) “Transport Phenomena in Helium II”

[24] L.D. Landau, Zh. Eksp. Teor. Fiz. **11**, 592 (1941); and J. Phys. (Moscow) **5**, 71 (1941)

[25] J. Bardeen, L.N. Cooper, and J.R. Schrieffer, Phys. Rev. **108**, 1175 (1957) “Theory of Superconductivity”

[26] N.N. Bogoliubov, Sov. Phys. JETP **34**, 41 (1958) “A new method in the theory of superconductivity I”

[27] D.D. Osheroff, R.C. Richardson, and D.M. Lee, Phys. Rev. Lett. **28**, 885 (1972) “Evidence for a New Phase of Solid He^3”; For a direct mention of superfluidity see T.A. Alvesalo, Yu.D. Anufriyev, H.K. Collan, O.V. Lounasmaa, and P. Wennerström, Phys. Rev. Lett. **30**, 962 (1973) “Evidence for Superfluidity in the Newly Found Phases of ^3He”

[28] V.L. Berezinskii, Zh. Eksp. Teor. Fiz. **59**, 907 (1970) [Sov. Phys. JETP **32**, 493 (1971)]; V.L. Berezinskii, Zh. Eksp. Teor. Fiz. **61**, 1144 (1971) [Sov. Phys. JETP **34**, 610 (1972)]

[29] J.M. Kosterlitz and D.J. Thouless, J. Phys. C **6**, 1181 (1973) “Ordering, Metastability and Phase Transitions in Two-Dimensional Systems”; J.M. Kosterlitz, J. Phys. C **7**, 1046 (1974) “The Critical Properties of the Two-Dimensional xy Model”

[30] J.G. Bednorz and A.K. Müller, Z. Phys. B **64**, 189 (1986) “Possible High-T_c Superconductivity in the Ba–La–Cu–O System”

[31] J.R. Schrieffer, US Patent App. 11/127,682 (2005) “Superconductors with Super High Critical Temperatures, Methods for Identification, Manufacture and Use”

[32] P. Dai, B.C. Chakoumakos, G.F. Sun, K.W. Wong, Y. Xin, D.F. Lu, Physica C **243**, 201 (1995) “Synthesis and neutron powder diffraction study of the superconductor $HgBa_2Ca_2Cu_3O_{8+\delta}$ by Tl substitution”

[33] M.H. Anderson, J.R. Ensher, M.R. Matthews, C.E. Wieman, and E.A. Cornell, Science **269**, (5221) 198 (1995) “Observation of BoseEinstein Condensation in a Dilute Atomic Vapor”

[34] A.F. Andreev and I.M. Lifshitz, Sov. Phys. JETP **29**, 1107 (1969); G.V. Chester, Phys. Rev. A **2**, 256 (1970) “Speculations on Bose-Einstein Condensation and Quantum Crystals”

[35] E. Kim and M.H.W. Chan, Nature **427**, 225 (2004) "Probable Observation of a Supersolid Helium Phase"; Science **305**, 1941 (2004) "Observation of Superflow in Solid Helium"

[36] A. Sudbø and W. Østreng (ed.), Complexity. Interdisciplinary Communications 2006/2007, 62 (2008) "Superconductors and Superfluids – Matter Wave Analogs of the LASER"

[37] C.F. Barenghi, R.J. Donnelly, and W.F. Vinen (ed.s), *Quantized Vortex Dynamics and Superfluid Turbulence*, Springer (2001)

[38] T.F. Buttke and A.J. Chorin, Applied Numerical Mathematics **12**, 47 (1993) "Turbulence Calculations in Magnetization Variables"

[39] G.A. Williams, Phys. Rev. Lett. **82**, 1201 (1999) "Vortex-Loop Phase Transitions in Liquid Helium, Cosmic Strings, and High-T_c Superconductors"

[40] G.A. Williams, J. Low Temp. Phys. **93**, 1079 (1993) "Vortex Dynamics at the Superfluid λ-Transition"

[41] J. Greensite, Prog. Part. Nucl. Phys. *51* 1 (2003) "The confinement problem in lattice gauge theory"

[42] T. Kibble, Phys. Today **60**, 47 (2007) "Phase-Transition Dynamics in the Lab and the Universe"; W.H. Zurek, Phys. Rep. **276**, 177 (1996) "Cosmological Experiments in Condensed Matter Systems"; A. Yates and W.H. Zurek, Phys. Rev. Lett. **80**, 5477 (1998) "Vortex Formation in Two Dimensions: When Symmetry Breaks, How Big Are the Pieces?"

[43] K.G. Lagoudakis, F. Manni, B. Pietka, M. Wouters, T.C.H. Liew, V. Savona, A.V. Kavokin, R. André, and B. Deveaud-Plédran, Phys. Rev. Lett. **106**, 115301 (2011) "Probing the Dynamics of Spontaneous Quantum Vortices in Polariton Superfluids"

[44] A.P. Young, J. Phys. C **11**, L453 (1978) "On the Theory of the Phase Transition in the Two-Dimensional Planar Spin Model"

[45] R.P. Feynman, Phys. Rev. **94**, 262 (1954) "Atomic Theory of the Two-Fluid Model of Liquid Helium"

[46] R.P. Feynman and M. Cohen, Phys. Rev. **102**, 1189 (1956) "Energy Spectrum of the Excitations in Liquid Helium"

[47] L. Reatto and G.L. Masserini, Phys. Rev. B **38**, 1 (1988) "Shadow Wave Function for Many-Boson Systems"

[48] D.E. Galli, E. Cecchetti, and L. Reatto, Phys. Rev. Lett. **77**, 5401 (1996) "Rotons and Roton Wave Packets in Superfluid ^{4}He"

[49] L. Reatto and D.E. Galli, Int. J. Mod. Phys. B **13**, 607 (1999) "What Is a Roton?"

[50] M. Sadd, G.V. Chester, and L. Reatto, Phys. Rev. Lett. **79**, 2490 (1997) "Structure of a Vortex in Superfluid ^{4}He"; Note the use of a "shadow wave function".

[51] V. Elser, Phys. Lett. A **161**, 541 (1992) "String Theory of the Roton"

[52] W. Wu, S.A. Vitiello, L. Reatto, M.H. Kalos, Phys. Rev. Lett. **67**, 1446 (1991) "Excited states in 4He described by a shadow wave function"

[53] C.A. Jones and P.H. Roberts, J. Phys. A: Math. Gen. **15** 2599 (1982) "Motions in a Bose Condensate: IV. Axisymmetric Solitary Waves"

[54] P.H. Roberts and N.G. Berloff, Ref. [37] 235 (2001) "The Nonlinear Schrödinger Equation as a Model of Superfluidity"

[55] P.H. Roberts and J. Grant, J. Phys. A: Gen. Phys. **4**, 55 (1971) "Motions in a Bose Condensate. I. The Structure of the Large Circular Vortex"

[56] S.J. Putterman, *Superfluid Hydrodynamics*, North-Holland / American Elsevier (1974). This book is an excellent introduction to superfluidity.

[57] A.K. Nguyen and A. Sudbø, Phys. Rev. B **60**, 15307 (1999) "Topological Phase Fluctuations, Amplitude Fluctuations, and Criticality in Extreme Type-II Superconductors"; The spin-waves discussed in this paper are second-sound waves.

[58] B. Chattopadhyay, M.C. Mahato, and S.R. Shenoy, Phys. Rev. B **47**, 15 159 (1993) "Vortex-Loop Crinkling in the Three-Dimensional XY Model: Numerical Evidence in Support of an Ansatz"

[59] R. Guida and J. Zinn-Justin, J. Phys. A **31**, 8103 (1998) "Critical exponents of the N-vector model"

[60] F. Jasch and H. Kleinert, J. Math. Phys. **42**, 52 (2001) "Fast-convergent resummation algorithm and critical exponents of ϕ^4-theory in three dimensions"

[61] V. Dohm, J. Low Temp. Phys. **69**, 51 (1987) "Renormalization-group theory of critical phenomena near the Lambda transition of ^4He"

[62] F.J. Wegner, Phys. Rev. B **5**, 4529 (1972) "Corrections to Scaling Laws"

[63] J. Rudnick and D. Jasnow, Phys. Rev. B **16**, 2032 (1977) "Renormalization-Group Proof of Josephson's Relation and ϵ Expansion for the Helicity Modulus (Superfluid Density)"

[64] M. Campostrini, M. Hasenbusch, A. Pelissetto, and E. Vicari, Phys. Rev. B **74**, 144506 (2006) “Theoretical Estimates of the Critical Exponents of the Superfluid Transition in ^{4}He by Lattice Methods”

[65] E. Burovski, J. Machta, N. Prokof’ev, and B. Svistunov, Phys. Rev. B **74**, 132502 (2006) “High-Precision Measurement of the Thermal Exponent for the Three-Dimensional XY Universality Class”

[66] J.A. Lipa, D.R. Swanson, J.A. Nissen, T.C.P. Chui, and U.E. Israelsson, Phys. Rev. Lett. **76**, 944 (1996) “Heat Capacity and Thermal Relaxation of Bulk Helium very near the Lambda Point” (The raw data was requested and obtained via email.)

[67] G. Ahlers, Phys. Rev. A **3**, 696 (1971) “Heat Capacity near the Superfluid Transition in ^{4}He at Saturated Vapor Pressure”

[68] G. Ahlers, Phys. Rev. A **8**, 530 (1973) “Thermodynamics and Experimental Tests of Static Scaling and Universality near the Superfluid Transition in He^4 under Pressure”

[69] R.J. Donnelly and C.F. Barenghi, “The Observed Properties of Liquid Helium at the Saturated Vapor Pressure” `<http://pages.uoregon.edu/rjd/vapor1.htm>` (accessed 2011 November 17)

[70] D.R. Tilley and J. Tilley, *Superfluidity and Superconductivity, Second Edition*, Adam Hilger Ltd (1986); See Fig. 2.3.

[71] J.S. Brooks and R.J. Donnelly, Journal of Physical and Chemical Reference Data **6**, 51 (1977) “The Calculated Thermodynamic Properties of Superfluid Helium-4”

[72] P.J. Flory, *Principles of Polymer Chemistry*, Chap. XII, Cornell University Press (1953)

[73] R.D. Kamien, J. Phys. I (France) **3**, 1663 (1993) “Flory Exponents from a Self-Consistent Renormalization Group”

[74] G.A. Williams, J. Phys.: Conf. Ser. **150**, 032120 (2009) “Finite-Frequency Dynamics of Vortex Loops at the ^{4}He Superfluid Phase Transition”

[75] R.J. Donnelly, Cambridge Studies in Low Temperature Physics 3: *Quantized Vortices in Helium II*, Cambridge University Press (1991); See pages 22–23.

[76] P.H. Roberts and R.J. Donnelly, Phys. Lett. **31A**, 137 (1970) “Dynamics of Vortex Rings”

[77] P.H. Roberts, Mathematika **19**, 169 (1972) “A Hamiltonian Theory for Weakly Interacting Vortices”; P.G. Saffman, *Vortex Dynamics*, Cambridge University Press (1992); See Section 10.4.

[78] S.R. Shenoy, Phys. Rev. B **40**, 5056 (1989) “Vortex-Loop Scaling in the Three-Dimensional XY Ferromagnet”

[79] D.S. Greywall and G. Ahlers, Phys. Rev. A **7**, 2145 (1973) “Second-Sound Velocity and Superfluid Density in ^{4}He under Pressure near T_λ”

[80] G. Agnolet, D.F. McQueeney, and J.D. Reppy, Phys. Rev. B **39**, 8934 (1989) “Kosterlitz-Thouless Transition in Helium Films”

[81] A. Jelić and L.F. Cugliandolo, J. Stat. Mech. (2011) P02032 “Quench Dynamics of the 2d XY Model”

[82] J. Villain, J. Phys. (Paris) **36**, 581 (1975) “Theory of One- and Two-Dimensional Magnets with an Easy Magnetization Plane: II. The Planar, Classical, Two-Dimensional Magnet”

[83] D.R. Nelson and J.M. Kosterlitz, Phys. Rev. Lett. **39**, 1201 (1977) “Universal Jump in the Superfluid Density of Two-Dimensional Superfluids”

[84] M. Hieda, K. Matsuda, T. Kato, T. Matsushita, and N. Wada, J. Phys. Soc. Japan **78**, 033604 (2009) “Extremely High Frequency Dependence of Two-Dimensional Superfluid Onset”

[85] H. Cho and G.A. Williams, Phys. Rev. Lett. **75**, 1562 (1995) “Vortex Core Size in Submonolayer Superfluid ^{4}He Films”

[86] G.A. Williams, Phys. Rev. Lett. **59**, 1926 (1987) “Vortex-Ring Model of the Superfluid λ Transition”

[87] G.A. Williams, J. Low Temp. Phys. **101**, 421 (1995) “Specific Heat and Superfluid Density of Bulk and Confined ^{4}He Near the λ-Transition”

[88] M. Ferer, Phys. Rev. Lett. **33**, 21 (1974) “New Universal Quantity for the He^4 Superfluid Transition”

[89] W.I. Glaberson, Phys. Lett. **38A**, 183 (1972) “Pressure Dependence of the Vortex Core Parameter in He II”

[90] W. I. Glaberson and M. Steingart, Phys. Rev. Lett. **26**, 1423 (1971) “Temperature Dependence of the Vortex-Core Parameter in He II”

[91] D.C. Samuels and R.J. Donnelly, Phys. Rev. Lett. **67**, 2505 (1991) "Motion of Charged Vortex Rings in Helium II"

[92] S. Balibar, J. Low Temp. Phys. **146**, 441 (2007) "The Discovery of Superfluidity"; See page 24 for the discussion on the nature of rotons.

[93] B.D. Josephson, Phys. Lett. **21**, 608 (1966) "Relation between the Superfluid Density and Order Parameter for Superfluid He near T_{c}"; Note that our α is written as "α'" and ν shows up as "$2\beta - \eta\nu'$", in particular, in equations (6) and (7).

[94] A.J. Bray, Adv. Phys. **43**, 357 (1994) "Theory of Phase Ordering Kinetics"; S. Puri and V.K. Wadhawan (ed.s), *Kinetics of Phase Transitions*, CRC Press (Taylor and Francis, Boca Raton, 2009)

[95] J.G. Amar and F. Family, Phys. Rev. A **41**, 3258 (1990) "Diffusion Annihilation in One Dimension and Kinetics of the Ising Model at Zero Temperature"; A. Coniglio and M. Zannetti, Europhys. Lett. **10**, 575 (1989) "Multiscaling in Growth Kinetics"

[96] J.J. Arenzon, A.J. Bray, L.F. Cugliandolo, and A. Sicilia, Phys. Rev. Lett. **98**, 145701 (2007) "Exact Results for Curvature-Driven Coarsening in Two Dimensions"

[97] P.C. Hohenberg and B.I. Halperin, Rev. Mod. Phys. **49**, 435 (1977) "Theory of Dynamic Critical Phenomena"

[98] A.J. Bray and S. Puri, Phys. Rev. Lett. **67**, 2670 (1991) "Asymptotic Structure Factor and Power-Law Tails for Phase Ordering in Systems with Continuous Symmetry"; H. Toyoki, Phys. Rev. B **45**, 1965 (1992) "Structure Factors of Vector-Order-Parameter Systems Containing Random Topological Defects"; A.J. Bray and K. Humayun, Phys. Rev. E **47**, R9 (1993) "Universal Amplitudes of Power-Law Tails in the Asymptotic Structure Factor of Systems with Topological Defects"

[99] R.E. Blundell and A.J. Bray, Phys. Rev. E **49**, 4925 (1994) "Phase-Ordering Dynamics of the O(n) Model: Exact Predictions and Numerical Results"

[100] M. Mondello and N. Goldenfeld, Phys. Rev. A **42**, 5865 (1990) "Scaling and Vortex Dynamics after the Quench of a System with a Continuous Symmetry"

[101] B. Yurke, A.N. Pargellis, T. Kovacs, and D.A. Huse, Phys. Rev. E **47**, 1525 (1993) "Coarsening Dynamics of the XY Model"

[102] A.J. Bray, A.J. Briant, and D.K. Jervis, Phys. Rev. Lett. **84**, 1503 (2000) "Breakdown of Scaling in the Nonequilibrium Critical Dynamics of the Two-Dimensional XY Model"

[103] H.-C. Chu and G.A. Williams, Phys. Rev. Lett. **86**, 2585 (2001) "Quenched Kosterlitz-Thouless Superfluid Transitions"

[104] V. Ambegaokar, B.I. Halperin, D.R. Nelson, and E.D. Siggia, Phys. Rev. B **21**, 1806 (1980) "Dynamics of Superfluid Films"

[105] A previous theory of quenches from below T_{KT} considered the two-point spin correlation function, but did not access the vortex dynamics: A.D. Rutenberg and A.J. Bray, Phys. Rev. E **51**, R1641 (1995) "Phase Ordering of Two-Dimensional XY Systems below the Kosterlitz-Thouless Transition Temperature"

[106] P. Minnhagen, O. Westman, A. Jonsson, and P. Olsson, Phys. Rev. Lett. **74**, 3672 (1995) "New Exponent for the Nonlinear IV Characteristics of a Two Dimensional Superconductor"; L.M. Jensen, B.J. Kim, P. Minnhagen, Phys. Rev. B **61**, 15412 (2000) "Dynamic Critical Exponent of Two-, Three-, and Four-Dimensional XY Models with Relaxational and Resistively Shunted Junction Dynamics"

[107] The proposal here, that a purely random arrangement of uncorrelated plus-minus vortices (at high temperatures and long length scales) has a distribution falling off as precisely r^{-4}, does not seem to have been previously noted in the literature, though this is probably the underlying reason for the Kosterlitz-Thouless result $2\pi K = 4$ at T_{KT} and $r = \infty$.

[108] A.K. Nguyen and A. Sudbø, Phys. Rev. B **57**, 3123 (1998) "Onsager Loop Transition and First-Order Flux-Line Lattice Melting in High-T_c Superconductors"; see Figure 5 for an example of the distribution $D(p)$ as a function of loop perimeter p.

[109] M. Tabor, *Chaos and Integrability in Nonlinear Dynamics: An Introduction*, John Wiley & Sons (1989); See Section 1.4.b for the fixed-point classification.

[110] R. Redheffer and D. Port, *Differential Equations: Theory and Applications*, Jones and Bartlett Publishers (1991); See Chapter 20, Fig. 1 for further fixed-point classification vocabulary.

[111] G.S. Pawley, R.H. Swendsen, D.J. Wallace, and K.G. Wilson, Phys. Rev. B **29**, 4030 (1984) "Monte Carlo Renormalization-Group Calculations of Critical Behavior in the Simple-Cubic Ising Model"

[112] D.F. Litim, Nucl. Phys. **B631**, 128 (2002) "Critical Exponents from Optimised Renormalisation Group Flows"

[113] S.-K. Ma, *Modern Theory of Critical Phenomena*, W. A. Benjamin, Inc. (1976); See Chapter VI, on Fixed Points and Exponents.

[114] P.M. Goldbart and F. Bora, J. Phys. A: Math. Theor. **42**, 185001 (2009) "Quantized Vortices and Superflow in Arbitrary Dimensions: Structure, Energetics and Dynamics"

[115] S. Chandrasekhar, Mod. Rev. Phys. **15**, 1 (1943) "Stochastic Problems in Physics and Astronomy"

[116] R.E. Wilde and S. Singh, *Statistical Mechanics: Fundamentals and Modern Applications*, John Wiley & Sons (1998)

[117] V.S. Anishchenko, V.V. Astakhov, A.B. Neiman, T.E. Vadivasova, and L. Schimansky-Geier, *Nonlinear Dynamics of Chaotic and Stochastic Systems: Tutorial and Modern Developments*, Springer (2002)

[118] C. Liu, R. Bammer, B. Acar, and M.E. Moseley, "Generalized Diffusion Tensor Imaging (GDTI) Using Higher Order Tensor (HOT) Statistics" `<http://cds.ismrm.org/ismrm-2003/0242.pdf>` (accessed 2009 February 13)

[119] D.E. Sheehy and L. Radzihovsky, Phys. Rev. Lett. **95**, 130401 (2005) "Quantum Decoupling Transition in a One-Dimensional Feshbach-Resonant Superfluid"